COPPE
Instituto Alberto Luiz Coimbra de Pós-Graduação e Pesquisa de Engenharia
UFRJ

# COPOLYMERIZATION OF COMPONENTS OF CASHEW NUT LIQUID WITH VINYL MONOMERS: EXPERIMENTAL AND MODELING STUDIES

Laura Pires da Mata Costa

Dissertação de Mestrado apresentada ao Programa de Pós-graduação em Engenharia Química, COPPE, da Universidade Federal do Rio de Janeiro, como parte dos requisitos necessários à obtenção do título de Mestre em Engenharia Química.

Orientadores: José Carlos Costa da Silva Pinto
Amanda Lemette Teixeira Brandão
Márcio Nele de Souza

Rio de Janeiro
Março de 2019

COPOLYMERIZATION OF COMPONENTS OF CASHEW NUT LIQUID WITH VINYL MONOMERS: EXPERIMENTAL AND MODELING STUDIES

Laura Pires da Mata Costa

DISSERTAÇÃO SUBMETIDA AO CORPO DOCENTE DO INSTITUTO ALBERTO LUIZ COIMBRA DE PÓS-GRADUAÇÃO E PESQUISA DE ENGENHARIA (COPPE) DA UNIVERSIDADE FEDERAL DO RIO DE JANEIRO COMO PARTE DOS REQUISITOS NECESSÁRIOS PARA A OBTENÇÃO DO GRAU DE MESTRE EM CIÊNCIAS EM ENGENHARIA QUÍMICA.

Examinada por:

Prof. José Carlos Costa da Silva Pinto, D.Sc.

Prof. Amanda Lemette Teixeira Brandão, D.Sc.

Prof. Fernando Gomes de Souza Jr, D.Sc.

Dr. Bruno Francisco Oechsler, D.Sc.

RIO DE JANEIRO, RJ – BRASIL
MARÇO DE 2019

Costa, Laura Pires da Mata

Copolymerization of components of cashew nut liquid with vinyl monomers: experimental and modeling studies/Laura Pires da Mata Costa. – Rio de Janeiro: UFRJ/COPPE, 2019.

XX, 201 p.: il.; 29,7cm.

Orientadores: José Carlos Costa da Silva Pinto
Amanda Lemette Teixeira Brandão
Márcio Nele de Souza

Dissertação (mestrado) – UFRJ/COPPE/Programa de Engenharia Química, 2019.

Referências Bibliográficas: p. 160 – 170.

1. LCC. 2. Cardanol. 3. Ácido anacárdico. 4. Copolímero. I. Pinto, José Carlos Costa da Silva *et al.* II. Universidade Federal do Rio de Janeiro, COPPE, Programa de Engenharia Química. III. Título.

*Eu dedico esta dissertação a minha mãe, Nilza Pires*

# Acknowledgments

Hoje, 20 de março, deveria ter acontecido no dia 29 de fevereiro. Apesar dos transtornos, não tem problema. De qualquer maneira, a chegada do 'hoje' foi uma caminhada que, apesar de início indeterminado, começou a muitos anos atrás. Posso afirmar, contudo, que se não tivesse sido um "paper" com o nome do Zé que me levou para o currículo dele, não haveria esse hoje.

Nessa caminhada, "meus sapatos" sempre foram minha família. Não poderia ter dado um único passo sem eles. O "Ultraboost" é a minha mãe que, por ser professora universitária, não poderia estar mais realizada em ver a filha passar por todos os estágios da formação superior. E eu não poderia ser mais grata a todas as oportunidades que ela me ofereceu e me oferece até hoje. Por exemplo, em 1998, tinha um computador em casa com uns joguinhos irados, mas que ela usava para rodar seus programas em Fortran e escrever seus artigos! Também me deixava presa na universidade e aprendi a mexer no PowerPoint e fazer apresentações "por osmose" no início dos anos 2000! Teve uma época que eu oferecia meus serviços de "consultoria gráfica" e realizava formatações para seus amigos professores! (...) Enfim, com certeza, gostaria de estar presente presencialmente no 'hoje' (pediu para filmar todos os instantes e, pasmem, tem uma pasta para guardar qualquer artigo, trabalho ou apresentação minha), mas está super ocupada dando aulas e participando de mesas redondas! Então, está meia complicado vir de Natal até o Rio! Te amo, mãe!

Mesmo com os melhores sapatos, pedras no caminho não foram evitadas. Porém, todo um arsenal surgiu nesse últimos dois anos a começar pelo Zé que sempre se mostrou "preocupado" e me criticava por não ter reuniões com ele... Acho que, no final, ficou até feliz em ver meu esforço em fazer várias coisas ao mesmo tempo e corrigir a dissertação noites adentro. Até começou a me zoar chamando de "menina do interior" por conta do trocadilho de palavras devido ao cansaço. Muito obrigada, Zé! É muito bacana trabalhar contigo!

Os comentários sobre o sotaque não ficaram isolados ao Zé, Marcio declarou que o meu sotaque seria "o melhor da COPPE"! Então, acho que não é tão ruim assim... Esse é o mesmo Márcio que achava minha dissertação super legal e incentivava sempre que me encontrava! Além de orientador, agora também converso com ele sobre viagens e preciso dar 'Kudos' para ele no Strava! Muito obrigada, Marcio!

Para dar mais cor aos dias, "uma tsuru encantado" chamada Amanda também me ajudou nesse processo. Além de me apoiar nos desabafos, sempre me incentivou... E incentivou tanto que passei a dever uns 20 artigos a ela! Muito obrigada, Amanda!

Muitos créditos também vão para meus amigos. Naiara e Nicolis se mostraram verdadeiras amigas. Sempre estamos lado a lado, uma apoiando as outras. É muito bom poder contar com vocês! Do I140, nenhum experimento teria sido feito sem "Thamiiyes" e Rafa que, ou me ajudavam, ou davam uns suportes piscoligicos rindo das minhas danças ou me zoando. Adoro vocês! Carol Sá também foi quem me introduziu ao laboratório, falando sobre GoT e corridas. Depois me enrosquei com ela e viramos amigas! Também teve Mateus, Ana, Lys, Marcel, Luciana, Débora Way, Diulia, Débora Vaz, Bruno Oechsler, Gustavo e Martina... Toda uma galera de peso! Também têm as engrenagens - Larissa, Camila, Nathaly, Natasha, Roberto, Ricardo e Vanessa! Obrigada! O que seria do laboratório sem vocês?

Não posso me esquecer de Angela do LADEQ que me ajudava sempre da maneira mais fofa e engraçada possível. Você é demais, Angela! André também me ajudou muito! Sempre colaborava com umas conversas legais! Muito obrigada, André! Também tem Ali que.. bem, ficava por último no Ladeq e me permitia ficar por lá até mais tarde!!! Também aparecia no RU e nas festas misteriosamente para divertir a galera!

Outros amigos também sempre estiveram presentes, mesmo que estando uns metros distantes... na G130! Para começar, Jonildo, Charles e Carol Bonita que vem me apoiando desde a época das disciplinas, incentivando uns aos outros em cada seminário, momentos difíceis e, claro, compartilhando ótimos momentos! Outros ótimos amigos são Carol Sá (novamente!), Sérgio, Thayná, Lucas, Rafa, Reinaldo, Felipe Gomide e Nayher. Adoro vocês!

Enfim, muito obrigada a todos vocês! Estão e sempre estarão guardados com um carinho especial nas minhas recordações! Mil beijos!

Resumo da Dissertação apresentada à COPPE/UFRJ como parte dos requisitos necessários para a obtenção do grau de Mestre em Ciências (M.Sc.)

# COPOLIMERIZAÇÃO DE COMPONENTES DO LÍQUIDO DA CASTANHA DE CAJU COM MONÔMEROS VINÍLICOS: ESTUDOS EXPERIMENTAIS E DE MODELAGEM

Laura Pires da Mata Costa

Março/2019

Orientadores: José Carlos Costa da Silva Pinto
Amanda Lemette Teixeira Brandão
Márcio Nele de Souza

Programa: Engenharia Química

O líquido da castanha de caju (LCC) é um sub-produto da indústria de produção de castanha de caju. Ele é riquissímo em compostos fenólicos que podem ser utilizados como comonômeros para funcionalização de polímeros. No presente trabalho, é estudada a polimerização radicalar desses materiais. Inicialmente, foi investigado a cinética da copolimerização em massa do cardanol ou LCC natural com estireno, metacrilato de metila, acetato de vinila ou ácido acrílico e diversas análises foram realizadas para caracterizar os copolímeros formados. Algumas vantagens obtidas com a copolimerização foram o aumento da estabilidade térmica e a redução da temperatura vítrea dos polímeros. Com base nos dados obtidos, um mecanismo cinético foi proposto e um modelo matemático foi derivado e implementado. Os parâmetros cinéticos do modelo foram estimados de modo a descrever os dados de conversão dos monômeros, massas molares médias e composição dos copolímeros. Foi observado que os monômeros renováveis exercem forte efeito inibitório nas polimerizações, fazendo com que a incorporação deles nas cadeias copoliméricas seja difícil. Polimerizações em suspensão foram realizadas nas condições que resultaram no melhor desempenho em massa. Os polímeros obtidos em suspensão foram mais hidrofílicos e a adição de cardanol nessas polimerizações constitui uma ótima alternativa para controlar o tamanho médio de partículas e manter as suspensões estáveis por longos períodos de tempo.

Abstract of Dissertation presented to COPPE/UFRJ as a partial fulfillment of the requirements for the degree of Master of Science (M.Sc.)

COPOLYMERIZATION OF COMPONENTS OF CASHEW NUT LIQUID WITH VINYL MONOMERS: EXPERIMENTAL AND MODELING STUDIES

Laura Pires da Mata Costa

March/2019

Advisors: José Carlos Costa da Silva Pinto
Amanda Lemette Teixeira Brandão
Márcio Nele de Souza

Department: Chemical Engineering

Cashew nut shell liquid (CNSL) is a by-product of cashew nut industry. CNSL is rich in phenolic compounds that can be used as comonomers for functionalization of polymers. In the present study, the radical polymerization of these materials is investigated. Initialy, the kinects of bulk copolymerization of cardanol or natural CNSL with styrene, methyl methacrylate, vinyl acetate or acrylic acid was studied and several analyses were carried out to characterize the obtained copolymers. Some advantages observed in the copolymerizations were the increase of thermal stability and reduction of the glass transition temperature of the polymers. Based on the obtained results, a kinetic mechanism was proposed and a mathematical model was derived and implemented. The unknown kinetic model parameters were estimated to guarantee an adequate model prediction of monomer conversion, average molecular weights and composition of the copolymers. It was observed that the renewable monomers exert strong inhibition effects on the polymerizations, making the incorporation of them into the copolymer chains difficult. Suspension polymerizations were performed at the conditions that resulted in the best bulk polymerization results. The obtained polymers were more hydrophilic in suspension. Besides, the addition of cardanol in suspension polymerizations constituted excellent alternative for control of average particle sizes and stabilization of suspensions for periods of time.

# Contents

# List of Figures

# List of Tables

# Chapter 1

# Introduction

Due to the increasing environmental concerns, different issues related to green chemistry and waste management are being discussed and studied in the 21th century. For instance, renewable sources are being increasingly used for manufacture of goods, especially by-product derivatives and wastes. In the polymerization industry, most of the polymers are still petroleum-derived. Because of this, the polymerization industry has been suffering harsh criticisms due to the negative environment impacts. Consequently, alternative sources of monomers have been investigated. One of them is cashew nut shell liquid (CNSL), which is a mixture of phenolic compounds obtained from the fruit of cashew tree (MUBOFU, 2016).

Even though many people think that the fruit of cashew tree is the cashew apple, the actual fruit is the nut with a kidney-shaped seed hidden inside, the cashew kernel. CNSL is found within of the cashew nut shells and can be extracted by thermal, solvent or mechanical processes. Depending on the method, the obtained CNSL can be classified as natural or technical. Natural CNSL is rich in anacardic acid, while technical CNSL is rich in cardanol. Cardanol is a salicylic acid with a long side chain, while anacardic acid contains a carboxylic acid group. The number of unsaturations in the side chain range from 0 to 3. Both compounds are amphiphilic and manufactured as a mixture of several closely related organic compounds (LUBI and THACHIL (2000), LOCHAB *et al.* (2014), OTSUKA *et al.* (2017)).

Although CNSL finds numerous applications, it is considered a by-product of the cashew almond industry, being frequently released to the environment and discarded as waste. Besides biological applications (as anticancer, antioxidant and antibacterial agent), CNSL has been used industrially for manufacture of brake linings, coatings, paints and varnishes. Additionally, CNSL can undergo many polymerization reactions because its compounds contain at least a phenolic group (polycondensation) and a long meta-substituted unsaturated aliphatic chain (C15) (polyaddition). Due to the hydroxyl group, cardanol has been used in polycondensation reactions with formalde-

hyde (or a less toxic alternative). However, very little is known about the radical addition polymerization of these monomers (BHUNIA *et al.* (1999), BALGUDE and SABNIS (2014), MUBOFU and MGAYA (2018)).

The worldwide annual production of raw cashew nuts stands at approximately 2.1 million tons (CEPAGRO/IBGE (2019)). Knowing that 25 wt% of the total cashew fruit constitutes the nut, and that 30-35 wt% of the shell is constituted by CNSL, depending on the method of extraction, 150 tons of CNSL are produced and obtained annually. However, the commercial demand for CNSL is not high. Therefore, the aim of the present study is on the use of CNSL and its derivatives (e.g. cardanol) as a comonomer to functionalize polymers through free radical polymerizations. This new application of CNSL can constitute a promising alternative to CNSL waste disposal (TIAN *et al.* (2012)).

Firstly, bulk copolymerizations of cardanol or natural CNSL with styrene, methyl methacrylate or vinyl acetate are studied. Kinetic experiments are carried out for monitoring of conversion data. The following copolymer properties were investigated: molecular weight distributions, copolymer compositions and transitions temperatures. Afterwards, a kinetic model is proposed and the unknown parameters are estimated. Because of the long side chain, steric hindrance is expected. Also, inhibitory effects can take place due to the phenolic moiety and generation of stable radicals (COSTA *et al.*, 2019).

Then, suspension polymerization runs are carried out and the kinetics is investigated. Experiments are performed in suspension based on those obtained previously in bulk. In this case, functionalized polymer particles were made, and the porosity, hydrophobicity and particle size distributions were studied. These particles can be used for bioconjugation, immobilization of enzyme and as a drug carriers in future applications.

The present study was performed in the "Laboratório de Engenharia de Polimerização" (EngePol) of the Programa de Engenharia Quimica (PEQ) of the Instituto Alberto Luiz Coimbra de Pós-Graduação e Pesquisa de Engenharia (COPPE) of the Universidade Federal do Rio de Janeiro (UFRJ). We thank the "Laboratório de Ressonância Magnética Nuclear de Líquidos" (LABRMN 2) of Chemistry Institute (IQ) of UFRJ and the "Laboratorio Multiusuários de Analised por RMN" (LAMAR) of the Center of Health Sciences of UFRJ, both for NMR analysis. We also thank the "Laboratório de Instrumentos e Pesquisa" of IF, UFRJ for FTIR analysis. Nonetheless, we thank "Laboratório de Apoio Instumental" (LAPIN) of the Instituto de Macromoleculas Professor Eloisa Mano (IMA) for differential scanning calorimetry (DSC) analyses.

## 1.1 Motivation

1. The enormous amount of CNSL obtained annually as a by-product of cashew nut production;

2. CNSL has low selling prices and can have its value aggregated by using it as a monomer;

3. Cardanol and anacardic acid are amphiphilic (polar and nonpolar functions in the same molecule) and can stabilize heterogeneous systems;

4. As cardanol and anacardic acid are polar, they can be used for modification of particle surface properties ;

5. The carboxylic group (anacardic acid) allows for posterior functionalization of the particles by means of the incorporation of proteins on the surface;

6. Functionalization through the carboxylic group constitutes the easiest and most efficient polymer functionalization method.

# Chapter 2

# Theoretical Foundation

## 2.1 Introduction

In this chapter, a brief theoretical introduction about polymers is presented. Polymers are macromolecules formed through reactions among smaller building blocks (monomers). However, there are several ways to build polymer molecules. First, the polymerization mechanism can follow chain or step-growth polymerizations. Second, different monomers can be used, enabling the formation of copolymers, terpolymers and so on. Also, a single monomer can form multiple bonds and create a network. Besides, a catalyst or a chain transfer agent can be added to control the polymerization and the properties of the final product. Additionally, the polymerization can be performed with different techniques such as bulk, solution, suspension or emulsion polymerizations. Every single aspect of the reaction changes the final characteristics of the produced polymer. Therefore, it is important to understand each process. Figure 2.1 shows different ways to classify a polymer.

## 2.2 Polymerization Types

Polymerization is the process though with molecules known as monomers react and form covalent bonds, building high-molecular-weight macromolecules (or polymers). Polymers can be made by two fundamental processes: chain-growth polymerization and step-growth polymerization. If the reaction is started by a special reactive site (a cation, an anion, a metal complex or a radical), then a chain-growth polymerization takes place. However, if complementary chemical functions are present, enabling the occurrence of chemical reactions between them, then a step-growth polymeriza-

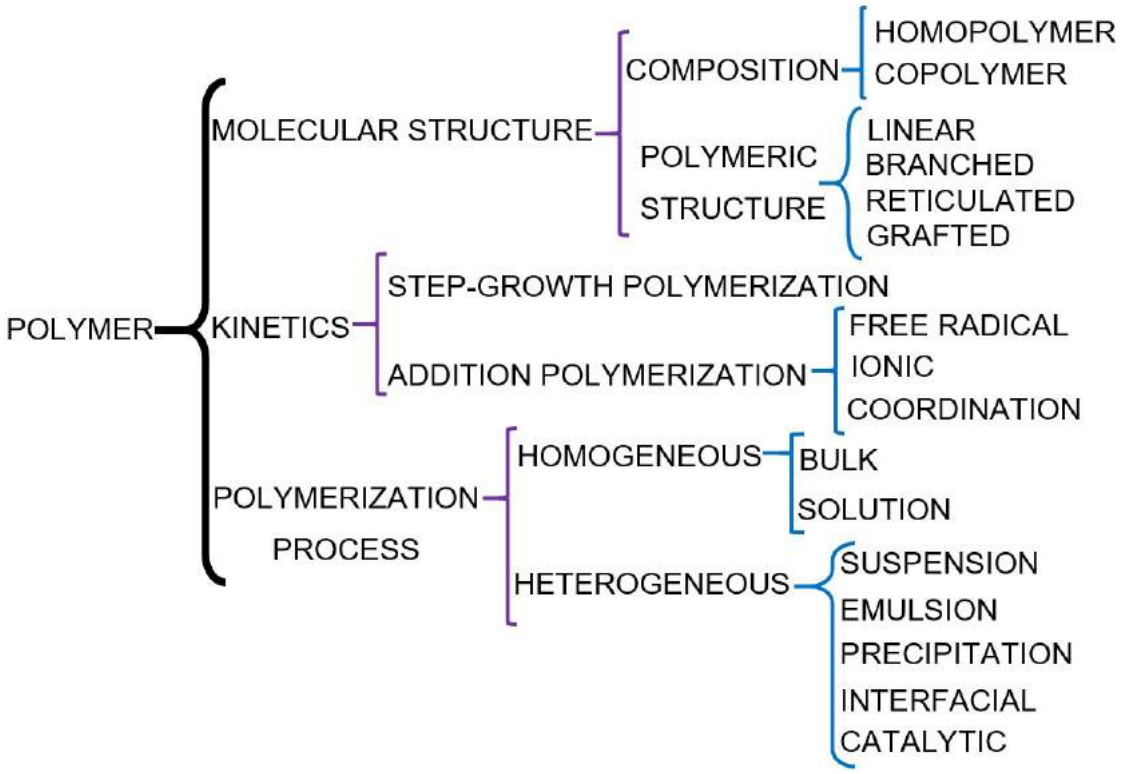


Figure 2.1: Some ways to classify a polymer material

tion takes place (ODIAN, 2004).

**Chain-Growth Polymerization**

Chain-growth polymerization (also called vinyl, olefin or addition polymerization) starts when a special reactive site (a cation, an anion, a metal complex or a radical) is formed. It represents 40% of the worldwide resin production (RODRIGUEZ *et al.*, 2015). Basically, three reaction stages take place, and high molecular mass polymers are formed during the first instants of the polymerization. These fundamental stages are:

- **Initiation:** this stage regards the creation of an active center - a free radical, a metal complex, a carbanion or a carbocation ion. The active specie reacts then with a monomer molecule through the double bond, generating another active species and initiating the polymerization. In the case of radical polymerization, radicals can be formed by thermal dissociation of peroxides (such as benzoyl peroxide, BPO) or azocompounds (such as azobisisobutyronitrile, AIBN) (BILLMEYER, 1984). Figure 2.2 summarizes the chemical reactions that take place during initiation. Monomers that polymerize through free radical polymerization contain at least one unsaturation. Taking the initiation of styrene with BPO as an example, the reaction happens as can be seen in Figure 2.3 (ODIAN, 2004).

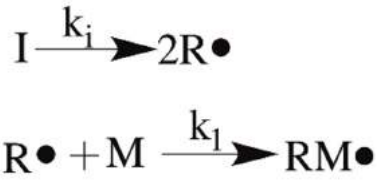


Figure 2.2: Schematic representation of initiation in the free radical polymerizations (ODIAN, 2004).

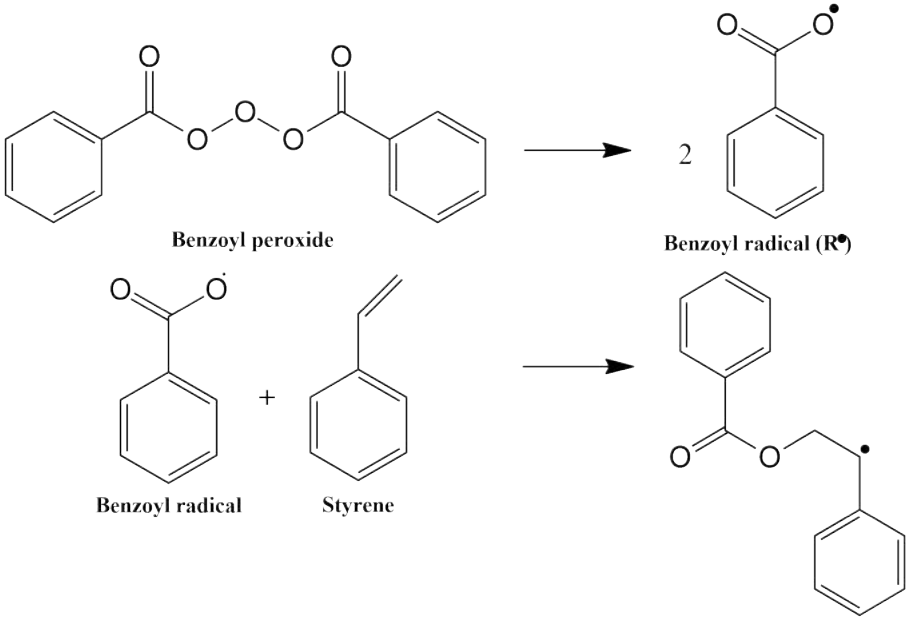


Figure 2.3: Schematic representation of the homolytic scission of BPO, followed by the initiation of the styrene polymerization (ODIAN, 2004).

In addition, the spontaneous thermal initiation of species, like the thermal initiation of styrene, can also take place as shown in Figure 2.4. Other ways to stimulate the creation of radicals include the use of light (ultraviolet, UV, or light emitting diode, LED), which allows for improved control of the polymerization rates (RODRIGUEZ *et al.*, 2015).

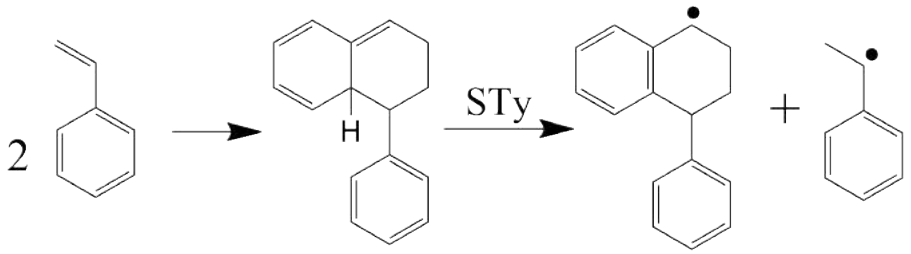


Figure 2.4: Schematic representation of the spontaneous thermal initiation of styrene (ODIAN, 2004).

- **Propagation:** this stage regards the repetitive addition of monomer molecules to the reactive site (or active center) at the growing chain end. A common hy-

pothesis is that the propagation rate constant ($k_p$) is the same for every living chain and does not depend on the chain length (long-chain hypothesis) (ODIAN (2004)). This is based on the idea that the reactivity of a growing polymer chain depends only on the last unit added. Again, taking the polymerization of styrene as an example, propagation takes place as shown in Figures 2.5 and 2.6.

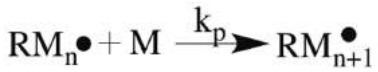


Figure 2.5: Schematic representation of propagation

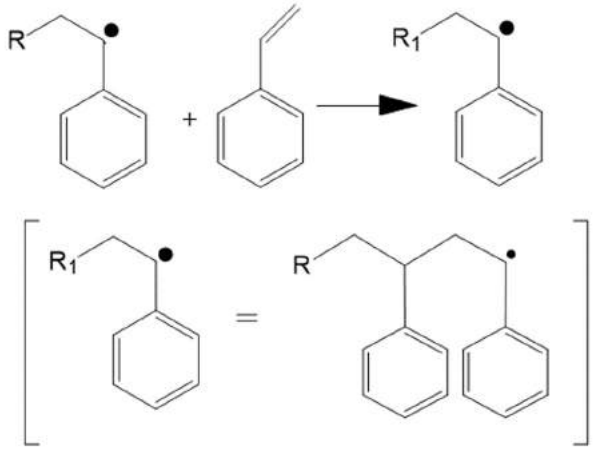


Figure 2.6: Schematic representation of propagation in styrene polymerizations (ODIAN, 2004).

- **Termination:** this stage regards the disappearance of living chain (active center) when they one react with each other. As the resulting chains lose the radicals activity, they cannot grow any longer and are called dead chains. In general, two types of termination can occur in free radical polymerization. If termination happens through combination (coupling), two living molecules form a single dead chain. However, if termination happens through disproportionation, two living molecules give birth to two distinct dead chains. Figure 2.7 illustrates the termination reaction. Disproportionation happens because one polymer chain transfers a hydrogen atom to another living chain, forming one saturated and one unsaturated dead chain. The final molecular weight of a dead polymer chain formed through combination is higher than the one obtained through disproportionation (RODRIGUEZ *et al.*, 2015). Termination reactions by disproportionation and coupling is shown in Figure 2.8 for the styrene polymerization.

**Step-Growth Polymerization**

If two monomers have complementary chemical functions and functionality equal or greater than two, the step-growth polymerization can take place. However, some-


Figure 2.7: Schematic representation of termination in free radical polymerizations (combination or disproportionation)

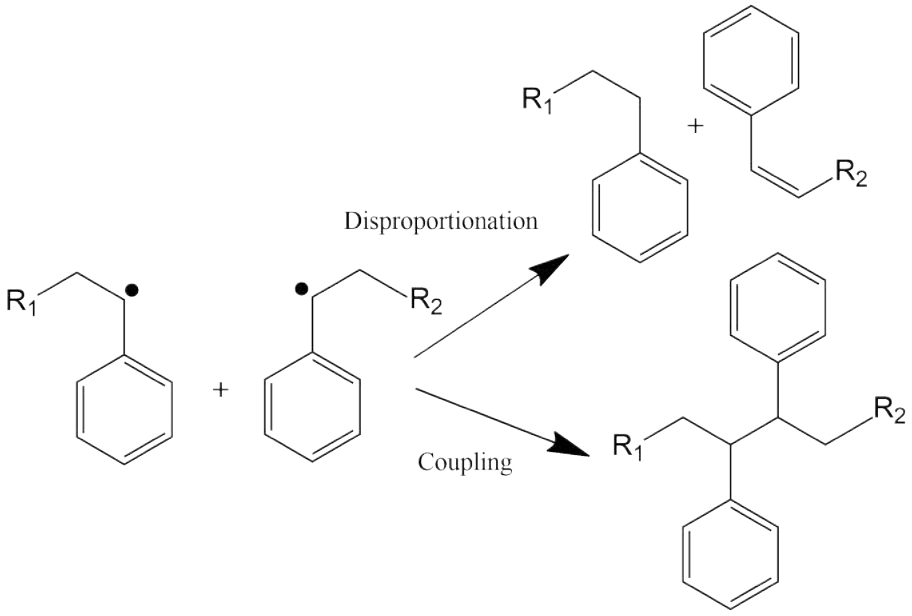


Figure 2.8: Schematic representation of termination in styrene polymerizations

times, a single monomer contains more than two reactive functional groups so that the presence of a second monomer may not be necessary. Figure 2.9 illustrates the synthesis of Nylon 66 by step-growth polymerization, where the carboxylic acid group reacts with the amine group, forming a polyamide.

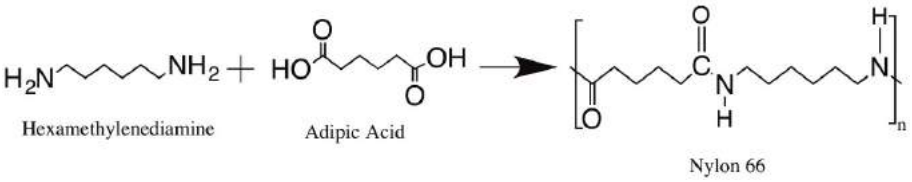


Figure 2.9: Schematic representation of the synthesis of Nylon 66 through step-growth polymerization.

The use of an initiator is not required in step-growth polymerizations, as the monomer molecules present reactive chemical functions. However, a catalyst can be used to accelerate the polymerization. The biggest difference between step-growth polymerization and chain-growth polymerization is the fact that polymer chains with large molecular weights are formed during step-growth reaction only when conversions are high. Moreover, throughout the step-growth process, small molecules are usually eliminated. For example, during esterification, which is a reaction between alcohol and acid groups, water molecules are formed. Therefore, conversion can be

controlled through the rate of removal of condensate molecules to force the shifting of the equilibrium towards the production of polymer products (BILLMEYER, 1984).

**Initiator and Half-Life Time**

Initiators are used to initiate the polymerization, as show in Figure 2.2. Benzoyl peroxide (BPO) and azobisisobutyronitrile (AIBN) are the commonest initiators used. Their chemical structures are shown in Figure 2.10. The peroxide and azo bonds cleave in the presence of an external stimulus (temperature or light), generating two radicals. The decomposition constitutes a first-order process (RODRIGUEZ *et al.*, 2015). Equations 2.1 and 2.2 show the initiator mass balance and respective solution.

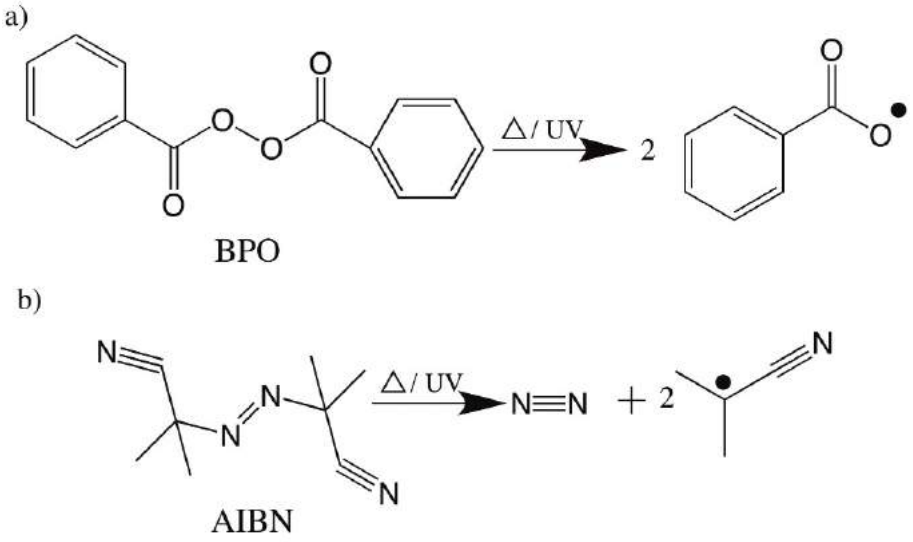


Figure 2.10: Schematic representation of decomposition of BPO (a) and AIBN (b).

$$-\frac{d[I]}{dt} = k_i[I] \tag{2.1}$$

$$ln\frac{[I]}{[I_0]} = -k_i t \tag{2.2}$$

When half of the initial initiator concentration is attained, the resulting reaction time is known as the initiator half-life time. In this case:

$$t_{1/2} = 0.693/k_i \tag{2.3}$$

$k_i$ can be correlated with temperature through the Arrhenius expression, as one can see in Equation 2.4, where $E_i$ is the activation energy for the decomposition process, $A$

is the collision frequency factor, $R$ is the universal gas constant and $T$ is the absolute temperature ($K$).

$$k_i = Aexp\left(\frac{-E_i}{RT}\right) \tag{2.4}$$

However, not every initiator molecule generates radicals that successfully react with the monomer, as only a certain fraction $f$ of the initiator starts the polymerization. Equation 2.5 shows how $f$ is defined. In general, f values are in the range of $0.8 \pm 0.2$ (RODRIGUEZ *et al.*, 2015); however, $f$ decays when the viscosity increases and the monomer concentration decreases (ODIAN, 2004).

$$f = \frac{initiation\,rate}{n * initiatior\,decomposition\,rate} \tag{2.5}$$

Where $n$ is the number of radicals generated by the initiator molecule.

**Chain Transfer**

Sometimes, the obtained molecular weights are smaller due to the occurrence of chain transfer reactions. In this case, some species present in the polymerization medium can act as chain transfer agents (CTAs): solvent, initiator, monomer, impurities or even the polymer. CTAs can capture, in an irreversible manner, the radical function through suppression of some weakly bound atom (normally, a hydrogen atom), resulting in a dead polymer chain and a new living radical (RODRIGUEZ *et al.*, 2015). Transfer to monomer with subsequent polymerization of the pendant double bond of the dead chain can lead to formation of branched molecules, broadening the molecular weight distribution (BILLMEYER, 1984).

**Inhibition and Retardation**

A retarder is a substance that can react with a radical to form products that are incapable of adding monomer, leading to reduction of the rates of polymerization and production of short chains. The induction period is the time needed to normalize the reaction rate (without retarders). If the retarder is very effective, it is called as an inhibitor. Therefore, inhibitors are species that react with radicals and form stable species, so that the polymerization rate ceases. Hydroquinone and diphenylamine are frequently used to prevent undesired polymerization reactions or to stop the reactions. Oxygen can also act as an inhibitor, so that the total removal of oxygen can be a key factor in some polymerizations systems (BILLMEYER, 1984).

**Gel and Glass Effects**

At high polymer concentrations, the overall reaction rate increases with time as monomer and initiator are consumed. This behavior is known as the gel effect (or autoaccelaration or Trommsdorff effect) (ODIAN, 2004). Gel effect happens because, as the conversion increases, viscosity also increases, causing the decrease of the rate at which polymer molecules diffuse through the medium, leading to reduction of termination and increase of propagation rates (BILLMEYER, 1984). The propagation rate is also affected by diffusion constraints, which is known as the glass effect (ODIAN, 2004). During the glass effect period, rates of monomer consumption decrease dramatically.

**Homo- and copolymerization**

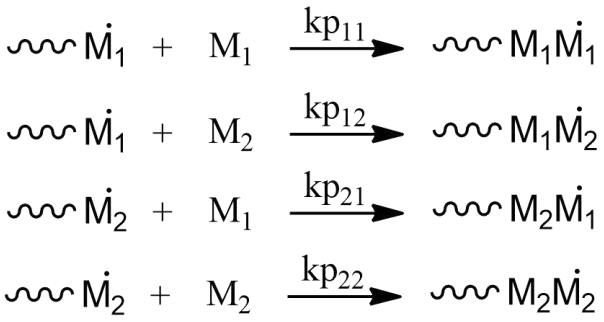


Figure 2.11: Schematic representation of the terminal model for copolymerization.

When more than one monomer is present in the reaction medium, polymers with different types of *mere* in the backbone are formed. Depending on the technique used and the reactivity of the monomers, different types of copolymers can be formed. A possible way to represent a polymerization is the terminal model, which considers that the reactivity of the polymer radical depends only on the nature of the last monomer added to the chain. This model is very popular for representation of copolymerizations, as illustrated in Figure 2.11. However, sometimes the penultimate model must be used (Figure 2.12). The penultimate model considers that the reactivity of the chain depends on the last pair of meres added to the chain. Instead of four propagation reactions, eight propagation reactions must be defined in this case; therefore, eight kinetic parameters must be known, which is not easy to determine experimentally (BILLMEYER, 1984). The use of the penultimate model becomes necessary when strong electronic and/or electrochemical effects can be assigned to the different chain configurations.

After writing the mass balance equations for the monomers and assuming the quasi-steady state for living chains, the copolymer equation (Equations 2.6, 2.7 and 2.8), also known as the Mayo-Lewis equation (MAYO and LEWIS, 1944) can be used to

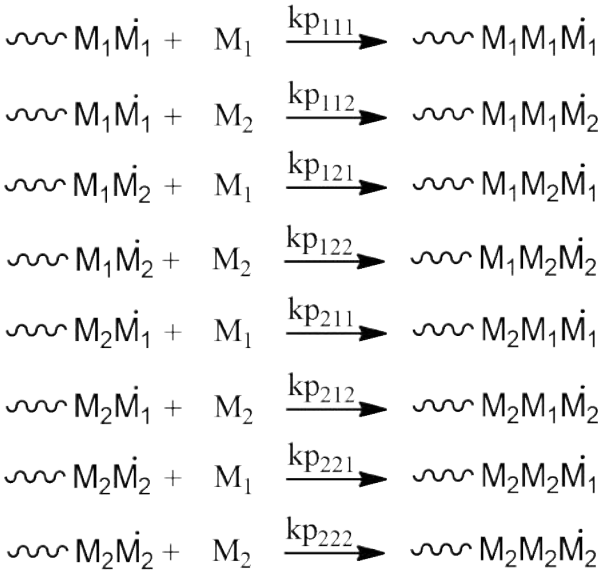


Figure 2.12: Schematic representation of the penultimate model for copolymerization

determine the composition of the copolymer. This equation shows that the copolymer composition does not depend either on the initiation and termination rates or the presence of inhibitors, CTAs or solvents. Therefore, in principle the same reactivity ratios obtained in bulk polymerizations can be used in heterogeneous reaction systems (BILLMEYER, 1984).

$$\frac{d[M_1]}{d[M_2]} = \frac{[M_1]}{[M_2]} \frac{r_1[M_1] + [M_2]}{[M_1] + r_2[M_2]} \tag{2.6}$$

$$r_1 = \frac{k_{p11}}{k_{p12}} \tag{2.7}$$

$$r_2 = \frac{k_{p22}}{k_{p21}} \tag{2.8}$$

The reactivity of monomers and radicals in copolymerizations is determined mainly by the nature of the substituents on the double bond of the monomer ODIAN (2004):

- The substituents may activate the double bond, making the monomer more reactive;
- The substituents may stabilize the resulting radical by resonance, making the radical less reactive;

- The substituents may provide steric hindrance at the reaction site, making the radical less reactive.

Besides the Mayo-Lewis equation, other methods can be used to calculate the copolymer composition using other models, such as the ones proposed by KELEN and TÜDŐS (1974), TIDWELL and MORTIMER (1965) and FINEMAN and ROSS (1950). These methods can provide distinct reactivity ratio values as shown by TIDWELL and MORTIMER (1970). Also, the experimental design and the technique used to analyze the data can affect the determined reactivity ratios (ZALDÍVAR *et al.*, 1998).

## 2.3 Polymerization Processes

Depending on the final desired application of the polymer, several polymerization methods can be used. If the polymerization occurs in a single phase, it is called homogeneous, as in bulk and solution polymerizations. If more than one phase is present, the polymerization is heterogeneous as in suspension and emulsion polymerizations. In this work, only bulk and suspension polymerizations were performed.

### 2.3.1 Bulk Polymerization

The main advantage of bulk polymerizations is the use of monomer and initiator only. Therefore, the final polymer has high purity. However, as the polymerization is exothermic and viscosity increases fast with the polymer concentration, the control of this system is very difficult. Heat removal is limited by the high viscosity and the low thermal conductivity. Also, the removal of unreacted monomer from the final product is difficult because of low diffusion rates and low surface-to-volume ratio of the reacting mass, compromising the purification of the final product (RODRIGUEZ *et al.*, 2015). As a consequence bulk polymerization are not performed frequently in industrial environments.

### 2.3.2 Solution Polymerization

The use of a solvent can be very beneficial for the polymerization process because it can allow for improved control of temperature and viscosity of the reacting system. The kinetics of the solution polymerization is similar to the kinetics of bulk polymerization, although the importance of the gel and glass effects is minimized. However, depending on the solvent that is used, undesired chemical reaction can take place between the living species and the solvent. Besides, purification and recirculation of the solvent increases the costs of the polymer production and reduces the productivity of

the process (CANEVAROLO JR., 2006).For these reasons, solution polymerization are rarely used in industrial environments.

### 2.3.3 Suspension Polymerization

If the monomer is insoluble in a dispersing continuous phase, bulk polymerization can occur inside droplets suspended in a suspension medium, such as water, which also acts as a heat transfer medium. Moreover, even though the viscosity inside the beads rises, increasing the reaction rate due to the gel effect, the viscosity of the continuous phase does not change much, improving the heat transfer. To avoid droplet coalescence, a suspension agent is commonly added to the system, frequently poly(vinyl alcohol) (PVA). Polymer particles produced through suspension polymerizations normally present average diameter of 10 to 1000 $\mu m$. Particle diameters can be changed through manipulation of the concentration of suspending agent and the stirring rate (PINTO *et al.*, 2013).

A typical suspension polymerization produce is described in the sequence. The reactor is initially filled with water contaning PVA (0.25% w/w in relation to $H_2O$). The solution is heated up to the reaction temperature under continuous stirring. Then the mixture of monomer and initiator is added to the reactor. After the specified reaction time, when the conversion is close to 100 %, heating and stirring can be turned off. Finally, the suspension can be filtrated to obtain pearl-like beads of polymer (RODRIGUEZ *et al.*, 2015).

### 2.3.4 Emulsion Polymerization

As in suspension polymerization, the monomer is initially dispersed in a continuous phase, frequently water . However, emulsion polymerizations also make use of an emulsifier (surfactant) which form micelles - with hydrophobic tails oriented inwards and hydrophilic head oriented outwards. Micelles appear when the concentration is higher than the critical micelle concentration (CMC). However, as the initiator is hydrophilic in this case and because the micelles are smaller than droplets, the surface area of micelle is high and enables the capture of free radicals generated in the aqueous phase. Therefore, in emulsion polymerization, the system comprises monomer-swollen polymer particles and monomer droplets that act as reservoirs of monomer for the reacting polymer particles. Polymer particles with characteristic diameters between 50 mm and 5 $\mu m$ can be obtained by this method (RODRIGUEZ *et al.*, 2015).

## 2.4 Molecular Weight Distribution (MWD)

Even when only homopolymerization reactions are considered, infinite reactions take place simultaneously. Although it is not possible to certainly know if a living chain is going to propagate or terminate, a certain probability can be associated with each effect. Therefore, some of the living chains propagate, while others terminate "prematurely". Thus, each reaction produces a mixture of polymer chains with the same composition, but different degrees of polymerization. Chain length distribution is a property that relates the chain size $i$ with the frequency of chains with size $i$, $P_i$. In terms of mass, the distribution becomes:

$$W_i = P_i i MM \tag{2.9}$$

where MM is the molar mass of the repeating unit.

Experimentally, the chain size distribution is determined through high performance liquid chromatography (HPLC) or size-exclusion chromatography (SEC). The chain frequencies are frequently normalized, enabling comparison between different distributions. Therefore, it is possible to define a probability density function (PDF) that treats the size of polymer chains as a random variable with a certain assigned probability (LEMOS, 2014).

$$P_i^{norm} = \frac{P_i}{\sum_{i=1}^{\infty} P_i} \tag{2.10}$$

$$W_i^{norm} = \frac{W_i}{\sum_{i=1}^{\infty} W_i} \tag{2.11}$$

The chain size distribution (known as the Most Probable Distribution, or the Schulz-Flory Distribution) is frequently found in many polymer reaction systems (Equation 2.12). The variable $q$ is the propagation probability and $P_{tot}$ is the total amount of polymer chains that follow the distribution (ODIAN, 2004).

$$P_i = P_{tot} q^{i-1}(1-q) \tag{2.12}$$

In order to simplify the representation of the distribution, it is common to use the moments of the distribution for comparative purposes, although the moments may be ambiguous, as different distrubitions can present similar moments. The number

average length $\overline{i_n}$ and the weight average length $\overline{i_w}$ are:

$$\overline{i_n} = \frac{\sum_{i=1}^{\infty} i N_i}{\sum_{i=1}^{\infty} N_i} \tag{2.13}$$

$$\overline{i_w} = \frac{\sum_{i=1}^{\infty} i W_i}{\sum_{i=1}^{\infty} W_i} \tag{2.14}$$

Therefore, the number average molar mass $\overline{M_n}$ and weight average molar mass $\overline{M_w}$ can be calculated as:

$$\overline{M_n} = \frac{\sum_{i=1}^{\infty} M_i N_i}{\sum_{i=1}^{\infty} N_i} = \overline{i_n} MM \tag{2.15}$$

$$\overline{M_w} = \frac{\sum_{i=1}^{\infty} M_i W_i}{\sum_{i=1}^{\infty} W_i} = \overline{i_w} MM \tag{2.16}$$

Finally, the polydispersity index (PI) is a measure of the variance of the chain size distribution, defined by Equation 2.17, where $\sigma^2$ is the variance of the distribution (ODIAN, 2004).

$$PDI = \frac{\overline{M_w}}{\overline{M_n}} = \frac{\overline{i_w}}{\overline{i_n}} = 1 + \frac{\sigma^2}{\overline{i_n}^2} \tag{2.17}$$

## 2.5 Concluding Remarks

Polymerization is a very well studied field. And there are several ways to produce polymers, depending on the reaction mechanism and the polymerization process. The kinetics of the polymerization reaction is complex and thousands of reactions may take place simultaneously, forming mixtures of macromolecules. In short, if a molecule presents unsaturated bonds or two reactive chemical groups, it is subject to polymerization. Such molecule can act as a monomer if the reaction is activated somehow and favorable conditions are present (for example, if a source of radicals is present, if enough thermal energy is provided, if inhibitors are absent). It is important to understand all aspects of the polymer synthesis because slight changes of the reaction conditions can affect enormously the properties of the final product. In the present study, the polymer is produced through chain-growth polymerization in bulk or aqueous suspension. The renewable chemical, cardanol or CNSL, can act as a comonomer, but also as an inhibitor and a chain transfer agent, as discussed in the next chapters.

# Chapter 3

# Cashew Nut Shell Liquid

## 3.1 Introduction

The cashew tree is a plant native to the Brazilian northeast, which was taken in the 16*th* and 17*th* centuries to India, Africa and other tropical countries. It belongs to the family *Anacardiaceae* and the species *Anacardium occidentale* is the most explored variation. From the cashew tree, one obtains the pseudo fruit (popularly known as cashew apple) and the cashew nut (the almond), two products of high economic interest. For illustrative purposes, Figure 3.1 shows the combination of the cashew nut (true fruit) and the peduncle (pseudo fruit), which is consumed as a fruit in nature or used to produce juices (such as cajuína), sweets and others (SERRANO, 2016).

Figure 3.1: The cashew fruit

In order to obtain the cashew nut, it is necessary to remove the shell (pericarp) that surrounds it. In Brazil, this process is about 90% mechanized. An example of this process is shown in Figure 3.2. However, mainly in the rural areas of the Brazilian Northeast, the artisan process is still very used.

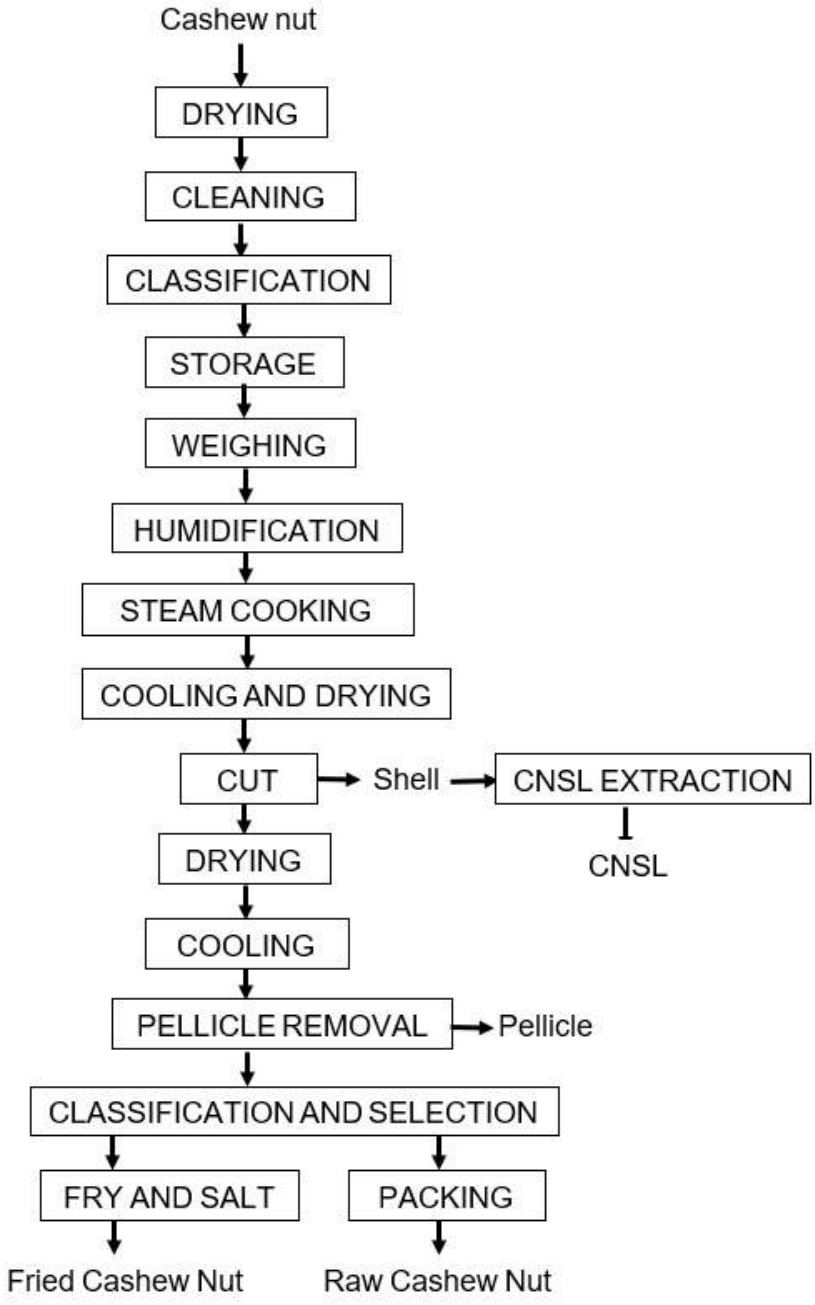


Figure 3.2: Schematic representation of the beneficiation process for Cashew Nut

Figure 3.3 illustrates the cashew nut, formed by the shell and the almond. The shell is constituted by the epicarp (outer layer), endocarp (inner layer) and the mesocarp (middle layer). It is in the mesocarp the cashew nut shell liquid (CNSL) is found, as an oil composed of several phenolic lipids, including anacardic acid and cardanol.

Figure 3.4 reveals the richness and diversity of products that can be obtained from

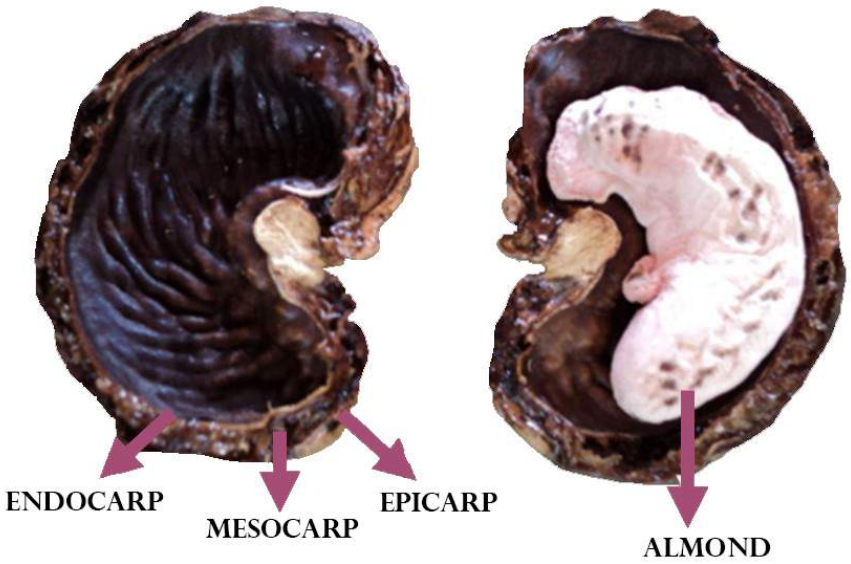


Figure 3.3: Cashew nut: the shell and the almond (adapted from SERRANO (2016)).

the cashew fruit (GONDINS (1973), PAIVA *et al.* (2000), SERRANO (2016)). Looking at the cashew nut ramification, followed by the shell, many different CNSL applications are described. However, while CNSL has the potential to be a valuable raw material, it is still regarded as a low value-added waste in the country. Therefore, research is this field is highly demanded, so innovative and sustainable products can be developed by the Brazilian industry and open room for new uses of CNSL.

Regarding the cashew production, since 1990 there were about 582 thousand hectares of plantations (IBGE 2018). Today, there are more than 607 thousand hectares of cashew plantations in Brazil. In relation to other fruits, the area planted with cashew trees only loses to the area planted with orange trees (IBGE, 2016). 75% of the cashew trees are located in the states of Ceará, Rio Grande do Norte and Piauí (IBGE, 2016).

According to the IBGE census of 2016, Ceará represents approximately 61% of the total amount of cashew nuts produced in Brazil, followed by the states of Rio Grande do Norte (19%), Piauí (13%), Bahia (3%), Maranhão (2%) and Pernambuco (1%). For 2018, 141.388 tons were produced in Brazil. However, due mainly to climatic conditions, production varies annually (Figure 3.5). In 2006 and 2008, the maximum production was obtained and corresponds to 243 thousand tons.

In relation to the world market, according to the latest data from Food and Agriculture Organization of the United Nations (FAOSTAT), Brazil is the 4th largest exporter of cashew nuts, behind Vietnam, India and the Gulf of Guinea (MUBOFU, 2016). The largest importers of the Brazilian cashew nuts are the United States, Canada, the Netherlands, Italy and Germany (SECEX/MDIC, 2019).

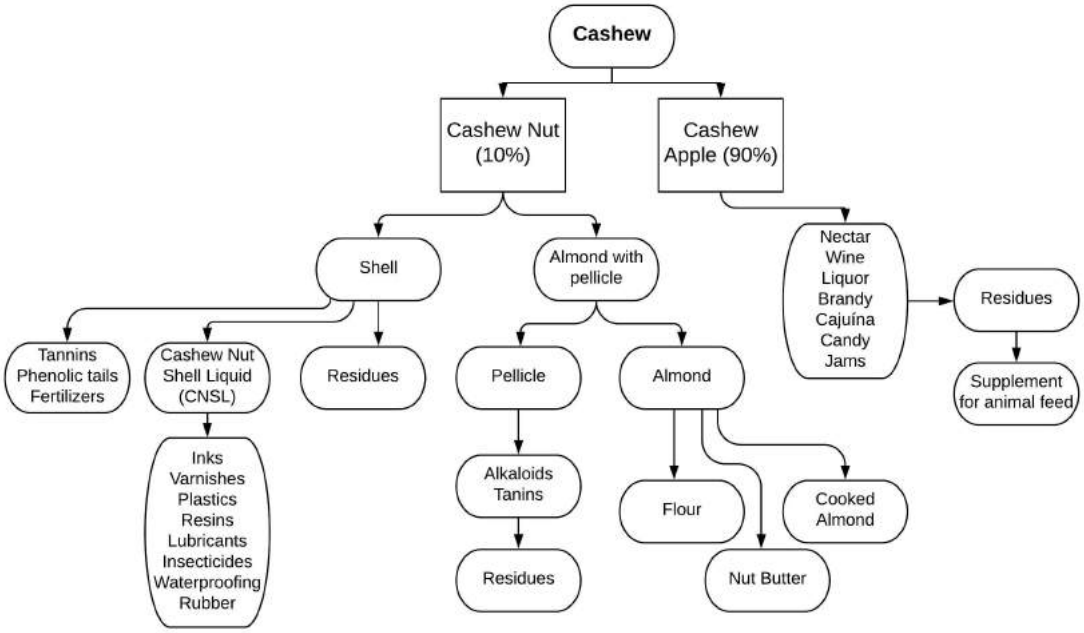


Figure 3.4: Products obtained from the cashew fruit (adapted from GONDINS (1973)).

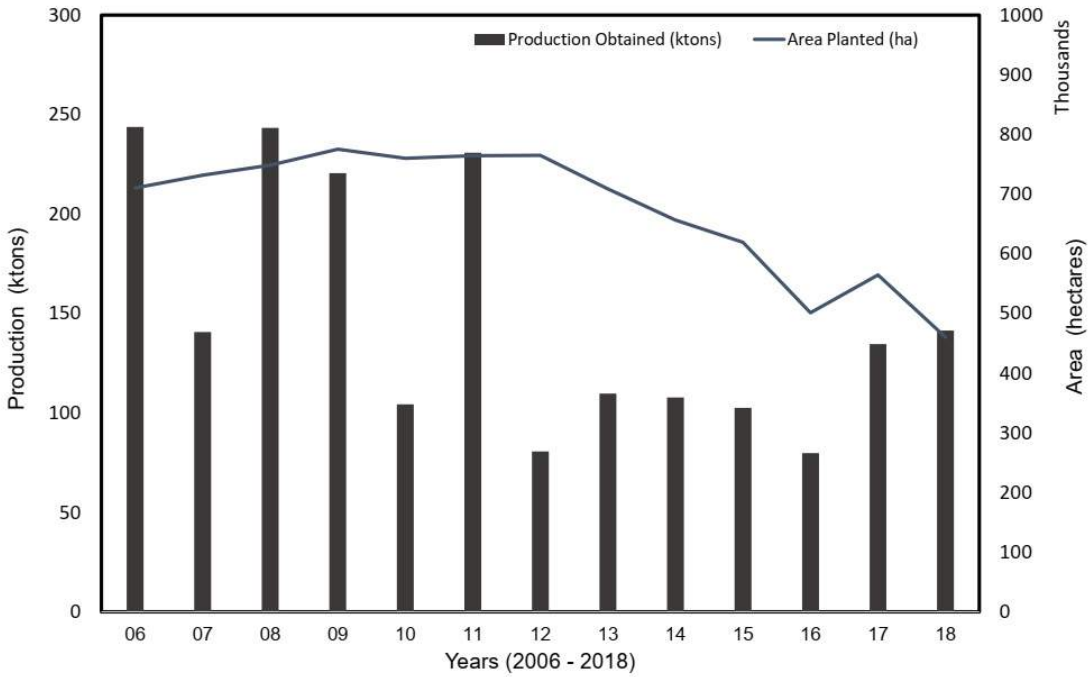


Figure 3.5: Production of cashew nuts between the years of 2006 and 2018 (CEPAGRO/IBGE, 2019)

## 3.2 Cashew Nut Shell Liquid (CNSL)

CNSL accounts for approximately 25% of the nut weight and is a by-product of cashew nut production (MAZZETTO *et al.*, 2009). Currently, CNSL has low added value

and is used commonly as an energy source (furnace fuel). However, the liquid is rich in non-isoprenoid phenolic lipids and is a good material for syntheses of organic products. Since 1970s, CNSL has been used as a raw material for manufacture of insecticides, germicides, antioxidants, thermal insulators, plasticizers, paints, vanishes and other materials (GEDAM and SAMPATHKUMARAN (1986), LUBI and THACHIL (2000), MUBOFU (2016)).

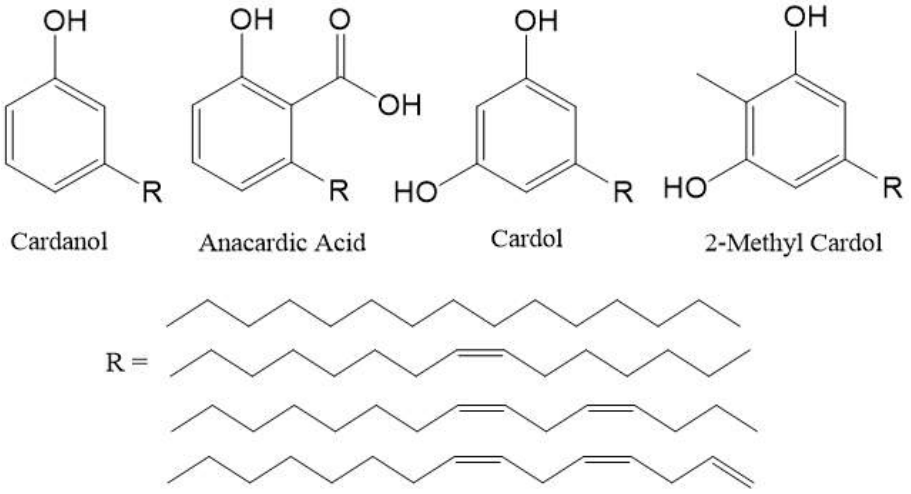


Figure 3.6: Typical components of the CNSL.

Figure 3.6 shows some of the phenolic lipids found in the CNSL. All of them have a side chain with fifteen carbon atoms located at the meta-position, in respect to the aromatic ring. The side chain may be saturated ($C_{15}H_{31}$) or mono- ($C_{15}H_{29}$), di- ($C_{15}H_{27}$) or tri- ($C_{15}H_{25}$) unsaturated, with double bonds placed at carbon 8, 11 and 14. Because of this side chain, polymers formed partially with these lipids are flexible, since the chain acts as a "plasticizer".

Cardanol (3-n-pentadecylphenol) has a hydroxyl group in the aromatic ring, as the other compounds have. However, anacardic acid (3-n-pentadecylsalicylic acid) has a carboxylic group in the ortho position; cardol (5-npentadecylresorcinol) has a second hydroxyl (diphenol) and 2-methyl-cardol (2-methyl-5-n-pentadecylresorcinol) has a methyl group located between two hydroxyl groups. These compounds are very interesting because of their multiple reactive sites, which can generate many derivatives and impart various functionalities to the target product. Figure 3.7 shows characteristics of cardanol and anacardic acid that can be related to their functional groups and final applications.

In order to extract the CNSL from the nut, the cold extraction method can be used, utilizing mechanical pressure or solvents. In this case, the CNSL is classified as natural. However, it can also be extracted with help of a thermal methods, such as hot oil bathing, roasting or solar cooking. In the former case, the hot CNSL can be used to heat the nuts and is the commonest method applied industrially (KUMAR *et al.*,

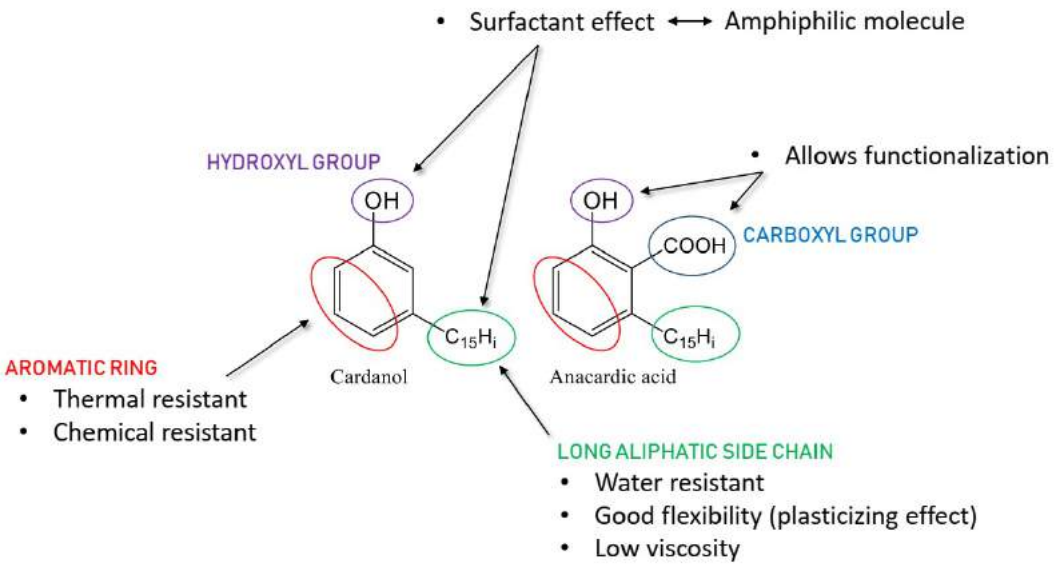


Figure 3.7: Practical properties than can be related to the functional groups of cardanol and anacardic acid.

2018). According to these methods, the cashew nuts are submitted to high temperatures (higher than 180 °*C*). As a consequence, the anacardic acid is decarboxylated and converted into cardanol, releasing carbon dioxide and providing the "technical CNSL" (Figure 3.8).

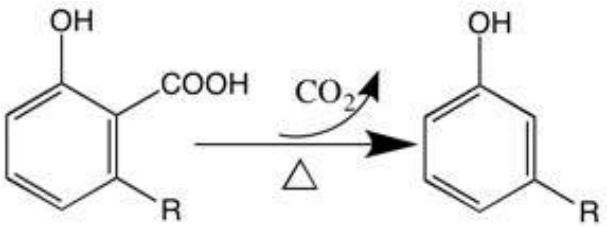


Figure 3.8: Schematic representation of the decarboxylation of anacardic acid.

In addition, during heating, at temperatures above 150 °*C* and in the presence of oxygen, polymeric substances can be produced. This means that thermal and oxidative polymerization occurs (MAHANWAR and KALE, 1996). Figure 3.9 shows a possible mechanism for the thermal polymerization of cardanol. Supercritical $CO_2$ extraction has also been reported, leading to the highests yield among the analyzed methods. However, the extract did not contain anacardic acid (PATEL *et al.*, 2006) and the process is not very common (KUMAR *et al.*, 2018).

Table 3.1 shows the typical compositions of natural and technical CNSL. In Brazil, the thermal-mechanic process is commonly used for production of CNSL, providing the technical CNSL that is rich in cardanol. The Table 3.1 also shows that anacardic

[1]The percentages describe the lower and upper limits using different analytical techniques. New, distilled and aged samples were analyzed. The dashed line represents absence of the material.

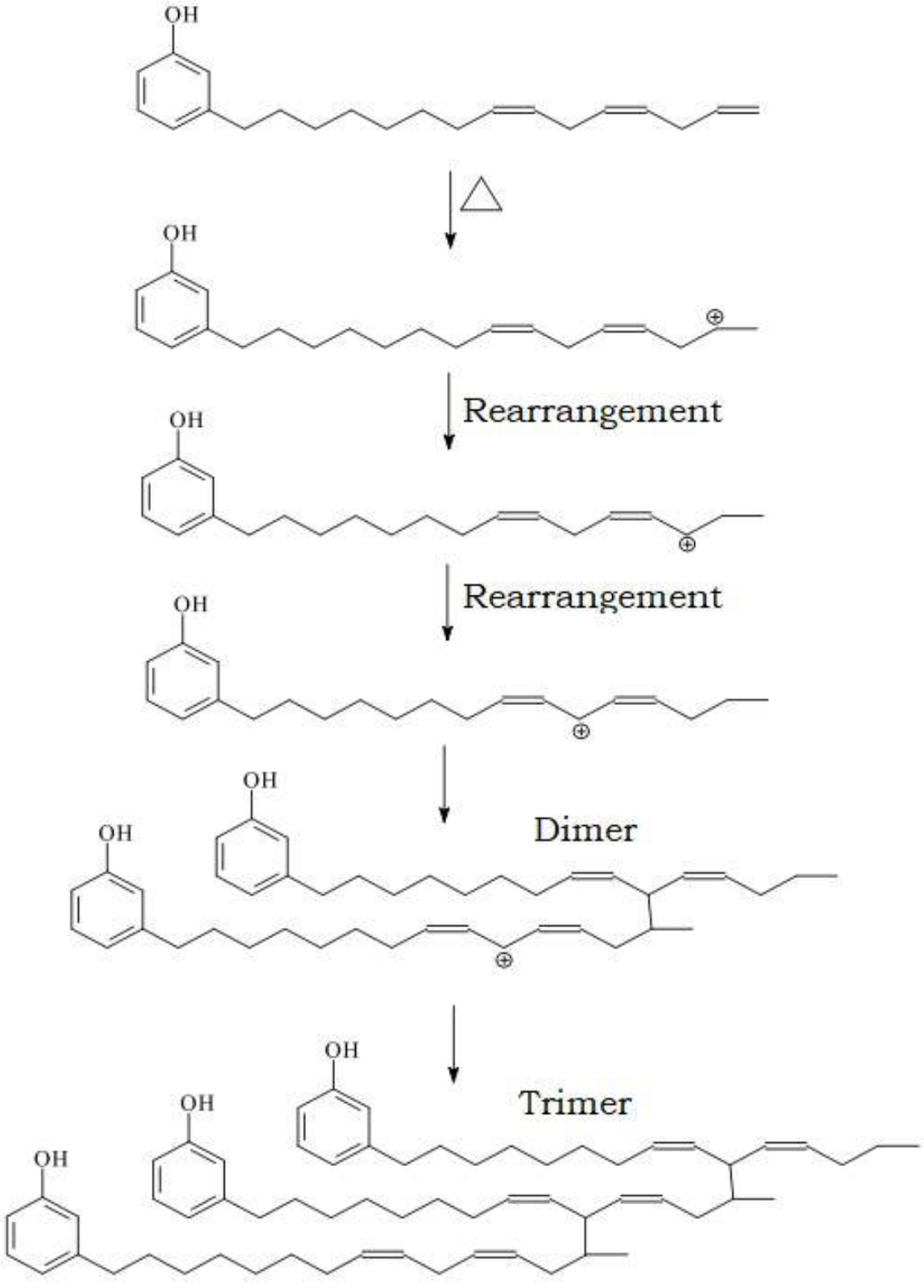


Figure 3.9: Schematic representation of the thermal polymerization of cardanol. Adapted from OLIVEIRA, L. D. M. DE (2007)

acid constitutes about 77% of natural CNSL. If solvent is used for cold extraction it is possible to obtain approximately 90% of anacardic acid and 10% of cardanol in CNSL

Table 3.1: Typical compositions of natural and technical CNSL (values are in wt%) (adapted from MAZZETTO *et al.* (2009)).

| Phenolic Compounds | Natural CNSL (%) | Technical CNSL (%) |
|---|---|---|
| Anacardic Acid | 71.70 – 82.00 | 1.09 – 1.75 |
| Cardanol | 1.60 – 9.20 | 67.82 – 94.60 |
| Cardol | 13.80 – 20.10 | 3.80 – 18.86 |
| 2-Methyl Cardol | 1.65 – 3.90 | 1.20 – 4.10 |
| Minority Components | 2.20 | 3.05 – 3.98 |
| Polymeric Material | - - - | 0.34 – 21.63 |

[1]

Table 3.2: Detailed compositions of natural CNSL as measured by coupled gas chromatography and mass spectroscopy (GC-MS) (values are in wt%) (adapted from MAZZETTO *et al.* (2009)).

| Constituent | Anacardic Acid (%) | Cardanol (%) | Cardol (%) | 2-Methyl cardol (%) |
|---|---|---|---|---|
| Saturated | 2.2 – 3.0 | 3.9 - 4.4 | 0.2 - 2.7 | 0.9 - 1.3 |
| Monoene (8') | 25.0 - 33.3 | 21.6 - 32.2 | 8.4 - 15.2 | 16.3 - 25.3 |
| Diene (8', 11') | 17.8 - 32.1 | 15.4 - 18.2 | 24.2 - 28.9 | 20.6 - 24.4 |
| Triene (8', 11', 14') | 36.3 - 50.4 | 45.2 - 59.0 | 36.5 - 67.2 | 49.8 - 62.2 |

(PATEL *et al.*, 2006).

Anacardic acid has called attention because of its antimicrobial, anticoagulant, antitumor, antifungal and molluscicide properties (CORREIA *et al.* (2006), MAZZETTO *et al.* (2009)). These properties are affected by the side chain. Cardanol and its derivatives have been used as plasticizers, surfactants, curing agents, doping agents, and for manufacture of phenolic and epoxy resins and in nano-composite films (LI *et al.*, 2018). The components of natural CNSL depending on the number of unsaturations is presented in Figure 3.10.

Table 3.2 presents the detailed composition of natural CNSL. Regarding the number of unsaturations present in the side chain, the triene is the side chain present more often in every phenolic compound. Values change inside an interval due to the regular variations of CNSL. The large quantities of trienes encourage the use of CNSL in polymerization reactions.

Monoene anacardic acid can be obtained by boiling the acid mixture in a solu-

Table 3.3: Physical properties of cardanol and anacardic acid.

| Property | Value | |
|---|---|---|
| | Cardanol | Anacardic Acid |
| Molecular Weight (Da) | 298.0 – 304.0 | 342.5- 348.5 |
| Density (g/$cm^3$) | 0.927 – 0.934 (30 °$C$) | 1.028 |
| Boiling Point (°$C$) | 228 – 235 | 496.4 |
| Viscosity (cP) | 95 (25 °$C$); 45 – 60 (30 °$C$) | 150 – 600 (25 °$C$) |

tion of isopropyl alcohol and ruthenium (III) chloride (catalyst) in acetone. Under these conditions, the diene and triene are hydrogenated to monoene (PERDRIAU *et al.*, 2012). The attained temperature reached does not promote the decarboxylation of the anacardic acid to cardanol (MUBOFU, 2016). Molecular weight, density, boiling point and viscosity of cardanol and anacardic acid are presented in Table 3.3 (RODRIGUES *et al.* (2011), MAZZETTO *et al.* (2009), BALGUDE and SABNIS (2014).

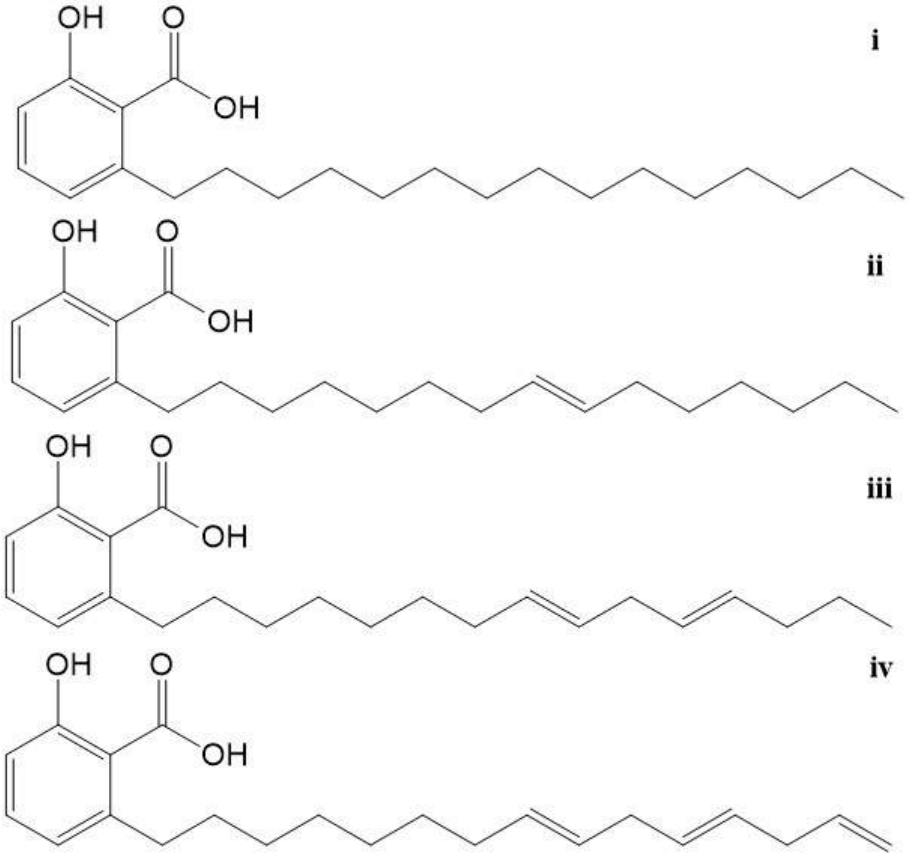


Figure 3.10: Anacardic acid: (i) 1-hydroxy-2-carboxy-3-pentadecyl benzene,
(ii) 1-hydroxy-2-carboxy-3-(8-penta-decenyl)benzene,
(iii) 1-hydroxy-2-carboxy-3-(8,11-pentadecadienyl)benzene, and
(iv) 1-hydroxy-2-carboxy-3-(8,11,14 pentadecatrienyl)benzene.

## 3.3 Synthesis of Polymers Using CNSL

Reports of polymer syntheses based on CNSL mainly describe condensation reactions in presence of electrophilic agents (such as formaldehyde), polymerizations of the side chains using acid catalysts and functionalizations of the hydroxyl group in order to obtain oligomers as functionalized prepolymers (BALGUDE and SABNIS, 2014). The polymers derived from the CNSL are known to present good flexibility, because of the long aliphatic chain, low wear, and high resistance to friction and impact. LUBI

and THACHIL (2000) reviewed most of the reactions (including polymerizations) and applications developed with CNSL until the late 1990s.

However, instead of using the mixture of compounds (CNSL), purified cardanol has been the most studied and used as substance obtained from CNSL for polymer syntheses. In the literature, one can find reports of oxidative (using acid catalysts), cationic, polycondensation and enzymatic polymerizations (IKEDA *et al.* (2000b), KIM *et al.* (2003)) used cardanol directly. Furthermore, cardanol derivatives, such as other monomers manufactured from cardanol, have also been used (BHUNIA *et al.*, 1999) as due to the hydroxyl moiety, many chemical transformations are possible with cardanol (Figure 3.11). A good review related to cardanol applications in the coating industry was prepared by BALGUDE and SABNIS (2014). LOCHAB *et al.* (2014) also prepared a great review regarding applications of natural phenolic compounds in the polymers field.

Regarding the oxidative polymerizations, the synthesis of polycardanol has been performed with the use of Fe-salen (iron-N,N-ethylenebis(salicylideneamine) complex as catalyst. IKEDA *et al.* (2000a) used Fe(II)-salen, which was posteriorly oxidized to Fe(III)-salen, the real catalyst of the polymerization. On a first study, the authors utilized pyridine to increase the yield, and tetrahydrofuran (THF) or 1,4-dioxane as solvents. After NMR and FTIR analyses, the obtained polymers were found to be a mixture of oxyphenylene and phenylene, classes of crosslinkable polyphones. Figure 3.12 shows the reaction done by the authors and Figure 3.13 illustrates the structure of Fe-salen complex.

In a second publication, IKEDA *et al.* (2000a) studied the same polymerization in bulk. They investigated the effects of concentration of catalyst, type of catalyst, concentration of hydrogen peroxide, time and additives (water or pyridine). It was found that the highest yield (80%) was obtained with the Fe-salen complex when the concentration of catalyst and hydrogen peroxide were high. However, the effect of time was not very significant in the range from half an hour to two hours. When compared to other metallic complexes, Fe-salen allowed for the highest polymer yields.

OTSUKA *et al.* (2017) reported the oxidative polymerization of cardanol in w/o emulsions, using larger amounts of cardanol is respect to water. To keep the system stable, polyamine and acetic acid were used. After 24 hours, depending on the analyzed conditions, 50% of conversion were achieved, average molecular weight of 6800 Da e polydispersity of 2.3 were achieved.

Besides the oxidative route, poly(cardanol) can be obtained through enzymatic polymerizations using peroxidases. The product is a mixture of oxyphenylene and phenylene units. Using soybean peroxidase, IKEDA *et al.* (2000b) obtained the highest yield (69%) with isopropanol as solvent (Mn = 6100 Da and PI = 1.8). Doubling the amounts of enzymes, KIM *et al.* (2003) studied the same polymerization reaction. They

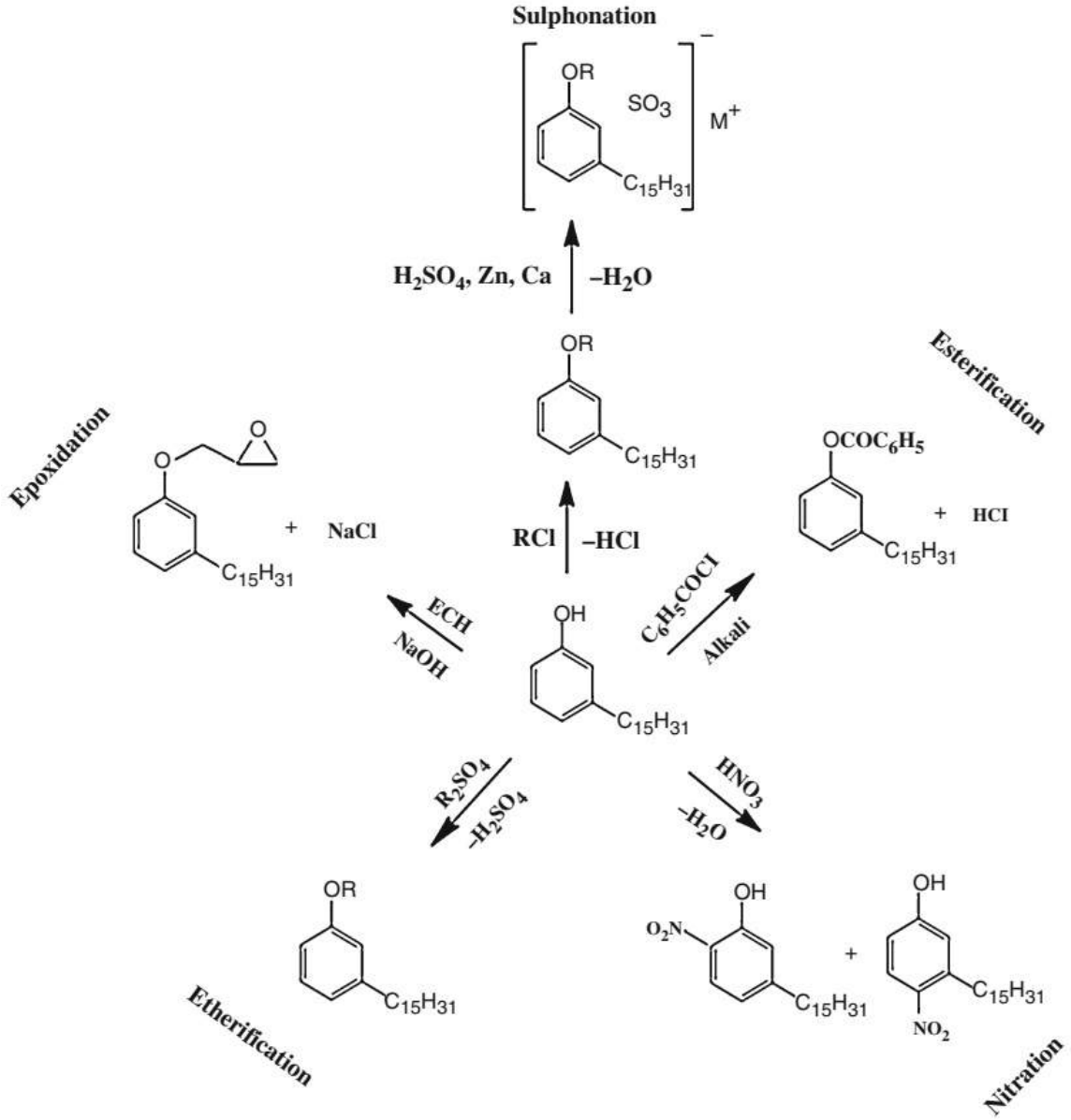


Figure 3.11: Possible chemical transformations of cardanol (BALGUDE and SABNIS, 2014)

obtained 62% of yield, $M_n$ of 3411 Da and $M_w$ of= 8221 Da (PDI of 2.41). The structure of the obtained polymer was similar to those obtained using the oxidative route.

Another possible route is polycondensation, which leads to oligomerization and production of functionalized pre-polymers. CNSL step-growth polymerization can be performed with electrophiles for reactions with hydroxyl group and an aldehyde (formaldehyde). In this case, a formaldehyde-cardanol resin can be obtained, forming a phenolic thermosetting resin. For example, MISRA and PANDEY (1984) (and also in a latter study: MISRA and PANDEY (1985)) studied this polymerization with help of a alkaline catalysis (NaOH). BISANDA and ANSELL (1992) found that the obtained material presented the strength for roofing applications.

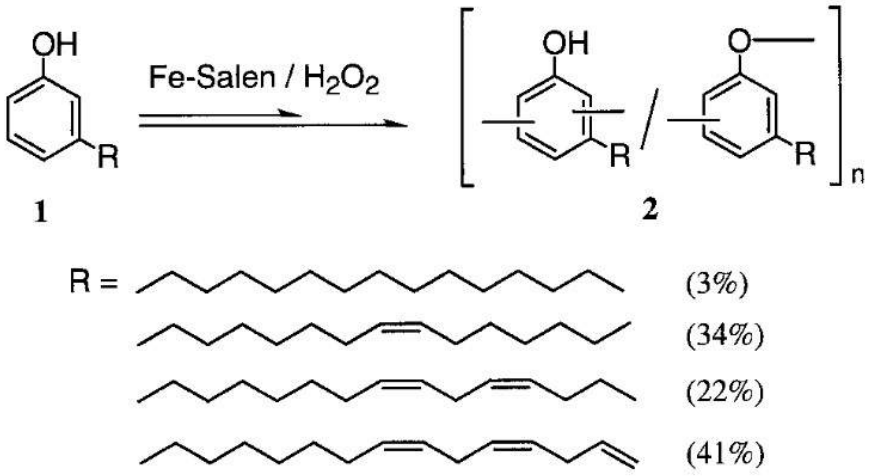


Figure 3.12: Schematic representation of oxidative polymerization of cardanol using Fe-salen as catalyst (IKEDA *et al.*, 2000a)

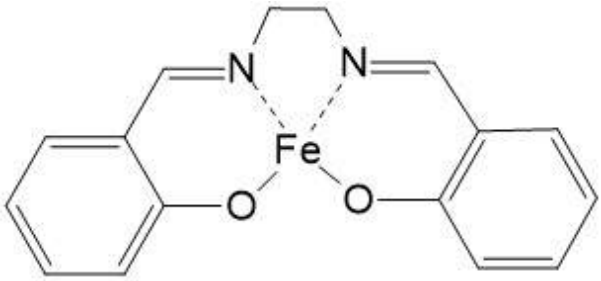


Figure 3.13: Structure of Fe-salen complex

In general, cardanol resins are more flexible and soluble in organic solvents than other phenol-formaldehyde resins. In addition, cardanol resins are hydrophobic and present better resistance to acids and bases. However, they present lower tensile strength and thermal stability than the traditional phenol-formaldehyde resins (LOCHAB *et al.*, 2014). This may be attributed to the side chain, which imparts steric hindrance and reduces the intermolecular interactions. Thus, an optimum replacement of phenol by cardanol can be required. For example, phenolic resins containing less than 15 wt% of cardanol present distinctly improved chemical resistance and mechanical properties, when compared to neat phenolic resins.

Cardanol polycondensations using acid catalysis have been reported using oxalic, succinic, citric and other acids (SATHIYALEKSHMI (1993), YADAV and SRIVASTAVA (2007a), LOUREIRO *et al.* (2017)). For example, SOUZA JR. *et al.* (2008a) prepared the resin in one step with $H_2SO_4$. The analyses of FTIR and XPS confirmed the polymerization. The presence of sulfur was also noticed in the polymer, which affects its acidity and was advantageous for preparation of mixtures with polyaniline (conductive polymer). In another work, SOUZA JR. *et al.* (2008b) used the cationic route to produce the same resin with $H_2SO_4$ catalysis.

Cationic polymerizations can also be used to synthesize poly(cardanol) with boron trifluoride etherate ($BF_3O(C_2H_5)_2$) as initiator (ANTONY *et al.* (1990), LOUREIRO *et al.* (2017)). Sulfuric or phosphoric acids can be used as catalysts (MANJULA *et al.*, 1992). The polymerization occurs on the side chain (Figure 3.14).

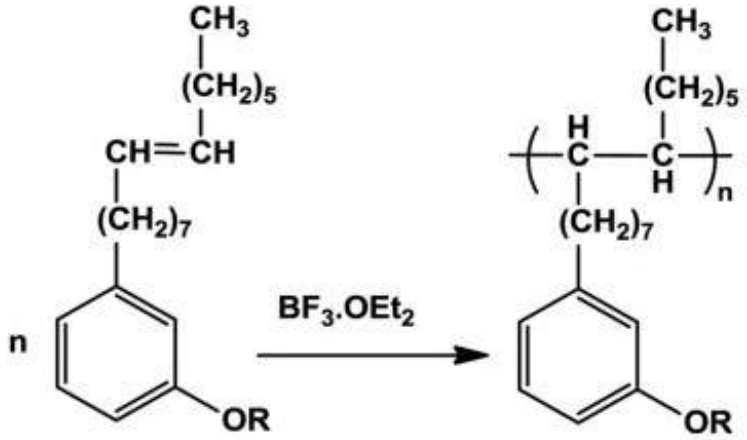


Figure 3.14: Schematic representation of the cationic polymerization of cardanol (adapted from ANTONY *et al.* (1990).)

BESTETI (2009) and GALVÃO (2016) studied the direct use of cardanol as comonomer using several polymerization methodologies: bulk, solution, suspension and emulsion polymerizations. However, due to the poor reactivity of the C15 unsaturations, obtained conversions were not very high, but the obtained products were shown to present attractive properties for some applications, mainly for enzyme immobilization, inspiring the present study.

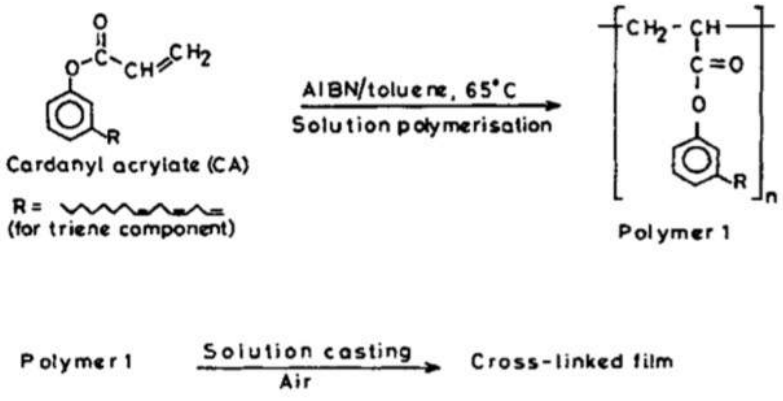


Figure 3.15: Schematic representation of the synthesis of poly(cardanyl acrylate) and respective films (MANJULA *et al.*, 1992).

As previously mentioned, cardanol can be used to prepare new monomers. Acrylates and methacrylates derived from cardanol have found more successful use as

monomers in radical polymerization than cardanol (LI *et al.*, 2018). For example example, cardanyl acrylate and cardanyl methacrylate polymerize through free radical polymerization to form lattice structures when exposed to air or ultraviolet light, resulting in thermoplastic and colorless polymers (MANJULA *et al.*, 1992). Figure 3.15 shows the chemical structure of cardanyl acrylate and its polymer.

Several companies have been using CNSL and cardanol to produce cardanol derivatives, polycarbonates, epoxy resins, detergents, foams, surfactants and other products. Table 3.4 presents some patents that use CNSL or cardanol as reagents. A prominent company is this field is Cardolite Inc. This American company is the world's largest cardanol producer. Besides cardanol (commercially available under the trade name Cardolite NC-700 or NX-2026), their most relevant products are cardanol derivatives, such as reactive diluents and flexible resins (NC-513, NC-514, NC-514 LV); epoxy novolac resins (NC-547), see Figure 3.16; phenalkamine curing agents, condensation product of cardanol, formaldehyde and polyamine (NC-540, NC-541, NC541LV, NC-556, NC-558, NC-559, NC-560, NX 2015) and polyols (NX-9001LV, GX-9005, GX- 9007, GX-9201, NX-4670).

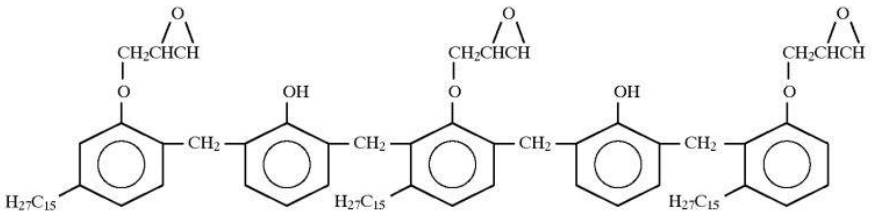


Figure 3.16: Schematic representation of an epoxy novolac resin structure sold by Cardolite.

Polyurethane resins have also been made with cardanol derivative polyols with a wide range of polyisocyanates (SURESH and KISHANPRASAD (2005); WO2006003668A1). There are several patents discussing this type of application (Table 3.5). A company that has been growing commercializing cardanol polyols and polyurethanes is Covestro, a Germany company and a spin-off of Bayer. The Dow Chemical Company (now DowDuPont, after merging with DuPont in 2017) is an American company that also works in this field.

Finally, very few studies can be found regarding the use of anacardic acid as a monomer. Even when the mixture of CNSL is used in polymerizations, normally it is the technical CNSL, which contains a small percentage of anacardic acid. CHELIKANI *et al.* (2009) polymerized anacardic acid through free radical oxidative coupling process, using soybean peroxidase for 24 hours (Figure 3.17). A redox mediator (phenothiazine-10-propionic acid, PPA) and hydrogen peroxide (as oxidant agent) were used in methanol or propanol in pH 7. Analyses of $^{1}$H-NMR and FTIR showed

Table 3.4: Patents using cardanol as a reactive molecule.

| Code | Priority Year | Status | Current Assignee | Name | Description | Application |
|---|---|---|---|---|---|---|
| WO2000034219A1 | 1998 | Grant in US | Cardolite Corp. | Derivative of cardanol and uses therefor | A method for the hydroxyalkylation of cardanol | Coatings, adhesives, sealants, rubber, plastic, elastomer, composites, and as a modifier in the ink composition |
| WO1998036015A1 | 1997 | Grant in US, EP, JP, CN, DE | Sabic | Redistribution of polyphenylene ethers and polyphenylene ethers with novel structure | Reaction with PPE, resulting in a solf-segment PPE which improves flow properties as well as compatibility with non-polar components. | Adhesives, sealants, thermosets, styrenic resins, polyolefines, polymer blends, providing better flow, tack, reactivity, oxidative stability and thermal properties |
| WO2003010218A1 | 2001 | Grant in US, EP, KR, CN, DE | General Electric Company | Method of polycarbonate preparation | Use of raw cardanol to prepare polycarbonates with more hydroxyl groups | Polycarbonates can be blended with additives such as heat/UV stabilizers, mold release agents, or with other polymeric materials and be molded (e.g. optical disks, optical lenses, automobile lamp components). |

| Code | Priority Year | Status | Current Assignee | Name | Description | Application |
|---|---|---|---|---|---|---|
| WO2008137706A1 | 2007 | Grant in CN and US | Cardolite Corp. | Cardanol based dimers and uses therefor | The cardanol dimers are formed by hydrosylylation with silanes. Cardanol based dimers may be further reacted to form epoxy curing agents and epoxies or friction particles or phenolic resins | Anti-fouling coatings on ship hulls and marine structures; friction particles or phenolic resins |
| WO2008131918A1 | 2007 | Application (2008) | Basf Se | Reactive surfactants and their use | Use of anionic cardanol or cardanol (poly)alkoxylate derivatives as polymerizable surfactants. The reactivity of the invented polymerizable surfactants can be further improved by conjugation of these double bonds. | Surfactants, stabilizers and/or dispersing agents in the preparation of polymer dispersions. And for coatings and binder compositions. Exemples: manufacture of paper or paperboard, paints, non-woven fabrics and building materials. Curable epoxy resin coating composition having a low viscosity which is useful in coating applications. |

| Code | Priority Year | Status | Current Assignee | Name | Description | Application |
|---|---|---|---|---|---|---|
| WO2014117351A1 | 2013 | Application (2014) | Dow Global Technologies Llc | An epoxy resin composition,and its applications | Production of a cardanol modified epoxy resin | Application in low volatile organic compounds (VOC) high solids coatings, and waterborne coating |
| WO2014179975A1 | 2013 | Application (2014) | Dow Global Technologies Llc | Epoxy resin compositions | Formation of a novel epoxy resin by reacting epoxy resins with cardanol | Coating films with balanced properties including good flexibility, good chemical resistance, short dry-hard time, desirable hardness, and good anti-corrosion performance; and the process of preparing the compositions. |
| WO2016086401A1 | 2014 | Application (2016) | Blue Cube Ip Llc or Dow Global Technologies Llc | Curable epoxy resin composition | Formation of "an advanced epoxy resin" by reacting an epoxy resin with a CNSL and a carboxylic acid | Curable epoxy resin coating composition having a low viscosity which is useful in coating applications. |

| Code | Priority Year | Status | Current Assignee | Name | Description | Application |
|---|---|---|---|---|---|---|
| WO2015054360A1 | 2013 | Grant in US | Cardolite Corp | CNSL-based hydrocarbon resins, preparation and uses thereof | Resins made from CNSL and vinyl hydrocarbons (e.g. alpha-methylstyrene) using a Lewis acid as an acid catalyst (e.g. para-toluenesulfonic acid). | Additives as non-reactive diluents for solvent-free coating formulations; tackifiers for structural adhesive, pressure sensitive and hot-melt adhesives; stabilizers for lubricants, fuel and polymer formulations; plasticizers for thermoplastic polymers and processing aid for rubber compounding and stabilizers for respective rubber artifacts. These resins are also valuable precursors for the manufacture of epoxy resins and polyols for coating, adhesive and composite formulations exhibiting ameliorated performance in water repellency, anti-corrosion, and fast hardness development during cure. |

Table 3.5: Patents using cardanol to produce polyurethanes.

| Code | Priority Year | Status | Current Assignee | Name | Description | Application |
|---|---|---|---|---|---|---|
| WO2006003668A1 | 2004 | Grant in EP and DE | Council Of Scientific And Industrial Research | Process for preparing polyurethane polyol and rigid foams therefrom from cardanol | Production of a) cardanol polyol and b) polyurethane | Thermal insulation |
| US20080139685A1 | 2006 | Grant in US and CN | Covestro LLC | Novel polyether polyols based on cashew nutshell liquid, a process for the production of these polyether polyols, flexible foams produced from these polyether polyols, and a process for the production of these foams | Production of a) polyether polyols by the alkoxylation of CNSL and b) production of flexible polyurethane foams | Industrial and consumer applications such as seats, dashboard and other cabin interior parts of automobiles |
| WO2011030197A2 | 2009 | Grant in US, EP, CN, DK, ES, FR | Coatex SAS | Cardanol-based associative polyurethanes, corresponding associative thickeners and uses thereof | Synthesis of a water-soluble polyurethane resulting from the condensation of an oxyalkylated cardanol, a polyalkylene glycol and polyisocyanate | Thickening agents for aqueous formulations. |
| WO2011030197A2 | 2009 | Grant in US, EP, CN, DK, ES and FR | Coatex SAS | Associative polyurethanes based on cardanol, corresponding associative thickeners and uses thereof | Synthesis of polyurethanes from polyalkylene glycol, polyisocyanates and optionally oxyethylated cardanol. | Thickening agents |

| Code | Priority Year | Status | Current Assignee | Name | Description | Application |
|---|---|---|---|---|---|---|
| WO2015077944A1 | 2013 | Grant in US, JP | Dow Global Technologies Llc | Cardanol modified epoxy polyol | Synthesis of a polyurethane resin by mixing cardanol, a cardanol-modified epoxy polyol, and an isocyanate component | Composites formed by filament winding and coatings |
| WO2014209704A1 | 2013 | Grant in US, EP, CN | Bayer or Covestro in US and EP | Polyurethane pultrusion formulations for the production of articles with improved coating adhesion and articles produced therefrom | Production of a polyurethane composite by a reaction of a polyisocyanate and a cashew oil-based polyether polyol | Use in pultrusion processes |
| WO2015077944A1 | 2013 | Grant in US and JP | Dow Global Technologies Llc | Cardanol modified epoxy polyol | Formation of a polyurethane resin system that includes an isocyanate-reactive component that has a first cardanol component and a cardanol-modified epoxy polyol | Composites formed by filament winding and coatings. |
| WO2015153399A1 | 2014 | Application (2015) | Dow Global Technologies Llc | Natural oil derived blocked prepolymers and acrylic plastisol compositions having the blocked prepolymers | Use of CNSL as a blocking agent to form a prepolymer. An isocyanate terminated prepolymer is also used. | Substitute for PVC-based plastisols |

| Code | Priority Year | Status | Current Assignee | Name | Description | Application |
|---|---|---|---|---|---|---|
| WO2017044402A1 | 2015 | Application (2017) | Dow Global Technologies Llc | Blocked polyurethane tougheners for epoxy adhesives | Use of cardanol as capping group for production of an epoxy adhesives as toughener | Tougheners for epoxy adhesives |
| WO2016167868A1 | 2015 | Application (2016) | 3M Innovative Properties Company | Fire spread prevention member and fire spread suppression method | Cardanol is present as a polyol to produce a polyurethane binder | Structures used in a fire prevention facility |
| WO2005082967A1 | 2004 | Grant in US, EP, CN, DE, ES | Covestro | Hydrophobic low-viscous polyols | The invention relates to new hydrophobic polyols of low viscosity, to a process for preparing them and to solvent-free binder mixtures based thereon | Primers of floor coatings. |
| US20080139685A1 | 2006 | Grant in US and CN | Covestro | Novel polyether polyols based on cashew nutshell liquid, a process for the production of these polyether polyols, flexible foams produced from these polyether polyols, and a process for the production of these foams | Production of polyether polyols which are prepared by alkoxylation of CNSL. And also the production of flexible polyurethane foams prepared from these polyols | Coatings, adhesives, sealants or molding compounds. |

| Code | Priority Year | Status | Current Assignee | Name | Description | Application |
|---|---|---|---|---|---|---|
| WO2016183073A1 | 2015 | Grant in US | Covestro | Filament winding processes using polyurethane resins and systems for making composites | The present invention is directed to, among other things, filament winding processes that use a low viscosity polyurethane-forming composition, systems for making a composite and the composites so made. | Pipe, pressure bottles and tanks, storage containers, among other things |

the polymer contained a mixture of oxyphenylene and phenylene units and that some decarboxylation took place during the polymerization. Therefore, the polymerization did not happen on any unsaturation of the pentadecyl side chain, being very selective. When methanol was used as solvent, the average molecular weight of the obtained polymer was equal to 5000 Da with 43% of yield. When propanol was used, the molecular weight was equal to 3900 Da with 61% of yield. Moreover, the polymers were crosslinked, and films were produced and submitted to biofouling tests for gram-negative or gram-positive bacteria, being more effective against gram-negative bacteria. In a similar study, YOON and KIM (2009) showed that both polymer films could reduce the number of adherent cells to its surface, but not presenting any antimicrobial activity.

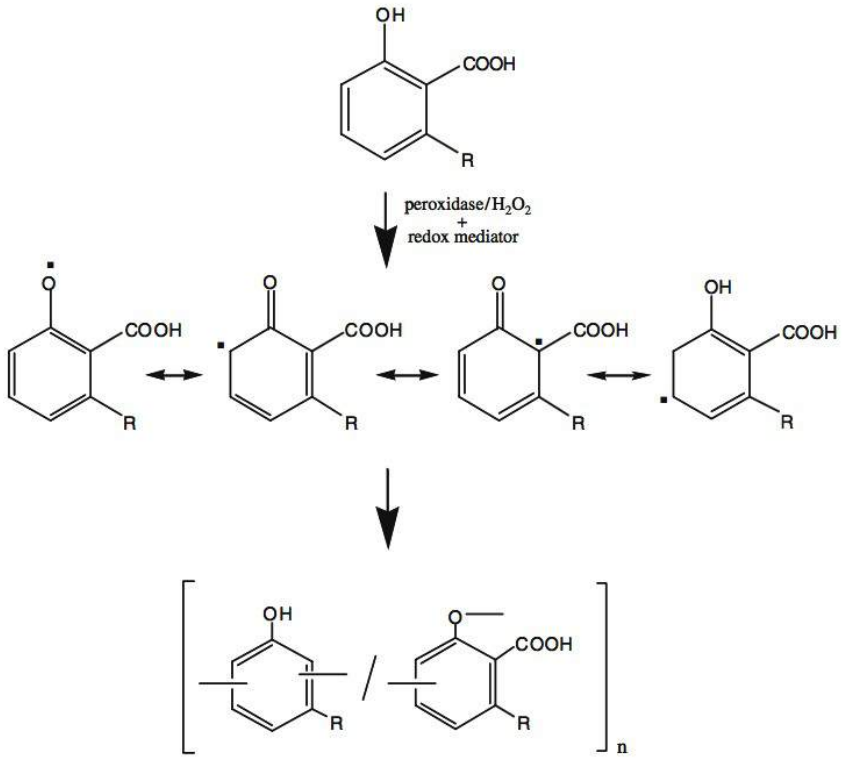


Figure 3.17: Reaction scheme of anacardic acid polymerization catalyzed by peroxidase (adapted from CHELIKANI *et al.* (2009))

PHILIP *et al.* (2007) tried to obtain molecularly imprinted polymers (MIPs), utilized the anacardic acid as monomer in toluene solution in presence of azobisisobutyronitrile (AIBN) and ethylene glycol dimethacrylate (EGDMA) or divinylbenzene (DVB) as crosslinking agent at 60 °*C*. In order to synthesize the MIP, (R,S)-propranolol hydrochloride, (R)-propranolol hydrochloride or (S)-propranolol hydrochloride were added as templates. The copolymerization was confirmed by FTIR analyses. However, the authors modified the anacardic acid through acylation and methacrylation, obtaining anacardanyl acrylate and anacardanyl methacrylate, respectively (Figure 3.18).

New copolymerizations were carried out in the same system successfully with these new monomers.

KAEWCHADA *et al.* (2012) copolymerized anacardic acid with divinylbenzene (DVB), utilizing benzoyl peroxide (BPO) and toluene, for 48h at 60 °*C*. As the main target was to synthesize a MIP, the authors added rice brain oil as template. At the end, a rigid mass of polymer was obtained. More detailed characterizations analyses were not mentioned.

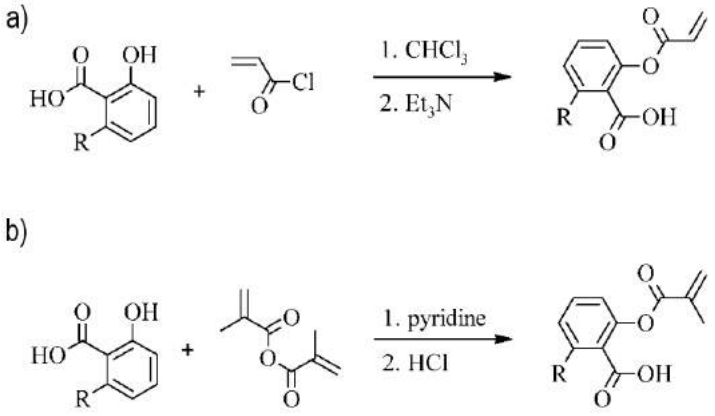


Figure 3.18: Schematic reperesentation of the synthesis of anacardanyl acrylate (a) and anacardanyl methacrylate (b) (adapted from PHILIP *et al.* (2007)).

## 3.4 Polymer Functionalization

Functionalization of polymers can be defined as the introduction of desired functional groups into the polymer structure to create specific chemical, physical, biological or pharmacological properties. Functionalization is important to enable further reactions, like bioconjugation, the selective binding of particular species, the transport of drugs, the catalytic activity and some specific final applications (PICHOT (2004), TIAN *et al.* (2012)). Functionalization can be implemented through physical adsorption by hydrophobic, hydrophilic or electrostatic interacting, through hydrogen and Van der Walls bonding and through covalent chemical bonding, due to the existence of chemical reactive groups such as amine, thiol, carboxyl and hydroxyl groups.

Functionalization through non-specific (physical) adsorption is the weakest one, since the molecule can be desorbed when the medium conditions like pH, temperature and ionic strength (WELSCH *et al.*, 2013) are changed. Conjugation through covalent bonding is more permanent and attractive because it provides a route for the formation of biofunctional layers, that are irreversibly and stable bounded (RAMOS, 2018).

As defined by IUPAC, a functional polymer is one that (MCNAUGHT and WILKINSON, 1997):

- bears specified chemical groups or;
- has specified physical, chemical, biological or pharmacological properties depending on specific chemical groups.

PICHOT (2004) specified the most used methods for fabrication of functionalized particles. Two of them are:

- heterogenous polymerizations, usually in aqueous medium and performed through free-radical polymerization, which enable the manufacture of particle dispersions with a wide size range that depends on the particular analyzed technique.
- self-organization of block or grafted copolymers by means of molecular or electrostatic interactions.

HERMANSON (2013) confirmed that reactive or functional groups can be created at the surface of particles for the subsequent coupling of binders with the aid of the monomer mixture in the polymerization. In this case, multiple factors, such as size and curvature of the particle surface and the chemical nature of the surface and the particle cores, can determine the final arrangement of the biomolecules and the extent of the functionalization (MAHON *et al.*, 2012).

PEIXOTO (2013) studied the functionalization of poly(methyl methacrylate) particles by copolymerizing methyl methacrylate with acrylic acid, methacrylic acid, 2-dimethylamino ethyl methacrylate and 2-hydroxyethyl methacrylate. The author observed the comonomers were concentrated in the particle surface due to their affinity with the aqueous medium, functionalizing the particle surfaces. Absorption tests with bovine serum albumin (BSA) indicated that 15 to 35% of the initial protein load was immobilized on the particle surfaces.

WAY (2017) studied click chemistry routes for functionalization of polymer particles. Successful thiol-ene reactions between styrene and 3-mercaptopropionic acid and between maleimide and functionalized polymers produced by RAFT polymerization were performed. The author detected the use of bioconjugated copolymer systems could cause the increase of nanoparticles uptake by cells, constituting promising alternatives for use in targeted drug delivery applications.

In the present study, suspension polymerizations are performed to functionalize polymer particles. Besides cardanol, the use of anacardic acid can be interesting due to the presence of the carboxylic group that can react with the amine groups of biomolecules, forming a peptide bound. This can be easily done with a

carbodiimide, such as 1-ethyl-3-(3-dimethylaminopropyl)carbodiimide (EDC) and N-hydroxysuccinimide (NHS). The formation of the amide group can be detected by FTIR analyses (RAMOS, 2018).

## 3.5 Concluding Remarks

Based on this literature review, it can be said that detailed experimental studies about the free-radical polymerization of cardanol or acid anacardic are not available. GALVÃO (2016) started investigating the copolymerization kinetics of cardanol with styrene in homogeneous and heterogeneous systems, confirming that cardanol can be incorporated into the polymer chains through one of its characteristic unsaturations. Besides, cardanol was shown to exert a stabilizing effect on suspension polymerizations. However, it also inhibited the polymerization, reducing the overall rates of polymerization. BESTETI *et al.* (2014) produced core-shell polymer particles containing cardanol through semibatch combined suspension-emulsion polymerizations for posterior enzyme immobilization. However, the authors were not able to copolymerize cardanol with styrene at usual suspension operation conditions. Regarding anacardic acid, only syntheses of MIPs have been reported. Therefore, comparative analyses of the kinetics of copolymerizations performed with anacardic acid and cardanol have yet to be done. Finally, the use of these renewable monomers for polymer functionalization sounds interesting as they can introduce long unsaturated aliphatic side chains and hydroxyl and carboxylic reactive groups into the polymer backbone, although this has not been performed in the literature yet.

# Kinetic Studies of Bulk Copolymerizations

## $1^{st}$ Section

# Chapter 4

# Bulk Copolimerizations: Methodology

## 4.1 Materials

Cardanol (Taian Health Chemical, minimum purity of de 99.5 wt%, Taian, China), natural CNSL (donated by Embrapa, Brazilian Agricultural Research Corporation, Fortaleza, Brazil), acrylic acid (AA) (VETEC, Rio de Janeiro, Brazil, with minimum purity of 99%), methyl methacrylate (MMA) (VETEC, Rio de Janeiro, Brazil, minimum purity of 99.5 wt%), styrene (Sty) (Sigma-Aldrich, Rio de Janeiro – Brazil, with minimum purity of 99.5 wt%) and vinyl acetate (VAc) (Sigma-Aldrich, Missouri - United States, with minimum purity of 99.5 wt%) were used as monomers. Hydroquinone (Tedia, Rio de Janeiro, Brazil, with minimum purity of 99 wt%) was used to halt the polymerization in solutions of ethanol (VETEC, Rio de Janeiro, Brazil, with minimum purity of 99.8 wt%). Benzoyl peroxide (BPO) (VETEC, Rio de Janeiro, Brazil,with minimum purity of 99 wt%, containing 25 wt% of humidity) was used as a initiator of the polymerizations. Tetrahydrofuran (THF) (Tedia, Rio de Janeiro, Brazil, with minimum purity of 99.5 wt%) was used as solvent for gel permeation chromatography analyses. Deuterated chloroform (Cambridge Isotope Laboratoies Inc., United States, minimum purity 99.8 wt%) was used as solvent for $^{1}$H-NMR analyses.

## 4.2 Set up for bulk polymerization

Reactions were performed in glass tubes. The reaction mixture (roughly 2 mL) was purged with nitrogen for one minute and placed in a silicone bath kept under constant stirring at the desired reaction temperature. The sample collected at time zero was taken when the temperature of the reaction mixture (measured with a thermocouple

placed inside the tube) reached the desired value. At specified sampling times, tubes were removed, cooled quickly and the reaction was interrupted by adding 10 droplets of ethanolic solution of hydroquinone (1 wt %).


Figure 4.1: Schematic representation of the experimental set up used to perform bulk copolymerizations.

## 4.3 Kinetic Experiments

All reaction mixtures (regardless of the comonomer) were prepared with 1 wt% of BPO. For each system, the concentration of cardanol or natural CNSL (0, 2.5, 5, 10 wt%) and the reaction temperature (85 - 110 °*C*) were manipulated. Depending on the comonomer and the concentration of cardanol/CNSL, the reaction time was also changed. When the reaction system presented smaller reactivities, longer sampling

Table 4.1: Experimental design of bulk copolymerizations

| Experiments | Monomers (% wt/wt) | | Initiator (% wt/wt) | Temperature (°C) |
|---|---|---|---|---|
| | Cardanol | Y | | |
| X.Y.T.1 | 0.0 | 99.0 | 1 | 85 |
| X.Y.T.2 | 2.5 | 96.5 | 1 | 85 |
| X.Y.T.3 | 5.0 | 94.0 | 1 | 85 |
| X.Y.T.4 | 10.0 | 89.0 | 1 | 85 |
| X.Y.T.5 | 0.0 | 99.0 | 1 | 110 |
| X.Y.T.6 | 2.5 | 96.5 | 1 | 110 |
| X.Y.T.7 | 5.0 | 94.0 | 1 | 110 |
| X.Y.T.8 | 10.0 | 89.0 | 1 | 110 |

times were taken. Table 4.1 summarizes the experiments that were performed. In total, at least 38 bulk polymerizations were carried out. In Table 4.1, X corresponds to cardanol and Y corresponds to the comonomer: MMA, Sty, VAc or AA, while T corresponds to the specified temperature. The reactions performed with MMA were repeated with natural CNSL, because PMMA is widely applied for many utilities. The obtained polymer samples were characterized by gravimetric analyses (for determination of overall monomer conversions). The polymer properties were characterized by GPC, NMR, FTIR, DSC and TGA analyses, as described below.

When necessary to remove residual cardanol, the polymeric samples were re-precipitated. For this, the sample was dissolved in toluene for a few hours until complete dissolution. Then, methanol was added to precipitate the polymer. Thus, the solid polymer phase was separated from the liquid phase and dried in a recirculating oven under vacuum. When this was performed, it is mentioned during the results discussion, naming re-precipitated copolymer.

## 4.4 Gravimetric Analysis

Monomer conversion was monitored by gravimetric analyses. The glass tube was weighed before the addition of the sample and the mass of hydroquinone added into each tube was recorded. The tubes containing the polymer material were dried in a recirculating oven under vacuum at ambient temperature, and weighed several times until constant mass. The overall monomer conversions were calculated in the form:

$$m_{monomer} = m_{initial} - m_{tube} - m_{BPO} \tag{4.1}$$

$$m_{polymer} = m_{dry} - m_{tube} - m_{BPO} - C_{sol.hydroquinone} * m_{hydroquinone} \tag{4.2}$$

$$conversion\,(\%) = \frac{m_{polymer}}{m_{monomer}} * 100\% \tag{4.3}$$

where $m_{monomer}$ is the initial mass of monomer, $m_{BPO}$ is the mass added of droplets of ethanolic solution of hydroquinone, $m_{polymer}$ is the mass of the polymer formed and $C_{sol.hydro}$ is the alcoholic solution of hydroquinone concentration (0.01 g/L).

## 4.5 Characterizations

### 4.5.1 Gel Permeation Chromatography (GPC)

Gel permeation chromatography (GPC) was used to determine the molecular weight distribution and average molecular weights of polymer samples. The sample was dissolved in THF and injected into a porous column filled with polymer. It takes longer times for small molecules to leave the column as they penetrate the interior of the porous gel phase. Bigger molecules are detected first because they do not penetrate the pores. As the operation was calibrated with standards of known molecular weights, it was possible to determine the molecular weight distribution of the polymer sample by analyzing the retention time inside the column.

Analyses were performed with a GPC chromatograph (Viscotek GPCmax, Malvern, Worcestershire, United Kingdom) equipped with Shodex GPC HFIP-803, Shodex GPC HFIP-804 and Shodex GPC HFIP-805 (Showa Denko, Tokyo, Japan) columns and a Viscotek refractive detector model VE3580 and Viscotek model 2500 UV detector, set to 255 mm and equipped with deuterium lamp. The equipment was calibrated with polystyrene standards having molecular weights ranging from 500 and $1.8 \cdot 10^6$ Da. Sample preparation consisted in solubilizing about 5 mg of the polymer in about 5 mL of THF. The solution was filtrated through a Teflon filter with pores of 0.45 $\mu$m pores. The filtrate was then injected into the chromatograph. The temperature of the columns was kept constant at 40 $°C$. 200 $\mu$l of the sample solution were injected into the mobile phase, flowing at volumetric flow rate of 1 mL/minute.

GPC data were also used to evaluate the conversion of homopolymers containing cardanol or CNSL. The characteristic monomer chromatograph was used as a benchmark for comparisons with the chromatographs of the copolymers. When a shoulder appeared in the region of higher molecular weights, indicating formation of polymer molecules, the mass fraction reported by the GPC of that fraction was assumed to correspond to the monomer conversion. However, as cardanol or CNSL were not purified, they also contained small fractions of oligomers which were subtracted from the value. A detailed explanation is presented in the Appendix.

### 4.5.2 Nuclear Magnetic Resonance (NMR)

The chemical structure of a material can be detected by nuclear magnetic resonance. This technique is based on the energy absorption at discrete frequencies when a compound is placed in a strong magnetic field and irradiated with a radio-frequency signal. The frequency is very sensitive to the atomic environment of the proton (ODIAN, 2004).

Samples for $^{1}$H-NMR were prepared solubilizing 15 mg of the polymer sample in 0.8 mL of deuterated chloroform. Analyses were performed at room temperature in a Varian Mercury, model VX300, 300.2 MHz of frequency and probe of 5 mm (California, the United States). In addition, for some samples (when announced in the discussion), the dry polymer material was redissolved in toluene, reprecipitated in methanol, filtrated and dried a second time in a drying oven under vacuum at 50 °$C$ until it reaching constant weight.

### 4.5.3 Fourier-Transform Infrared Spectroscopy (FTIR)

Fourier-transform infrared spectroscopy (FTIR) is based on the fact that atoms vibrate at specific frequencies of the electromagnetic spectra, depending on their chemical structure. The vibration changes when the chemical neighborhood changes. For this reason, this technique is used to detected chemical compounds and detect the appearance or disappearance of functional groups (ODIAN, 2004).

FTIR analyses were carried out in the range of 4000 – 400 $cm^{-1}$, with resolution of 4 $cm^{-1}$, in a Thermo equipment, model Nicolet 6700 (Madison, the United States) equipped with a ATR Smart Orbit in reflectance mode, that ensures application of a constant pressure in the samples.Soectra were reported as averages of 128 scans. KBr pellets were prepared according to the Standard Practice for Rubber Chemicals (ASTM D2702).

### 4.5.4 Thermogravimetric Analysis (TGA)

Thermogravimetric analysis (TGA) is a destructive technique used to determine the thermal stability of polymer samples placed under inert reactive atmospheres. It can also be used to evaluate the presence of solvent, residual monomer or any other volatile compound in the sample. During the analysis, temperature increases at specified rates and the mass of the sample decreases. Then, the equipment provides a mass graph (thermogram) as a function of the temperature.

Samples of 10 mg were analyzed in a Perkin Elmer STA 600 equipment (Massachusetts, the United States) with temperature ranging from 30 to 700 °$C$ with a heating rate of 10 °$C$/min under inert nitrogen atmosphere.

### 4.5.5 Differential Scanning Calorimetry (DSC)

To determine the $T_g$ and and $T_m$ of a polymer, Differential Scanning Calorimetry (DSC) analyses can be used. DSC reflects the change in heat capacity of a sample as a function of temperature by measuring the heat flow required to maintain a zero temperature differential between an inert reference material and the polymer sample. This analysis is interesting because the values of $T_g$ and and $T_m$ for a polymer affect its mechanical properties at any particular temperature and determine the temperature range in which that polymer can be employed. As the two thermal transitions are generally affected in the same manner by the molecular symmetry, structural rigidity, and secondary attractive forces of polymer chains, the presence of a plasticizer increases the mobility of macromolecules, reducing the transition temperatures (ODIAN, 2004).

For Differential Scanning Calorimetry (DSC) analyses, polymer samples of 5 mg were placed in aluminum pans under nitrogen atmosphere. Analyses were performed in the range from 0 to 280 $°C$ at heating rate of 10 $°C.\text{min}^{-1}$. As usual, the second heating scan was used to record thermal transition temperatures in order to erase the thermal history of the sample.

# Chapter 5

# Bulk Copolymerizations: Experimental Results

## 5.1 Introduction

As far we have knowledge, kinetic studies about the free radical copolymerization of cardanol with vinyl monomers had never been reported before the work of GALVÃO (2016). The author studied the copolymerization of cardanol with styrene in bulk, suspension and emulsion reactors. As previously detected, several problems may arise when cardanol is used as a comonomer. Firstly, steric hindrance is expected to occur due to the long side chain of cardanol. Secondly, the hydroxyl group may interact with other compound and lead to secondary reactions. Thirdly, stable radicals may be formed due to internal unsaturations, retarding the polymerization (RODRIGUES *et al.* (2006)). Figure 5.1 shows the reactivity sites of cardanol.

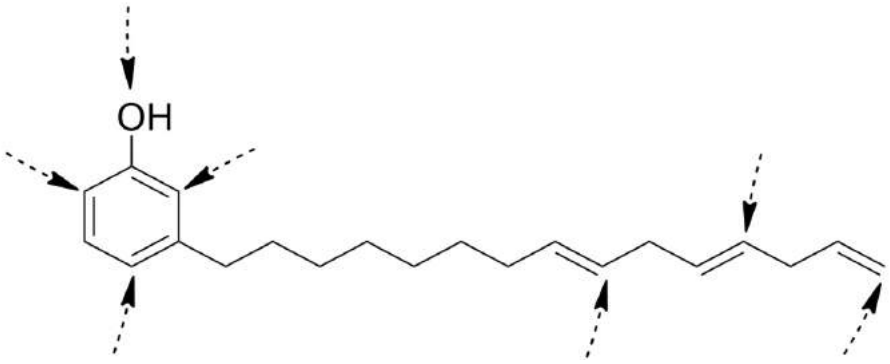


Figure 5.1: Reactive sites of cardanol

The bulk copolymerizations of cardanol with methyl methacrylate, vinyl acetate, acrylic acid and styrene are studied in this first section. As these monomers present different functional groups, reactivities and applications, it may be interesting to check if copolymerizations are possible in these systems.

It is important to observe that free radical copolymerizations of anacardic acid with these monomers have never been reported. For this reason, copolymerizations of natural CNSL with methyl methacrylate is also studied in this section. This copolymerization can be even more challenging due to the presence of a carboxylic group. Theoretically, as it is expected the polymerization will occur through one of the double bonds of the side chain, the reactivity ratios should be similar to the ones obtained when cardanol is used as a comonomer.

## 5.2 Homopolymerizations of Cardanol and Anacardic Acid

Cardanol and anacardic acid are very similar phenolic compounds as both compounds have side chains with 15 carbon atoms and 0 to 3 unsaturations, but anacardic acid presents a carboxylic group in the ortho position in respect to the hydroxyl group. Although anacardic acid can be purified from CNSL (PARAMASHIVAPPA *et al.* (2001)), this increases the cost of the reagent and, consequently, of the homo- and copolymerizations performed with this compound. Therefore, in order to evaluate the effect of the functional groups of CNSL on the copolymerizations, natural CNSL was used as reagent.

The homopolymerization of cardanol and natural CNSL were performed with 1 wt % of BPO at 85 and 110 °*C*, using the same reaction procedure already described for copolymerizations. However, as the boiling point of CNSL is very high (225 °*C* at 0.013 atm) (HARVEY), monomer may not be removed efficiently under vacuum at low temperatures. Therefore, monomer conversions for this polymerization systems were obtained from gel permeation chromatograph (GPC) data, as shown in Table 5.1. More explanation about the calculation is present in the Appendix.

Table 5.1: Conversions for homopolymerizations of cardanol with 1 wt% of BPO.

| 85 °*C* | | 110 °*C* | |
|---|---|---|---|
| Reaction Time (h) | Conversion (%) | Reaction Time (h) | Conversion (%) |
| 2 | 1.6 | 1 | 4.4 |
| 4 | 2.1 | 3 | 7.6 |
| 7 | 2.1 | 5 | 7.8 |
| 8.5 | 1.8 | 6 | 4.5 |
| 10.5 | 1.5 | 8 | 8.4 |

Even though the conversion values were small (Table 5.2), it indicates that some oligomerization took place. The fast stabilization of monomer conversions at 110 °C is related to the fast decomposition of BPO and absence of spontaneous initiation at this

Table 5.2: Conversions for homopolymerizations of natural CNSL with 1 wt% of BPO.

| 85 °C | | 110 °C | |
|---|---|---|---|
| Reaction Time (h) | Conversion (%) | Reaction Time (h) | Conversion (%) |
| 2 | 3.00 | 1 | 10.25 |
| 4 | 2.90 | 3 | 9.25 |
| 7 | 4.93 | 5 | 9.45 |
| 8.5 | 3.90 | 6 | 5.65 |
| 9 | 2.90 | 8 | 5.85 |

Table 5.3: Average molecular weights for cardanol and natural CNSL with 1 wt% of BPO.

| | $85^o$C | | |
|---|---|---|---|
| | Mn | Mw | PDI |
| Cardanol | 971 ±24 | 1217 ± 66 | 1.25±0.04 |
| Natural CNSL | 1130 ± 45 | 1499 ± 52 | 1.33±0.02 |
| | $110^o$C | | |
| | Mn | Mw | PDI |
| Cardanol | 1185 ±64 | 1690 ± 64 | 1.43±0.06 |
| Natural CNSL | 1179 ±37 | 1684 ±103 | 1.43±0.06 |

condition. Figure 5.2 show characteristic GPC chromatograms of samples collected at 85 and 110 °*C*. Oligomers were obtained at both temperatures as can be seen in Table 5.3 (the average molecular weights for each point of a same reaction is similar, thus, for each point, values of $M_n$ and $M_w$ are present in the Appendix). It is possible to observe in Figure 5.2 the presence of small shoulders positioned in the region of low molecular weights that may be due to impurities, as also observed for natural CNSL and illustrated in Figure 5.3. Conversions for CNSL homopolymerizations are presented in Table 5.2. As one can see, conversions were similar for cardanol and natural CNSL homopolymerizations, as one might already expect if reactions involve the unsaturations of the pendant side chains. However, conversions appeared to be consistently larger for CNSL samples, which may indicate that the functional group exert some influence on the course of the reaction.

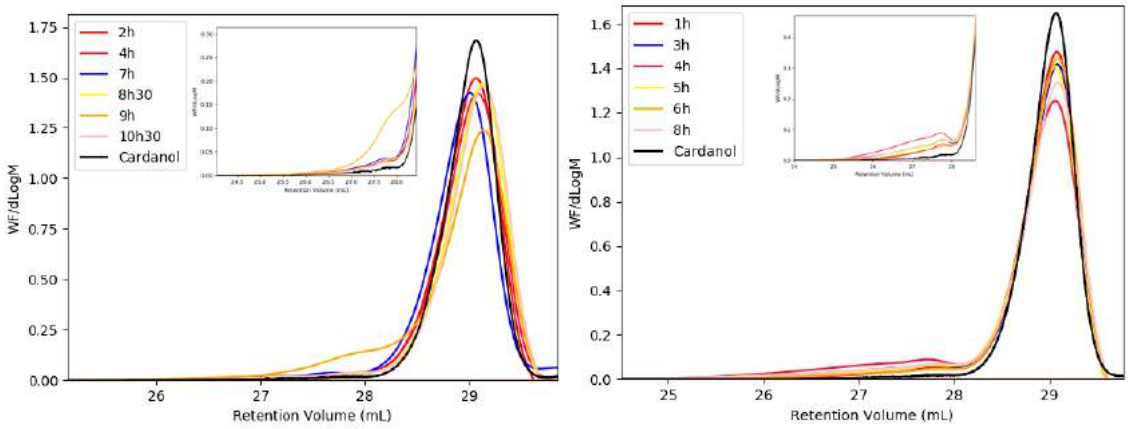


(a) (b)

Figure 5.2: GPC chromatographies of samples collected at 85 °*C* (a) and 110 °*C* (b) for cardanol homopolymerizations (differential molecular weight distribution versus retention volume).

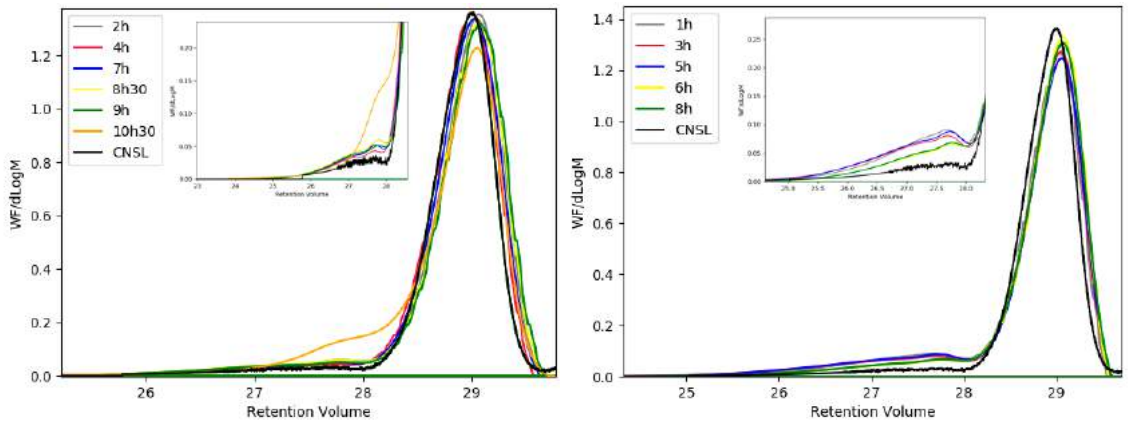


(a) (b)

Figure 5.3: GPC chromatographies of samples collected at 85 °*C* (a) and 110 °*C* (b) for natural CNSL homopolymerizations (differential molecular weight distribution versus retention volume).

$^1$H-NMR analyses for cardanol samples were performed to evaluate the chemical bonds present and propose a possible reaction mechanism. However, the obtained spectra were very complex, with many signals (GALVÃO (2016), FERREIRA *et al.* (2015)). Figure 5.4 shows the $^1$H NMR spectrum of cardanol with identified peaks. The formation of higher molecular weight compounds can be monitored through the peak placed at $\delta$ = 2.5 ppm (*f*). Hydrogen (2H) related to peak *f* were selected because they are present in all analyzed molecules. Figure 5.5 shows the spectrum of a sample collected after 4h of polymerization, while Figure 5.6 shows the spectrum of a sample collected after 8h of reaction at 110 °C. One can observe that peaks *c, e, g* and *j* experience a relative increase while peaks *b* or *d* that correspond to the terminal double bonds remained constant. So, as it seems that the relative proportion of saturated car-

danol decreased, while the mono and diene fractions increased, reactions did not take place through the terminal double bond. Similarly, peaks *a* did not change, showing that a mechanism similar to the oxidative or enzymatic polymerization of cardanol did not happen. The appearance of a very broad peak within the range of 3 to 5 ppm, which corresponds to the R-O-R (ether) bonds, indicates that some reaction with the hydroxyl group may have happened (PRETSCH *et al.*, 2000). Analyses were performed in duplicates and the obtained results were essentially the same.

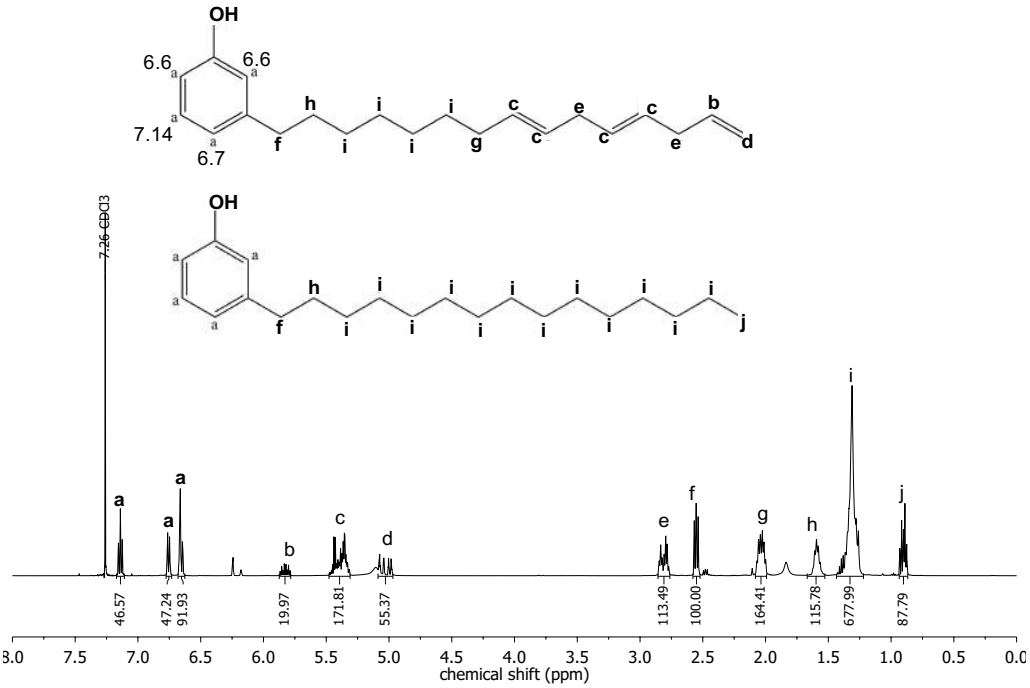


Figure 5.4: $^{1}$H NMR spectrum of cardanol.

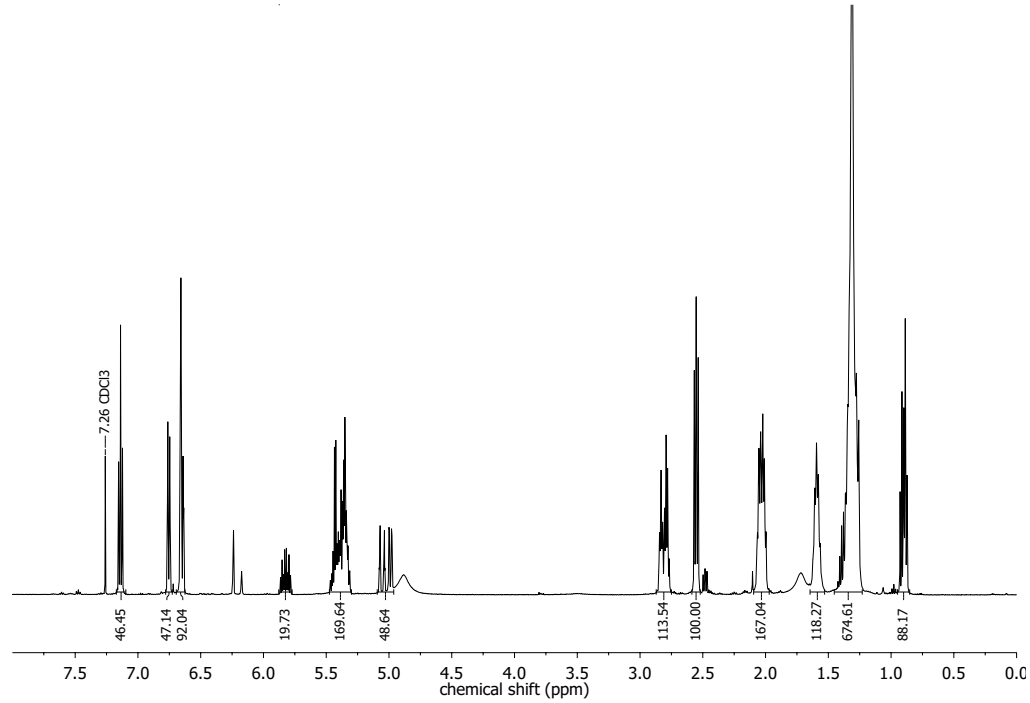


Figure 5.5: $^{1}$H NMR spectrum sample collected after 4h of reaction at 110°C with cardanol.

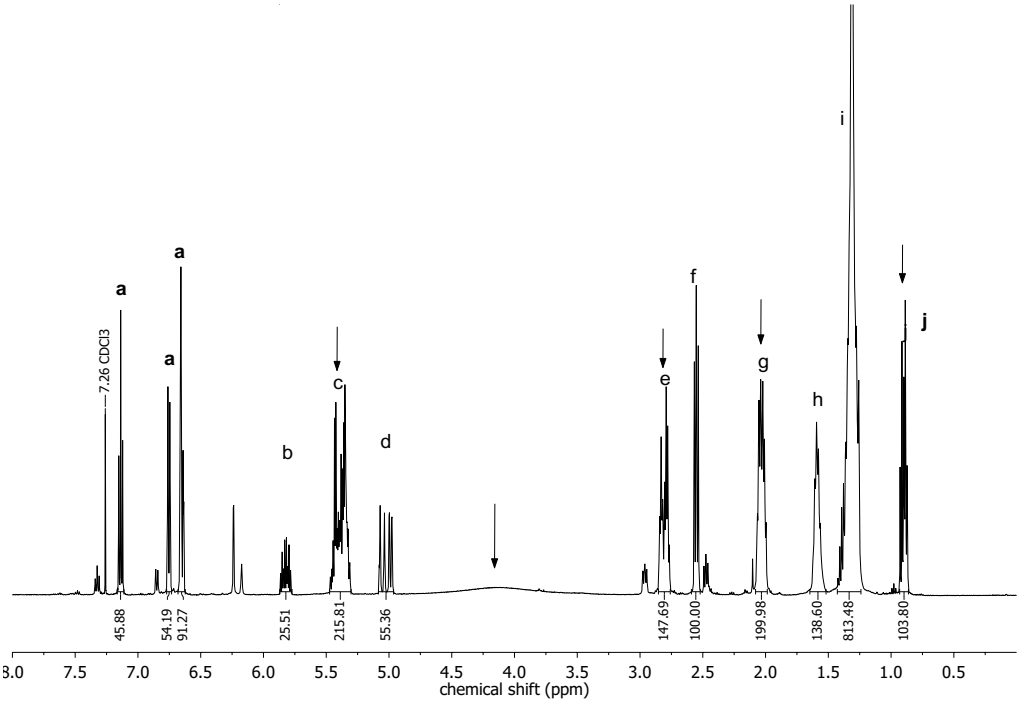


Figure 5.6: $^{1}$H NMR spectrum of a sample collected after 8 hours of reaction at 110°C with cardanol.

For natural CNSL, the composition of the mixture and the respective $^{1}$H NMR spec-

trum was even more complex than the observed for cardanol. The $^1$H NMR spectrum is presented in Figure 5.7 and identification of the peaks is similar to the one presented for cardanol. However, after 8 hours of reaction at 110°*C*, a reference peak could not be selected as the intensities of all peaks seemed to have changed, as pointed by the arrows of Figure 5.8. Also, a peak located in the region between 4.0 and 4.9 ppm appeared indicating the ether function.

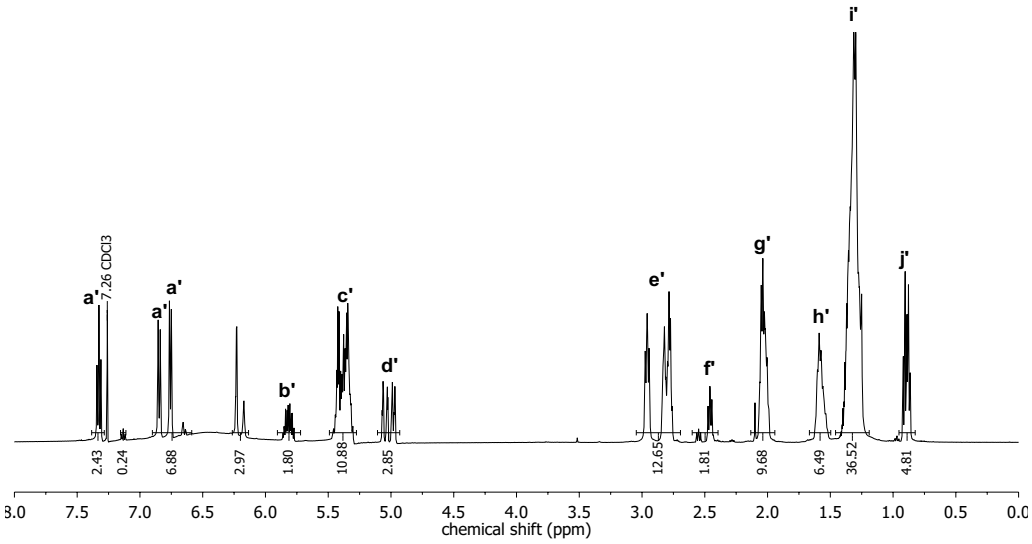


Figure 5.7: $^1$H NMR spectrum of CNSL.

The $^1$H NMR spectra of cardanol and CNSL can be used to evaluate the percentage of the triene component(s), by comparing the peaks *f* or *h* with peaks *b* or *d*. Therefore, the triene fractions were equal to $44.41 \pm 7.8$ % in cardanol and $49.69 \pm 6.0$ % in natural CNSL. Monoene and diene fractions cannot be obtained only by $^1$H NMR analysis. Gas chromatography can be used to obtain their compositions in further investigations.

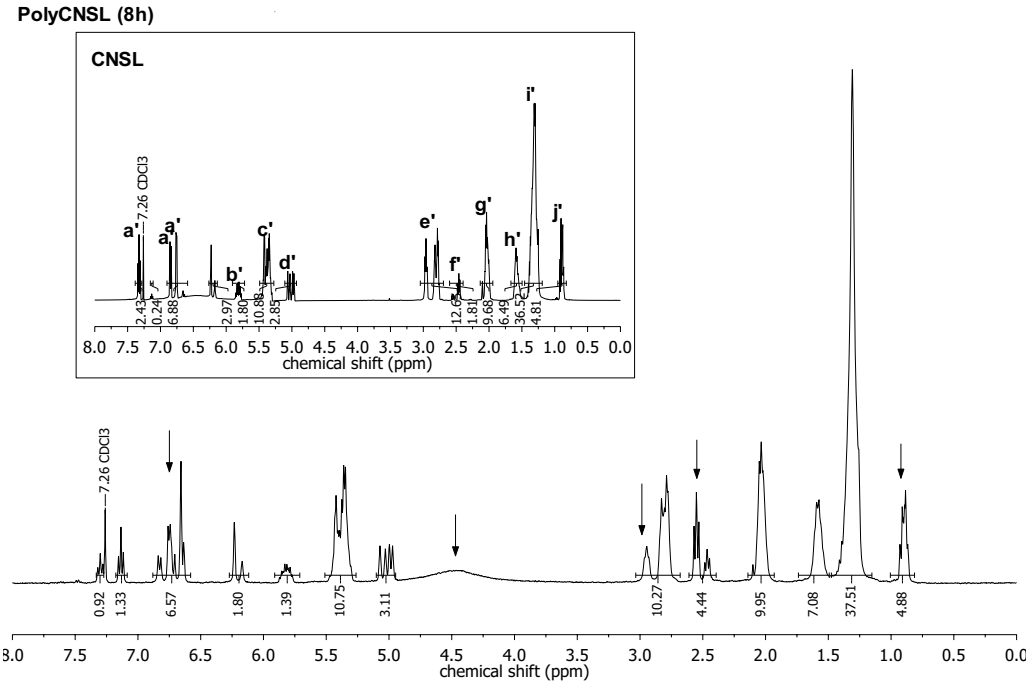


Figure 5.8: $^{1}$H NMR spectrum of sample collected after 8h of reaction at 110 °C with CNSL.

FTIR analyses were also performed to detect functional groups present in the samples. FTIR spectra of samples collected at 110 °*C* (Figure 5.9) show that the relative intensity of peaks decreased with time, indicating consumption of functional groups. Reduction of intensity took place mainly at 3300, 1250 and 1150 cm$^{-1}$, which are related to the hydroxyl moiety (SMITH, 1998). Therefore, reactions with this group may have happened. Moreover, the relative intensity of peaks related to double bonds also diminished with time, such as the one related to the terminal double bond at 3050 cm$^{-1}$ and those located at 1000 - 600 cm$^{-1}$ corresponding to internal and terminal unsaturations (SMITH, 1998). FTIR spectra of samples collected after 4 hours and 8 hours of reaction at 110 °C were not different with linear correlation of 0.9563 (Figure 5.10). The FTIR spectra were similar to the one of pure cardanol reported by YADAV and SRIVASTAVA (2007b). Therefore, cardanol may present multiple reactive sites: hydroxyl groups, internal and terminal unsaturations. All of them can react in the presence of a suitable initiator (such as BPO) in different magnitudes. The reaction with the hydroxyl moiety can happen because phenolic compounds are donors of hydrogen atoms, as shown in Figure 5.11 (TYCHOPOULOS and TYMAN, 1990). This reaction is faster than the transfer reaction of an alkyl radical (LARTIGUE-PEYROU (1996). Moreover, the presence of oxygen can cause the formation of peroxy radicals, reinforcing the need for nitrogen purging before reaction.

For natural CNSL, it is hard to analyze the FTIR spectra because the peaks were

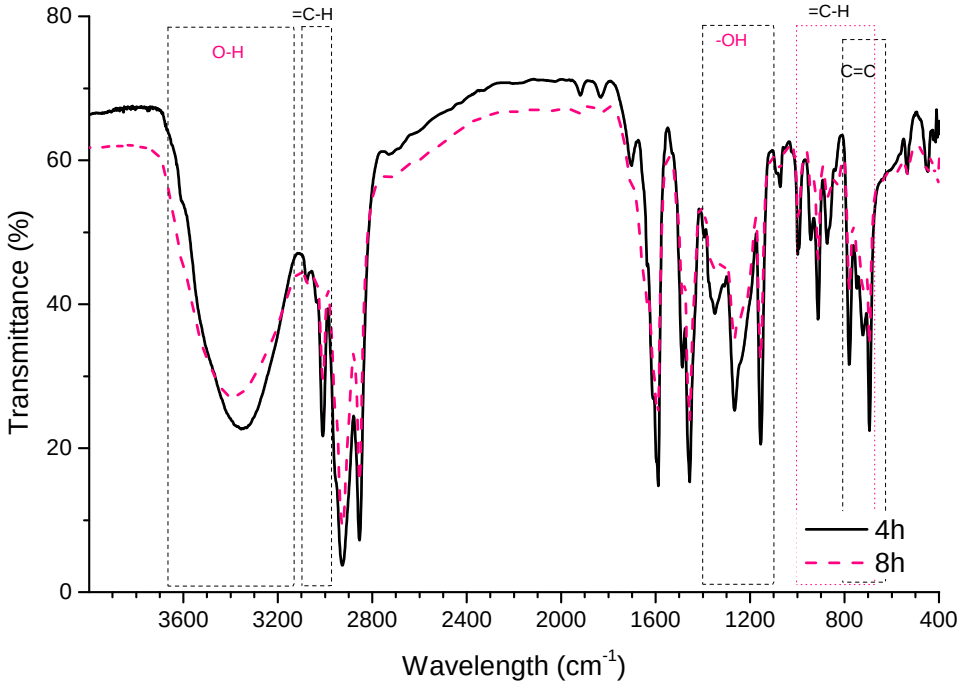


Figure 5.9: FTIR spectra of samples collected after 4 and 8 hours of reaction at 110 °C with cardanol.

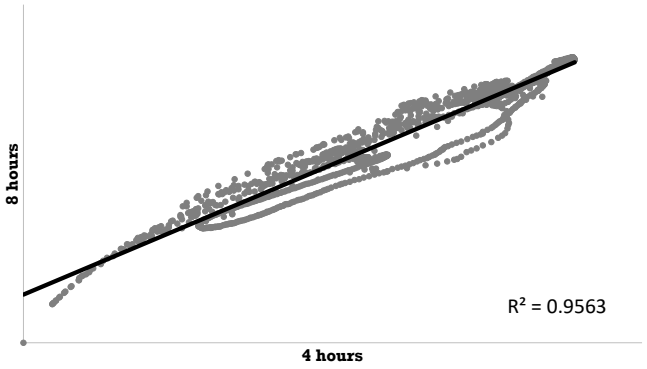


Figure 5.10: Graphic comparison between FTIR transmittance of collected cardanol samples at 110 °C after 4 hours and 8 hours.

overlapped and very broad. As one can seen in Figure 5.12, FTIR spectra of samples collected after 4 and 8 hours of reaction at 110 °C were not very different, with linear correlation of 0.9291 (Figure 5.13). However, absorption at 1600-1700 $cm^{-1}$ apparently indicate consumption of double bonds. Even though unsaturated internal C=C bonds permits radical addition for subsequent polymerization, the formed radical is very stable, retarding the polymerization by trapping of free radicals. Therefore, a way

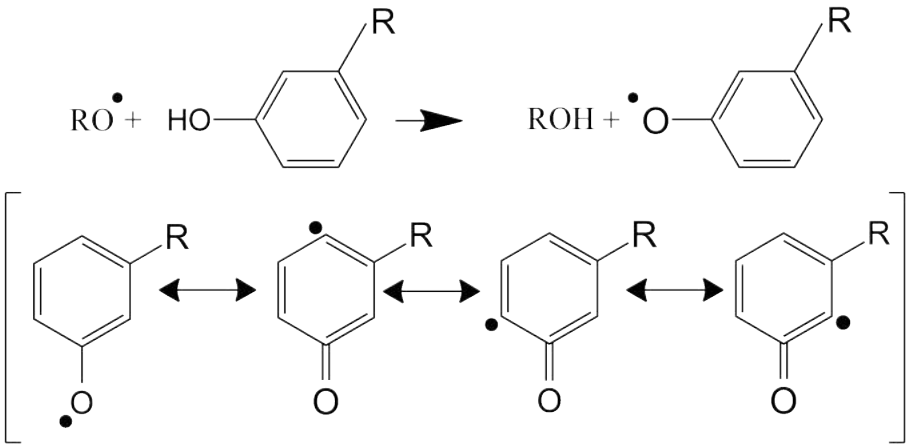


Figure 5.11: Schematic representation of the inhibition mechanism of cardanol.

to enhance the reactivity could make use of activation functionalization or conjugation strategies. Acrylation and epoxidation are some options. Cardolite NC 513 or NC 2513 (from Cardolite, Inc), for example, are epoxidized cardanol materials (ECL) used as reactant (CHISHOLM *et al.*, 2014).

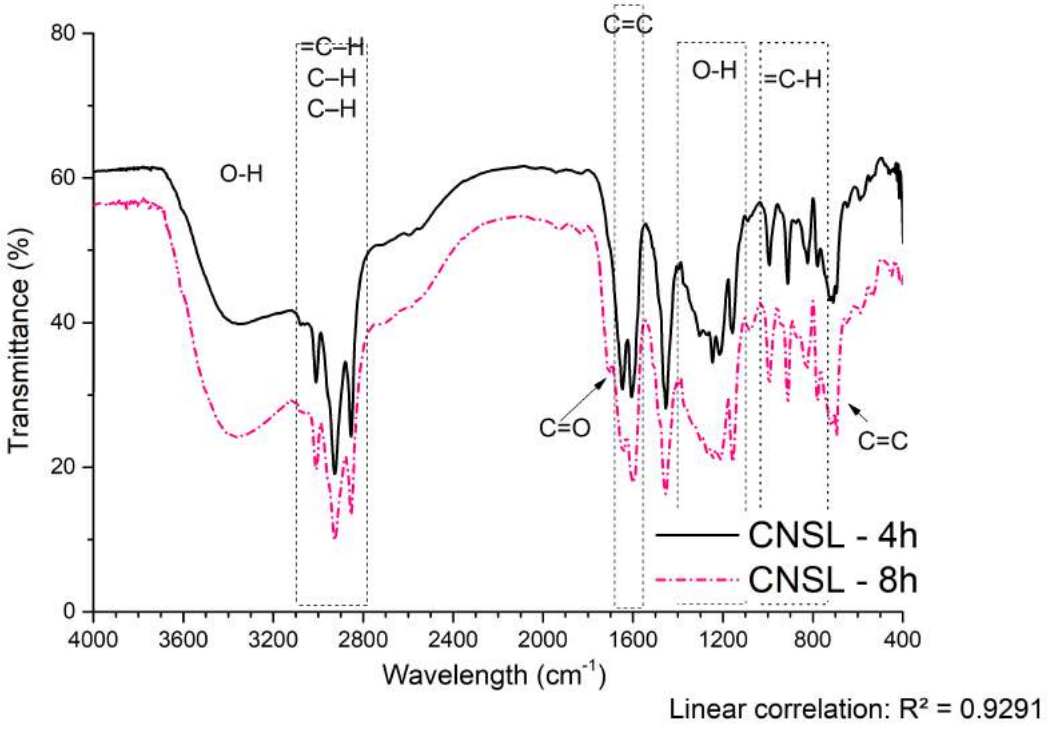


Figure 5.12: FTIR spectra of samples collected after 4 and 8 hours of reaction at 110 °C with natural CNSL.

Thermogravimetric analysis were performed to evaluate the thermal stability of the raw materials. CNSL presented higher thermal stability than cardanol, although volatilization started at 150 °*C* in both cases. However, while cardanol presented a single volatilization stage, CNSL presented three. The first stage of CNSL volatilization

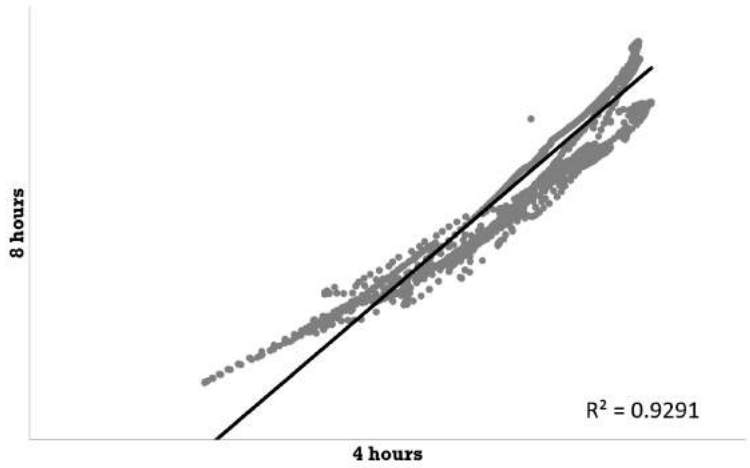


Figure 5.13: Graphic comparison between FTIR transmittance of collected CNSL samples at 110 °C after 4 hours and 8 hours.

may be related with the descarboxylation of anacardic acid, which happens at temperatures above 180 °*C* and transforms anacardic acid into cardanol while liberating carbon dioxide (MAZZETTO *et al.*, 2009). The second stage of CNSL degradation may be related to cardanol, which is present in small amounts in natural CNSL (< 10 wt %), but it is also generated by descarboxylation of anacardic acid. While cardanol is fully volatilized at 325°C, the presence of impurities in CNSL extends volatilization and degradation to higher temperature, over 500 °*C*. The TGA analysis for CNSL is similar to the obtained by RODRIGUES *et al.* (2011).

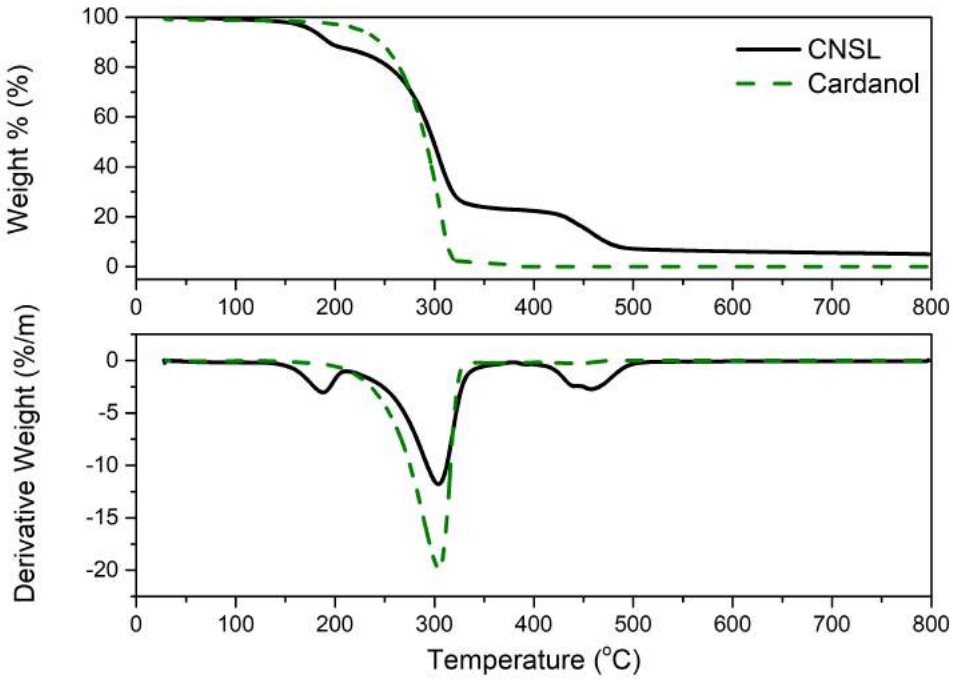


Figure 5.14: TGA and DTG thermograms of cardanol and natural CNSL.

## 5.3 Copolymerization of cardanol and styrene

Polystyrene is a very known polymer, being transparent, it is used in a large variety of applications, including food packaging and appliances. Polystyrene is also used for manufacture of foams as expanded polystyrene (EPS), which are used for thermal insulation and protective packaging (RODRIGUEZ *et al.*, 2015). The chemical structure of polystyrene is presented in Figure 5.15.

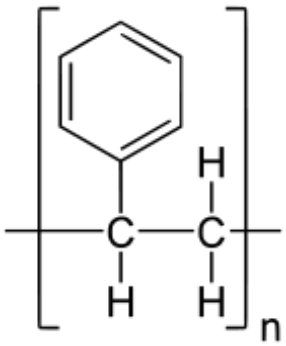


Figure 5.15: Chemical structure of polystyrene.


Figure 5.16: Photographs of samples of polystyrene and poly(styrene-co-cardanol) prepared at 110°*C*

Reactions between cardanol and polystyrene were performed with 2.5, 5 and 10 wt% of cardanol at 85 and 110 °*C* using 1 wt % of BPO. Figure 5.16 shows photographs of the copolymers produced at 110 °*C*, showing the color of the material changes with the increase of the cardanol concentration and indicating the copolymerization may have happened. For copolymer samples re-precipitated (photographs were not taken), the brownish color for copolymers was also noticed. Conversions and molecular weights of polymer samples collected for reactions performed at 85 °*C* are presented in Figure 5.17. Although styrene reactions achieved very high conversions in less than three hours, it took longer times for reactions with cardanol to achieve high conversions. Reaction performed with 10 wt % of cardanol reached a plateau just after 30 minutes of

reaction, which can indicate the presence of unreacted cardanol. As one can see in Figure 5.17, cardanol acts retarding and inhibiting the styrene polymerization. As expected, the average molecular weights of the polymer samples diminished. This may have happened because the phenolic group and the internal unsaturations form stable radicals very stable, retarding or stopping the polymerization. Therefore, cardanol consumes living radicals, reducing the radical concentration in the reaction medium. For reactions with 10 wt% of cardanol, average molecular weight data indicated that polymer was not formed.

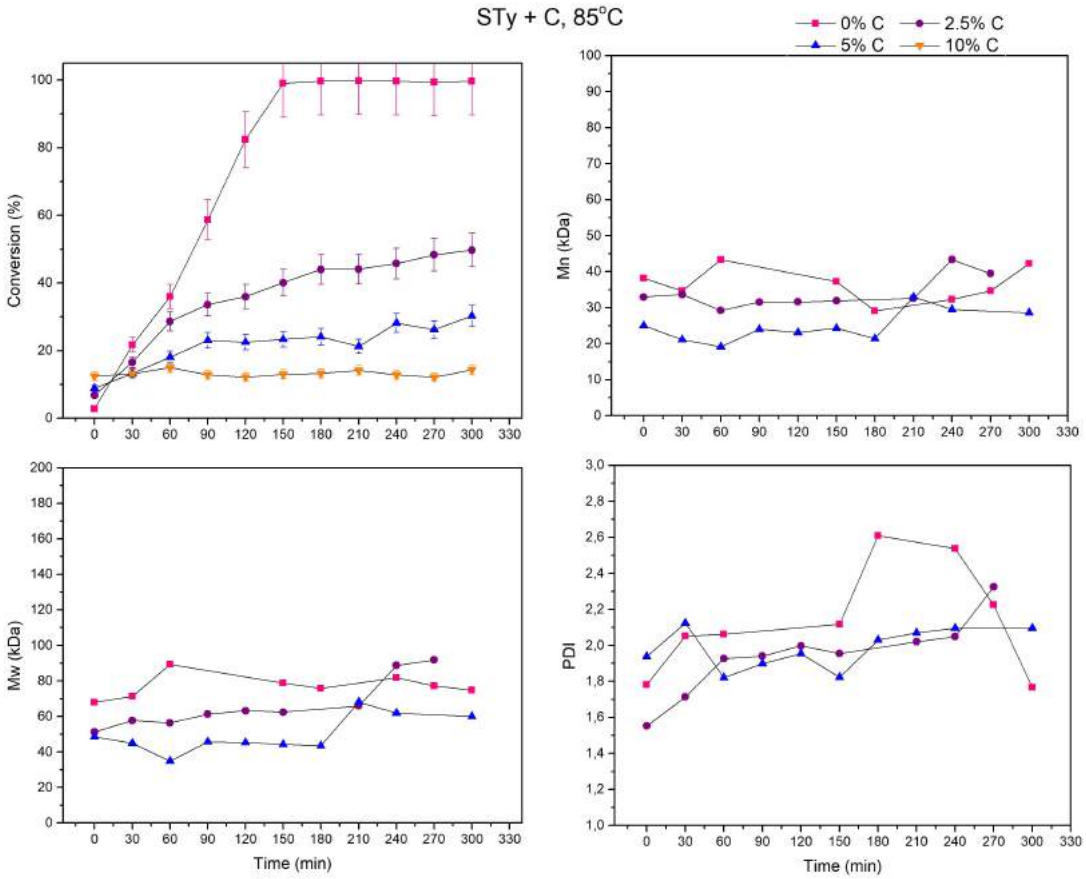


Figure 5.17: Conversions and average molecular weights of polymer samples collected at 85 °*C* in copolymerizations of styrene and cardanol.

At 110°*C*, a similar behavior could be observed, as shown in Figure 5.18, although reaction rates were higher. Molecular weights were also reduced, but the PDI values were higher because of the faster decomposition of initiator and the continuous thermal initiation of styrene, which becomes more relevant at this temperature and kept the continuous growth of monomer conversions.

Thermogravimetric analyses were used to compare the thermal stabilities of the copolymers produced with pure polystyrene and cardanol. For reactions performed at 85 °*C* (Figure 5.19), the addition of cardanol shifts the TGA curve towards the TGA curve of pure cardanol located below 400 °*C*, showing that weaker chemical bonds

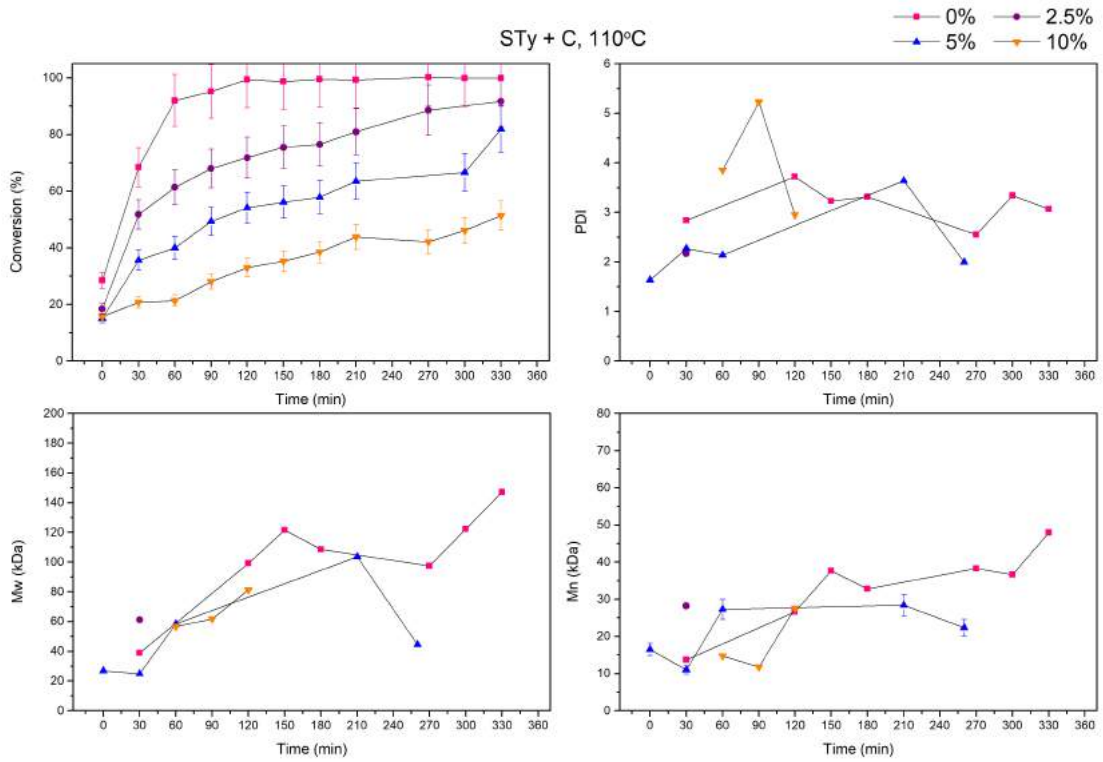


Figure 5.18: Conversions and average molecular weights of polymer samples collected at 110 °*C* in copolymerizations of styrene and cardanol.

were formed with the addition of cardanol or indicating the decomposition of the side chain of cardanol takes place first. This suggests that the presence of cardanol reduced the thermal stability of the copolymer and indicates the occurrence of the copolymerization. However, at higher temperatures, the presence of cardanol increased the residual thermal stability of the copolymer, which can also indicate the occurrence of the copolymerization. This can be due to the addition of the phenolic group of cardanol to the copolymer chains. For 10 wt% of cardanol, higher amounts of residual monomer might be present in the sample (styrene boils at 145 °*C*). However, almost 20 wt % is left afterwards, which corresponded to the copolymer, leading to the highest residual thermal stability. Similar behavior could be noticed at 110 °*C* (Figure 5.20), although the shifting effect towards the curve of cardanol was less pronunced, maybe due to the significant increase in styrene conversions and reduction of the cardanol content of the copolymer.

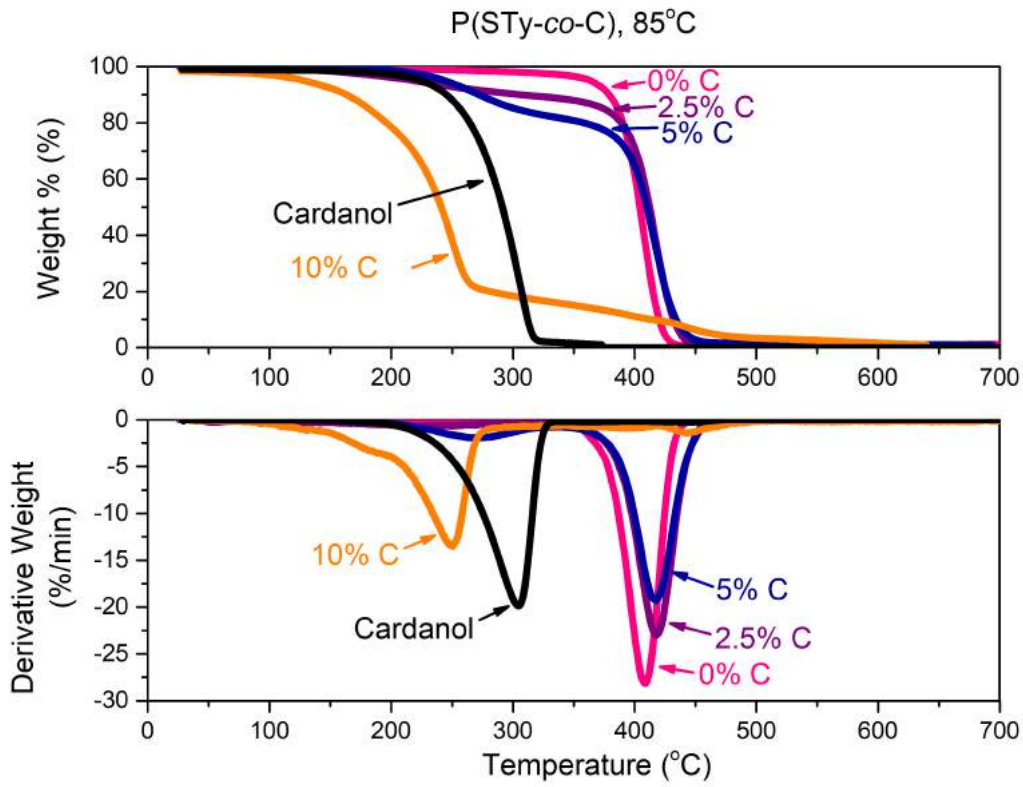


Figure 5.19: TGA and DTG thermograms of samples collected after 5 hours of reaction at 85 °*C* in copolymerizations of styrene and cardanol.

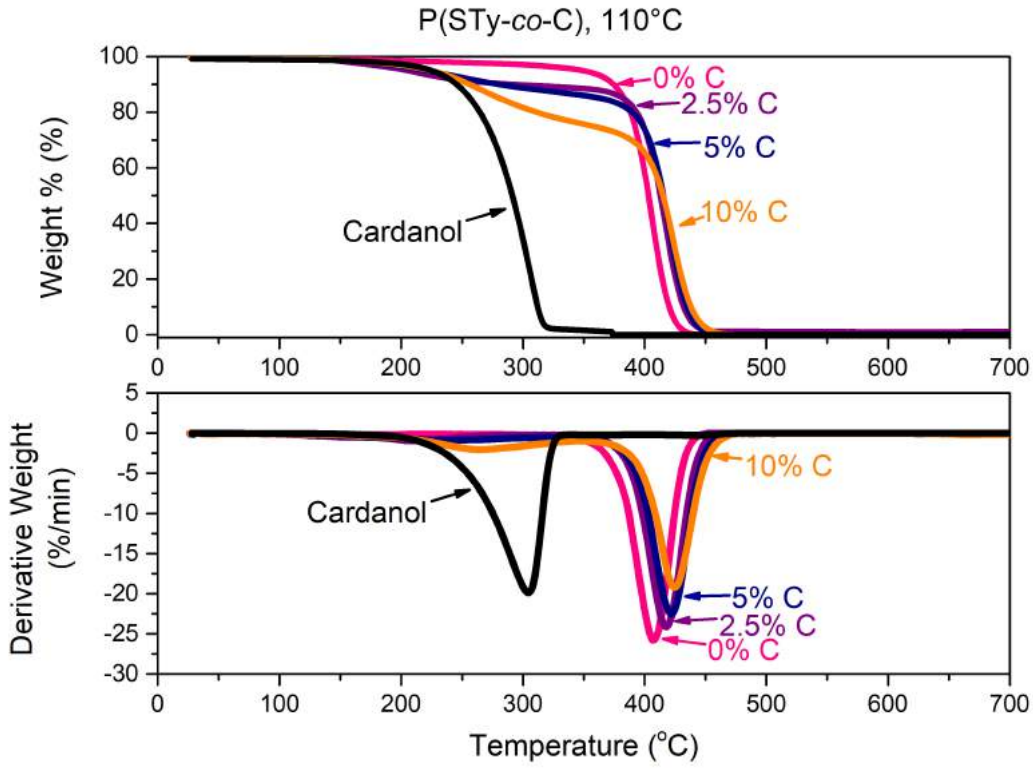


Figure 5.20: TGA and DTG thermograms of samples collected after 5.5 hours of reaction at 110 °*C* in copolymerizations of styrene and cardanol.

Although some effects on the thermal stability of the obtained copolymers could be noticed with the introduction of cardanol, the observed effects were very subtle, probably indicating the low incorporation of cardanol into the copolymer chains. For this reason, DSC analyses were carried out, as shown in Table 5.4. The obtained results showed the significant reduction of the glass transition temperature ($T_g$) with the increase of the cardanol feed content, indicating the incorporation of cardanol molecules into the copolymer chains. The reduction of the $T_g$ values is related to the large sizes of cardanol molecules and incorporation of long pendant groups, which enhance the mobility of the polymer chains.

$^1$H-NMR analyses were carried out to evaluate if cardanol had been in fact incorporated into the copolymer chains. Figure 5.21 shows the $^1$H-NMR spectrum of the polymer sample produced with 5 wt% of cardanol at 110 °$C$ as an example and indicates the occurrence of styrene-cardanol bonds. It is important to emphasize that residual styrene was removed from polymer samples through vacuum drying and residual cardanol was removed by reprecipitation in methanol . The $^1$H-NMR spectra of the other polymer samples are present only in the Appendix because they were qualitatively similar to the $^1$H-NMR spectrum of polymer sample presented in Figure 5.21. Based on the $^1$H-NMR spectrum, it is possible to calculate the mol and weight cardanol copolymer compositions respectively as:

$$\varphi_C(mol\,\%) = \frac{(f/2)}{(f/2)+q} \tag{5.1}$$

$$\omega_C(wt\,\%) = \frac{\frac{\varphi_C}{MW_{STy}}}{\frac{1}{MW_C} + \varphi_C(\frac{1}{MW_{Sty}} - \frac{1}{MW_C})} \tag{5.2}$$

where $f$ and $q$ are the areas of the corresponding peaks. The obtained degrees of cardanol incorporation are shown in Table 5.5. Samples collected after 3 and 5 hours of reaction were selected for modeling purposes. In order to evaluate the possible effect of the purification procedure, $^1$H-NMR analyses were performed for samples obtained

Table 5.4: Glass transition temperatures of samples collected after 5 hours of reaction in copolymerizations of styrene and cardanol.

| $T_g$ (°$C$) | | |
|---|---|---|
| | 85 °$C$ | 110 °$C$ |
| 0% C | 97.5 | 92.1 |
| 2.5% C | 78.4 | 83.0 |
| 5.0% C | 44.3 | 66.6 |
| 10% C | - - - | 57.2 |

after 5 hours of reaction before and after reprecipitation in methanol. As one can see, most results were similar and within the expected experimental fluctuation of 1%. In one case, however, the observed difference was significant, indicating the incomplete removal of cardanol during the initial drying step or loss of copolymer during the second reprecipitation step. For 10 wt% of cardanol at 85 °*C*, it was clear from TGA and DSC analyses that the amounts of residual cardanol were high. Therefore, it is possible that the value reported in Table 5.5 does not correspond to the true cardanol content of the sample. Moreover, a value was not reported for this point because nothing precipitated with methanol, indicating the low polymer content of the sample. Nevertheless, it seems clear that cardanol was incorporated into the polymer chains during the polymerization trials.

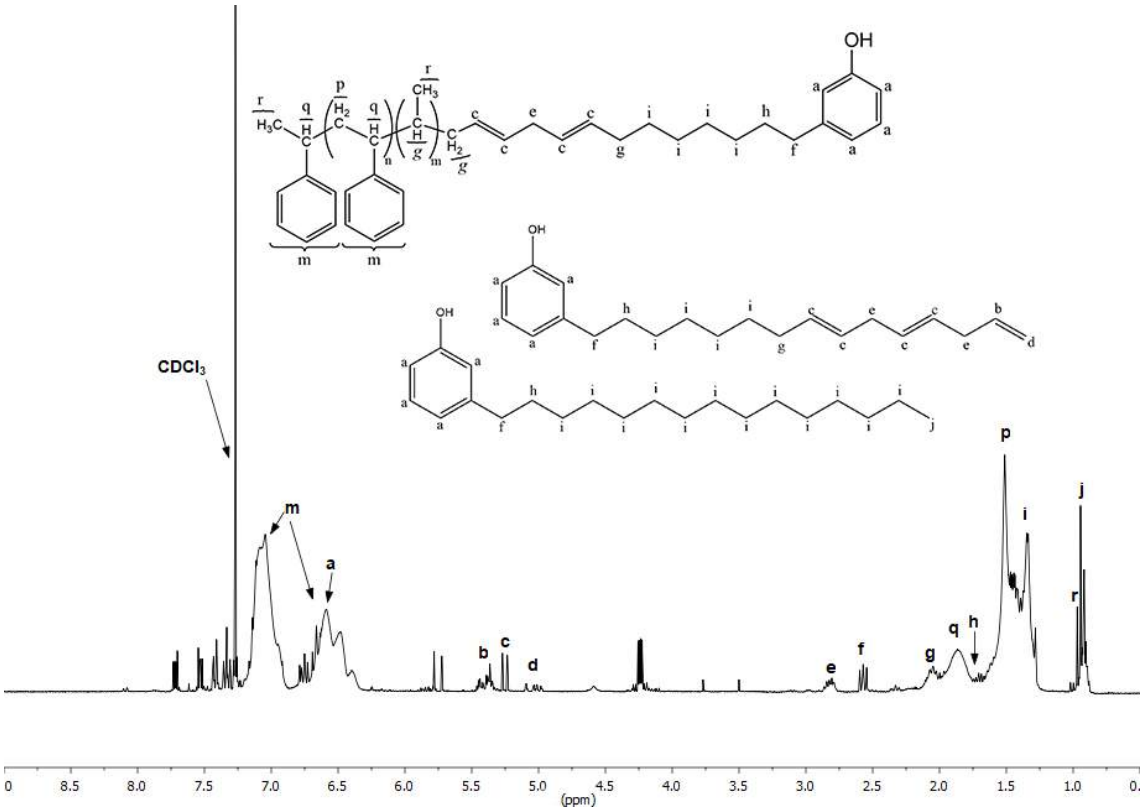


Figure 5.21: $^{1}$H-NMR spectrum of polymer sample collected after 5 hours of reaction and prepared with 5 wt% of cardanol at 110 °*C*.

When the $^{1}$H-NMR spectrum of Figure 5.21 is compared with the $^{1}$H-NMR spectrum of cardanol, shown in Figure 5.4, one can see the characteristic polystyrene peaks are present at 1.8, 2.2 and 7.1 ppm, although confounded with peaks that are characteristic of cardanol. Moreover, the relative intensities of peaks corresponding to protons *b* and *d* decreased due to the incorporation of cardanol through the terminal double bond. It is important to observe that the peaks placed between 6.5 and 7.0 ppm in the cardanol spectrum became much broader, which may indicate the reaction of the hydroxyl group and the occurrence of inhibition and chain transfer reactions. Finally, the

Table 5.5: Cardanol contents of copolymer samples collected after 3 and 5 hours in copolymerization of styrene and cardanol.

| Exp. Cond. | 85 °C | | | 110 °C | | |
|---|---|---|---|---|---|---|
| | 2.5% C | 5% C | 10% C | 2.5% C | 5% C | 10% C |
| 3h | 6.83 | 5.78 | - - - | 6.13 | 8.24 | 8.67 |
| 5h | 5.60 | 20.16 | 74.32 | 5.60 | 8.24 | 22.98 |
| 5h (reprecipitated) | 5.54 | 5.38 | - - - | 5.33 | 7.35 | 7.26 |

presence of additional peaks in the spectra of cardanol and poly(styrene-co-cardanol) probably indicates the existence of other impurities in the comonomer feed (which is provided as a complex mixture of cardanol derivatives, as already explained), which may also affect the kinetics of the copolymerization reactions. Nevertheless, it is important to emphasize that additional purification of available commercial feed streams is not feasible, due to both economical and technical constraints, imposing the use of similar commercial feeds to perform the polymerizations.

One may raise the question whether the terminal unsaturation is most reactive group and responsible for the copolymerization. In this case, only 40 wt% of the cardanol load should be accounted, as this is roughly the weight fraction of the cardanol triene. However, in addition to changes detected in the $^{1}$H-NMR spectrum of the copolymer, the styrene-cardanol polymer produced with 2.5 wt % at 110 °C reached very high conversions while the composition data for samples collected after 5 hours of reaction showed that 5.33 wt% of cardanol was present in the copolymer, which would correspond to total consumption of cardanol. Therefore, the whole cardanol stream seems to be reactive.

Finally, FTIR analyses were carried out to verify the presence of functional groups. As both cardanol and styrene have aromatic rings, many peaks overlap. Regions indentified in green are present mainly in cardanol, while those in black are present in both monomers. In Figure 5.22, it is possible observe the hydroxyl group of cardanol between 3600 and 3200 cm$^{-1}$, which also appears with smaller intensity between 1350 and 1050 cm$^{-1}$. Figure 5.23 presents the FTIR spectra of samples collected in reactions performed at 110 °C. The less intense hydroxyl peaks in samples collected at 85 °C may indicate that inhibition may have happened due to reaction with hydroxyl groups.

As it can be noticed the relative intensity of hydroxyl peaks changed, samples collected at earlier reaction times (1, 3 and 5 hours) for the same reaction were also analyzed. For reaction performed with 2.5 wt% of cardanol at 85 °C (Figure 5.24), for example, from one to five hours, the band located at 3600-3500 cm$^{-1}$ (O-H bond) disappeared completely, while the peak located at 1250-1180 cm$^{-1}$, also related with the phenolic moiety, became less intense too. One may notice that the main difference between samples collected after 3 and 5 hours of reaction was the intensity of the peak

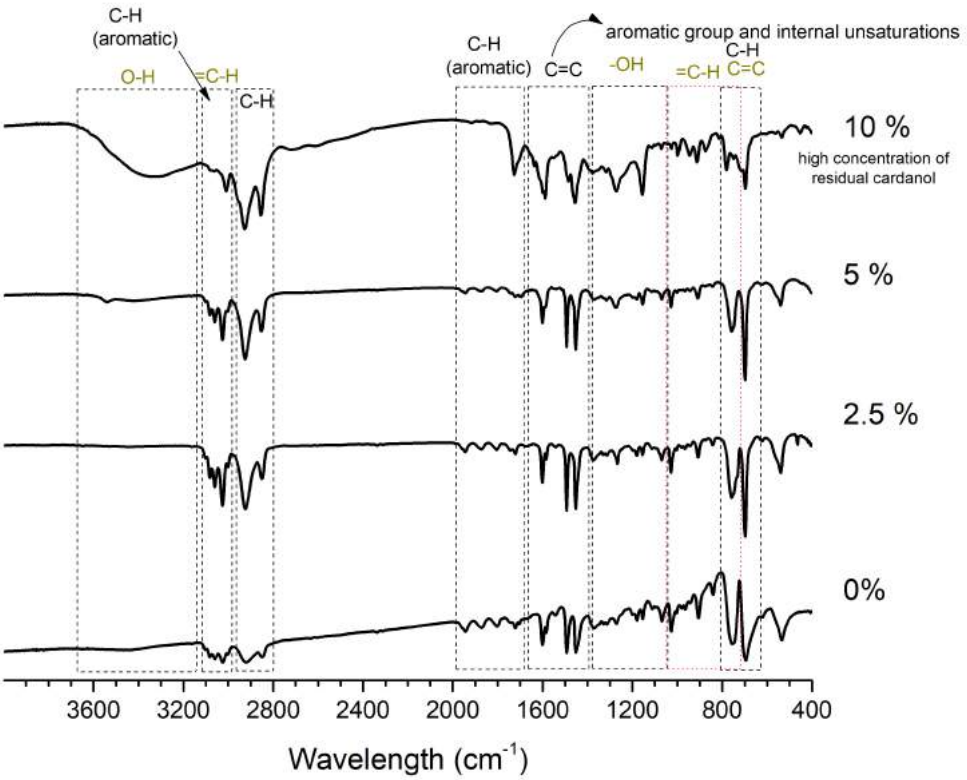


Figure 5.22: FTIR spectrum of poly(styrene-co-cardanol) prepared with at 85 °*C*.

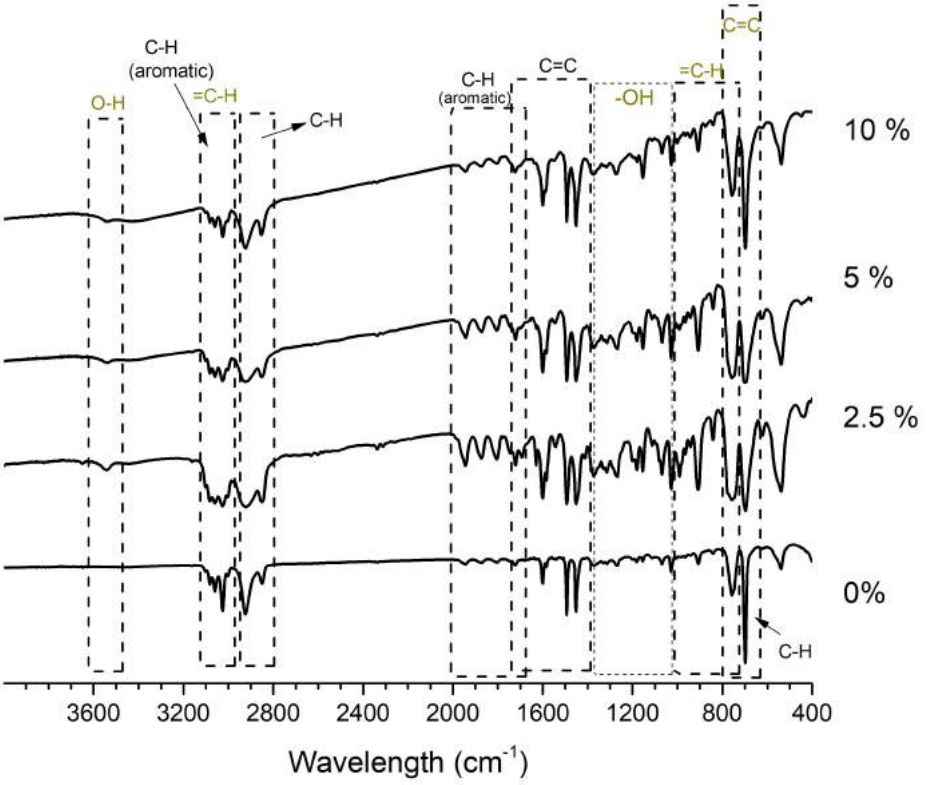


Figure 5.23: FTIR spectrum of poly(styrene-co-cardanol) at 110 °*C*.

placed at 3600 - 3500 $cm^{-1}$, so that the phenolic ring may have been suppressed by newly formed radicals. Moreover, the peak placed at 900 $cm^{-1}$ decreased, which may indicate that the terminal double bond was consumed. The peak located at 1700 $cm^{-1}$, not present in styrene, was reduced as well. As the conversion increased throughout the reaction course, this may be related with the styrene incorporation. However, the formation of a C=O bond due to hydrogen donation from the phenolic group should appear around this same range. Nonetheless, the intensities of the peaks between 3100 and 2800 $cm^{-1}$ were much higher than for styrene, showing that cardanol was incorporated into the molecules.

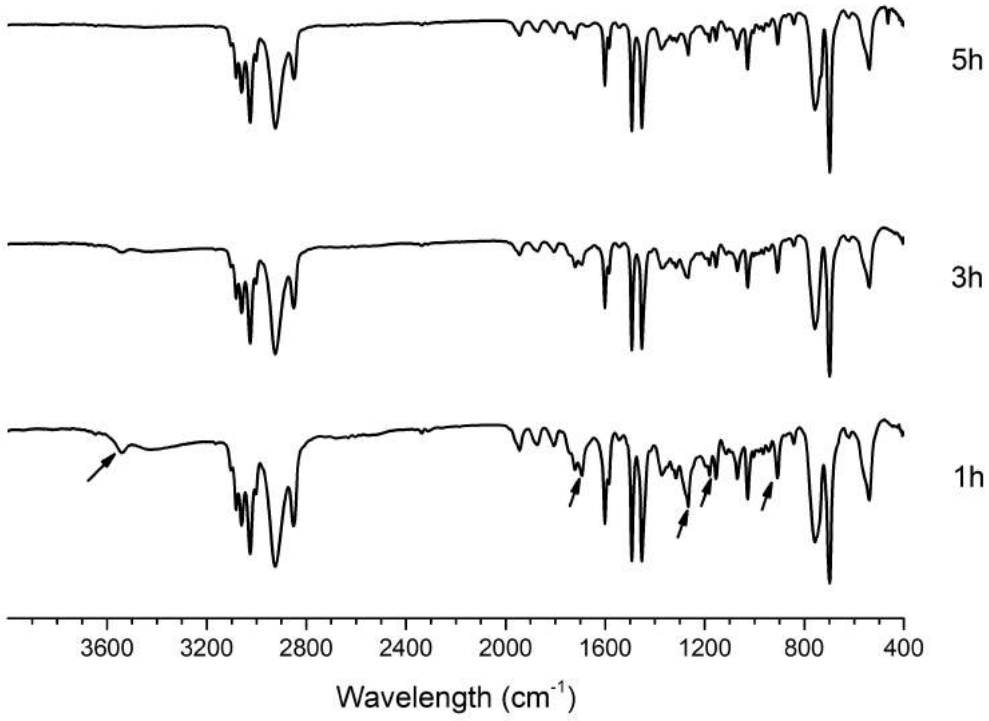


Figure 5.24: FTIR spectra of poly(styrene-co-cardanol) samples prepared with 2.5 wt% of cardanol at 85 °*C* and different reaction times.

For reactions performed with 2.5 wt % of cardanol at 110 °*C* (Figure 5.25), the reduction of the hydroxyl peak around 3500 $cm^{-1}$ did not occur. However, peaks from 3200 - 2800 $cm^{-1}$ resembled the peaks of pure polystyrene, indicating higher styrene incorporation in the polymer molecules. The increase of the intensity of peaks placed between 2000 - 1650 $cm^{-1}$ and related to the aromatic ring also shows the higher styrene incorporation. One cannot notice the increase of the peak located at 1700 $cm^{-1}$, which corresponds to the carbonyl bond that would be formed by the phenolic inhibition. Peaks at 750 and 550 $cm^{-1}$ were not present in the polystyrene spectrum, showing that a different structure was present. Therefore, these peaks might be related with the formation of different chemical bonds with cardanol. The peaks placed at 1000-800 $cm^{-1}$

should present lower intensities, as they are related with the terminal double bonds and the cardanol concentration. The observed increase may indicate the incorporation of cardanol though unknown reaction mechanisms. A similar behavior was observed with 10 wt% of cardanol at 110 °C (Figure 5.26) and with 5 wt% of cardanol at the same temperature. But, for these cases, a slight reduction of the peaks placed at 3600, 1250 and 1190 $cm^{-1}$ was observed. One cannot notice the increase of the peak at 1700 $cm^{-1}$, which corresponds to the carbonyl bond. So, the obtained FTIR data suggest that the hydroxyl group is a radical inhibitor and is consumed during the reaction course.

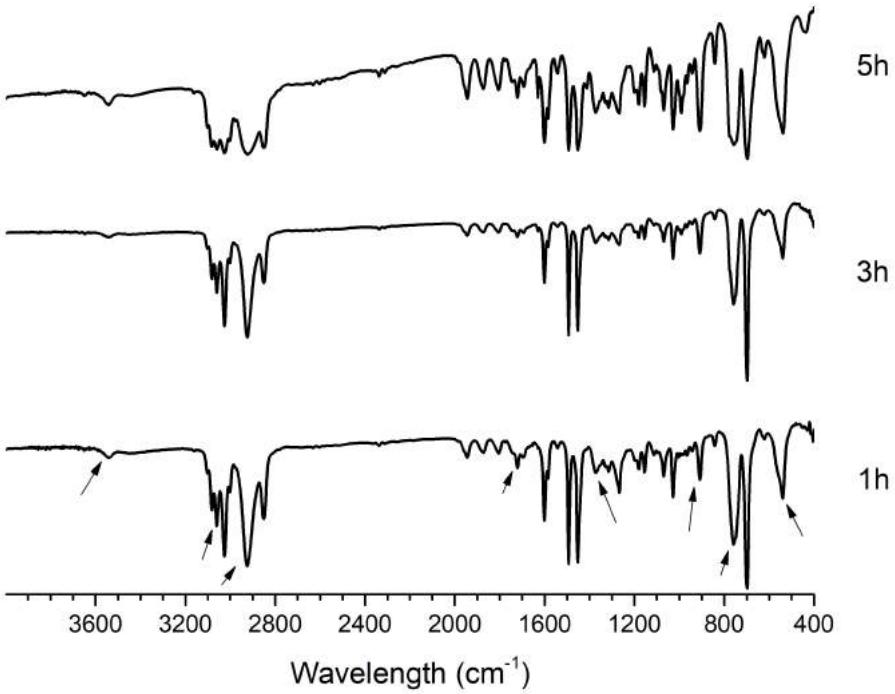


Figure 5.25: FTIR spectra of poly(styrene-co-cardanol) samples prepared in reactions with 2.5 wt% of cardanol at 110 °*C*.

Finally, as purified copolymer samples were needed to evaluate the copolymer composition (as calculated by $^1$H-NMR), additional FTIR analyses were performed with the reprecipitated copolymer samples for reactions performed at 110 °C. The new FTIR spectra were very similar to each other and the peak placed at 3600 $cm^{-1}$ disappeared, although the other peaks located at 1400 – 800 $cm^{-1}$ remained with smaller intensity. Besides, when comparative analyses were performed between the FTIR spectra of polystyrene and of the copolymers, significant differences were observed because the linear correlations ($R^2$) calculated were very far from 1 (0.30 for 2.5 wt%; 0.21 for 5.0 wt%; 0.43 for 10 wt%). Graphic comparisons are present in the Appendix. Therefore, despite the difficulty to analyze the FTIR spectra of the copolymers, as peaks over-

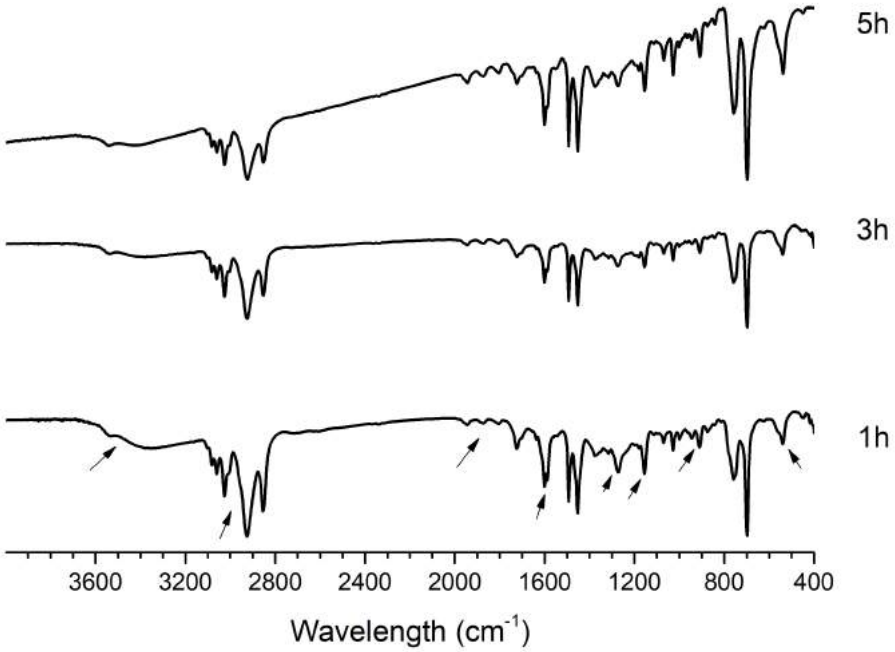


Figure 5.26: FTIR spectra of poly(styrene-co-cardanol) samples prepared in reactions with 10 wt% of cardanol at 110 °*C*.

lapped, it seems clear that structural modifications of the molecules were caused by the copolymerization.

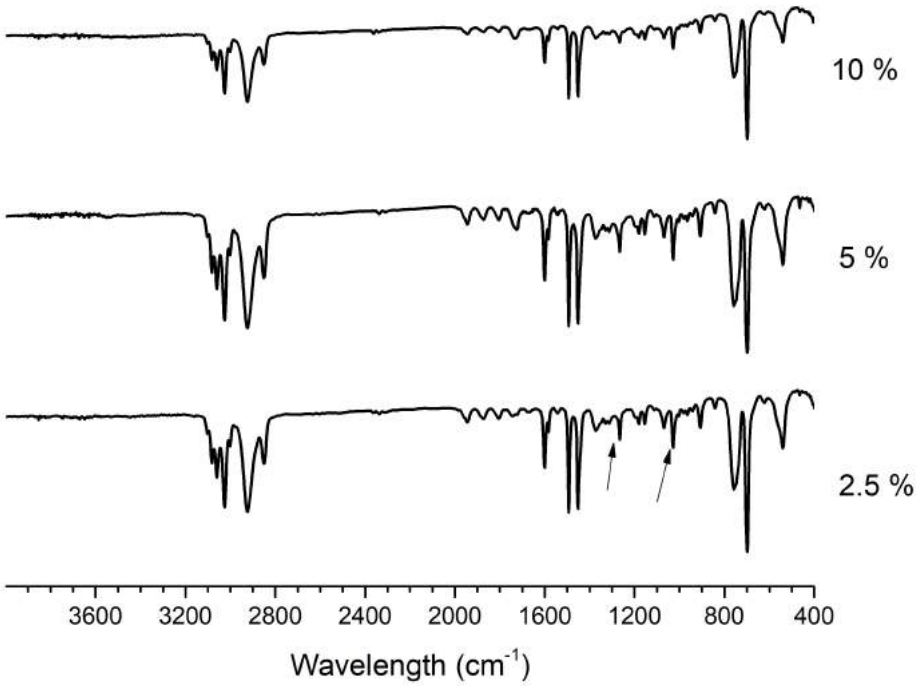


Figure 5.27: FTIR spectra of reprecipitated poly(styrene-co-cardanol) samples prepared at 110 °*C*.

## 5.4 Copolymerization of cardanol and MMA

MMA (Figure 5.28) is a vinyl monomer used for manufacture of PMMA. PMMA is amorphous, presents high strength and has excellent dimensional stability due to its rigid polymer chains (ODIAN, 2004). Additionally, PMMA has exceptional clarity, very good weatherability, good impact resistance, it can be machined and is resistant to most chemicals, although it can be attacked by different organic solvents. For these reasons, PMMA finds inumerous commercial applications, particularly in the biomedical field.

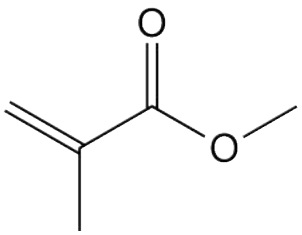


Figure 5.28: Molecular structure of methyl methacrylate

Copolymerizations of cardanol with MMA were performed at 85 and 110 °*C*. Figure 5.29 presents monomer conversions and average molecular weights for P(MMA-*co*-C) at 85 °*C*. Although complete MMA conversion could be obtained in less than one hour,

it took almost 2 and 4 hours to reach complete monomer conversion when for 2.5 wt % and 5 wt % of cardanol were added, respectively. The average molecular weights were also reduced when cardanol was added due to cardanol inhibitory effect. Therefore, the observed kinetic effects were similar in reactions performed with styrene.

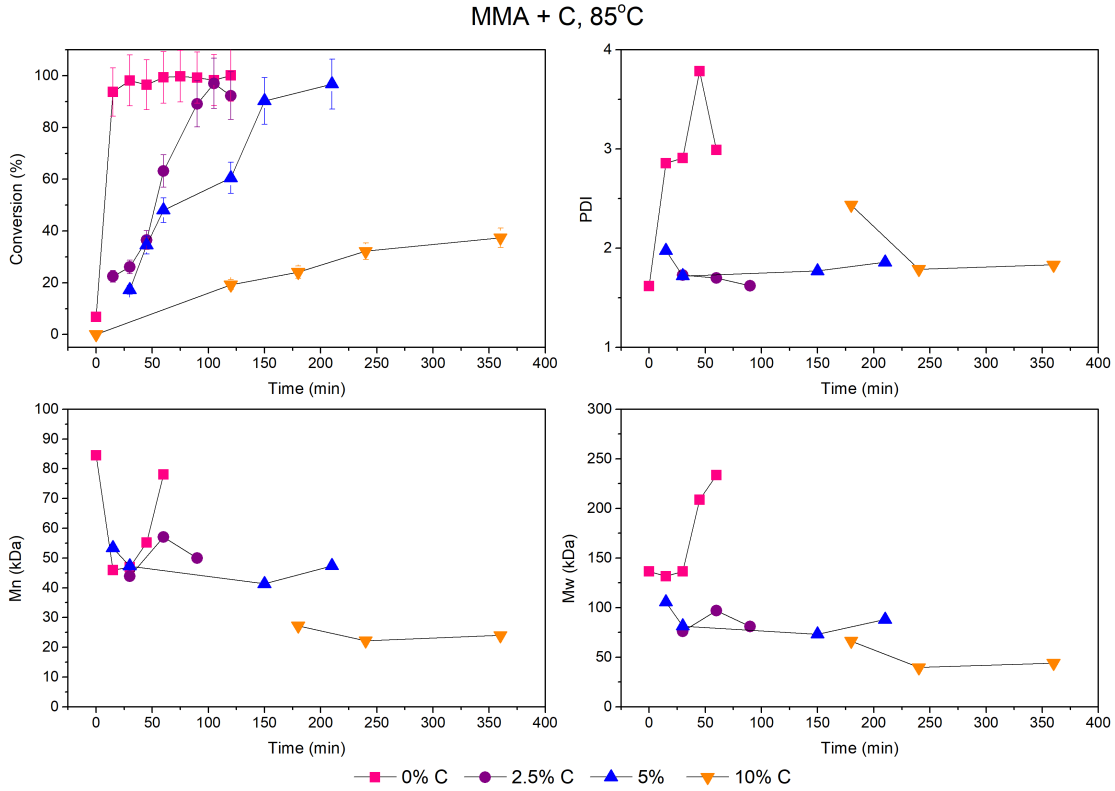


Figure 5.29: Monomer conversions and average molecular weights of samples collected at 85 °*C* in copolymerizations of MMA and cardanol.

At 110 °*C*, the retardant effect could also be noticed, although reaction rates were higher. When 10 wt% of cardanol was added, conversions reached 60% and stabilized, as MMA does not polymerize spontaneously like styrene. Reactions with the internal unsaturations and the phenolic group are the causes for retardation and inhibition as they form stable radicals.

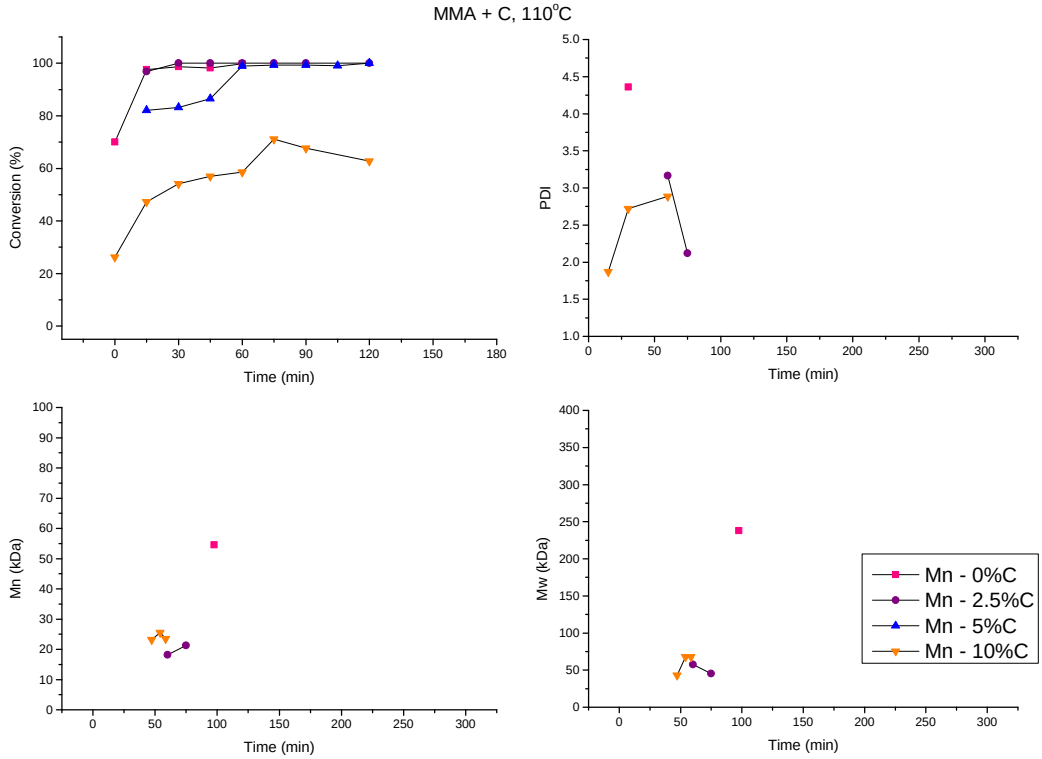


Figure 5.30: Monomer conversions and average molecular weights of samples collected at 110 °*C* in copolymerizations of MMA and cardanol.

Despite the decrease of the reaction rates, the addition of cardanol increased the polymer thermal stabilities as detected by TGA analyses. Figures 5.31 and 5.32 show that cardanol volatilizes around 250 °*C*, which is roughly the same temperature at which PMMA begins to degrade. However, for copolymers, the degradation starts afterwards and fully degrades around 450 °*C*, which is a very positive and interesting effect that has never been reported before. Therefore, TGA curves are shifted to the right (in direction of higher temperatures). The observed degradation of PMMA was similar to others reported in the literature (FERRIOL *et al.*, 2003). Although two degradation stages can be clearly seen, there are in fact three degradation stages. The first step (close to 165 °*C*) is initiated by scissions of head-to-head linkages, as the bond dissociation energy of these linkages are lower due to occurrence of steric hindrance and inductive effect of vicinal ester groups (KASHIWAGI *et al.*, 1986). The second degradation step for PMMA (around 270 °*C*) is related to the unsaturated ends (resulting from termination by disproportionation) and involves the homolytic scission of the vinyl group (MANRING *et al.*, 1989). The last degradation step for PMMA (around 350 °*C*) is related to the random scission of the polymer chain. Apparently, the presence of small amounts of cardanol in the backbone causes significant changes of the PMMA thermal degradation mechanism preventing the homolitic $\beta$-scission of the terminal vinyl group. Due to the inhibitory effects, it is plausible to assume that cardanol molecules

occupy the extremities of many polymer chains, inhibiting the second characteristic PMMA degradation step.

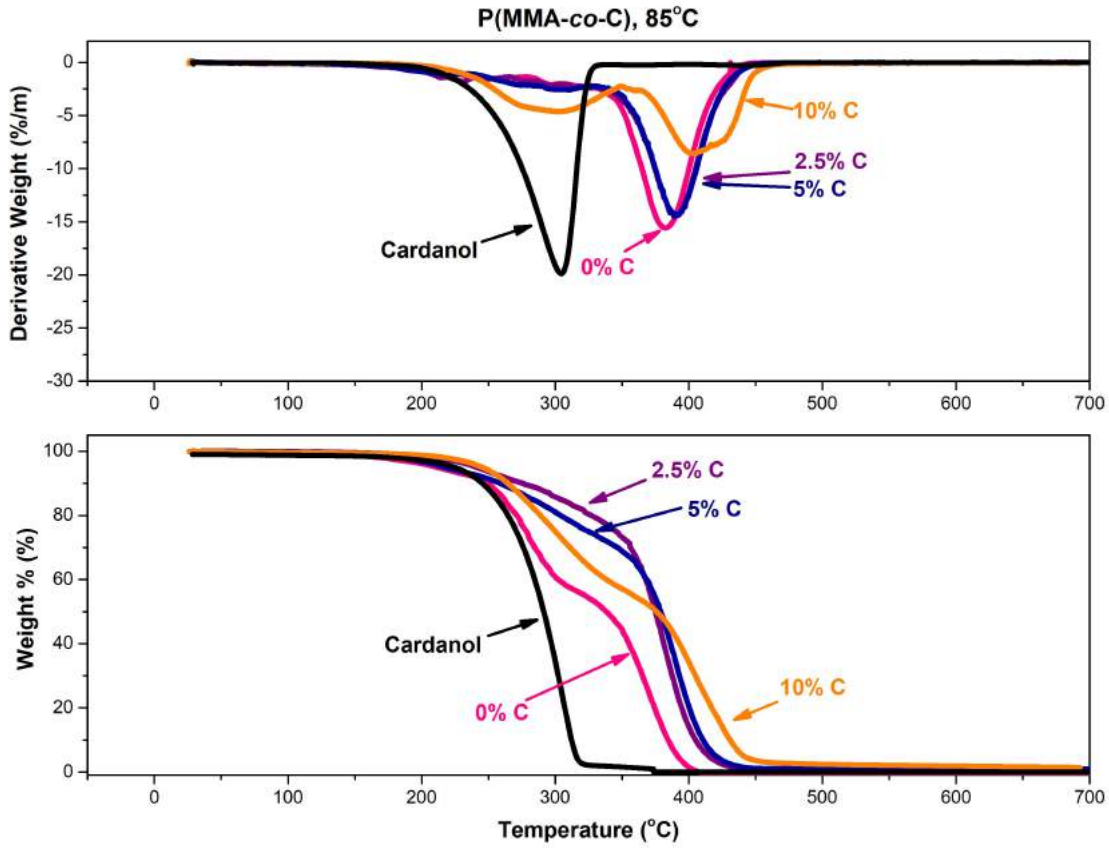


Figure 5.31: TGA and DTG thermograms of samples collected after 2 hours for 0 and 2.5 wt% of cardanol, after 4 hours for 5 wt% of cardanol and after 6 hours of reaction for 10 wt% of cardanol at 85 °*C* in copolymerizations of MMA and cardanol.

In addition, due to the long side chain of cardanol, it exerts some plastificant effect, reducing the glass transition temperature ($T_g$) of copolymer samples, as shown in Table 5.6. When 10 wt % of cardanol was used, the $T_g$ could not be detected, as it was probably lower than 0 °*C* (the polymer was completely flexible at room temperature).

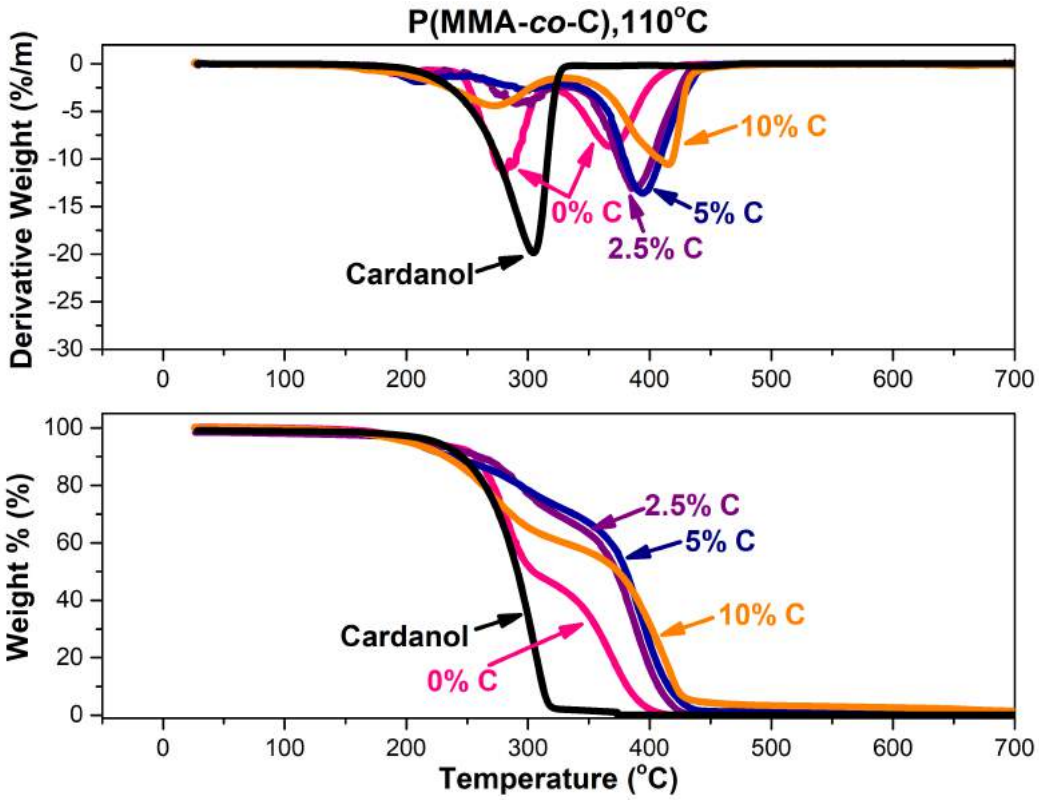


Figure 5.32: TGA and DTG curves thermograms of samples collected after 2 hours of reaction at 110 °*C* in copolymerizations of MMA and cardanol.

Table 5.6: Glass transition temperatures of samples collected after 2, 4 and 6 hours of reaction for 0 and 2.5 wt%, 5 wt% and 10 wt% of cardanol respectively at 85 °*C* in copolymerizations of MMA and cardanol, and also for samples collected after 2 hours of reaction at 110 °*C*.

| | **85 °C** | **110 °C** |
|---|---|---|
| **0%** | 104.8 | 105.3 |
| **2.5%** | 84.92 | 84.13 |
| **5%** | 72.36 | 71.25 |
| **10%** | - - - | - - - |

FTIR analyses of the final reaction products were performed (Figures 5.33 and 5.34). The largest difference between the FTIR spectra of PMMA and of the copolymers was the presence of the peak at 3450 $cm^{-1}$, related to the phenolic group. It was not possible to see the presence of the carbonyl group (C=O) that might have been formed after hydrogen donation by the phenolic moiety around 1700 $cm^{-1}$, as this bond overlap with characteristic bonds of PMMA. At 85 °*C* (Figure 5.33), although some reaction with the hydroxyl group may have taken place, the peak was still present with 5 wt% (that reached full conversion) and for 10 wt% of cardanol. So this functional group may still be used for functionalization of the polymers. However, at 110 °C (Figure 5.34), the presence of the phenolic group was much less significant, indicating additional -OH consumption. Thus, although the inhibitory effect was not so intense, radicals were probably suppressed through reactions with the phenolic group.

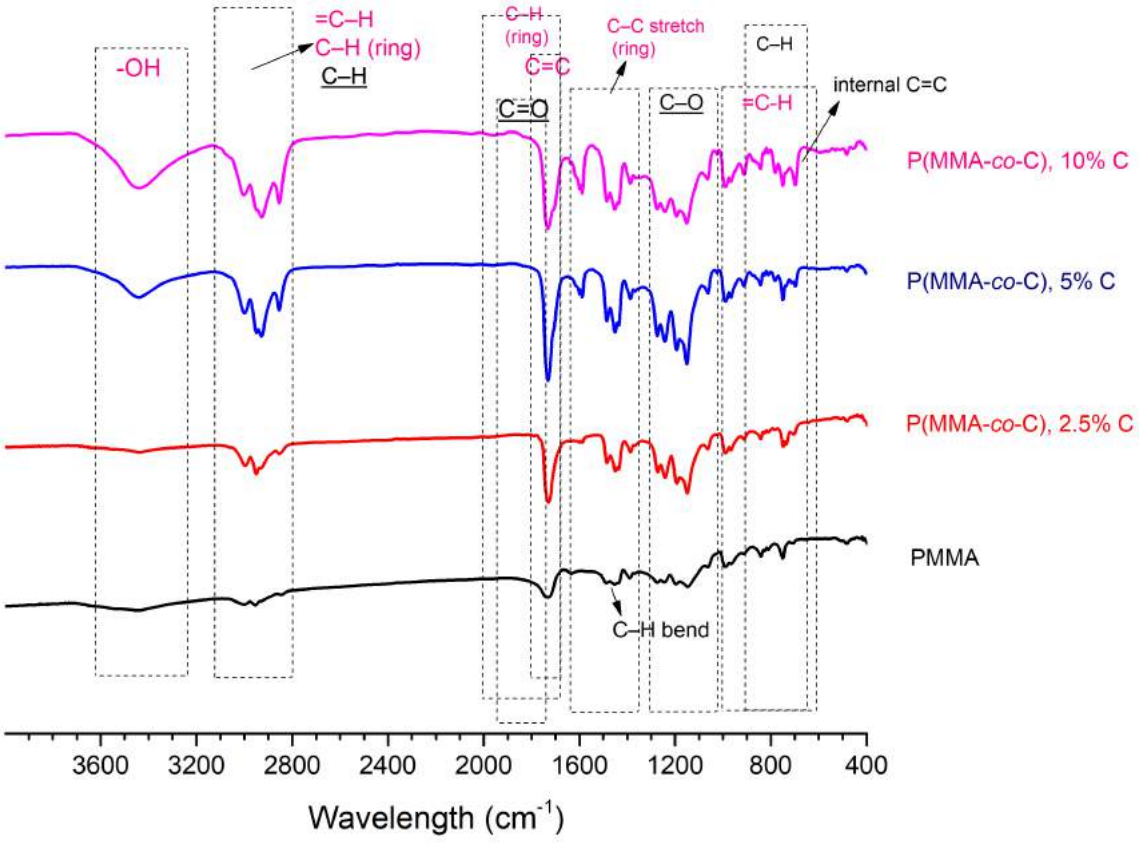


Figure 5.33: FTIR spectra for the final reaction product at 85 °*C* in copolymerizations of MMA and cardanol.

Comparing FTIR spectra collected at different times for reactions performed with 5 wt% of cardanol at 85 °C, the peaks remained essentially constant, with linear correlation of 0.99 between spectra collected after 30 minutes and 1h 30, and of 0.96 for spectra collected after 30 min and 3h of reaction. Graphic comparisons are present in the Appendix. The main difference was observed at 1700 $cm^{-1}$, which corresponds to the unsaturation of cardanol and the C=O bond of MMA, indicating changes of the

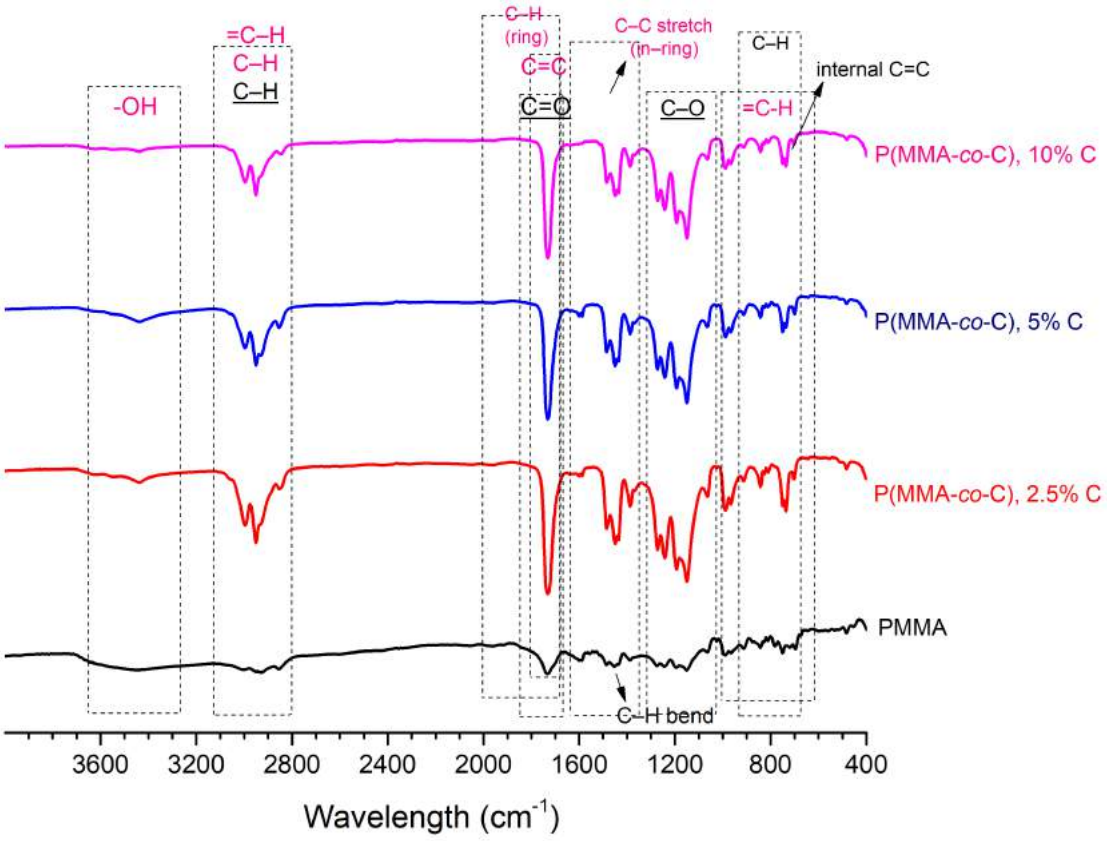


Figure 5.34: FTIR spectra for the final reaction product at 110 °*C* in copolymerizations of MMA and cardanol.

copolymers composition. Therefore, this indicates the increase of the MMA composition in the copolymer, meaning that cardanol is incorporated faster initially and that MMA molecules are incorporated more efficiently after consumption of cardanol.

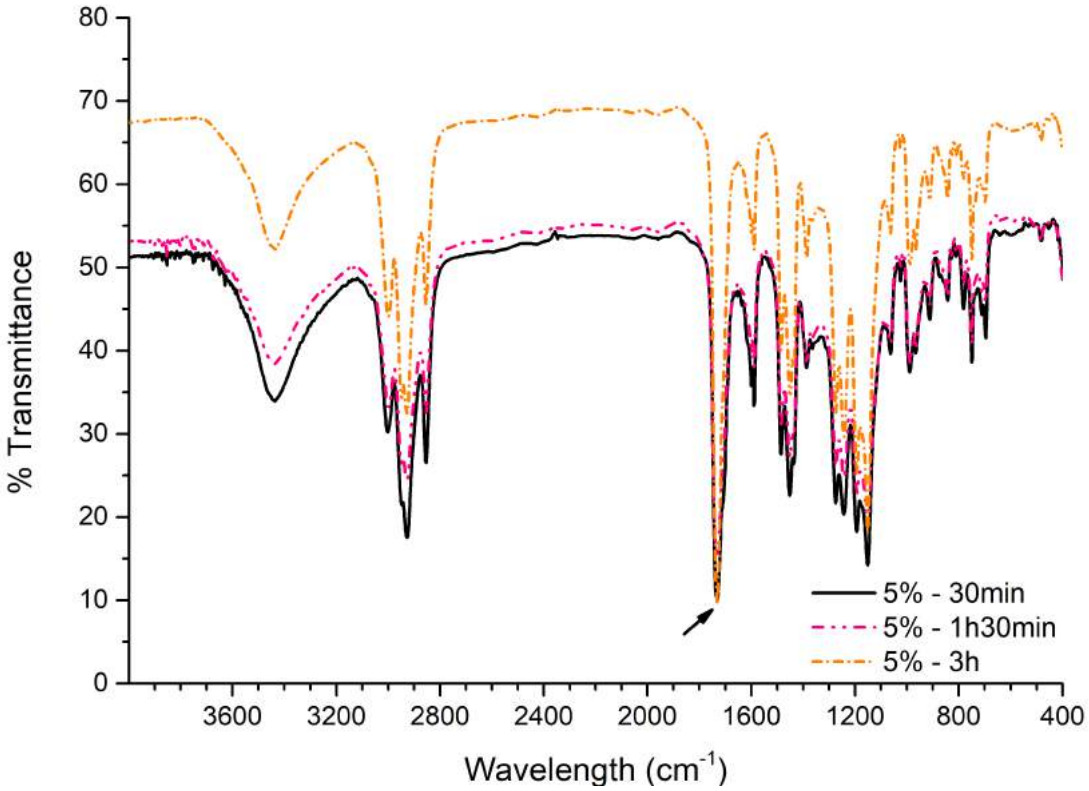


Figure 5.35: FTIR spectra for the samples collected after 30, 1h 30 and 3 hours of reaction at 85 °*C* in copolymerizations of MMA with 5 wt% of cardanol.

In order to evaluate the copolymer composition, $^{1}$H-NMR analyses were performed and the areas of the peaks *m* and *f* of cardanol were compared. Figure 5.36 shows the spectrum of P(MMA-*co*-C) prepared at 85 °*C* with 5 wt% of cardanol as an example. The other spectra are presented in the Appendix. As *m* represents three hydrogens, while *f* represents two, the following equations were used to calculate the copolymer composition as molar and mass fractions:

$$\varphi_C(mol\,\%) = \frac{(f/2)}{(f/2)+(m/3)} \tag{5.3}$$

$$\omega_C(wt\,\%) = \frac{\frac{\varphi_C}{MW_{MMA}}}{\frac{1}{MW_C}+\varphi_C(\frac{1}{MW_{MMA}}-\frac{1}{MW_C})} \tag{5.4}$$

However, as some unreacted cardanol could still be present within the polymeric samples, they were dissolved in toluene and precipitated in methanol. The values of the copolymer compositions before and after purification are shown in Tables 5.7 and 5.8. Significant differences were observed for reactions performed with 10 wt% of cardanol. Surprisingly, reactions performed at 110 °*C* incorporated less cardanol than

Table 5.7: Copolymer compositions of final polymer samples collected at 85 °C in copolymerizations of MMA and cardanol.

| | Not Reprecipitated | | Reprecipitated | |
|---|---|---|---|---|
| | Mol (%) | Mass (%) | Mol (%) | Mass (%) |
| 2.5 | 0.01 | 1.32 | 0.01 | 1.30 |
| 5 | 0.03 | 2.87 | 0.03 | 2.87 |
| 10 | 0.19 | 18.93 | 0.02 | 2.40 |

Table 5.8: Copolymer compositions of samples collected after 2 hours of reaction at 110 °*C* in copolymerizations of MMA and cardanol.

| | Not Reprecipitated | | Reprecipitated | |
|---|---|---|---|---|
| | Mol (%) | Mass (%) | Mol (%) | Mass (%) |
| 2.5 | 0.02 | 1.79 | 0.01 | 1.32 |
| 5 | 0.04 | 4.38 | 0.01 | 1.44 |
| 10 | 0.12 | 13.29 | 0.01 | 1.20 |

reactions performed at 85 °*C*, due to the higher MMA conversion. One must notice at every spectrum that the relative proportion between peaks *d/f*, *c/f* or *b/f* decreased in the copolymers, meaning that reactions through cardanol unsaturations took place. It is interesting to observe, though, that although the cardanol incorporation at 110 °*C* was relatively smaller, similar $T_g$ values were obtained for copolymers prepared with similar cardanol contents at both temperatures. This possibly indicates the plasticizing effect of the pendant side chain of cardanol.

FTIR analyses were performed for the purified copolymer samples prepared at 110 °C (Figure 5.37) and the three spectra looked similar. Although the peak placed at 3600 $cm^{-1}$ disappeared, other peaks were more intense than in the spectrum of pure PMMA. For example, peaks placed at 3100-2800 $cm^{-1}$ are clearly present. Comparing the FTIR spectra of samples with different cardanol concentrations, the linear correlations ($R^2$) were high ($R^2$ = 0.9487 for 2.5 wt% and 5 wt%, $R^2$ = 0.9249 for 2.5 wt% and 10 wt%, $R^2$ = 0.9872 for 5 and 10 wt%), showing the copolymers presented similar compositions, as shown in Tables 5.7 and 5.8. Comparing the linear correlation values of FTIR spectra of samples that were reprecipitated versus not-reprecipitated, the observed values were $R^2$ = 0.9196 for 2.5 wt%, $R^2$ = 0.9727 for 5 wt% and $R^2$ = 0.2989 for 10 wt% of cardanol. Graphic comparisons are presented in the Appendix. The obvious non-linear correlation for samples prepared with 10 wt% of cardanol is due to the presence of excess residual cardanol before purification.

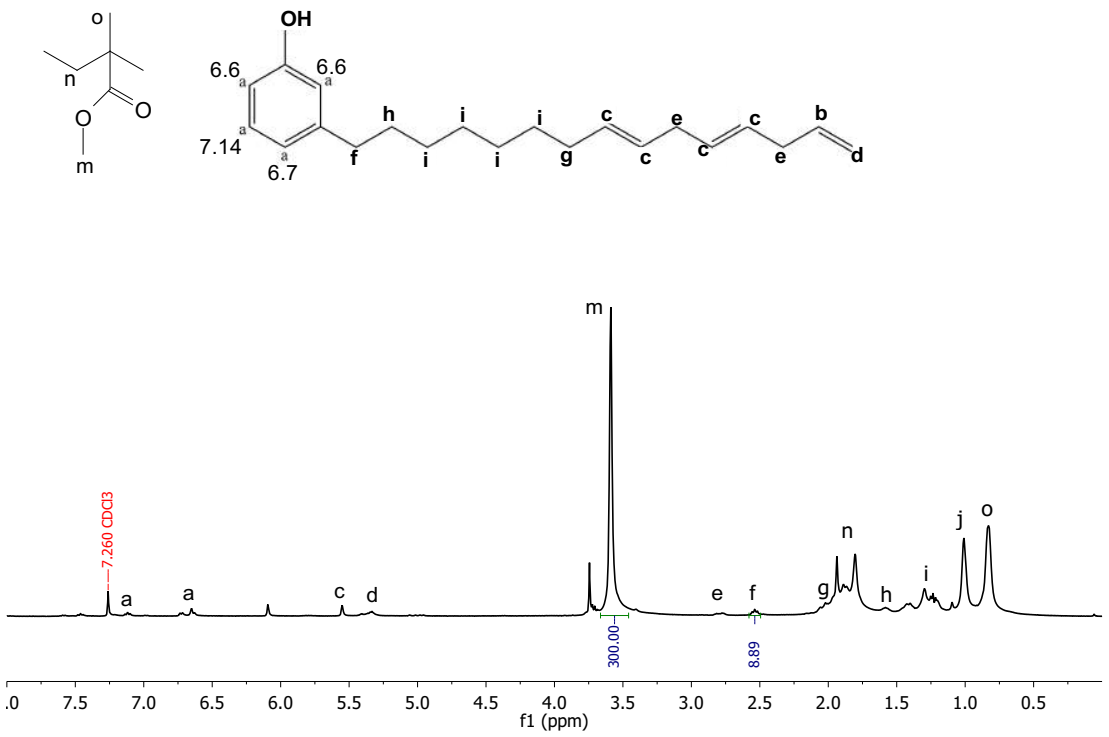


Figure 5.36: $^{1}$ H NMR spectrum of P(MMA-*co*-C) prepared with 5 wt% of cardanol at 110 °C after 2 hours of reaction.

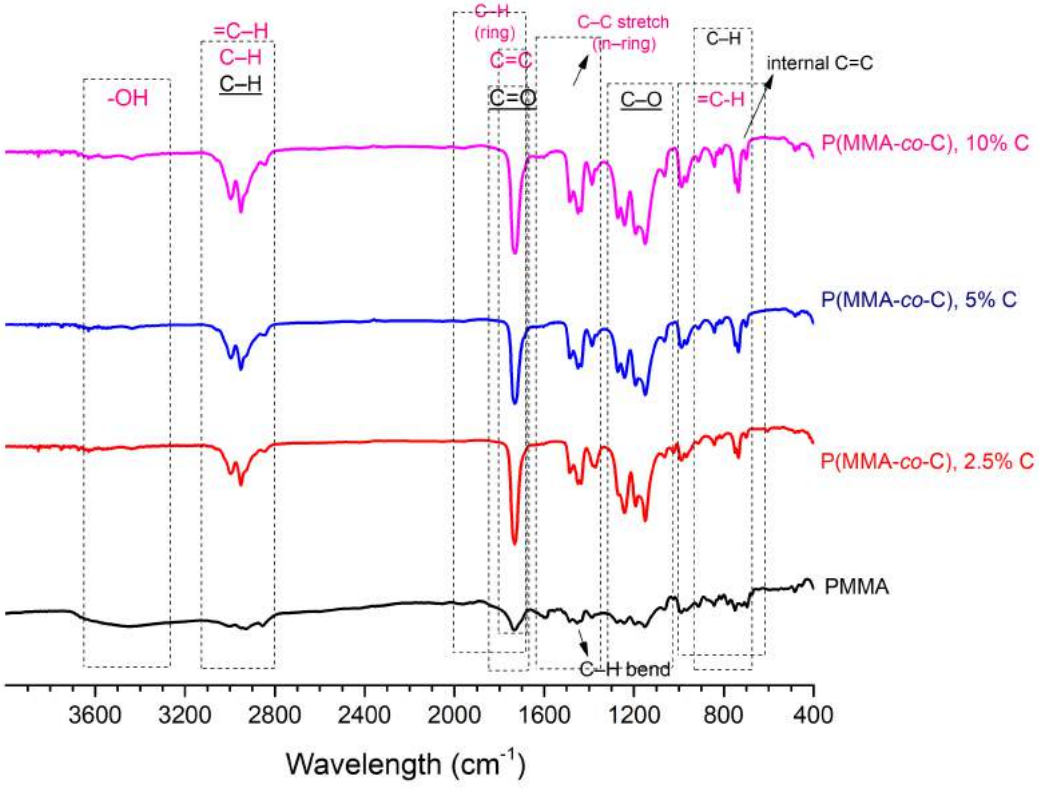


Figure 5.37: FTIR spectroscopy for purified samples of P(MMA-*co*-C), 110 °*C*

## 5.5 Copolymerization of natural CNSL and MMA

In order to compare the reactivities of anacardic acid and cardanol, copolymerizations with natural CNSL and MMA were performed at the same conditions analyzed previously. Figure 5.38 shows the conversions at 85 °*C* and 110 °*C*. Although conversions were similar for cardanol and natural CNSL at both temperatures (Figures 5.39 and 5.40), the copolymerizations with natural CNSL were faster at 85 °*C*, when the highest inhibitory effect was observed. This is interesting because natural CNSL also contains cardol (< 21 wt %) and 2-methyl cardanol (< 4 wt %). Perhaps, the presence of the carboxylic group affects the inhibitory effect of the phenolic group, as both groups are electronegative and prone to proton donation. Tables 5.9 and 5.10 presents the average molecular weights for MMA/CNSL copolymer samples. The average molecular weights obtained for the this system was similar to those average molecular weights of samples in copolymerizations of MMA and cardanol.

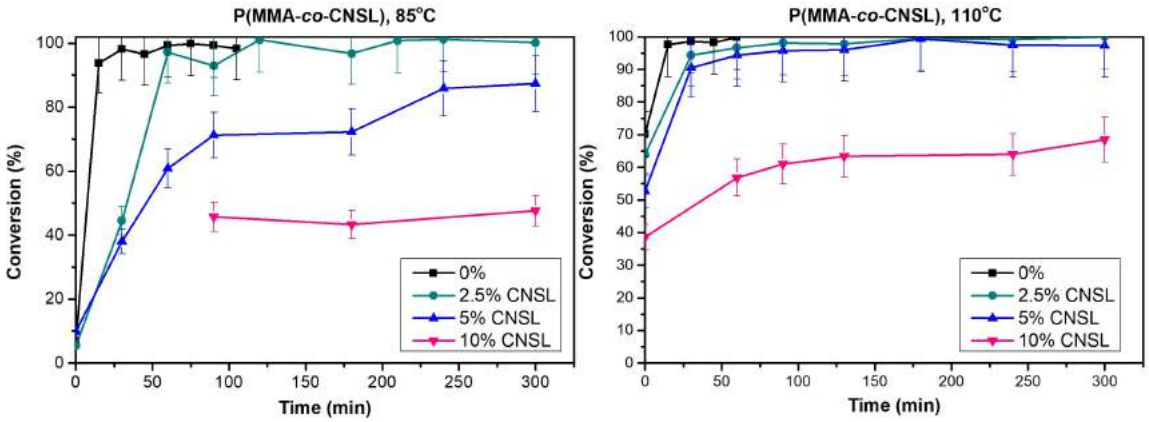


Figure 5.38: Monomer conversions of samples collected at 85 and 110 °*C* in copolymerizations of MMA and CNSL.

Table 5.9: Average molecular weights for samples collected at 85 °C in copolymerizations of MMA and CNSL.

| | **2.5 wt% of CNSL** | | |
|---|---|---|---|
| Time (min) | Mn (Da) | Mw (Da) | PDI |
| 300 | 47187 | 96736 | 2.05 |
| | **5 wt% of CNSL** | | |
| Time (min) | Mn (Da) | Mw (Da) | PDI |
| 300 | 27906 | 42938 | 1.539 |
| | **10 wt% of CNSL** | | |
| Time (min) | Mn (Da) | Mw (Da) | PDI |
| 300 | 20785 | 27509 | 1.323 |

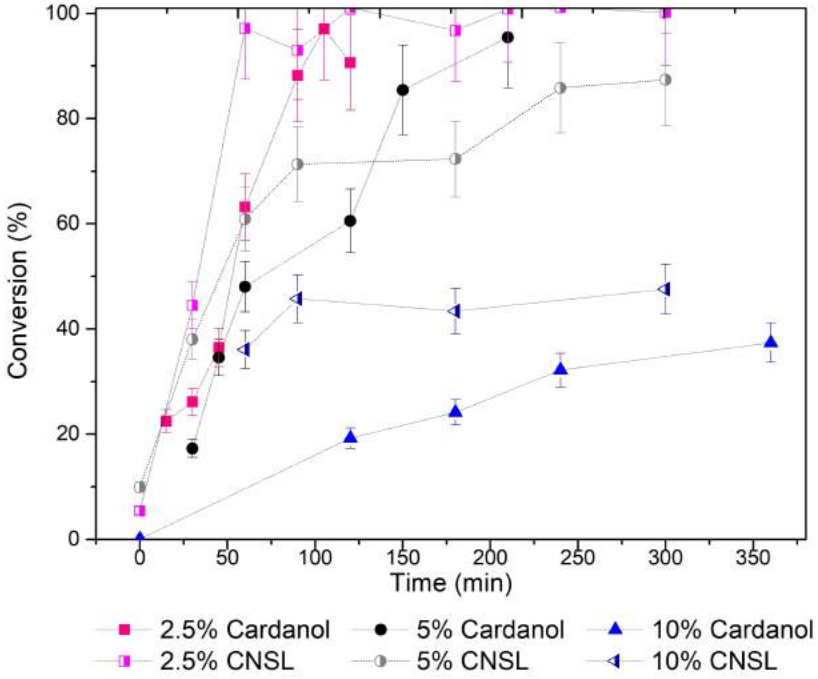


Figure 5.39: Monomer conversions of samples collected at 85 °*C* in copolymerizations of MMA and CNSL and also MMA and cardanol.

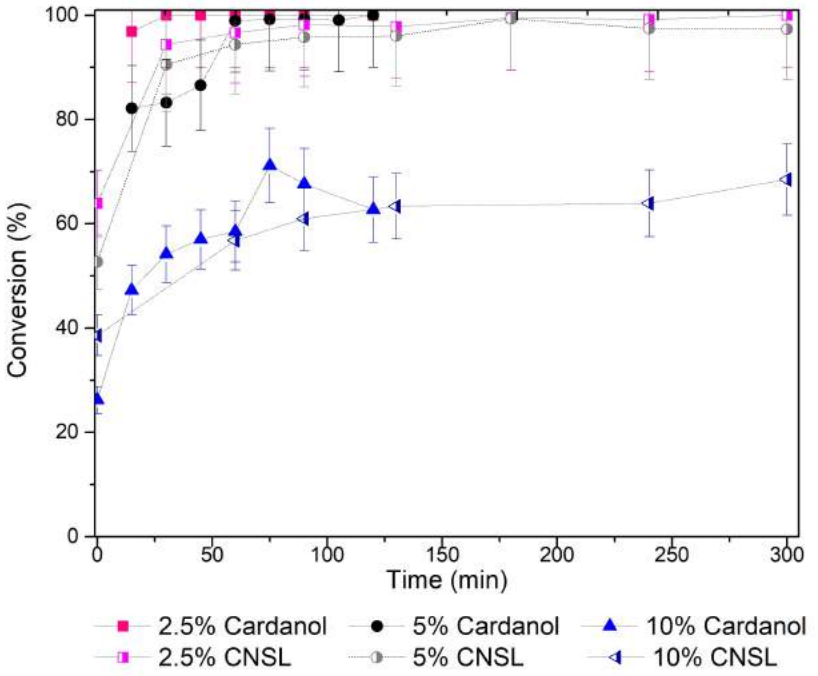


Figure 5.40: Monomer conversions of samples collected at 110 °*C* in copolymerizations of MMA and CNSL and also MMA and cardanol.

When it comes to thermal stability, CNSL helps to improve the thermal stability even more than cardanol. Figures 5.41 and 5.42 present TGA curves for the polymers prepared at 85 °*C* and 110 °*C* respectively. While PMMA degrades at approximately 400 °*C*, the copolymers degraded only over 425 °*C*, shifting the TGA curves to the right

Table 5.10: Average molecular weights for samples collected at 110 °C in copolymerizations of MMA and CNSL.

| | **2.5 wt% of CNSL** | | |
|---|---|---|---|
| Time (min) | Mn (Da) | Mw (Da) | PDI |
| 90 | 30453 | 79561 | 2.613 |
| | **5 wt% of CNSL** | | |
| Time (min) | Mn (Da) | Mw (Da) | PDI |
| 30 | 33075 | 64521 | 1.951 |
| 90 | 34208 | 74503 | 2.178 |
| | **10 wt% of CNSL** | | |
| Time (min) | Mn (Da) | Mw (Da) | PDI |
| 90 | 33697 | 54915 | 1.63 |

(in direction of higher temperatures). Also, the first stage of degradation of PMMA was significantly reduced. Based on the TGA thermograms, it can be affirmed that a copolymer was formed due to the significant changes observed in the TGA curves.

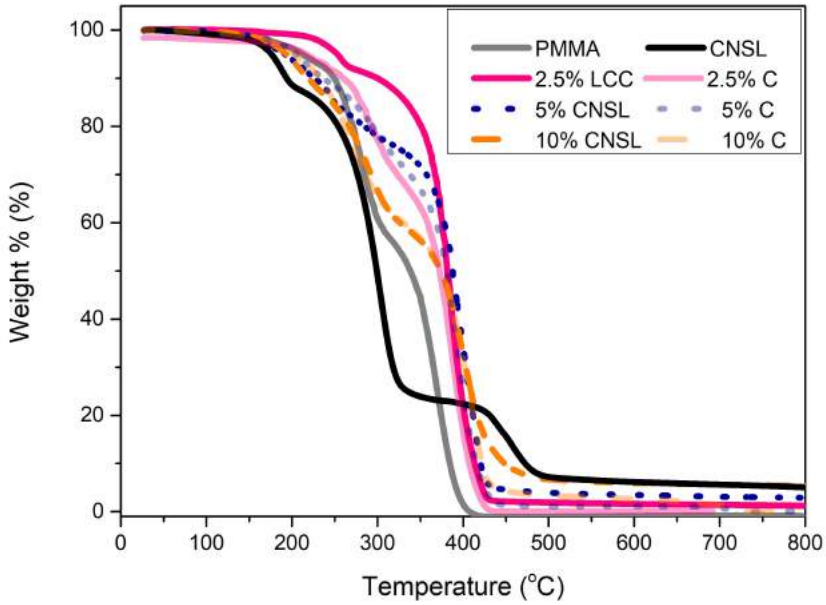


Figure 5.41: TGA thermograms of final reaction products collected at 85 °*C* in copolymerizations of MMA and natural CNSL and also for copolymerizations of MMA and cardanol.

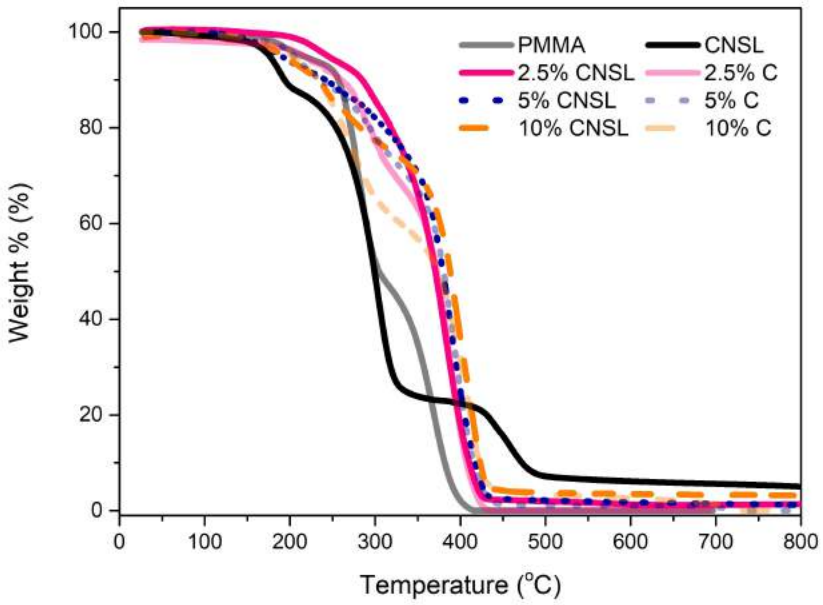


Figure 5.42: TGA thermograms of final reaction products collected at 110 °*C* in copolymerizations of MMA and natural CNSL and also for copolymerizations of MMA and cardanol.

DSC analyses (Table 5.11) showed the glass transition temperature ($T_g$) decreased with the addition of CNSL because of the incorporation of anacardic acid and the other CNSL compounds. This occurred due to the presence of the long side, which increases the mobility of the polymer chains, reducing the $T_g$. The $T_g$ for sample prepared with 10 wt% of CNSL at 85 °*C* was not obtained because it was lower than 0 °*C*. $^1$H-NMR was performed for only one sample of P(MMA-*co*-CNSL) prepared with 10 wt% of CNSL at 110 °*C* (Figure 5.43). Using Equations 5.3 and 5.4, the CNSL composition in the copolymer corresponded to 2.75 wt% in mass, roughly the double of the composition obtained with cardanol. This constitutes an additional evidence of the slightly higher reactivity of the CNSL mixture in respect to cardanol.

Table 5.11: Glass transition temperatures of the final reaction products collected at 85 and 110 °C of MMA and CNSL polymerizations.

| | **85 °C** | **110 °C** |
|---|---|---|
| **0%** | 104.8 | 105.3 |
| **2.5%** | 101.67 | 98.00 |
| **5%** | 68.37 | 88.08 |
| **10%** | - - - | 60.43 |

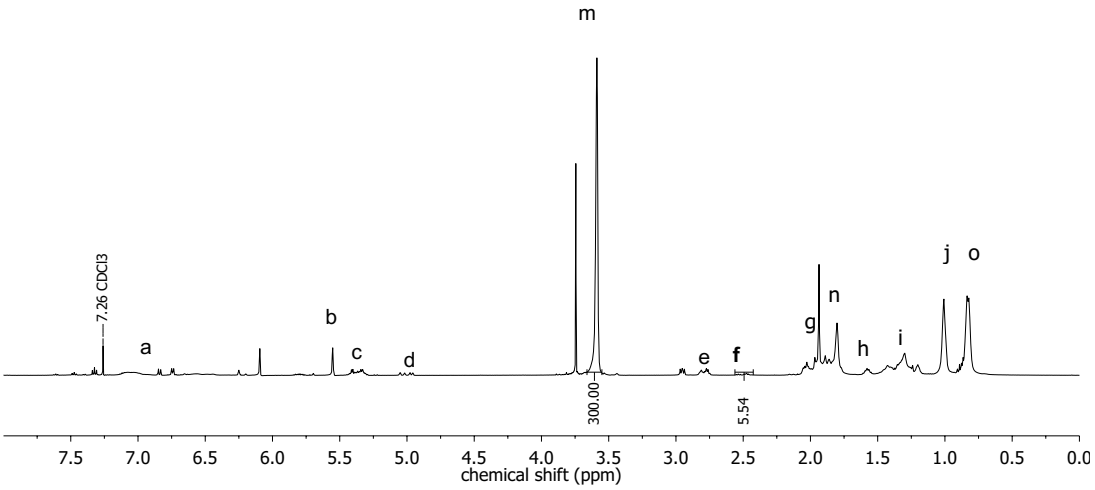


Figure 5.43: $^{1}$H-NMR spectrum of P(MMA-*co*-C) prepared with 10 wt% of cardanol at 110 °*C* after 5 hours of reaction

## 5.6 Copolymerization of cardanol and vinyl acetate

Poly(vinyl acetate) (PVA or PVAc) is a polymer known for its adhesive properties. Its molecular structure is presented in Figure 5.44. It belongs to the poly(vinyl esters) family and is a type of thermoplastic. Copolymerizations of vinyl acetate and cardanol were performed at 70, 85 and 110 °*C*. However, at 110 °*C* the acquired conversion and average molecular weight data were bad because the boiling temperature of vinyl acetate is 72.7 °*C* and the glass tubes, although threaded, could not avoid evaporation. For this reason, some characterizations revealed irregular patterns were and not trustable. Some results obtained at 85 °*C* were also poor and were removed from the discussion. At 70 °*C*, the reaction rates were significant low and monomer conversion reached a maximum of 20% after 5 hours of reaction even without the presence of cardanol. Figure 5.45 shows the monomer conversion and average molecular weights of samples prepared at 85 °*C*. As also noticed for copolymerizations with styrene and methyl methacrylate, cardanol retards the polymerization, limiting the monomer conversion to 50% even when the smallest concentration of cardanol was used. Values of average molecular weights were also very small in presence of cardanol. Therefore, the cardanol inhibition effect was much more pronounced in vinyl acetate copolymerizations than in other analyzed reactions.

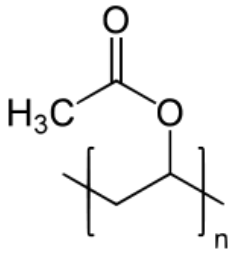


Figure 5.44: Molecular structure of poly(vinyl acetate)

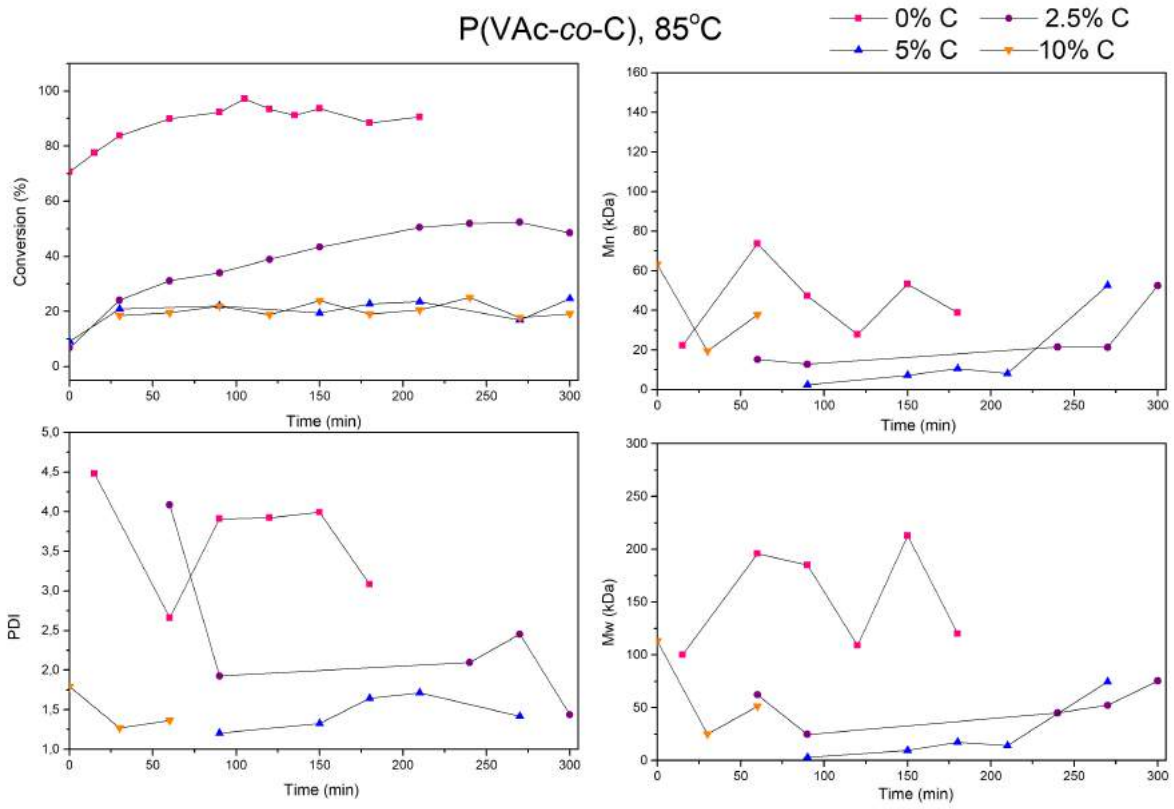


Figure 5.45: Monomer conversions and average molecular weights for samples collected at 85 °*C* in copolymerizations of VAc and cardanol.

Based on the NMR data, copolymer compositions could be calculated with help of Equations 5.5 and 5.6, as shown in 5.12. The $^{1}$H NMR spectrum for the copolymer prepared with 5 wt% of cardanol is shown in Figure 5.46. The higher amounts in the obtained products can indicate a strong inhibitory effect of cardanol in the VAc polymerization. For 10 wt%, a high amount of residual cardanol is present because conversion was small and the vinyl acetate not reacted, but cardanol remained in the copolymer sample.

$$\varphi_C(mol\,\%) = \frac{(f/2)}{(f/2)+(m/3)} \tag{5.5}$$

Table 5.12: Copolymer compositions of samples collected at 85 °*C* in copolymerizations of VAc and cardanol.

| | mol (%) | mass (%) |
|---|---|---|
| 2.5% C | 0.04 | 3.85 |
| 5.0% C | 0.12 | 12.96 |
| 10% C | 0.49 | 76.32 |

$$\omega_C(wt\%) = \frac{\frac{\varphi_C}{MW_{VAc}}}{\frac{1}{MW_C} + \varphi_C(\frac{1}{MW_{VAc}} - \frac{1}{MW_C})} \tag{5.6}$$

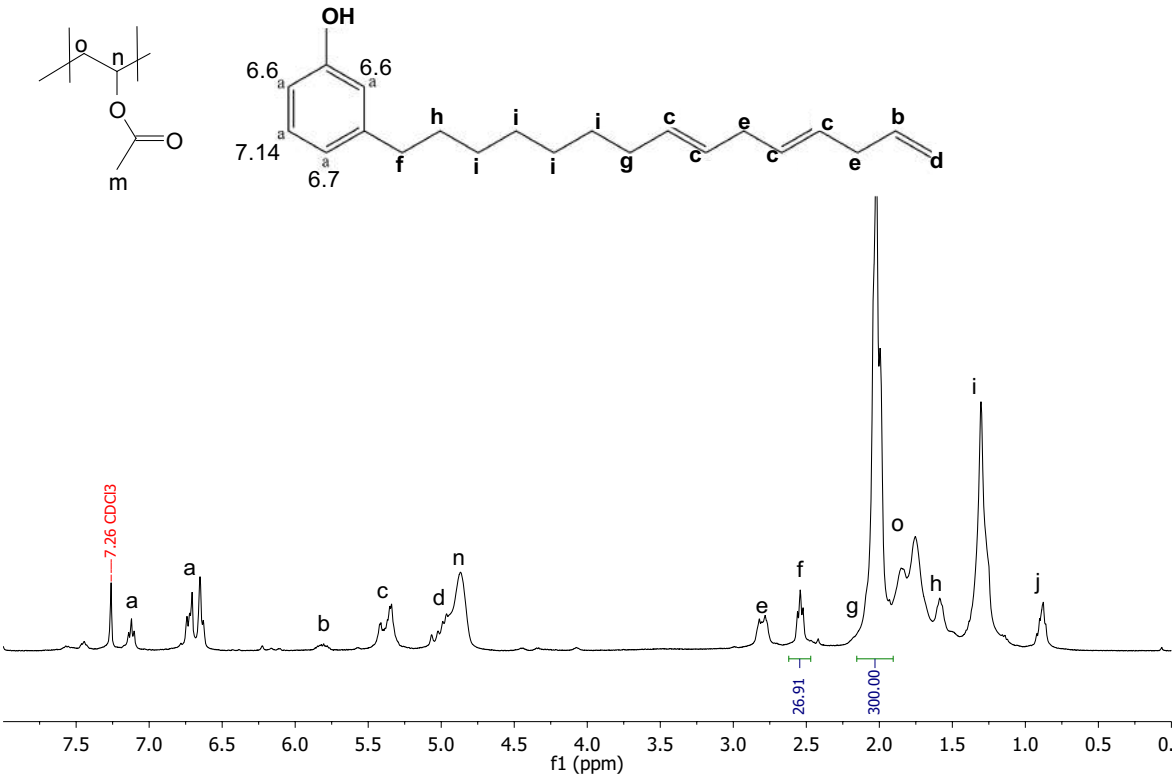


Figure 5.46: $^1$H NMR for P(VAc-*co*-C), 5% w/w, 85 °*C*

According to the TGA analyses, the copolymers presented lower thermal stability than PVAc, as shown in Figure 5.47. PVAc thermal degradation presents two characteristic stages, one close to 350 °C and another one close to 475 °C. Addition of cardanol shifts the TGA curves downwards, below the volatilization temperature of cardanol and suggesting the formation of volatile oligomers (CERVANTES-UC *et al.* (2006)). DSC analyses were not performed because the obtained copolymers were viscous liquids at room temperature.

FTIR analyses showed that both vinyl acetate and cardanol groups were present in

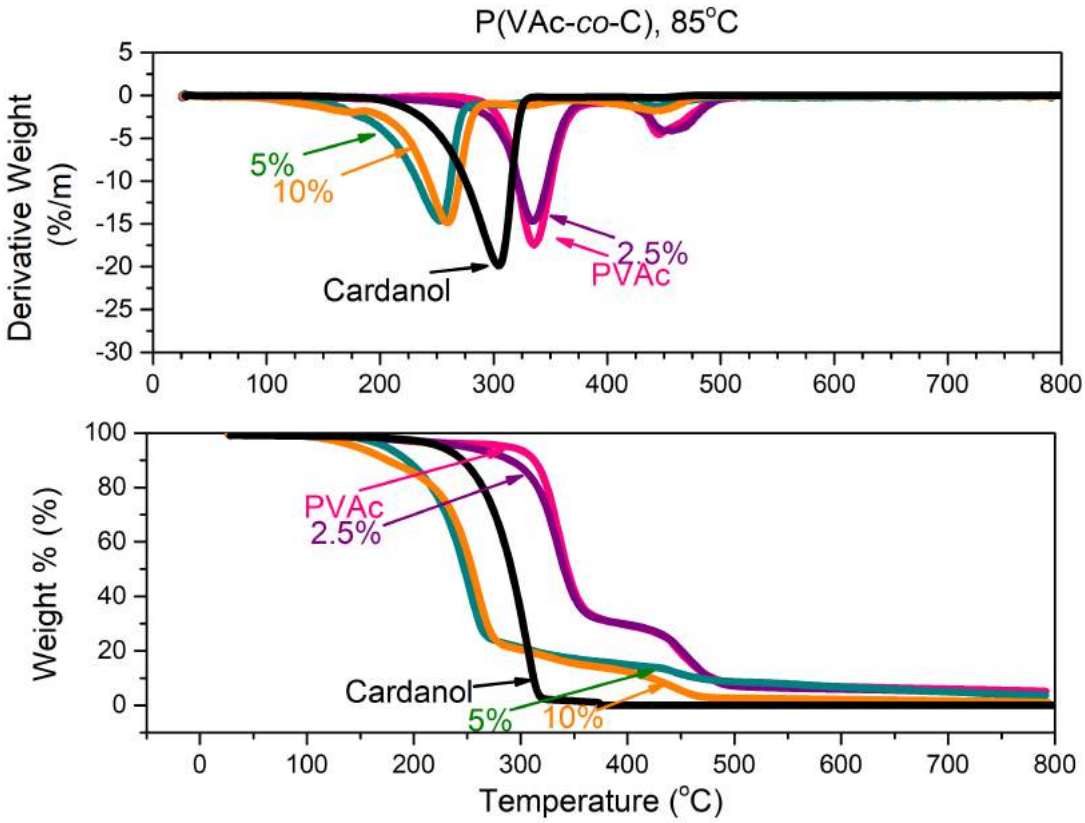


Figure 5.47: TGA and DTG thermograms for P(VAc-*co*-C) samples prepared in reactions at 85 °*C*.

samples prepared with 2.5 and 5 wt% of cardanol. However, at 10 wt%, the presence of high concentrations of residual cardanol was likely because the peaks related to PVAc were weak.

In summary, copolymerizations of cardanol with vinyl acetate were not performed successfully at the analyzed conditions. Cardanol exerts a very strong inhibitory effect on vinyl acetate polymerizations and conversions were always small. Moreover, the thermal stability of the copolymer was also prejudiced by addition of cardanol. Perhaps reactions should be performed at higher temperatures and pressures in the future, although these are not the conditions normally employed for production of PVAc products commercially.

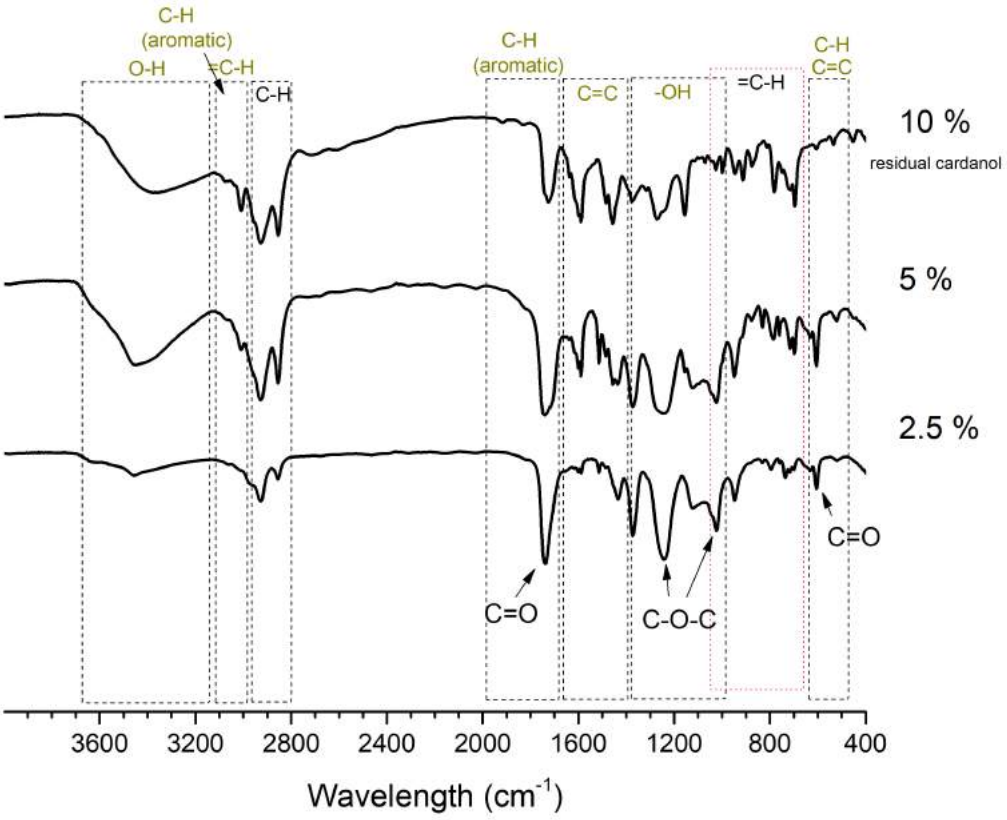


Figure 5.48: FTIR spectrum for P(VAc-*co*-C) samples prepared in reactions at 85 °*C*.

## 5.7 Copolymerization of cardanol and acrylic acid

Poly(acrylic acid) (PAA) is a water soluble, hygroscopic, brittle and colorless polymer, with $T_g$ of 106 °*C*. Its molecular structure is presented in Figure 5.49. As PAA is an anionic polymer, it has the ability to absorb and retain water and swell to many times its original volume. This explains why PAA is used in diapers and menstrual pads. When it is dry, PAA is used in paints, cosmetics, pharmaceutical and personal care products as thickener, dispersing agent, suspending agent, and emulsifier agent. However, many polymer products contain acrylic acid as a comonomer, including polymers that respond to modification of temperature or pH.

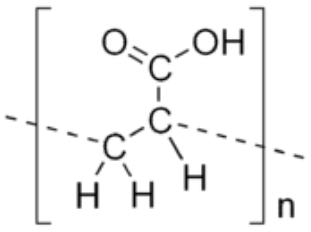


Figure 5.49: Molecular structure of poly(acrylic acid).

Reactions of cardanol and PAA were performed at 85 and 110 °*C*. However, reactions were so fast that was not possible to analyze the kinetics behavior of the reacting

systems. As Figure 5.50 shows, the monomer was completely consumed almost instantaneously even when 10 wt % cardanol was added to the reacting media. Figure 5.51 presents TGA thermograms of the obtained copolymer samples. As one can see, the addition of cardanol shifts downwards in the direction of the TGA of pure cardanol. Therefore, addition of cardanol did not increase the thermal stability of the copolymer. The first stage of degradation matches with the boiling point of acrylic acid, equal to 139 °*C*. So this first stage seems to be related to the loss of residual acrylic acid. The second stage matches with the cardanol curve, suggesting that it correponds to loss of residual cardanol. The third stage is similar to the PAA degrdation curve and might represent the degradation of pure PAA without incorporation of cardanol. So, it can be speculated that cardanol incorporation was not high even at high conversions.

As the reaction was very fast even at 85 °*C*, another reaction was performed at 60 °*C*. However, as the initiator decomposition rate also decreased, the kinetics became much slower, and the monomer conversion did not reach 40% after 6 hrs of reaction. Therefore the much slower kinetics makes the inhibition of cardanol more significant. Therefore, copolymerizations of AA and conditions were unsuccessful at the analyzed experimental conditions and should be studied at alternative polymerization conditions with more detail in the near future (MINARI *et al.* (2011), SILVA *et al.* (2004)).

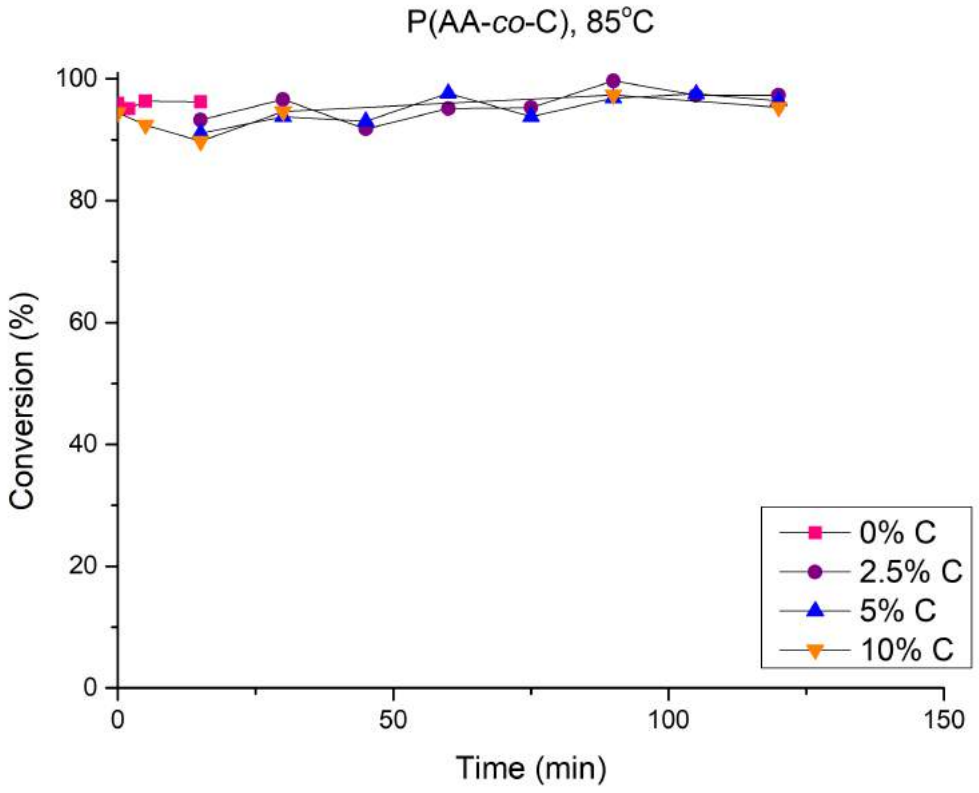


Figure 5.50: Monomer conversions for samples collected at 85 °*C* in copolymerizations of AA and cardanol.

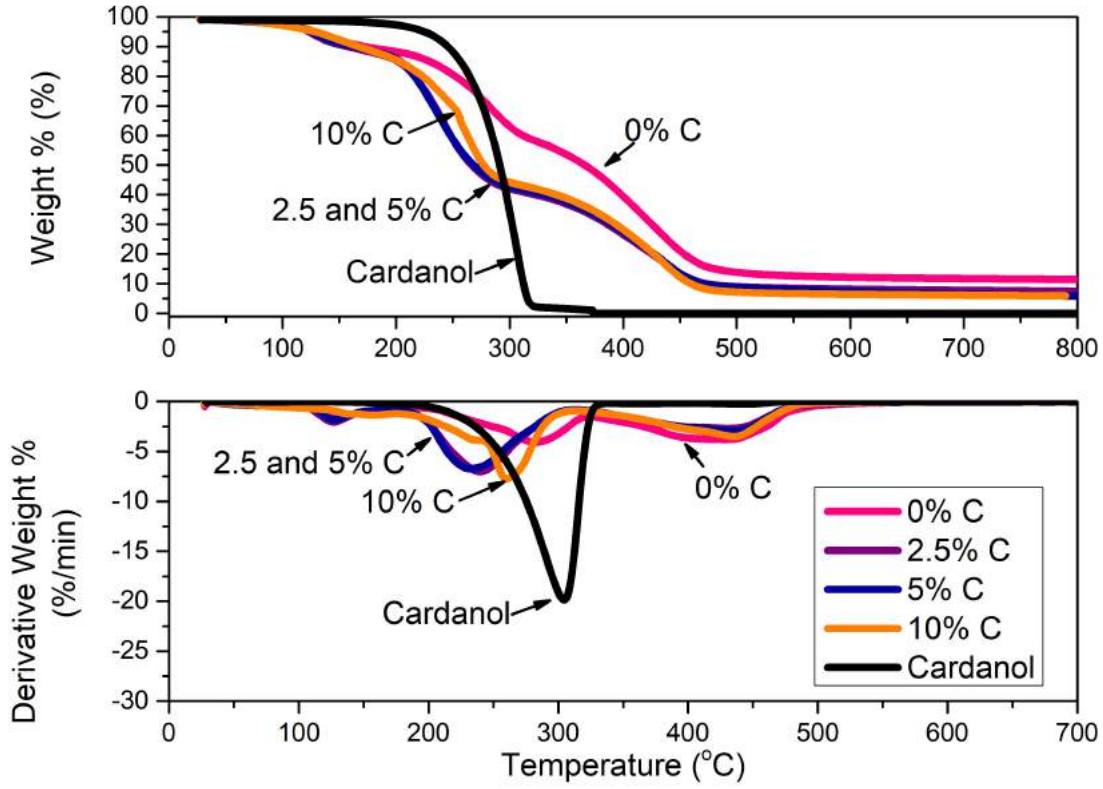


Figure 5.51: TGA and DTG thermograms for P(AA-*co*-C) samples prepared in reactions at 85 °*C*.

## 5.8 Concluding Remarks

In the present chapter, it was shown that cardanol and natural CNSL can react successfully through free radical mechanisms. In the case homopolymerizations reactions were very slow and reached very small conversions. However, $^{1}$H-NMR, FTIR and TGA analyses proved there are differences between the reaction product collected after 8 or 10 hours of reaction. When added to styrene and MMA polymerizations, both cardanol and natural CNSL inhibit the polymerizations. Nonetheless, the obtained conversions can be close to 100% and cardanol and CNSL incorporation can be high, allowing for functionalization of the polymer molecules. The addition of cardanol or natural CNSL can also be used to reduce the $T_g$ or increase the thermal stability of the material. However, the copolymerization experiments performed with vinyl acetate and acrylic acid were not satisfactory as addition of cardanol did not enhance the thermal stability of the products.

Based on available $^{1}$H-NMR and FTIR spectra, it was shown that the phenolic compounds were able to react with free radical through several reactive sites. The hydroxyl group was responsible for inhibition as its concentration was sensitive to reaction conditions. Despite the steric hindrance, the internal unsaturations probably reacted as

detected by $^{1}$H-NMR and FTIR analyses. The terminal unsaturation was the functional group most likely to continue propagation and incorporate cardanol and natural CNSL in polymer chains. Although they are present in less than 50% in phenolic lumps, it is considered that the whole lump is reactive because the compounds have many reactive sites. The carboxylic group of anacardic acid apparently did not affect the polymerization kinetics very significant, although carboxylic moiety reduce the inhibition for reactions performed with MMA at 85 °C.

# Chapter 6

# Bulk Copolymerization: Modeling

## 6.1 Introduction

In this chapter, a mathematical model is proposed for the copolymerization in bulk through free radical bulk polymerization. The terminal model and quasi-steady state assumption are used. Based on experimental results, model parameters are estimated to allow for appropriate description of monomer conversions, average molecular weights and copolymer compositions of the produced copolymer. For methyl methacrylate or styrene, classical thermal-kinetic parameters available in the literate were used. As cardanol behaved similarly to natural CNSL, the model parameters are also expected to be similar. Regarding the model parameters related to cardanol, the parameters are not available in the literature. Besides, it was shown that the phenolic compounds exerted strong inhibitory effects on the polymerizations, so that this effect must be take into account. Therefore, a parameter, referenced as $f_{inh}$, that describes the decreasing concentrations of living free radicals in the system is estimated.

Given the fact that other molecules may be eventually present in the naturally occurring cardanol stream and different reactive sites (such as the phenolic group) can take part in the reaction mechanism, the whole cardanol stream was treated as a lumped monomer stream for purposes of kinetic modeling. However, as cardanol polymerizes at slow rates and only produces oligomers at the analyzed reaction conditions through free-radical polymerizations, as observed experimentally, for the sake of simplicity, some model parameters were initially assumed to be either null or equal to the styrene polymerization parameters.

The parameter estimation procedure was performed with the computation package ESTIMA, implemented in Fortran, which combines particle swarm optimization (PSO) and Gauss-Newton algorithms (SCHWAAB *et al.*, 2008). 180 particles were used and a thousand iterations were carried out with statistical confidence level of 95 %.

## 6.2 Kinetic Mechanism

The proposed dynamic model describes the copolymerization in bulk via the standard free radical mechanism. The terminal model assumes that only the last species added to the living chain controls the reactivity of the living active molecule. Therefore, the propagation step is extended to represent the different reactions between monomers and the reactive macro-radicals presented in the reaction medium. Similarly, other steps that involve the reaction of a living species with another molecule are also extended (ODIAN, 2004).

Every free radical chain initiated thermally by an initiator (BPO or AIBN) is subject to initiation, propagation and termination steps. Depending on the monomer, thermal initiation may take place and should be included. Chain transfer reactions (to one of the monomers or to impurities) do not affect the monomer conversion; however, change the average molar mass of the final products. Therefore, a generic kinetic mechanism is represented below with 18 mechanistic steps. One must notice that the thermal initiation is represented in the form usually considered for styrene (Equation 6.4).

Initiation:

$$I \xrightarrow{k_d} 2R \tag{6.1}$$

$$R + M_1 \xrightarrow{k_{r1}} P_{1,0} \tag{6.2}$$

$$R + M_2 \xrightarrow{k_{r2}} Q_{0,1} \tag{6.3}$$

$$3M_1 \xrightarrow{k_{dm}} 2P^*_{1,0} \tag{6.4}$$

Propagation:

$$P_{i,j} + M_1 \xrightarrow{k_{p11}} P_{i+1,j} \tag{6.5}$$

$$P_{i,j} + M_2 \xrightarrow{k_{p12}} Q_{i,j+1} \tag{6.6}$$

$$Q_{i,j} + M_1 \xrightarrow{k_{p21}} P_{i+1,j} \tag{6.7}$$

$$Q_{i,j} + M_2 \xrightarrow{k_{p22}} Q_{i,j+1} \tag{6.8}$$

Transfer to monomer:

$$P_{i,j} + M_1 \xrightarrow{k_{tm11}} P_{1,0} + \Gamma_{i,j} \tag{6.9}$$

$$P_{i,j} + M_2 \xrightarrow{k_{tm12}} Q_{0,1} + \Gamma_{i,j} \tag{6.10}$$

$$Q_{i,j} + M_1 \xrightarrow{k_{tm21}} P_{1,0} + \Gamma_{i,j} \tag{6.11}$$

$$Q_{i,j} + M_2 \xrightarrow{k_{tm22}} Q_{0,1} + \Gamma_{i,j} \tag{6.12}$$

Termination:

$$P_{i,j} + P_{m,n} \xrightarrow{k_{tc11}} \Gamma_{i+m,j+n} \tag{6.13}$$

$$P_{i,j} + Q_{m,n} \xrightarrow{k_{tc12}} \Gamma_{i+m,j+n} \tag{6.14}$$

$$Q_{i,j} + Q_{m,n} \xrightarrow{k_{tc22}} \Gamma_{i+m,j+n} \tag{6.15}$$

$$P_{i,j} + P_{m,n} \xrightarrow{k_{td11}} \Gamma_{i,j} + \Gamma_{m,n} \tag{6.16}$$

$$P_{i,j} + Q_{m,n} \xrightarrow{k_{td12}} \Gamma_{i,j} + \Gamma_{m,n} \tag{6.17}$$

$$Q_{i,j} + Q_{m,n} \xrightarrow{k_{td22}} \Gamma_{i,j} + \Gamma_{m,n} \tag{6.18}$$

In the proposed mechanism, $I$ represents a molecule of initiator, $R^*$ is a dissociated initiator radical, $M_1$ is a molecule of styrene (Sty) or methyl methacrylate (MMA), depending on the analyzed system. $M_2$ is a molecule of cardanol or a molecule that represents the mixture of natural CNSL.

$P^*_{i,j}$ represents a living chain with $i$ units of monomer 1 (Sty or MMA) and $j$ units of monomer 2 (cardanol or CNSL) with active center located in a Sty/MMA-terminated unit. $Q^*_{i,j}$ represents a living chain with i units of monomer 1 and j units of monomer 2 with active center located in a CNSL molecule-terminated unit.

Although dead chains are different from each other in terms of composition and molar mass, they are represented by one unique species $\Gamma_{i,j}$, with $i$ units of monomer 1 and $j$ units of monomer 2.

In addition, the reactivity ratios ($r_{11}$ and $r_{22}$) are used to relate the specific homo-propagation reaction rates to the hetero-propagation reaction rates in the form:

$$r_{i,j} = \frac{k_{p,ii}}{k_{p,ij}} \tag{6.19}$$

$$r_{j,i} = \frac{k_{p,jj}}{k_{p,ji}} \tag{6.20}$$

Moreover, the relative efficiency factor of hetero-termination measures how fast

hetero-termination is in relation to a reference value (OECHSLER (2016)), in the form:

$$\psi_{ii} = \frac{k_{tii}}{\sqrt{k_{tii}k_{tji}}} \tag{6.21}$$

$$\psi_{jj} = \frac{k_{tjj}}{\sqrt{k_{tii}k_{tjj}}} \tag{6.22}$$

The gel ($g_{tij}$) and glass ($g_{pij}$) effects cannot be ignored either. They multiply the propagation/termination rates constant (Equations 6.23 and 6.24). $k^0_{pij}$ and $k^0_{tij}$ represent the specific rates of propagation and termination in the absence of polymer, while $g_{pij}$ and $g_{tij}$ are the correlations for glass and gel effects, respectively. These can be calculated by Equations 6.25 to 6.27, which are based on the Free Volume Theory (PINTO and RAY, 1995).

$$k_{pij} = k^{\circ}_{pij} g_{pij} \tag{6.23}$$

$$k_{tij} = k^{\circ}_{tij} g_{tij} \tag{6.24}$$

$$g_{pij} = 1 \qquad (v_f \geq v_{fcr}) \tag{6.25}$$

$$g_{pij} = \exp\left[-A\left(\frac{1}{v_f} - \frac{1}{v_{fcr}}\right)\right] \qquad (v_f < v_{fcr}) \tag{6.26}$$

$$g_{tij} = \exp\left[-A\left(\frac{1}{v_f} - \frac{1}{v_{f0}}\right)\right] \tag{6.27}$$

While $v_{fcr}$ values are tabulated for each monomer, the free volumes calculated at the beginning of the reaction ($v_{f0}$) and at time $t$ ($v_f$) can be obtained with Equations 6.28 and 6.29, where $\sigma_i$ is the volume fraction of species $i$, time $t$ and $\sigma_{fi}$ is the volume fraction of species $i$ at the initial time.

$$v_f = \sigma_{m1} v_{fm1} + \sigma_{m2} v_{fm2} + \sigma_p v_{fp} \tag{6.28}$$

$$v_{f0} = \sigma_{fm1} v_{fm1} + \sigma_{fm2} v_{fm2} + \sigma_{fp} v_{fp} \tag{6.29}$$

Finally, the free volumes ($v_{fi}$) for monomers and polymer were calculated with Equation 6.30. $\alpha_i$ is the thermal expansion coefficient and $T_{gi}$ is the glass transition temperature of species i.

$$v_{fi} = 0.025 + \alpha_i (T - T_{gi}) \tag{6.30}$$

## 6.3 Mass Balances

First of all, the glass and gel effects were only considered for styrene or methyl methacrylate homo-polymerization steps, as there is not any information about these effects for cardanol/CNSL. Also, the phenolic compounds exert strong inhibitory effects on the course of the polymerization and do not polymerize to high conversions at the analyzed conditions utilized. Moreover, the validity of volume additivity and of the long chain assumption was assumed.

Mass balance for initiator $I$:

$$\frac{dI}{dt} = -k_d I \tag{6.31}$$

Mass balance for monomer 1, $M_1$:

$$\frac{dM_1}{dt} = -\left[ R_{ckr} \frac{M_1}{V} + (k_{p11} + k_{tm11}) \frac{M_1}{V} \gamma_{0,0} + (k_{p21} + k_{tm21}) \frac{M_1}{V} \Pi_{0,0} \right] V - 2 k_{dm} \left[ \frac{M_1}{V} \right]^3 V \tag{6.32}$$

Mass balance for monomer 2, $M_2$:

$$\frac{dM_2}{dt} = -\left[ R_{ckr} \frac{M_2}{V} + (k_{p12} + k_{tm12}) \frac{M_2}{V} \gamma_{0,0} + (k_{p22} + k_{tm22}) \frac{M_2}{V} \Pi_{0,0} \right] V \tag{6.33}$$

Mass balance for radicals, $R^*$:

$$\frac{dR^*}{dt} = \left[ 2 f k_d \frac{I}{V} - k_{r1} \frac{M_1}{V} \frac{R}{V} - k_{r2} \frac{M_2}{V} \frac{R}{V} \right] V \tag{6.34}$$

Assuming the quasi-steady state assumption and that $k_{r1} = k_{r2}$, it is possible to

obtain the normalized rate of initiation for $k_{r1} = k_{r2}$ as:

$$R_{ckr} = k_r \frac{R}{V} = \frac{2 f k_d C_i}{C_{m1} + C_{m2}} \tag{6.35}$$

where $C_i = {}^{I}/_{V}$, $C_{m1} = {}^{M_1}/_{V}$ and $C_{m2} = {}^{M_2}/_{V}$.

Mass balance for living chains, $P_{1,0}$:

$$\begin{aligned}
\frac{dP_{1,0}}{dt} = & \left[ k_{r1} \left(\frac{R}{V}\right)\left(\frac{M_1}{V}\right) - k_{p11} \left(\frac{P_{1,0}}{V}\right)\left(\frac{M_1}{V}\right) - k_{p12} \left(\frac{P_{1,0}}{V}\right)\left(\frac{M_2}{V}\right) \right] V \\
& + \left[ -k_{tm11} \left(\frac{P_{1,0}}{V}\right)\left(\frac{M_1}{V}\right) - k_{tm12} \left(\frac{P_{1,0}}{V}\right)\left(\frac{M_2}{V}\right) \right] V \\
& + \left[ k_{tm11} \sum_{i=1}^{\infty}\sum_{j=0}^{\infty} \left(\frac{P_{i,j}}{V}\right)\left(\frac{M_1}{V}\right) + k_{tm21} \sum_{i=0}^{\infty}\sum_{j=1}^{\infty} \left(\frac{Q_{i,j}}{V}\right)\left(\frac{M_1}{V}\right) \right] V \\
& + \left[ 2 k_{dm} \left(\frac{M_1}{V}\right)^3 \right] V
\end{aligned} \tag{6.36}$$

Considering:

$$i = 2, \ldots, \infty \tag{6.37}$$

$$j = 0, \ldots, \infty \tag{6.38}$$

Mass balance for living chains, $P_{i,j}$:

$$\begin{aligned}
\frac{dP_{i,j}}{dt} = & \left[ -k_{p11} \left(\frac{P_{i,j}}{V}\right)\left(\frac{M_1}{V}\right) - k_{p12} \left(\frac{P_{i,j}}{V}\right)\left(\frac{M_2}{V}\right) \right] V \\
& \left[ k_{p11} \left(\frac{P_{i-1,j}}{V}\right)\left(\frac{M_1}{V}\right) + k_{p21} \left(\frac{Q_{i-1,j}}{V}\right)\left(\frac{M_1}{V}\right) \right] V \\
& + \left[ -k_{tm11} \left(\frac{P_{i,j}}{V}\right)\left(\frac{M_1}{V}\right) - k_{tm12} \left(\frac{P_{i,j}}{V}\right)\left(\frac{M_2}{V}\right) \right] V \\
& + \left[ -k_{tc11} \left(\frac{P_{i,j}}{V}\right) \sum_{m=1}^{\infty}\sum_{n=0}^{\infty} \left(\frac{P_{m,n}}{V}\right) - k_{td11} \left(\frac{P_{i,j}}{V}\right) \sum_{m=1}^{\infty}\sum_{n=0}^{\infty} \left(\frac{P_{m,n}}{V}\right) \right] V \\
& + \left[ -k_{tc12} \left(\frac{P_{i,j}}{V}\right) \sum_{m=0}^{\infty}\sum_{n=1}^{\infty} \left(\frac{Q_{m,n}}{V}\right) - k_{td12} \left(\frac{P_{i,j}}{V}\right) \sum_{m=0}^{\infty}\sum_{n=1}^{\infty} \left(\frac{Q_{m,n}}{V}\right) \right] V
\end{aligned} \tag{6.39}$$

Mass balance for living chains, $Q_{0,1}$:

$$\begin{aligned}\frac{dQ_{0,1}}{dt} &= \left[k_{r2}\left(\frac{R}{V}\right)\left(\frac{M_2}{V}\right) - k_{p21}\left(\frac{Q_{0,1}}{V}\right)\left(\frac{M_1}{V}\right) - k_{p22}\left(\frac{Q_{0,1}}{V}\right)\left(\frac{M_2}{V}\right)\right]V \\ &+ \left[-k_{tm21}\left(\frac{Q_{0,1}}{V}\right)\left(\frac{M_1}{V}\right) - k_{tm22}\left(\frac{Q_{0,1}}{V}\right)\left(\frac{M_2}{V}\right)\right]V \\ &+ \left[k_{tm12}\sum_{i=1}^{\infty}\sum_{j=0}^{\infty}\left(\frac{P_{i,j}}{V}\right)\left(\frac{M_2}{V}\right) + k_{tm22}\sum_{i=0}^{\infty}\sum_{j=1}^{\infty}\left(\frac{Q_{i,j}}{V}\right)\left(\frac{M_2}{V}\right)\right]V\end{aligned} \tag{6.40}$$

Mass balance for living chains, $Q_{i,j}$:

$$\begin{aligned}\frac{dQ_{i,j}}{dt} &= \left[-k_{p21}\left(\frac{Q_{i,j}}{V}\right)\left(\frac{M_1}{V}\right) - k_{p22}\left(\frac{Q_{i,j}}{V}\right)\left(\frac{M_2}{V}\right)\right]V \\ &+ \left[k_{p12}\left(\frac{P_{i,j-1}}{V}\right)\left(\frac{M_2}{V}\right) + k_{p22}\left(\frac{Q_{i,j-1}}{V}\right)\left(\frac{M_2}{V}\right)\right]V \\ &+ \left[-k_{tm21}\left(\frac{Q_{i,j}}{V}\right)\left(\frac{M_1}{V}\right) - k_{tm22}\left(\frac{Q_{i,j}}{V}\right)\left(\frac{M_2}{V}\right)\right]V \\ &+ \left[-k_{tc12}\left(\frac{Q_{i,j}}{V}\right)\sum_{m=1}^{\infty}\sum_{n=0}^{\infty}\left(\frac{P_{m,n}}{V}\right) - k_{td12}\left(\frac{Q_{i,j}}{V}\right)\sum_{m=1}^{\infty}\sum_{n=0}^{\infty}\left(\frac{P_{m,n}}{V}\right)\right]V \\ &+ \left[-k_{tc22}\left(\frac{Q_{i,j}}{V}\right)\sum_{m=0}^{\infty}\sum_{n=1}^{\infty}\left(\frac{Q_{m,n}}{V}\right) - k_{td22}\left(\frac{Q_{i,j}}{V}\right)\sum_{m=0}^{\infty}\sum_{n=1}^{\infty}\left(\frac{Q_{m,n}}{V}\right)\right]V\end{aligned} \tag{6.41}$$

Mass balance for dead chains, $\Gamma_{i,j}$:

$$\begin{aligned}\frac{d}{dt}\left[\Gamma_{i,j}\right] &= k_{tm11}\frac{M_1}{V}P_{i,j}V + k_{tm12}\frac{M_2}{V}P_{i,j}V + k_{tm21}\frac{M_1}{V}Q_{i,j}V + k_{tm22}\frac{M_2}{V}Q_{i,j}V \\ &+ \frac{ktc_{11}}{2}\sum_{r=1}^{i-1}\sum_{q=o}^{j}P_{r,q}P_{i-r,j-q}V + k_{tc12}\sum_{r=1}^{i-1}\sum_{q=o}^{j}P_{r,q}Q_{i-r,j-q}V \\ &+ \frac{ktd_{11}}{2}P_{i,j}\sum_{i=0}^{\infty}\sum_{j=o}^{\infty}P_{i,j}V + k_{td12}\left[P_{i,j}\sum_{i=0}^{\infty}\sum_{j=o}^{\infty}Q_{i,j} + Q_{i,j}\sum_{i=0}^{\infty}\sum_{j=o}^{\infty}P_{i,j}\right]V \\ &+ \left[-k_{tc12}\left(\frac{Q_{i,j}}{V}\right)\sum_{m=1}^{\infty}\sum_{n=0}^{\infty}\left(\frac{P_{m,n}}{V}\right) - k_{td12}\left(\frac{Q_{i,j}}{V}\right)\sum_{m=1}^{\infty}\sum_{n=0}^{\infty}\left(\frac{P_{m,n}}{V}\right)\right]V \\ &+ \frac{ktd_{22}}{2}Q_{i,j}\sum_{i=0}^{\infty}\sum_{j=o}^{\infty}Q_{i,j}V + \frac{k_{tc22}}{2}\sum_{r=1}^{i}\sum_{q=o}^{j-1}Q_{r,q}Q_{i-r,j-q}V\end{aligned} \tag{6.42}$$

As the volume changes on the course of reaction, volume balance was calculated

as:

$$\frac{dV}{dt} = \left[\left(\frac{1}{\rho_{m1}} - \frac{1}{\rho_p}\right) R_{m1} + \left(\frac{1}{\rho_{m2}} - \frac{1}{\rho_p}\right) R_{m2}\right] V \tag{6.43}$$

Thus, the overall monomer conversion (X) can be obtained as:

$$X = \frac{\rho_p \upsilon_P}{\rho_{m1}\upsilon_{m1} + \rho_{m2}\upsilon_{m2} + \rho_p \upsilon_p} \tag{6.44}$$

where $\rho_i$ is the density of the component $i$ ($g.L^{-1}$) and $\upsilon_i$ is the volume fraction of component $i$.

## 6.4 Numerical Solution

There are seven types of reacting species in the system (not counting the radical, $R^{(}*)$), although it is necessary to account for volume changes in the batch reaction. Moreover, eighteen specific reaction rates must be found. Hetero-propagation rates can be defined in terms of the reactivity ratios. Hetero-termination rates can be defined in terms of the relative efficiency factor of hetero-termination. Mn, Mw and PDI values must be calculated along the polymerization course. In order to do that, the moment technique is very popular, using the statistical moments of the molar mass distributions. An advantage is the fact that an infinite number of balance equations of the method is transformed into a finite set of moment equations. The moments for living and dead chain size distributions can be defined as (OECHSLER (2016)):

$$\gamma_{k,l} = \sum_{i=0}^{\infty} \sum_{j=o}^{\infty} i^k j^m P_{i,j} \tag{6.45}$$

$$\pi_{k,l} = \sum_{i=0}^{\infty} \sum_{j=o}^{\infty} i^k j^m Q_{i,j} \tag{6.46}$$

$$\lambda_{k,l} = \sum_{i=0}^{\infty} \sum_{j=o}^{\infty} i^k j^m \Gamma_{i,j} \tag{6.47}$$

However, if one is interested in the average molar masses, few moments are needed considering that:

$$k_{t12} = (k_{tc12} + k_{td12}) \tag{6.48}$$

$$k_{t11} = (k_{tc11} + k_{td11}) \tag{6.49}$$

$$k_{t22} = (k_{tc22} + k_{td22}) \tag{6.50}$$

Considering the quasi-steady state assumption, $\gamma_{0,0}$ and $\pi_{0,0}$ are defined as:

$$\gamma_{0,0} = \sqrt{\frac{R_{ckr}(M_1/V)(M_2/V) + 2k_{dm}(M_1/V)^3}{k_{t11} + k_{t12}K_s + k_{t22}K_S^2}} \tag{6.51}$$

$$\pi_{0,0} = K_s\gamma_{0,0} \tag{6.52}$$

With:

$$K_s = \frac{(k_{p12} + k_{tm12})(M_2/V)}{(k_{p21} + k_{tm21})(M_1/V)} \tag{6.53}$$

Then $\gamma_{1,0}$ & $\pi_{1,0}$:

$$\begin{aligned}\frac{d\gamma_{1,0}}{dt} &= k_{p21}\left(\frac{M_1}{V}\right)\left(\frac{\pi_{1,0}}{V}\right)V \\ &- \left[\left(k_{p12} + k_{tm12}\right)\left(\frac{M_2}{V}\right) + k_{tm11}\left(\frac{M_1}{V}\right) + k_{t11}\left(\frac{\gamma_{0,0}}{V}\right) + k_{t12}\left(\frac{\pi_{0,0}}{V}\right)\right]\left(\frac{\gamma_{1,0}}{V}\right)V \\ &+ \left[k_{r1}\left(\frac{R}{V}\right) + k_{tm11}\left(\frac{\gamma_{0,0}}{V}\right) + k_{tm21}\left(\frac{\pi_{0,0}}{V}\right) + k_{p11}\left(\frac{\gamma_{0,0}}{V}\right) + k_{p21}\left(\frac{\pi_{0,0}}{V}\right)\right]\left(\frac{M_1}{V}\right)V\end{aligned} \tag{6.54}$$

$$\begin{aligned}\frac{d\pi_{1,0}}{dt} = &- \left[\left(k_{p21} + k_{tm21}\right)\left(\frac{M_1}{V}\right) + k_{tm22}\left(\frac{M_2}{V}\right) + k_{t22}\left(\frac{\pi_{0,0}}{V}\right) + k_{t12}\left(\frac{\gamma_{0,0}}{V}\right)\right]\left(\frac{\pi_{1,0}}{V}\right)V \\ &+ k_{p12}\left(\frac{M_2}{V}\right)\left(\frac{\gamma_{1,0}}{V}\right)V\end{aligned} \tag{6.55}$$

$\gamma_{0,1}$ & $\pi_{0,1}$:

$$\frac{d\gamma_{0,1}}{dt} = k_{p21}\left(\frac{\pi_{0,1}}{V}\right)\left(\frac{M_1}{V}\right)V - \left[\left(k_{p12}+k_{tm12}\right)\left(\frac{M_2}{V}\right)+k_{tm11}\left(\frac{M_1}{V}\right)+k_{t11}\left(\frac{\gamma_{0,0}}{V}\right)+k_{t12}\left(\frac{\pi_{0,0}}{V}\right)\right]\left(\frac{\gamma_{0,1}}{V}\right)V \tag{6.56}$$

$$\begin{aligned}\frac{d\pi_{0,1}}{dt} = &-\left[k_{tm22}\left(\frac{M_2}{V}\right)+\left(k_{p21}+k_{tm21}\right)\left(\frac{M_1}{V}\right)+k_{t22}\left(\frac{\pi_{0,0}}{V}\right)+k_{t12}\left(\frac{\gamma_{0,0}}{V}\right)\right]\left(\frac{\pi_{0,1}}{V}\right)V \\ &+k_{p12}\left(\frac{M_2}{V}\right)\left(\frac{\gamma_{0,1}}{V}\right)V \\ &+\left[k_{r2}\left(\frac{R}{V}\right)+\left(k_{p22}+k_{tm22}\right)\left(\frac{\pi_{0,0}}{V}\right)+\left(k_{p12}+k_{tm12}\right)\left(\frac{\gamma_{0,0}}{V}\right)\right]\left(\frac{M_2}{V}\right)V\end{aligned} \tag{6.57}$$

$\gamma_{2,0}$ & $\pi_{2,0}$:

$$\begin{aligned}\frac{d\gamma_{2,0}}{dt} = &k_{p21}\left(\frac{M_1}{V}\right)\left(\frac{\pi_{2,0}}{V}\right)V \\ &-\left[k_{tm11}\left(\frac{M_1}{V}\right)+\left(k_{p12}+k_{tm12}\right)\left(\frac{M_2}{V}\right)+k_{t11}\left(\frac{\gamma_{0,0}}{V}\right)+k_{t12}\left(\frac{\pi_{0,0}}{V}\right)\right]\left(\frac{\gamma_{2,0}}{V}\right)V \\ &+\left[k_{r1}\left(\frac{R}{V}\right)+k_{tm11}\left(\frac{\gamma_{0,0}}{V}\right)+k_{tm21}\left(\frac{\pi_{0,0}}{V}\right)+k_{p11}\left[2\left(\frac{\gamma_{1,0}}{V}\right)+\left(\frac{\gamma_{0,0}}{V}\right)\right]\right]\left(\frac{M_1}{V}\right)V \\ &+k_{p21}\left[2\left(\frac{\pi_{1,0}}{V}\right)+\left(\frac{\pi_{0,0}}{V}\right)\right]\left(\frac{M_1}{V}\right)V\end{aligned} \tag{6.58}$$

$$\begin{aligned}\frac{d\pi_{2,0}}{dt} = &-\left[\left(k_{p21}+k_{tm21}\right)\left(\frac{M_1}{V}\right)+k_{tm22}\left(\frac{M_2}{V}\right)+k_{t22}\left(\frac{\pi_{0,0}}{V}\right)+k_{t12}\left(\frac{\gamma_{0,0}}{V}\right)\right]\left(\frac{\pi_{2,0}}{V}\right)V \\ &+k_{p12}\left(\frac{M_2}{V}\right)\left(\frac{\gamma_{2,0}}{V}\right)V\end{aligned} \tag{6.59}$$

$\gamma_{0,2}$ & $\pi_{0,2}$:

$$\frac{d\gamma_{0,2}}{dt} = k_{p21}\left(\frac{M_1}{V}\right)\left(\frac{\pi_{0,2}}{V}\right)V - \left[\left(k_{p12}+k_{tm12}\right)\left(\frac{M_2}{V}\right)+k_{tm11}\left(\frac{M_1}{V}\right)+k_{t11}\left(\frac{\gamma_{0,0}}{V}\right)+k_{t12}\left(\frac{\pi_{0,0}}{V}\right)\right]\left(\frac{\gamma_{0,2}}{V}\right)V \tag{6.60}$$

$$\begin{aligned}\frac{d\pi_{0,2}}{dt} = &-\left[\left(k_{p21}+k_{tm21}\right)\left(\frac{M_1}{V}\right)+k_{tm22}\left(\frac{M_2}{V}\right)+k_{t22}\left(\frac{\pi_{0,0}}{V}\right)+k_{t12}\left(\frac{\gamma_{0,0}}{V}\right)\right]\left(\frac{\pi_{0,2}}{V}\right)V\\ &+k_{p12}\left(\frac{M_2}{V}\right)\left(\frac{\gamma_{0,2}}{V}\right)V\\ &+\left[k_{r2}\left(\frac{R}{V}\right)+k_{tm22}\left(\frac{\pi_{0,0}}{V}\right)+k_{tm12}\left(\frac{\gamma_{0,0}}{V}\right)+k_{p22}\left[2\left(\frac{\pi_{0,1}}{V}\right)+\left(\frac{\pi_{0,0}}{V}\right)\right]\right]\left(\frac{M_2}{V}\right)V\\ &+k_{p12}\left[2\left(\frac{\gamma_{0,1}}{V}\right)+\left(\frac{\gamma_{0,0}}{V}\right)\right]\left(\frac{M_2}{V}\right)V\end{aligned} \tag{6.61}$$

$\gamma_{1,1}$ & $\pi_{1,1}$:

$$\begin{aligned}\frac{d\gamma_{1,1}}{dt} = &\,k_{p21}\left(\frac{M_1}{V}\right)\left(\frac{\pi_{1,1}}{V}\right)V\\ &-\left[k_{tm11}\left(\frac{M_1}{V}\right)+\left(k_{p12}+k_{tm12}\right)\left(\frac{M_2}{V}\right)+k_{t11}\left(\frac{\gamma_{0,0}}{V}\right)+k_{t12}\left(\frac{\pi_{0,0}}{V}\right)\right]\left(\frac{\gamma_{1,1}}{V}\right)V\\ &+\left[k_{p11}\left(\frac{\gamma_{0,1}}{V}\right)\left(\frac{M_1}{V}\right)+k_{p21}\left(\frac{\pi_{0,1}}{V}\right)\left(\frac{M_1}{V}\right)\right]V\end{aligned} \tag{6.62}$$

$$\begin{aligned}\frac{d\pi_{1,1}}{dt} = &-\left[k_{tm22}\left(\frac{M_2}{V}\right)+\left(k_{p21}+k_{tm21}\right)\left(\frac{M_1}{V}\right)+k_{t22}\left(\frac{\pi_{0,0}}{V}\right)+k_{t12}\left(\frac{\gamma_{0,0}}{V}\right)\right]\left(\frac{\pi_{1,1}}{V}\right)V\\ &+k_{p12}\left(\frac{M_2}{V}\right)\left(\frac{\gamma_{1,1}}{V}\right)V\\ &+\left[k_{p22}\left(\frac{\pi_{1,0}}{V}\right)+k_{p12}\left(\frac{\gamma_{1,0}}{V}\right)\right]\left(\frac{M_2}{V}\right)V\end{aligned} \tag{6.63}$$

The moment balances for dead chains are:

$$\begin{aligned}\frac{d}{dt}\left[V\lambda_{k,l}\right] = &\,k_{tm11}\frac{M_1}{V}\gamma_{k,l}V+k_{tm12}\frac{M_2}{V}\gamma_{k,l}V+k_{tm21}\frac{M_1}{V}\pi_{k,l}V\\ &+k_{tm22}\frac{M_2}{V}\pi_{k,l}V+k_{td11}\gamma_{k,l}\gamma_{0,0}V\\ &+k_{td12}\left[\gamma_{k,l}\pi_{0,0}+\gamma_{0,0}\pi_{k,l}\right]V+k_{td22}\pi_{k,l}\pi_{0,0}V\\ &+\frac{k_{tc11}}{2}\sum_{i=o}^{k}\sum_{j=0}^{l}\left(\binom{k}{l}\binom{l}{j}\gamma_{i,j}\gamma_{k-i,l-j}V\right)\\ &+k_{tc12}\sum_{i=o}^{k}\sum_{j=0}^{l}\binom{k}{i}\binom{l}{j}\gamma_{i,j}\pi_{k-i,l-j}V\\ &+\frac{k_{tc22}}{2}\sum_{i=o}^{k}\sum_{j=0}^{l}\binom{k}{i}\binom{l}{j}\pi_{i,j}\pi_{k-i,l-j}V\end{aligned} \tag{6.64}$$

Making $k$ and $l$ equal to 0, 1 or 2, the following moments of the dead chain size

distributions can be obtained:

$$\begin{aligned}\frac{d}{dt}\left[\lambda_{0,0}\right] &= k_{td11}\left(\frac{\gamma_{0,0}}{V}\right)^2 V + k_{tm11}\frac{M_1}{V}\frac{\gamma_{0,0}}{V}V \\ &+ k_{td12}\left(\frac{\gamma_{0,0}}{V}\frac{\pi_{0,0}}{V} + \frac{\gamma_{0,0}}{V}\frac{\pi_{0,0}}{V}\right)V + k_{tc12}\frac{\gamma_{0,0}}{V}\frac{\pi_{0,0}}{V}V \\ &+ \frac{k_{tm12}}{2}\frac{M_2}{V}\frac{\gamma_{0,0}}{V}V + k_{tm21}\frac{M_1}{V}\frac{\pi_{0,0}}{V}V + k_{tm22}\frac{M_2}{V}\frac{\pi_{0,0}}{V}V \\ &+ \left(k_{td22} + \frac{k_{tc22}}{2}\right)\left(\frac{\pi_{0,0}}{V}\right)^2 V + \frac{k_{tc11}}{2}\left(\frac{\gamma_{0,0}}{V}\right)^2 V\end{aligned} \tag{6.65}$$

$$\begin{aligned}\frac{d}{dt}\left[\lambda_{1,0}\right] &= k_{td11}\left(\frac{\gamma_{1,0}}{V}\right)\left(\frac{\gamma_{0,0}}{V}\right)V + k_{td12}\left(\frac{\gamma_{0,0}}{V}\frac{\pi_{1,0}}{V} + \frac{\pi_{0,0}}{V}\frac{\gamma_{1,0}}{V}\right)V \\ &+ k_{tm11}\frac{M_1}{V}\frac{\gamma_{1,0}}{V}V + k_{tm12}\frac{M_2}{V}\frac{\gamma_{1,0}}{V}V + k_{tm21}\frac{M_1}{V}\frac{\pi_{1,0}}{V}V + k_{tm22}\frac{M_2}{V}\frac{\pi_{1,0}}{V}V \\ &+ k_{tc11}\frac{\gamma_{0,0}}{V}\frac{\gamma_{1,0}}{V}V + k_{tc12}\left(\frac{\gamma_{0,0}}{V}\frac{\pi_{1,0}}{V} + \frac{\pi_{0,0}}{V}\frac{\gamma_{1,0}}{V}\right)V \\ &+ k_{tc22}\frac{\pi_{0,0}}{V}\frac{\pi_{1,0}}{V}V + k_{td22}\frac{\pi_{0,0}}{V}\frac{\pi_{1,0}}{V}V\end{aligned} \tag{6.66}$$

$$\begin{aligned}\frac{d}{dt}\left[\lambda_{1,1}\right] &= k_{td11}\left(\frac{\gamma_{1,1}}{V}\right)\left(\frac{\gamma_{0,0}}{V}\right)V + k_{td12}\left(\frac{\gamma_{1,1}}{V}\frac{\pi_{0,0}}{V} + \frac{\pi_{1,1}}{V}\frac{\gamma_{0,0}}{V}\right)V \\ &+ k_{td22}\frac{\pi_{1,1}}{V}\frac{\pi_{0,0}}{V}V + k_{tm11}\frac{M_1}{V}\frac{\gamma_{1,1}}{V}V + k_{tm12}\frac{M_2}{V}\frac{\gamma_{1,1}}{V}V \\ &+ k_{tm21}\frac{M_1}{V}\frac{\pi_{1,1}}{V}V + k_{tm22}\frac{M_2}{V}\frac{\pi_{1,1}}{V}V \\ &+ k_{tc11}\left(\frac{\gamma_{0,0}}{V}\frac{\gamma_{1,1}}{V} + \frac{\gamma_{1,0}}{V}\frac{\gamma_{0,1}}{V}\right)V + k_{tc22}\left(\frac{\pi_{0,0}}{V}\frac{\pi_{1,1}}{V} + \frac{\pi_{1,0}}{V}\frac{\pi_{0,1}}{V}\right)V \\ &+ k_{tc12}\left(\frac{\gamma_{0,0}}{V}\frac{\pi_{1,1}}{V} + \frac{\pi_{0,0}}{V}\frac{\gamma_{1,1}}{V}\right)V + k_{tc12}\left(\frac{\gamma_{1,0}}{V}\frac{\pi_{0,1}}{V} + \frac{\pi_{1,0}}{V}\frac{\gamma_{0,1}}{V}\right)V\end{aligned} \tag{6.67}$$

$$\begin{aligned}\frac{d}{dt}\left[\lambda_{0,1}\right] &= k_{td11}\left(\frac{\gamma_{0,1}}{V}\right)\left(\frac{\gamma_{0,0}}{V}\right)V + k_{td12}\left(\frac{\gamma_{0,1}}{V}\frac{\pi_{0,0}}{V} + \frac{\pi_{0,1}}{V}\frac{\gamma_{0,0}}{V}\right)V \\ &+ k_{tm11}\frac{M_1}{V}\frac{\gamma_{0,1}}{V}V + k_{tm12}\frac{M_2}{V}\frac{\gamma_{0,1}}{V}V + k_{tm21}\frac{M_1}{V}\frac{\pi_{0,1}}{V}V + k_{tm22}\frac{M_2}{V}\frac{\pi_{0,1}}{V}V \\ &+ k_{tc11}\frac{\gamma_{0,0}}{V}\frac{\gamma_{0,1}}{V}V + k_{tc12}\left(\frac{\gamma_{0,0}}{V}\frac{\pi_{0,1}}{V} + \frac{\pi_{0,0}}{V}\frac{\gamma_{0,1}}{V}\right)V \\ &+ k_{tc22}\frac{\pi_{0,0}}{V}\frac{\pi_{0,1}}{V}V + k_{td22}\frac{\pi_{0,0}}{V}\frac{\pi_{0,1}}{V}V\end{aligned} \tag{6.68}$$

$$\begin{aligned}\frac{d}{dt}\left[\lambda_{2,0}\right] = {} & k_{td11}\left(\frac{\gamma_{2,0}}{V}\right)\left(\frac{\gamma_{0,0}}{V}\right)V + k_{td12}\left(\frac{\gamma_{0,0}}{V}\frac{\pi_{2,0}}{V} + \frac{\pi_{0,0}}{V}\frac{\gamma_{2,0}}{V}\right)V \\ & + k_{tm11}\frac{M_1}{V}\frac{\gamma_{2,0}}{V}V + k_{tm12}\frac{M_2}{V}\frac{\gamma_{2,0}}{V}V + k_{tm21}\frac{M_1}{V}\frac{\pi_{2,0}}{V}V + k_{tm22}\frac{M_2}{V}\frac{\pi_{2,0}}{V}V \\ & + k_{tc11}\left(\frac{\gamma_{0,0}}{V}\frac{\gamma_{2,0}}{V} + \left(\frac{\gamma_{1,0}}{V}\right)^2\right)V + k_{tc12}\left(\frac{\gamma_{0,0}}{V}\frac{\pi_{2,0}}{V} + \frac{\pi_{0,0}}{V}\frac{\gamma_{2,0}}{V}\right)V \\ & + 2.0\cdot k_{tc12}\frac{\gamma_{1,0}}{V}\frac{\pi_{1,0}}{V}V \\ & + k_{tc22}\left(\frac{\pi_{0,0}}{V}\frac{\pi_{2,0}}{V} + \left(\frac{\pi_{1,0}}{V}\right)^2\right)V + k_{td22}\frac{\pi_{0,0}}{V}\frac{\pi_{2,0}}{V}V\end{aligned} \tag{6.69}$$

$$\begin{aligned}\frac{d}{dt}\left[\lambda_{0,2}\right] = {} & k_{td11}\left(\frac{\gamma_{0,2}}{V}\right)\left(\frac{\gamma_{0,0}}{V}\right)V + k_{td12}\left(\frac{\gamma_{0,2}}{V}\frac{\pi_{0,0}}{V} + \frac{\pi_{0,2}}{V}\frac{\gamma_{0,0}}{V}\right)V \\ & + k_{td22}\frac{\pi_{0,0}}{V}\frac{\pi_{0,2}}{V}V \\ & + k_{tm11}\frac{M_1}{V}\frac{\gamma_{0,2}}{V}V + k_{tm12}\frac{M_2}{V}\frac{\gamma_{0,2}}{V}V + k_{tm21}\frac{M_1}{V}\frac{\pi_{0,2}}{V}V + k_{tm22}\frac{M_2}{V}\frac{\pi_{0,2}}{V}V \\ & + k_{tc11}\left(\frac{\gamma_{0,0}}{V}\frac{\gamma_{0,2}}{V} + \left(\frac{\gamma_{0,1}}{V}\right)^2\right)V + k_{tc12}\left(\frac{\gamma_{0,0}}{V}\frac{\pi_{0,2}}{V} + \frac{\pi_{0,0}}{V}\frac{\gamma_{0,2}}{V}\right)V \\ & + 2.0\cdot k_{tc12}\frac{\gamma_{0,1}}{V}\frac{\pi_{0,1}}{V}V \\ & + k_{tc22}\left(\frac{\pi_{0,0}}{V}\frac{\pi_{0,2}}{V} + \left(\frac{\pi_{0,1}}{V}\right)^2\right)V\end{aligned} \tag{6.70}$$

Because of the fast dynamic responses of the living chains when compared to the other species present in the polymerization system, the quasi-steady state hypothesis can be used for $P_{i,j}$ and $Q_{i,j}$. Finally, average molecular weights can be calculated with Equations 6.71 and 6.72, where Mn and Mw are the number and weight average molecular weights and $\overline{M_1}$ and $\overline{M_2}$ are the molecular weights of monomer 1 (Sty or MMA) and cardanol, respectively.

$$M_n = \frac{\left(\gamma_{1,0}+\pi_{1,0}+\lambda_{1,0}\right)\overline{M_1} + \left(\gamma_{0,1}+\pi_{0,1}+\lambda_{0,1}\right)\overline{M_2}}{\gamma_{1,0}+\pi_{1,0}+\lambda_{1,0}} \tag{6.71}$$

$$M_w = \frac{\left(\gamma_{2,0}+\pi_{2,0}+\lambda_{2,0}\right)\overline{M_1^2} + \left(\gamma_{1,1}+\pi_{1,1}+\lambda_{1,1}\right)\overline{M_1 M_2} + \left(\gamma_{0,2}+\pi_{0,2}+\lambda_{0,2}\right)\overline{M_2^2}}{\left(\gamma_{1,0}+\pi_{1,0}+\lambda_{1,0}\right)\overline{M_1} + \left(\gamma_{0,1}+\pi_{0,1}+\lambda_{0,1}\right)\overline{M_2}} \tag{6.72}$$

Cardanol copolymer composition and cardanol weight fraction in the reaction

medium can be calculated with Equations 6.73 and 6.74.

$$C_{n_{M2}} = \frac{\lambda_{0,1}}{\lambda_{1,0} + \lambda_{0,1}} \tag{6.73}$$

$$\omega_{M2} = \frac{\rho_{m2} v_{m2}}{\rho_{m1} v_{m1} + \rho_{m2} v_{m2} + \rho_p v_p} \tag{6.74}$$

## 6.5 Parameters for homopolymerization

MMA and styrene have been used for decades, so that the kinetics of these reactions are well known and the kinetics parameters are available. Every parameter is a function of the reaction temperature and is correlated by an Arrhenius expression (Equation 6.75). Thus, for each monomer, a set of characteristic kinetic parameters were used. As reactions were initiated by benzoyl peroxide (BPO), the same dissociation parameter was used in all simulation. The universal gas constant (R) is equal to $1.987 cal.gmol^{-1}.K^{-1}$.

$$k_i = A \exp\left(\frac{-E_I}{RT}\right) \tag{6.75}$$

$$T(K) = T(°C) + 273.15 \tag{6.76}$$

Table 6.2 shows the kinetic parameters and physicochemical properties used to describe the homopolymerization of styrene ($M_1$) with benzoyl peroxide initiator (BPO). These parameters were obtained from several works published in the literature. Table 6.3 shows the kinetic parameters and physicochemical properties used to describe the homopolymerization of methyl methacrylate (also labeled as $M_1$). Equations used for glass and gel effect are presented in Table 6.4 (PINTO and RAY, 1995). Regarding the parameters related to cardanol, they are not available in the literature. Therefore, they must be estimated.

Table 6.1: Dissociation parameter used for benzoyl peroxide.

| Parameter | Unit | Reference |
|---|---|---|
| $k_d^0 = 6.120 \cdot 10^{17} \exp\left(\frac{-30000}{RT(K)}\right)$ | $h^{-1}$ | KALFAS and RAY (1993) |

Table 6.2: Kinetic parameters of styrene homopolymerizations.

| Parameter | Unit | Reference |
|---|---|---|
| $\rho_{m1} = 924 - 0.918(T(K) - 273.15)$ | $g \cdot L^{-1}$ | SCORAH *et al.* (2006) |
| $\rho_p = 1080 - 0.6058(T(K) - 273.15)$ | $g \cdot L^{-1}$ | SCORAH *et al.* (2006) |
| $k_{dm} = 2.190 \cdot 10^5 \exp\left(\frac{-27440}{RT(K)}\right)$ | $L^2 \cdot mol^{-2} \cdot s^{-1}$ | KIM and CHOI (1989) |
| $k_{p11} = 3.816 \cdot 10^{10} \exp\left(\frac{-7067}{RT(K)}\right)$ | $L \cdot mol^{-1} \cdot h^{-1}$ | TSOUKAS *et al.* (1982) |
| $k_{tc11} = 1.26 \cdot 10^9 \exp\left(\frac{-1680}{RT(K)}\right)$ | $L \cdot mol^{-1} \cdot s^{-1}$ | KALFAS and RAY (1993) |
| $k_{td11} = 2.052 \cdot 10^{18} \exp\left(\frac{-153000}{RT(K)}\right)$ | $L \cdot mol^{-1} \cdot h^{-1}$ | MELO *et al.* (2014) |
| $k_{tm11} = 2.463 \cdot 10^5 \exp\left(\frac{-10280}{RT(K)}\right)$ | $L \cdot mol^{-1} \cdot s^{-1}$ | KIM *et al.* (1992) |
| $f = 0.70$ | - | SCORAH *et al.* (2006) |
| $\alpha_{m1} = 0.001$ | $K^{-1}$ | VILLALOBOS *et al.* (1993) |
| $\alpha_p = 0.00048$ | $K^{-1}$ | VILLALOBOS *et al.* (1993) |
| $T_{gm1} = 185.0$ | $K$ | VILLALOBOS *et al.* (1993) |
| $T_{gp} = 370.0K$ | $K$ | VILLALOBOS *et al.* (1993) |
| $v_{fcr} = 0.036$ | - | VIVALDO-LIMA *et al.* (1998) |
| $A_{gel} = 0.32$ | - | MELO *et al.* (2014) |
| $A_{glass} = 1.7$ | - | MELO *et al.* (2014) |
| $MM_{m1} = 104.15$ | Da | |

Table 6.3: Kinetic parameters of MMA homopolimerizations.

| Parameter | Unit | Reference |
|---|---|---|
| $\rho_{m1} = 0.9654 - \frac{1.09}{10^3}(T - 273.15) - \frac{9.7}{10^7}(T - 273.15)^2$ | $g \cdot cm^{-3}$ | PINTO and RAY (1995) |
| $\rho_p = \rho_{m1}(0.754 - \frac{9.0}{10^4}(T - 343.15))^{-1}$ | $g \cdot cm^{-3}$ | PINTO and RAY (1995) |
| $k_{dm} = 0.0$ | $L^2 \cdot mol^{-2} \cdot s^{-1}$ | Considered in this work |
| $k_{p11} = 4.92 \cdot 10^5 \exp\left(\frac{-4353}{RT(K)}\right)$ | $L \cdot mol^{-1} \cdot s^{-1}$ | MAHABADI and O'DRISCOLL (1977) |
| $k^0_{tc11} = 9.8 \cdot 10^7 \exp\left(\frac{-701}{RT(K)}\right)$ | $L \cdot mol^{-1} \cdot s^{-1}$ | MAHABADI and O'DRISCOLL (1977) |
| $k^0_{td11} = 3.956 \cdot 10^{-4} \exp\left(\frac{-4090}{RT(K)}\right) * k^0_{tc11}$ | $L \cdot mol^{-1} \cdot s^{-1}$ | BEVINGTON *et al.* (1954) |
| $k_{tm11} = 4.66 \cdot 10^9 \exp\left(\frac{-76290}{8.3144621 * T(K)}\right)$ | $L \cdot mol^{-1} \cdot s^{-1}$ | PEKLAK *et al.* (2006) |
| $f = 0.80$ | - | LOUIE *et al.* (1985) |
| $\alpha_{m1} = 0.001$ | $K^{-1}$ | PINTO and RAY (1995) |
| $\alpha_{\mathrm{p}} = 0.00048$ | $K^{-1}$ | PINTO and RAY (1995) |
| $T_{gm1} = 167.0$ | $K$ | PINTO and RAY (1995) |
| $T_{gp} = 387.15$ | $K$ | PINTO and RAY (1995) |
| $v_{fcr} = 0.04227$ | - | Considered in this work |
| $v_{ftc} = 0.01856 - 2.965 \cdot 10^{-4}(T - 273.15)$ | - | PINTO and RAY (1995) |
| $MM_{m1} = 100.121$ | Da | - |

Table 6.4: Equations used to describe gel and glass effects for MMA.

| $g_{T,MMA}$ | |
|---|---|
| $0.10575 \cdot \exp(17.15 v_f - 0.01715(T - 273.15)$ | $v_f > v_{ftc}$ |
| $2.3 \cdot 10^{-6} \exp(75 v_f)$ | $v_f \leq v_{ftc}$ |
| $g_{P,MMA}$ | |
| 1 | $v_f > v_{fcr}$ |
| $7.1 \cdot 10^{-5} \exp(171.53 v_f)$ | $v_f > v_{ftc}$ |

## 6.6 Parameter estimation

As discussed by SCHWAAB and PINTO (2007), parameter estimation consists in utilizing a reference model and changing the parameters until the predictions of the model fits the experimental data, respecting the uncertainties of the measurements.

Thus, all balance equations were solved numerically using backward differentiation formula (BDF), as available in the DASSL code with relative and absolute tolerances of $10^{-4}$. Model parameters were estimated with the computational package ESTIMA, implemented in Fortran, which combines particle swarm (stochastic) optimization (PSO) and the deterministic Gauss-Newton algorithms (SCHWAAB *et al.* (2008)) with the accelerator of LAW and BAILEY (1963).

The Gauss-Newton method frequently fails when dealing with ill-posed problems, making impossible the determination of parameter uncertainties (as the covariance matrix of parameter uncertainties cannot be obtained). In these cases, first, particle swarm optimization can be applied. Then, with the point of minimum obtained with the PSO technique, an identifiability procedure can be applied to determine which set of model parameters can have the uncertainties evaluated. Afterwards, the Gauss-Newton procedure can be applied to estimate the selected parameters and refine the minimum of the previously estimated model parameters (BRANDÃO (2017)).

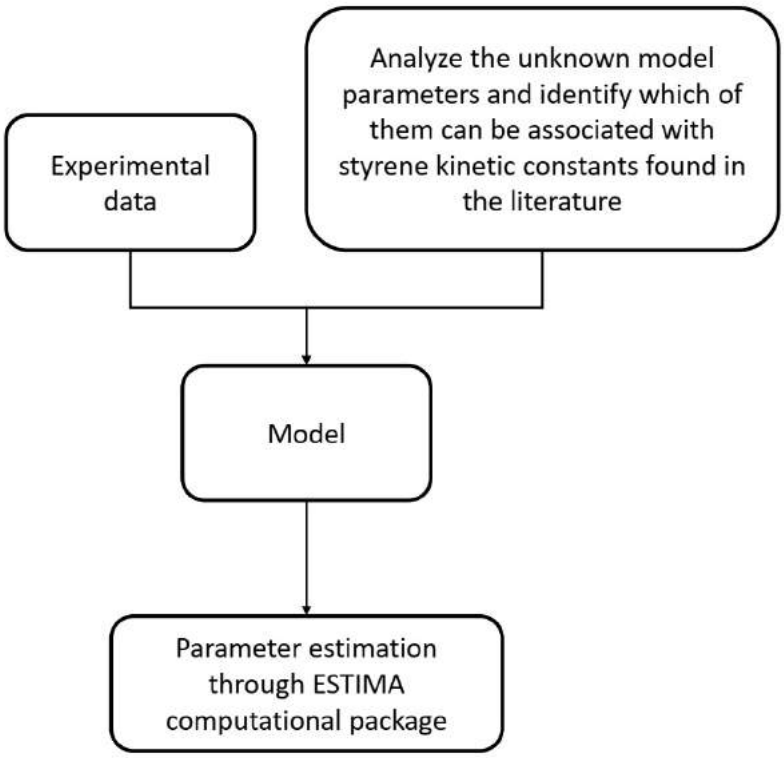


Figure 6.1: Employed parameter estimation procedure.

One hundred particles were used and ten thousand iterations were carried out with

statistical confidence level of 95%. To avoid numerical problems, due to the differences of orders of magnitude among the parameter values, some model parameters were estimated in their logarithmic form.

For the sake of simplicity, for each experimental condition, it was executed one model parameters estimation procedure. Then, the estimated parameters were analyzed together in order to evaluate the consistency of the obtained results. The objective function used in the present work was defined as follows:

$$F_{obj} = \left(y^e - y^m\left(x^m, \theta\right)\right)^T V_y^{-1} \left(y^e - y^m\left(x^m, \theta\right)\right) \tag{6.77}$$

where $y$ and $y^m$ are the vectors of the measured and predicted dependent variables, respectively; $V_y$ is the covariance matrix of the measured outputs (assumed to be diagonal); and $x^m$ and $\theta$ are the vectors of the measured independent variables and model parameters, respectively. The measured variables considered were conversion, number and weight average molecular weights ($\bar{M}_n$ and $\bar{M}_w$).

## 6.7 Simulations

For poly(styrene-*co*-cardanol) simulations, besides the data previously reported for overall monomer conversions and average molecular weights of polymer samples, data provided by GALVÃO (2016) were also included to increase the degrees of freedom and the reliability of the estimations, as shown in 6.5.

Regarding the parameters related to cardanol or CNSL, they are not available in the literature. However, as cardanol and natural CNSL led to similar kinetic behaviors when copolymerized with methyl methacrylate, the respective kinetic parameters were assumed to be the same. Also, based on their structures, if one assumes that only terminal double bonds can react through free-radical polymerization mechanisms, one

Table 6.5: Experimental conditions used for parameter estimation for styrene/cardanol copolymerization, as provided by GALVÃO (2016).

| Experimental Condition | Styrene (wt%) | Cardanol (wt%) | BPO (wt%) | T (°C) | Reaction Duration (h) | Sample Interval (min) |
|---|---|---|---|---|---|---|
| A1 | 96.5 | 2.5 | 1.0 | 110 | 5 | 30 |
| A2 | 94.0 | 5.0 | 1.0 | 110 | 5 | 30 |
| A3 | 96.5 | 2.5 | 1.0 | 90 | 5 | 30 |
| A4 | 94.0 | 5.0 | 1.0 | 90 | 5 | 30 |
| A5 | 99.0 | 0.0 | 1.0 | 90 | 3 | 15 |
| A6 | 99.0 | 0.0 | 1.0 | 110 | 3 | 15 |

Table 6.6: Parameters used for cardanol

| Parameter | Unit | Reference |
|---|---|---|
| $k_{tm21} = k_{tm12} = k_{p22} = 0$ | $L \cdot mol^{-1} \cdot h^{-1}$ | Considered in this work |
| $k_{tc22} = k_{td22} = k_{tc11}$ | $L \cdot mol^{-1} \cdot h^{-1}$ | Considered in this work |

will conclude that just 40% of the phenolic stream can be available as monomer for the polymerization. Despite that, given the fact that other molecules may be eventually present in the naturally occurring cardanol or anacardic acid stream and that different reactive sites (such as the phenolic group) can take part in the reaction mechanism, the whole stream is treated as a lumped monomer stream for purposes of kinetic modeling.

It is important to emphasize that cardanol polymerizes at slow rates at the analyzed reaction conditions through free-radical polymerizations, as observed experimentally. Therefore, for the sake of simplicity, some model parameters were initially assumed to be either null or equal to the styrene or methyl methacrylate polymerization parameters, as shown in Table 6.6. Particularly, one must observe that $kp_{22}$ was assumed to be equal to zero, imposing the modification of the normal reactivity ratio scheme used to describe the copolymerization.

Therefore, the parameters to be found are $k_{p12}$ and $k_{p21}$, which are dependent only of $k_{p11}$. Thus $r_{1,2}$ and $r_{2,1}$ were estimated as defined:

$$k_{p12} = k_{p11} \cdot r_{1,2} \tag{6.78}$$

$$k_{p21} = k_{p11} \cdot r_{2,1} \tag{6.79}$$

Although $r_{1,2}$ and $r_{2,1}$ resemble the classical reactivity ratios, they are not the reactivity ratios, as $k_{p22}$ is assumed to be equal to zero because cardanol practically does not homopolymerize through regular free-radical polymerizations at the analyzed conditions. Despite that,$r_{1,2}$ and $r_{2,1}$ are parameters that indicate the relative magnitudes of the rates of cross propagation in respect to the rate of styrene homopropagation. Moreover, $f_{inh}$ is also estimated. This constant corresponds to the inhibition effect of cardanol and is used to reduce the number of living radicals in the reaction media. Thus, the initial initiator concentration is multiplied by this inhibition factor, which implies that inhibitors can react very fast with the primary radicals and interrupt the course of the polymerization, reducing the efficiency of the initiation step.

Table 6.7: Estimated model parameters for styrene homopolymerization reactions.

| Exp. Cond. | $F_{obj}$ | $\chi^2_{inf}$ | $\chi^2_{sup}$ | $\delta_{tm}$ |
|---|---|---|---|---|
| A5 | 37.58 | 16.85 | 45.72 | $0.849 \pm 0.129$ |
| A6 | 35.40 | 16.85 | 45.72 | $1.211 \pm 0.113$ |

### 6.7.1 Styrene Homopolymerization

Using experimental conditions A5 and A6, the kinetic parameters of Table 6.2 can be tested. A correction factor $\delta_{tm}$ was estimated for the kinetic constant for chain transfer to monomer ($k_{tm11} = \delta_{tm} k_t m11$) to account for possible presence of impurities. Table 6.7 presents the estimated parameters for reactions at both temperatures.

As shown in Table 6.7, estimated values of the kinetic constant for chain transfer to monomer $k_{tm11}$ were very close to the real reference literature parameter value $k_{tm11}$, indicating the adequacy of the proposed modeling approach. The quality of the model fit was evaluated with the chi-square statistical test. According to this test, the model can be considered suitable, since the final objective function value, $F_{obj}$, lay between the limits provided by the $\chi^2$ distribution. Therefore, as shown in Figures 6.2 and 6.3, the proposed model fits the available experimental data adequately. Thus, the homopolymerization model is trustable and ready for copolymerization analyses.

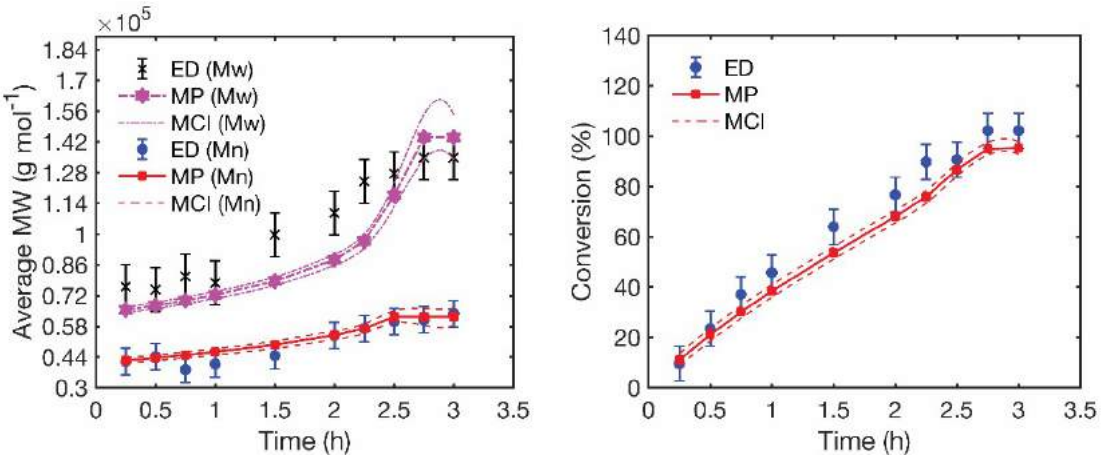


(a) (b)

Figure 6.2: Predicted and experimental results for styrene homopolymerizations performed at 90 °$C$ (condition A5). (MCI = model confidence interval; MP = model predictions and ED = experimental data).

Thus, for copolymerization parameter estimation, except for the constant of chain transfer to styrene, that was fixed as $k_{tm11} = 1.211 k^0_{tm11}$, which corresponds to the estimated value of this kinetic constant for experimental condition A6, all the remaining kinetic parameters used are the ones presented in Table 6.2.

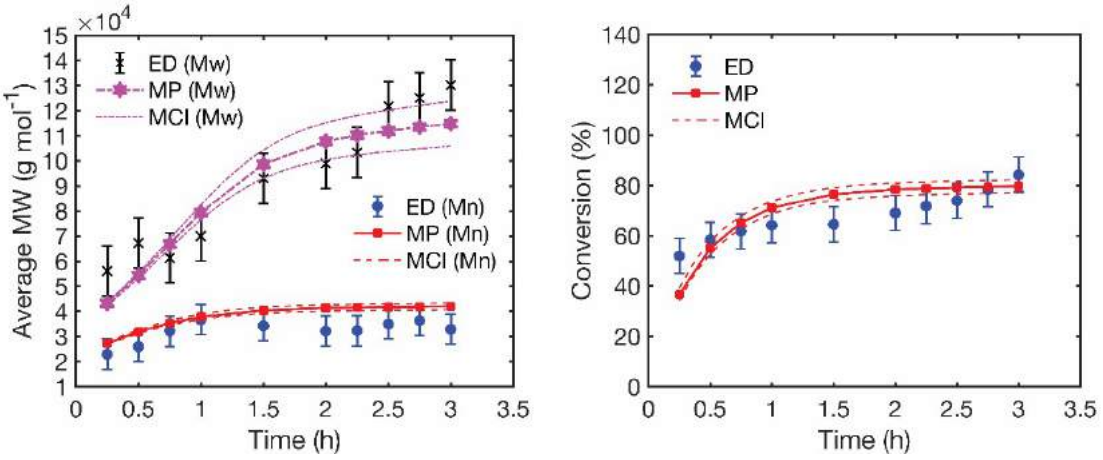


(a) (b)

Figure 6.3: Predicted and experimental results for styrene homopolymerizations at 110 °$C$ (condition A6). (MCI = model confidence interval; MP = model predictions and ED = experimental data).

### 6.7.2 Styrene/Cardanol Copolymerizations at 110 °$C$

Table 6.8 presents the estimated model parameters for styrene/cardanol copolymerization reactions. At both conditions, A1 and A2, the final objective function values lay inside the most likely range defined by the $\chi^2$ distribution distribution, indicating the adequacy of the proposed model. Figure 6.4 shows the joint confidence region for parameters $r_{1,2}$ and $r_{2,1}$ when parameter $f_{inh}$ was fixed at its optimal value shown in Table 6.8. To generate this figure, a new estimation procedure was run but this time $f_{inh}$ was fixed at 0.731. The new objective function obtained was equal to 21.34 and the estimated values for $r_{1,2}$ and $r_{2,1}$ were equal to 1.628 and 0.026, respectively.

As one can see in Table 6.8, $f_{inh}$ decreased with the cardanol feed concentration, which caused the simultaneous increase of the inhibitor concentration in the reacting medium, as already described. Therefore, the concentration of active radicals is expected to diminish with the amount of cardanol in the feed. Regarding the estimated values of $r_{1,2}$ and $r_{2,1}$, it must be considered that the incorporation of cardanol

Table 6.8: Estimated model parameters for cardanol/styrene copolymerization reactions performed at 110 °$C$.

| | A2 | | A1 | |
|---|---|---|---|---|
| Exp. Cond. | Estimated Value | Confidence Interval | Estimated Value | Confidence Interval |
| $F_{obj}$ | 21.34 | 15.31 - 44.46 | 41.39 | 16.79 - 46.98 |
| $f_{inh}$ | 0.731 | 0.721 - 0.740 | 0.888 | 0.814 - 0.962 |
| $r_{1,2}$ | 1.627 | 1.589 - 1.666 | $r_{1,2}$estimated at A2 | |
| $r_{2,1}$ | 0.023 | 0.022 - 0.031 | $r_{2,1}$estimated at A2 | |

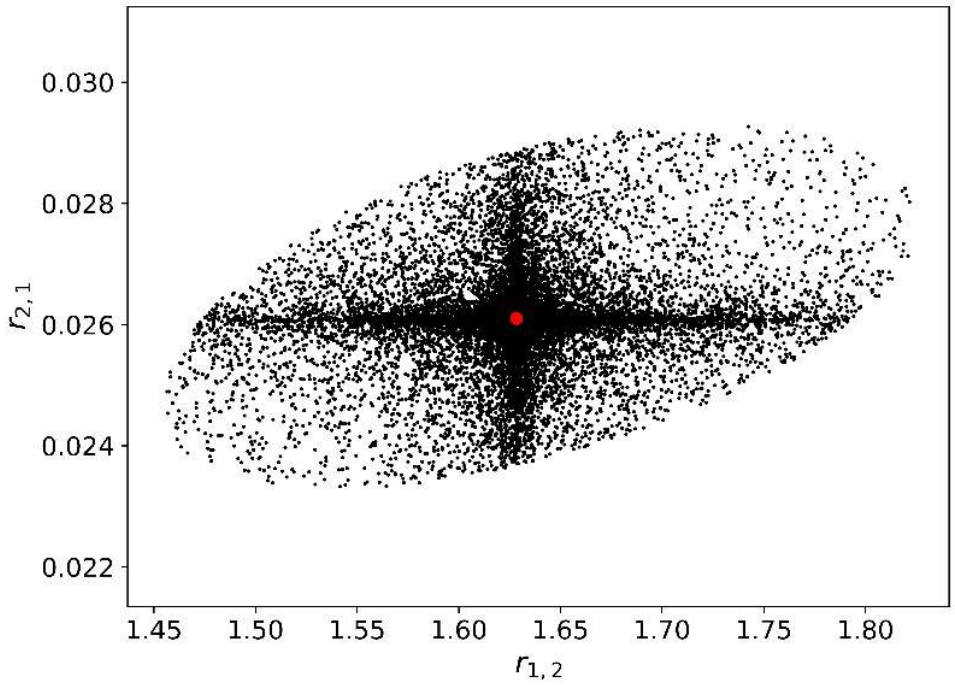


Figure 6.4: Joint confidence region for parameters $r_{1,2}$ and $r_{2,1}$ when parameter $f_{inh}$ was fixed at 0.731. The red center dot is the estimated values of $r_{1,2}$ and $r_{2,1}$ (1.628, 0.026).

molecules by propagating chains can cause the steric hindrance of the active centers of growing macroradicals, justifying the low $k_{p21}$ values ($k_{p21} = 0.026 \cdot k^0_{p11}$). Also, one must consider that more stable radicals can be formed due to the presence of the phenolic ring and internal unsaturation, retarding the polymerization rate. It is interesting to observe that the incorporation of cardanol molecules seems preferable than the incorporation of styrene at initial times because styrene forms radicals that are more stable and less reactive due to the proximity of the aromatic ring, while cardanol forms secondary radicals that are not stabilized by the phenolic ring. Moreover, although only the terminal double bond seems responsible for the usual addition steps, cardanol presents multiple reactive sites that are also prone to reaction and formation of radicals (as suggested by the $^1H-NMR$ spectra), which can also retard the polymerization, leading to small $k_{p21}$ values. Figures 6.5 and 6.6 present the available experimental data and simulation results for monomer conversion and average molecular weights, illustrating the very good quality of the obtained model fits.

The obtained results are strongly connected to the relative decrease of radical concentration ($P_{(i,j)} and Q_{(i,j)}$) in the reacting system, due to the previously described inhibitory effects of phenolic compounds. As one can see in Figures 6.5 and 6.6, monomer conversions were smaller at condition A2 (with 5 wt% of cardanol) than at

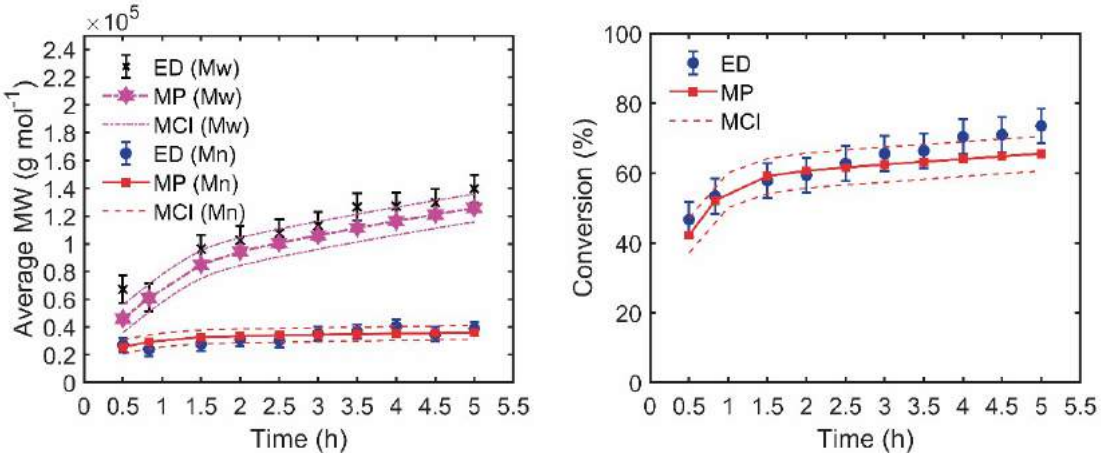


(a) (b)

Figure 6.5: Predicted and experimental results for styrene/cardanol copolymerization at condition A1. (MCI = model confidence interval; MP = model predictions and ED = experimental data).

condition A1 (2.5 wt% of cardanol). Nevertheless, as illustrated in Figure 6.7-a, despite the inhibitory effect exerted by cardanol, it was possible to obtain copolymers with relatively high amounts of cardanol incorporated into copolymer chains at both conditions, due to the relatively high cardanol reactivity of the polyunsaturated cardanol molecules. Since styrene thermal initiation is more pronounced at 110°C, reaction rates were kept almost constant (although at low values) after approximately 1 hour of reaction (Figure 6.5b and 6.6b). Regarding the cardanol composition, it is possible to observe in Figure 6.7 - a that model simulations indicated that cardanol copolymer compositions did not change very significantly during the reaction course. Besides, Figure 6.7 suggests that cardanol was almost completely consumed at experimental condition A1, while at condition A2 a residual amount of nonreacted cardanol remained in the reacting medium. Despite the larger amount of cardanol incorporated into copolymer chains at condition A2, higher inhibition effects could also be noticed at this condition.

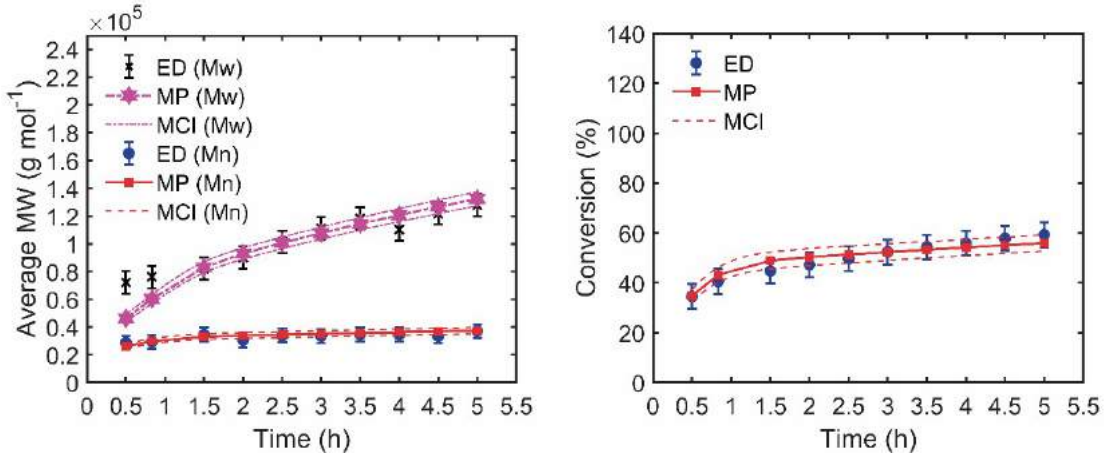


(a) (b)

Figure 6.6: Predicted and experimental results for styrene/cardanol copolymerization at condition A2. (MCI = model confidence interval; MP = model predictions and ED = experimental data).

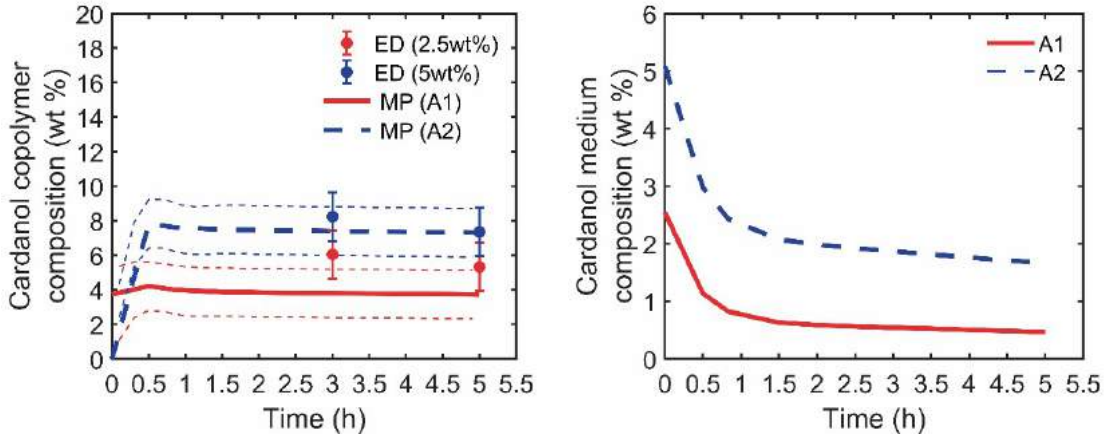


(a) (b)

Figure 6.7: Predicted and experimental results for cardanol compositions at conditions A1 and A2. (MP = model predictions and ED = experimental data).

### 6.7.3 Styrene/Cardanol Copolymerizations at 90°C

At 90°C, all three parameters were selected for estimation again. The constant of chain transfer to styrene was fixed as $k_{tm11} = 0.849 \cdot k^0_{tm11}$ which corresponds to the estimated value of this kinetic constant for experimental condition A5. Table 6.9 presents the estimated model parameters for styrene/cardanol copolymerization reactions performed at 90 °C. As one can observe, cardanol exerted stronger inhibitory effects at the lower temperature. At 90 °C, lower concentrations of radicals are expected due to the smaller decomposition rates of BPO and thermal initiation rates of styrene. In addition, as radicals react with cardanol due to $r_{1,2}$, they get stabilized and react more slowly due to steric hindrance, making more difficult the propagation of cardanol terminated radicals. Figure 6.8 shows the joint confidence region for parameters $r_{1,2}$ and $r_{2,1}$ when parameter $f_{inh}$ was fixed at its optimal value shown in Table 6.9. To generate this figure, a new estimation procedure was run, but this time $f_{inh}$ was fixed at 0.628. The new objective function obtained was equal to 43.44 and the estimated values for $r_{1,2}$ and $r_{2,1}$ were equal to 3.172 and 0.015, respectively.

As one can see in Table 6.9, the values estimated for the cross-propagation rate constants at 90 °C were not much different from the ones estimated at 110 °C (Table 6.8), mainly for $r_{2,1}$. This indicates that the reaction temperature does not seem to exert a strong effect on the relative kinetic constants for cardanol incorporation. The apparent increase of $r_{1,2}$ can possibly be related to more complex mechanistic effects, such as penultimate cross-propagation and cross-termination effects, which can become more evident at lower rates of reaction. Moreover, other effects, such as the less intense thermal initiation of styrene and the lower reactivity of benzene radicals, can also lead to lower rates of reaction. Again, the obtained objective function values lay in the chi-square confidence interval, showing that the model could predict well the available experimental data. Figures 6.9 and 6.10 illustrate the obtained experimental data and simulation results for monomer conversion and average molecular weights.

As previously discussed, conversion and average molecular weights presented lower values at condition A4 (with 5 wt% of cardanol) than the ones obtained at con-

Table 6.9: Estimated model parameters for cardanol/styrene copolymerization reactions performed at 90 °.

| | A3 | | A4 | |
|---|---|---|---|---|
| Exp. Cond. | Estimated Value | Confidence Interval | Estimated Value | Confidence Interval |
| $F_{obj}$ | 43.44 | 15.31 - 44.46 | 36.29 | 16.79 - 46.98 |
| $f_{inh}$ | 0.628 | 0.609 - 0.649 | 0.572 | 0.552 - 0.593 |
| $r_{1,2}$ | 3.210 | 2.356 - 4.372 | $r_{1,2}$estimated at A3 | |
| $r_{2,1}$ | 0.015 | 0.010 - 0.025 | $r_{2,1}$estimated at A3 | |

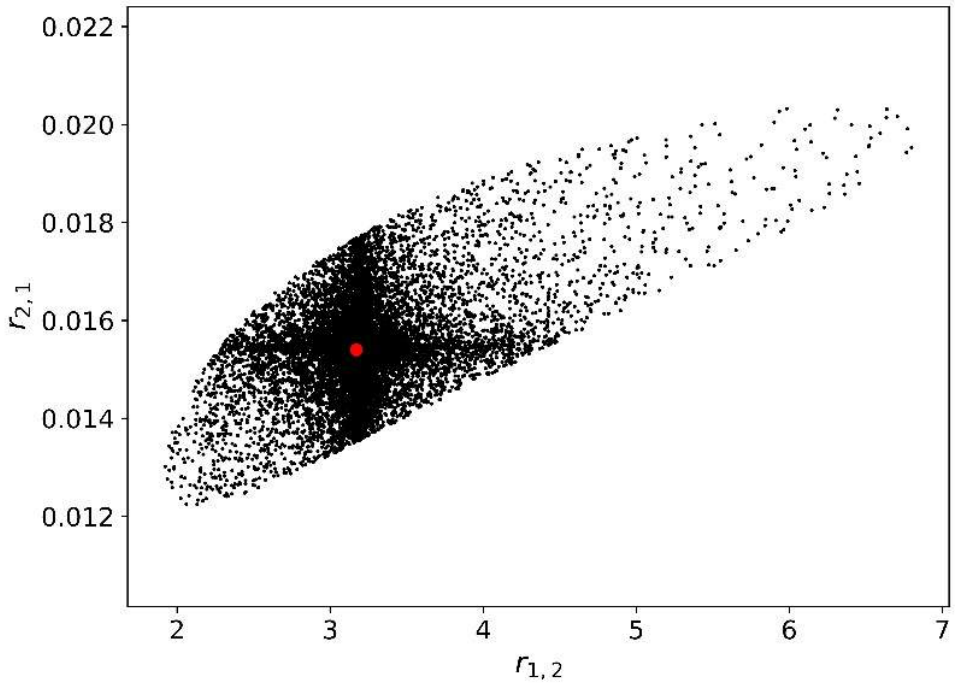


Figure 6.8: Joint confidence region for parameters $r_{1,2}$ and $r_{2,1}$ when parameter $f_{inh}$ was fixed at 0.628. The red center dot is the estimated values of $r_{1,2}$ and $r_{2,1}$ (3.172, 0.015).

dition A3 (with 2.5 wt% of cardanol), due to inhibition effects. Regarding the cardanol copolymer and medium compositions for conditions A3 and A4, the obtained model indicates higher cardanol copolymer compositions at condition A4 than at condition A3, as shown in Figure 6.11, despite the lower reaction rates at condition A4, as a consequence of the higher cardanol concentrations in the feed. However, cardanol copolymer compositions obtained in copolymerizations performed at 90 °C were expected to be lower than the ones obtained at 110 °C, due to the lower rates of radical generation by thermal styrene initiation at 90 °C.

### 6.7.4 Styrene/Cardanol Copolymerizations at 110 °C for 10 wt %

Using the experimental values obtained for the copolymerization at 110 °C for 10 wt %, the kinetic model can be validated once again. The experimental values obtained for 85 °C were not used because they were not satisfactory, as the inhibition was very high and average molecular weights and composition could not be obtained with good precision. Figure 6.12 shows the conversion and average molecular weights obtained experimentally and the model prediction. It can be seen the model was able to fit the data correctly with the parameters shown in Table 6.10.

For conditions A1 and A2, $r_{1,2}$ and $r_{2,1}$ values were equal to 1.627 and 0.023, re-

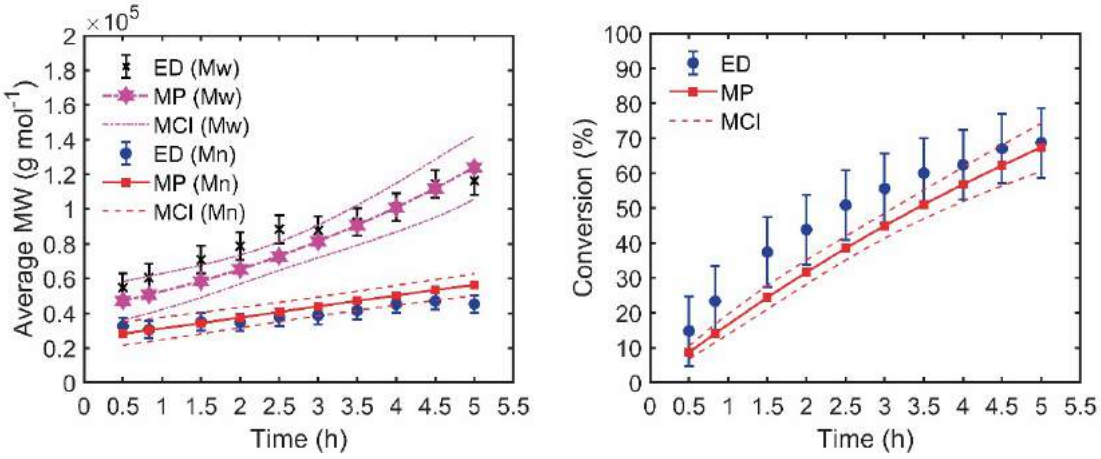


(a) (b)

Figure 6.9: Predicted and experimental results for styrene/cardanol copolymerization at condition A3. (MCI = model confidence interval; MP = model predictions and ED = experimental data).

Table 6.10: Estimated model parameters for cardanol/styrene copolymerization reactions performed with 10 wt % at 110 °C.

| | **10 wt %; 110°C** | |
|---|---|---|
| **Exp. Cond.** | **Estimated Value** | **Confidence Interval** |
| $F_{obj}$ | 15.00 | 6.26 - 27.49 |
| $f_{inh}$ | 0.478 | 0.439 - 0.519 |
| $r_{1,2}$ | 1.765 | 1.699 - 1.833 |
| $r_{2,1}$ | 0.016 | 0.012 - 0.021 |

spectively. They were similar to the other values obtained at this same temperature. Besides, $f_{inh}$ corresponded to 0.888 for 2.5 wt % (condition A1), 0.731 for 5.0 wt % (condition A2) and 0.478 for this condition, which could be expected since the inhibition is expected to increase with cardanol content. Figure 6.13 shows the copolymer composition for this condition and the model was also able to fit these data. Therefore, the model is capable of reproducing available experimental results in the analyzed ranges of concentrations and temperatures, following conversion, average molecular weights and copolymer composition trajectories successfully.

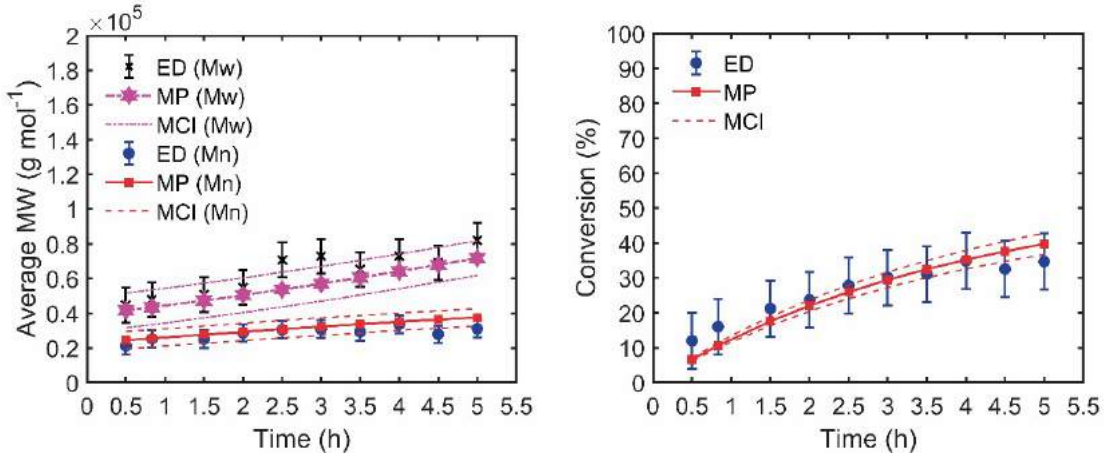


(a) (b)

Figure 6.10: Predicted and experimental results for styrene/cardanol copolymerization at condition A4. (MCI = model confidence interval; MP = model predictions and ED = experimental data).

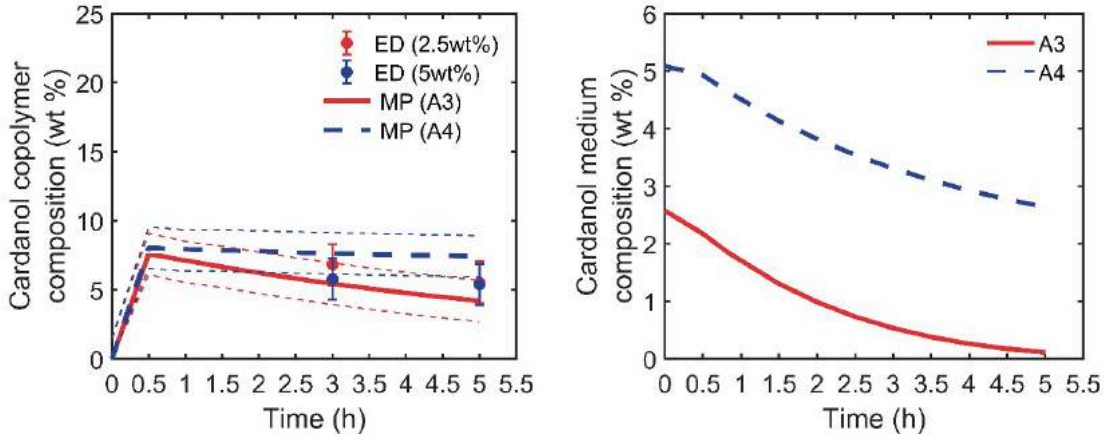


(a) (b)

Figure 6.11: Predicted and experimental results for cardanol compositions at conditions A3 and A4 (MP = model predictions).

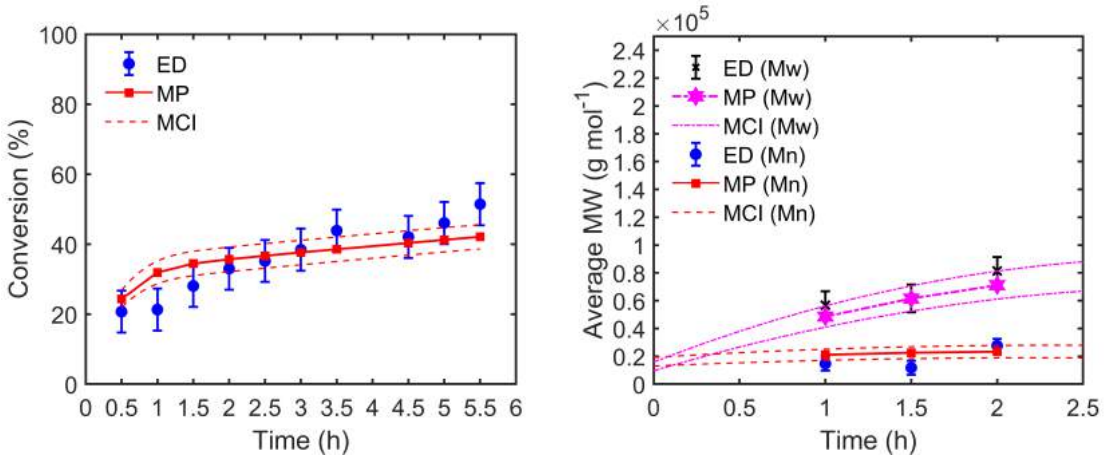


(a) (b)

Figure 6.12: Predicted and experimental results for cardanol copolymerization at 110 °C for 10 wt % (MCI = model confidence interval; MP = model predictions and ED = experimental data).

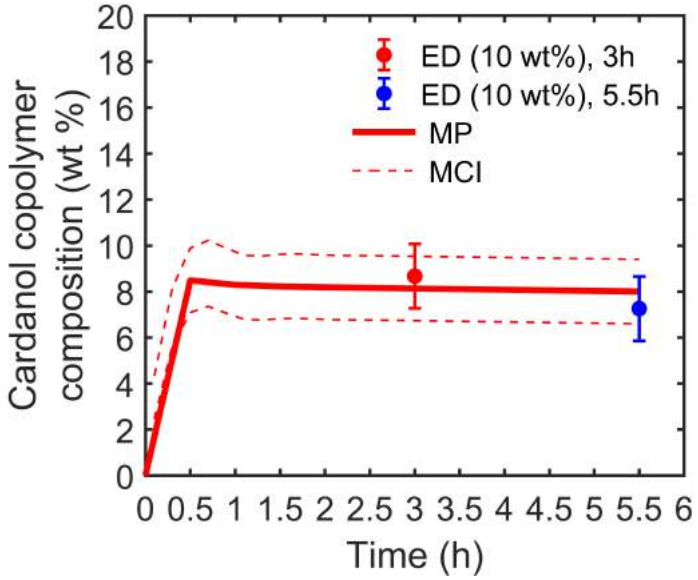


Figure 6.13: Predicted and experimental results for cardanol compositions at 110 °C for 10 wt % (MCI = model confidence interval; MP = model predictions and ED = experimental data).

### 6.7.5 Methyl Methacrylate/Cardanol Copolymerizations at 85 °C

For both temperatures (85 and 110 °C), kinetic parameters for methyl methacrylate/cardanol copolymerization were also estimated. However, due to the small number of experimental data, results were not so accurate. Nonetheless, the same kinetic model proposed for styrene-cardanol copolymerization was used in this case. Using the previous estimation strategy, the parameters estimates were obtained in the logarithmic form. Esimated model parameters are shown in Tables 6.11 and 6.12. Although $F_{obj}$ values were sometimes higher than imposed by the chi-square distribution, the experimental values were in general represented well, as shown in Figures 6.17 to 6.19. The parameters estimated indicate that MMA radical preferentially reacts with MMA molecules, as expected; that cardanol radicals react very slowly with MMA molecules, leading to the retardation effect; and that inhibition is smaller in MMA reactions than in styrene reactions, as observed experimentally.

As average molecular weight and copolymer composition could not be fitted simultaneously well in some cases, the model was adapted by adding a transfer to monomer reaction step. This modification was proposed because transfer reactions do not affect the conversion, but affect the molecular weights. $k_{tm22}$ was considered to be null because radicals present a cardanol terminal unit are not reactive. Kinetic parameter $k_{tm21}$ was also maintained as null for the same reason. Thus, a fourth parameter was estimated to represent $k_{tm12}$ in the form of Equation 6.80. To initiate the estimation, parameter boundaries were set as presented in Table 6.13.

$$k_{tm,12} = k_{tm,11} \cdot t_{1,2} \tag{6.80}$$

Values obtained for the 4 parameters and the objective function are presented in Tables 6.14 and 6.15. It can be seen that $r_{1,2}$, $r_{2,1}$ and $t_{1,2}$ were similar in all concentrations and that estimation trials were much better, as illustrated in Figures 6.17 to 6.19. Parameter $t_{1,2}$ values were high, showing that MMA radicals probably transfer activity to cardanol molecules, probably through the phenolic group. Besides, $f_{inh}$ decreased with the initial mount of cardanol, as expected, increasing the inhibition effect and

Table 6.11: Estimated parameters for cardanol-MMA copolymerization reactions at 85 °C.

| Exp. Cond. | 2.5 wt% | 5 wt% | 10 wt% |
|---|---|---|---|
| $10^{r_{1,2}}$ | $-0.354 \leq -0.275 \leq -0.195$ | Same for 2.5 wt% | Same for 2.5 wt% |
| $10^{r_{2,1}}$ | $-5.606 \leq -4.362 \leq -3.118$ | $-4.682 \leq -4.339 \leq -3.996$ | $-5.705 \leq -4.629 \leq -3.553$ |
| $10^{f_{inh}}$ | $-0.040 \leq -0.035 \leq -0.030$ | $\approx 0$ | $-0.428 \leq -0.358 \leq -0.287$ |
| $F_{obj}$ | 27.14 ($3.25 \leq \chi^2 \leq 20.48$) | 83.06 ($3.25 \leq \chi^2 \leq 20.48$) | 3.96 ($2.18 \leq \chi^2 \leq 17.53$) |

Table 6.12: Estimated model parameters (without exponentials) for cardanol-MMA copolymerization reactions at 85 °$C$.

| Exp. Cond. | 2.5 wt% | 5 wt% | 10 wt% |
|---|---|---|---|
| $r_{1,2}$ | $0.4429 \leq 0.5314 \leq 0.6377$ | Same for 2.5 wt% | Same for 2.5 wt% |
| $r_{2,1}$ | $2.48 \cdot 10^{-6} \leq 4.35 \cdot 10^{-5} \leq 7.62 \cdot 10^{-4}$ | $2.08 \leq 4.58 \leq 10.00$ $(\cdot 10^{-5})$ | $1.97 \cdot 10^{-6} \leq 2.35 \cdot 10^{-5} \leq 2.80 \cdot 10^{-4}$ |
| $f_{inh}$ | $0.913 \leq 0.923 \leq 0.933$ | $\approx 1.000$ | $0.373 \leq 0.439 \leq 0.517$ |

Table 6.13: Boundaries for estimated model parameters considering $k_{tm12}$.

| | Par Inf | Par Sup |
|---|---|---|
| $10^{r_{1,2}}$ | -4.0 | 0.0 |
| $10^{r_{2,1}}$ | -5.0 | 0.0 |
| $10^{f_{inh}}$ | -1.5 | 0.0 |
| $10^{t_{1,2}}$ | -2.0 | 5.0 |

simultaneously reducing conversion and average molecular weights.

Figure 6.20 represents the confidence regions of parameter uncertainties obtained with the PSO and after generation of model parameters values, considering $k_{tm12}$ for the MMA/copolymer produced at 85 °C with 5 wt% of cardanol. Confidence regions for the 2.5 and 10 wt% of cardanol are similar to the one presented. The confidence regions were generated considering all 4 parameters varying simultaneously, as obtained through the PSO using 1000 interactions and 160 particles. The red dot represents the model parameter value that resulted in the minimum value of the objective function. It can be seen that the parameter $r_{2,1}$ wants to decrease as much as possible because the parameter $t_{1,2}$ is able achieve the cardanol composition in the copolymer.

Table 6.14: Estimated parameters for cardanol/MMA copolymerization reactions considering $k_{tm12}$, 85 °$C$.

| | $2.5wt\,\%$ | $5wt\,\%$ | $10wt\,\%$ |
|---|---|---|---|
| $10^{r_{1,2}}$ | -0.563 | -0.655 | -0.608 |
| $10^{r_{2,1}}$ | -4.367 | -4.266 | -4.338 |
| $10^{f_{inh}}$ | -0.260 | -0.481 | -1.000 |
| $10^{t_{1,2}}$ | 3.522 | 3.202 | 3.716 |
| $F_{obj}$ | 25.34 ($2.70 \leq \chi^2 \leq 19.02$) | 31.19 ($2.70 \leq \chi^2 \leq 19.02$) | 2.19 ($1.69 \leq \chi^2 \leq 16.01$) |

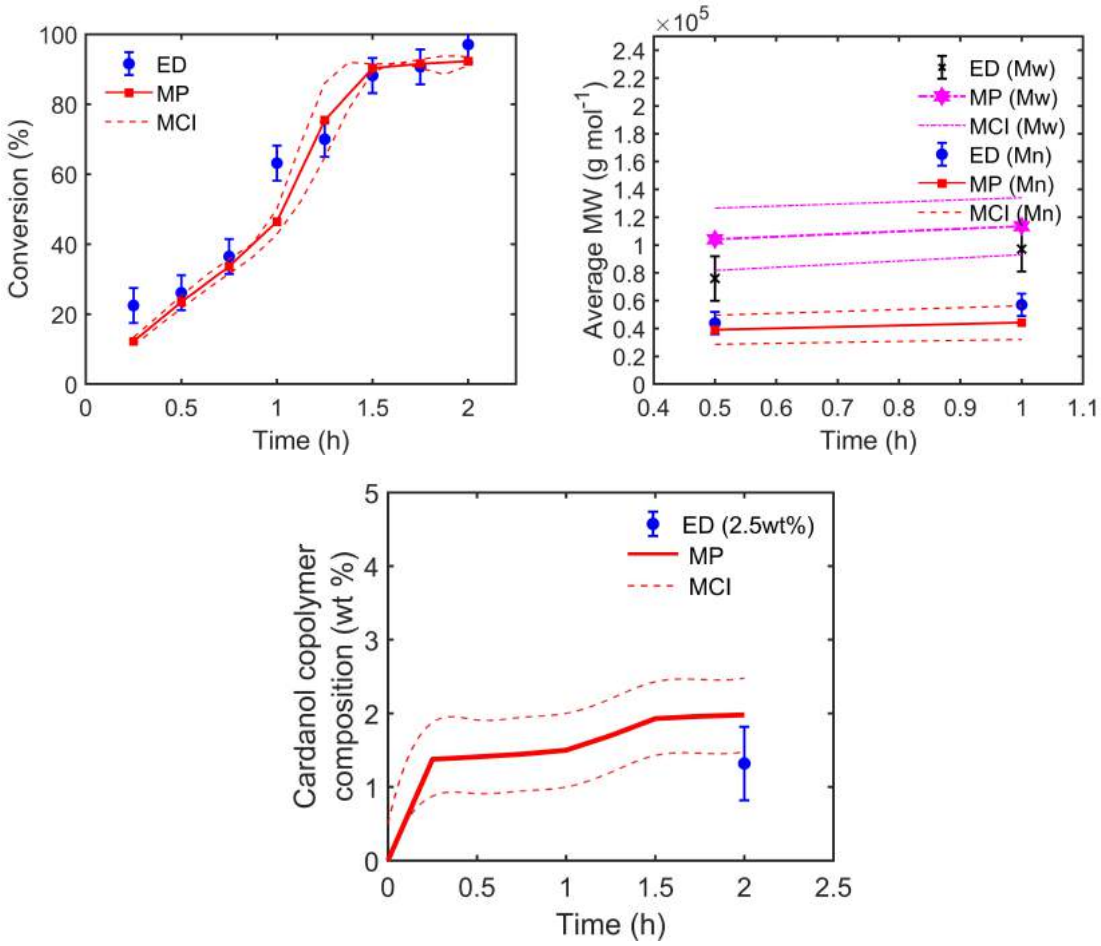


Figure 6.14: Predicted and experimental results for MMA/cardanol copolymer conversion, molecular weights and cardanol composition at conditions 2.5 wt % and 85°C (MCI = model confidence interval; MP = model predictions and ED = experimental data).

Table 6.15: Estimated model parameters (without the exponentials) for cardanol/MMA copolymerization reactions considering $k_{tm12}$, 85 °$C$.

| | $2.5wt\,\%$ | $5wt\,\%$ | $10wt\,\%$ |
|---|---|---|---|
| $r_{1,2}$ | 0.273 (0.237;0.315) | 0.221 (0.189;0.259) | 0.247 (0.026;0.517) |
| $r_{2,1}$ | $4.29\cdot10^{-5}$ ($8.38\cdot10^{-7}$;$2.20\cdot10^{-3}$) | $5.42\cdot10^{-5}$ ($3.57\cdot10^{-5}$;$8.23\cdot10^{-5}$) | $6.73\cdot10^{-5}$ ($4.53\cdot10^{-12}$;$1.14\cdot10^{-4}$) |
| $f_{inh}$ | 0.550 (0.417;0.725) | 0.330 (0.293;0.373) | 0.100 (0.0001;0.420) |
| $t_{1,2}$ | 3322.77 (119.83;92140.38) | 1591.77 (1114.55;2273.26) | 5205.00 (0.00;5205.00) |

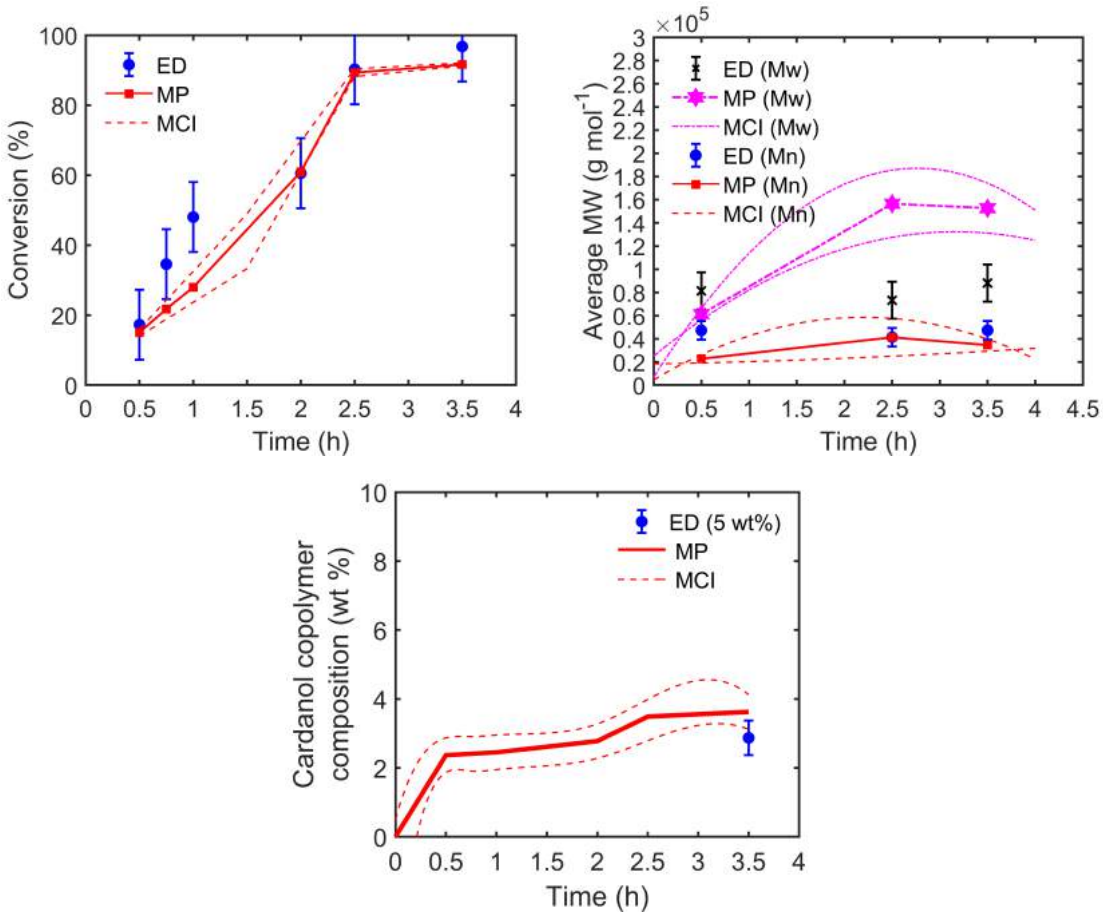


Figure 6.15: Predicted and experimental results for MMA/cardanol copolymer conversion, molecular weights and cardanol composition at conditions 5 wt % (MCI = model confidence interval; MP = model predictions and ED = experimental data).

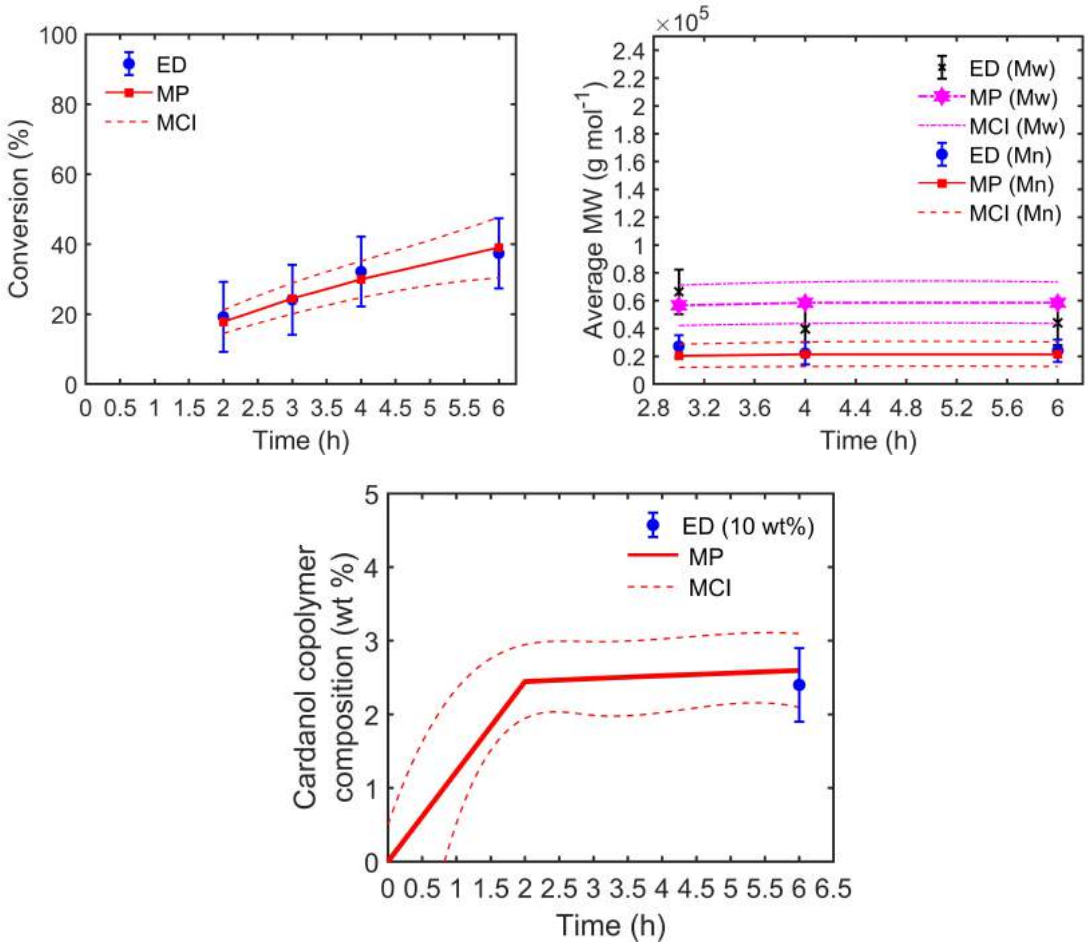


Figure 6.16: Predicted and experimental results for MMA/cardanol copolymer conversion and molecular weights at conditions 10.0 wt % (MCI = model confidence interval; MP = model predictions and ED = experimental data).

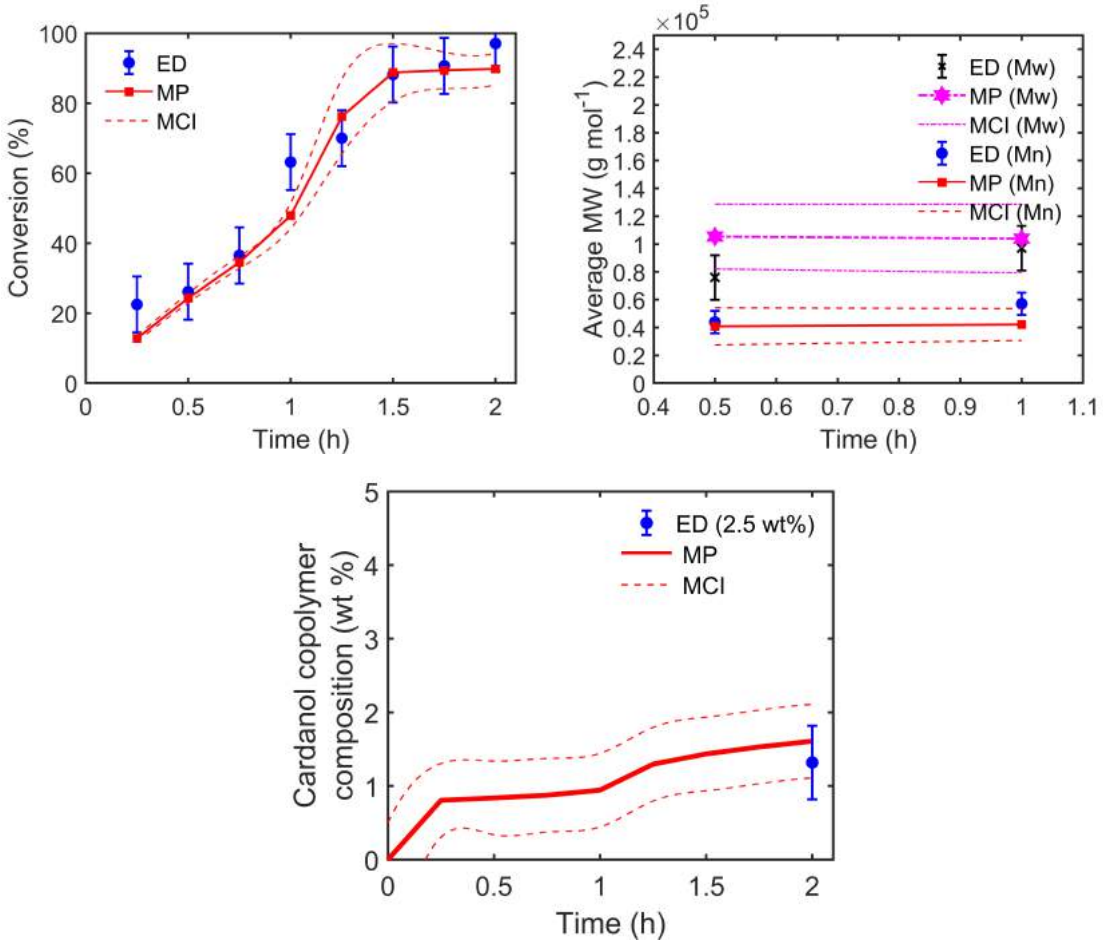


Figure 6.17: Predicted and experimental results for MMA/cardanol copolymer conversion, molecular weights and cardanol composition at conditions 2.5 wt % considering a $4^{th}$ parameter, $t_{1,2}$ (MCI = model confidence interval; MP = model predictions and ED = experimental data).

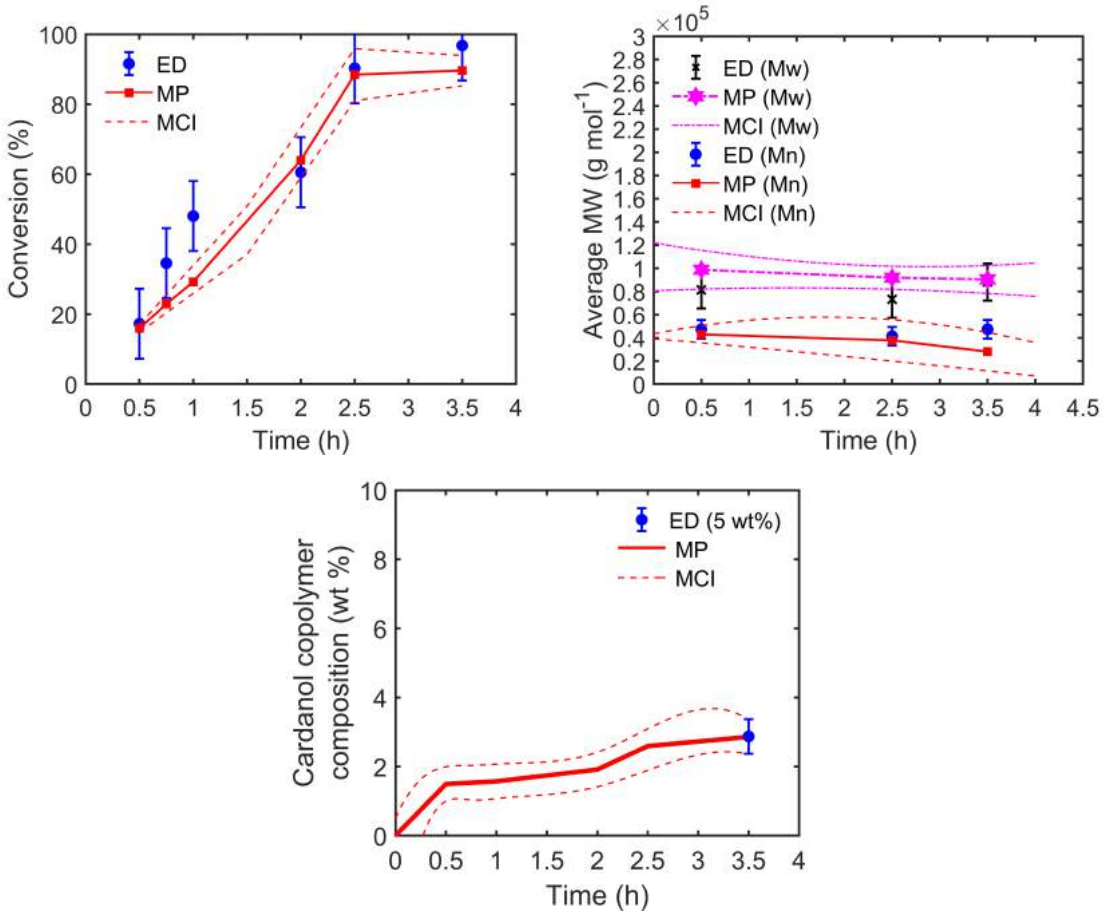


Figure 6.18: Predicted and experimental results for MMA/cardanol copolymer conversion, molecular weights and cardanol composition at 85 °C and 5 wt % considering a $4^{th}$ parameter, $t_{1,2}$ (MCI = model confidence interval; MP = model predictions and ED = experimental data).

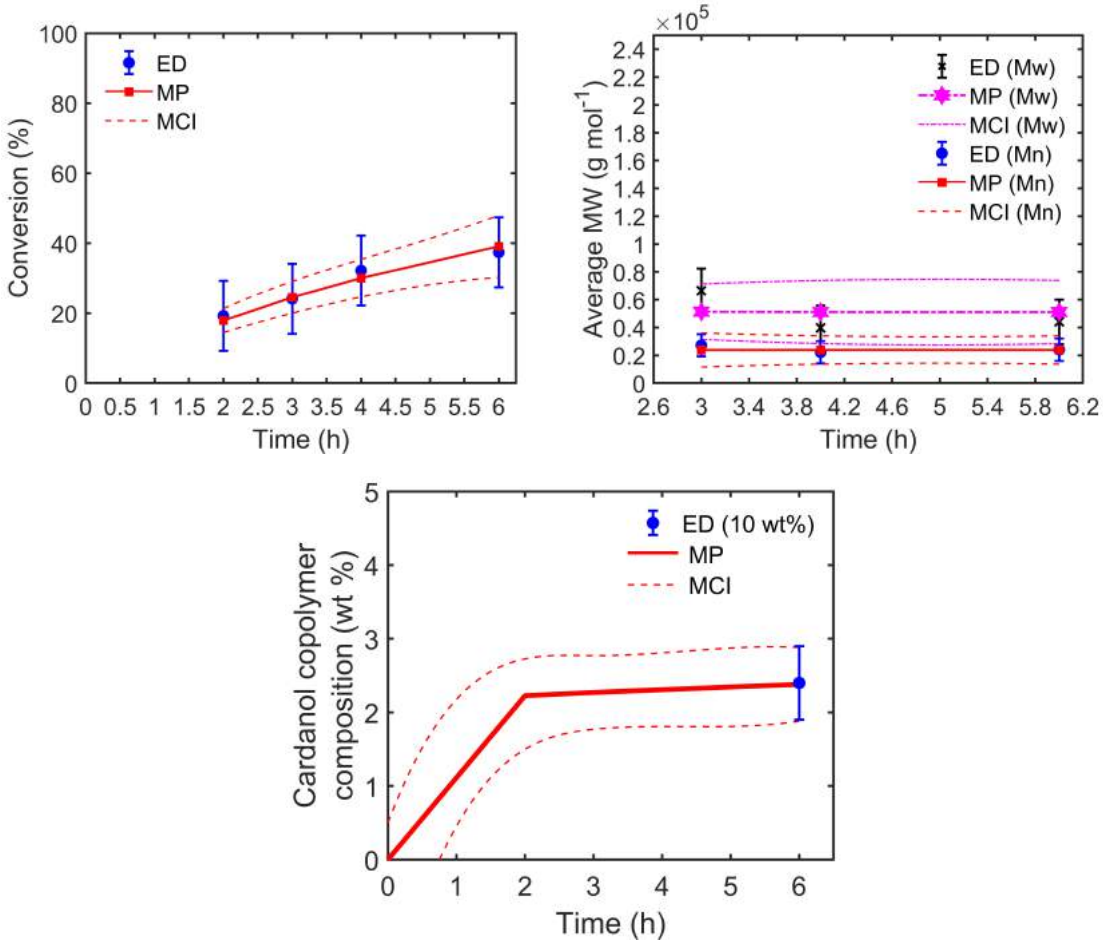


Figure 6.19: Predicted and experimental results for MMA/cardanol copolymer conversion, molecular weights and cardanol composition at 85 °C and 10 wt % considering a $4^{th}$ parameter, $t_{1,2}$ (MCI = model confidence interval; MP = model predictions and ED = experimental data).

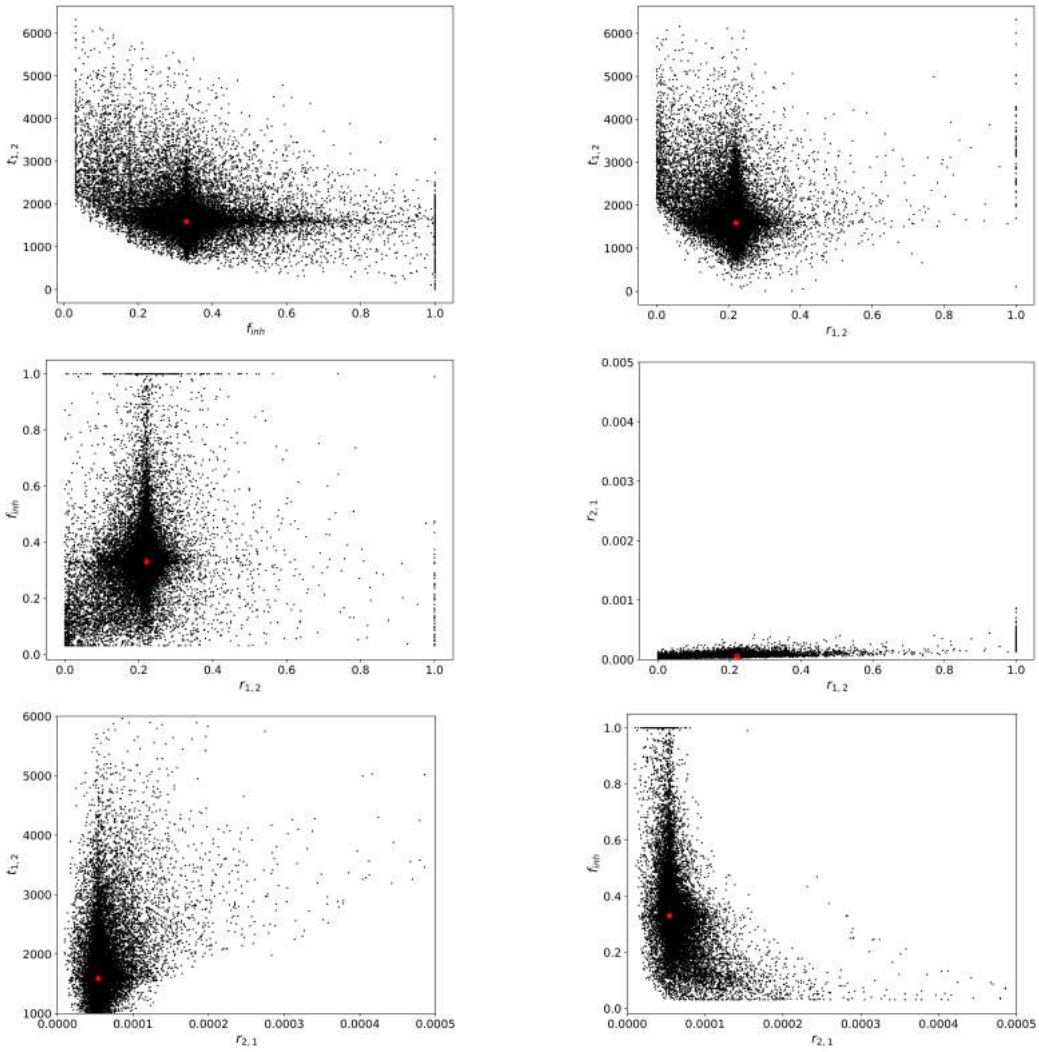


Figure 6.20: Confidence regions for 5 wt% MMA/cardanol copolymer, 85 °C.

### 6.7.6 Methyl Methacrylate/Cardanol Copolymerizations at 110 °C

At 110 °C, the average molecular weights for samples prepared with 5 wt% of cardanol were not available, until the presentation of the date. So, only parameters for 2.5 and 10 wt% were estimated. Not considering $t_{1,2}$, objective functions were 38.24 and 35.21 for 2.5 and 10 wt% of cardanol, respectively. Again, when cardanol compositions were good, molecular weights were not represented well. When $t_{1,2}$, values were estimated, objective function for both concentrations decreased and remained inside the chi-square confidence interval. $t_{1,2}$ values were lower than those obtained at 85 °C, but still high. $r_{1,2}$ decreased quite significantly, because MMA became even more reactive at higher temperatures, but cardanol still retarded the polymerization (maintaining small value for $f_{inh}$). However, $r_{2,1}$ remained the same, showing that cardanol concentration did not increase with temperature. Obtained results are presented in Tables 6.16 and 6.17 and in Figures 6.21 and 6.22.

Figure 6.23 represents the confidence regions of parameter uncertainties obtained with the PSO and after generation of model parameters values, considering $k_{tm12}$. The confidence regions were generated considering all 4 parameters varying simultaneously, as obtained through the PSO using 400 interactions and 160 particles. Moreover, the confidence regions for 2.5 wt% were similar to the obtained for 10 wt% of cardanol. To obtain these confidence regions, the limits of Table 6.13 were considered, but the graphics limits were changed to improve the visibility of the optimal value. The red dot represents the model parameter value that resulted in the minimum value of the objective function. As cardanol composition in the copolymer was not high (almost 1 wt%) the model tries to increase inhibition as much as possible, but the parameter $f_{inh}$ was limited to 0.03. As one can see, the confidence limits were severely influenced by the physical boundaries of the parameter values. Therefore, perhaps additional parameter estimation procedures should be executed with additional data in order to improve the parameter estimates.

Table 6.16: Estimated parameters for cardanol/MMA copolymerization reactions considering $k_{tm12}$, 110 °$C$.

| | $2.5 wt\,\%$ | $10 wt\,\%$ |
|---|---|---|
| $10^{r_{1,2}}$ | -3.956 | Same as 2.5 wt % |
| $10^{r_{2,1}}$ | -4.000 | Same as 2.5 wt % |
| $10^{f_{inh}}$ | -0.730 | -0.957 |
| $10^{t_{1,2}}$ | 3.267 | 3.090 |
| $F_{obj}$ | 11.46 ($2.70 \leq \chi^2 \leq 19.02$) | 21.21 ($3.82 \leq \chi^2 \leq 21.92$) |

Table 6.17: Estimated model parameters (without exponentials) for cardanol/MMA copolymerization reactions considering $k_{tm12}$, 110 °C.

| | $2.5 wt\,\%$ | $10 wt\,\%$ |
|---|---|---|
| $r_{1,2}$ | $10^{-5} \leq 1.11 \cdot 10^{-4} \leq 10^{-3}$ | Same as 2.5 wt % |
| $r_{2,1}$ | $3.33 \cdot 10^{-5} \leq 10^{-4} \leq 1.1 \cdot 10^{-4}$ | Same as 2.5 wt % |
| $f_{inh}$ | $0.10 \leq 0.19 \leq 1.00$ | $0.08 \leq 0.11 \leq 0.15$ |
| $t_{1,2}$ | $335.46 \leq 1849.70 \leq 1.06 \cdot 10^{4}$ | $304.41 \leq 1231.40 \leq 4981.27$ |

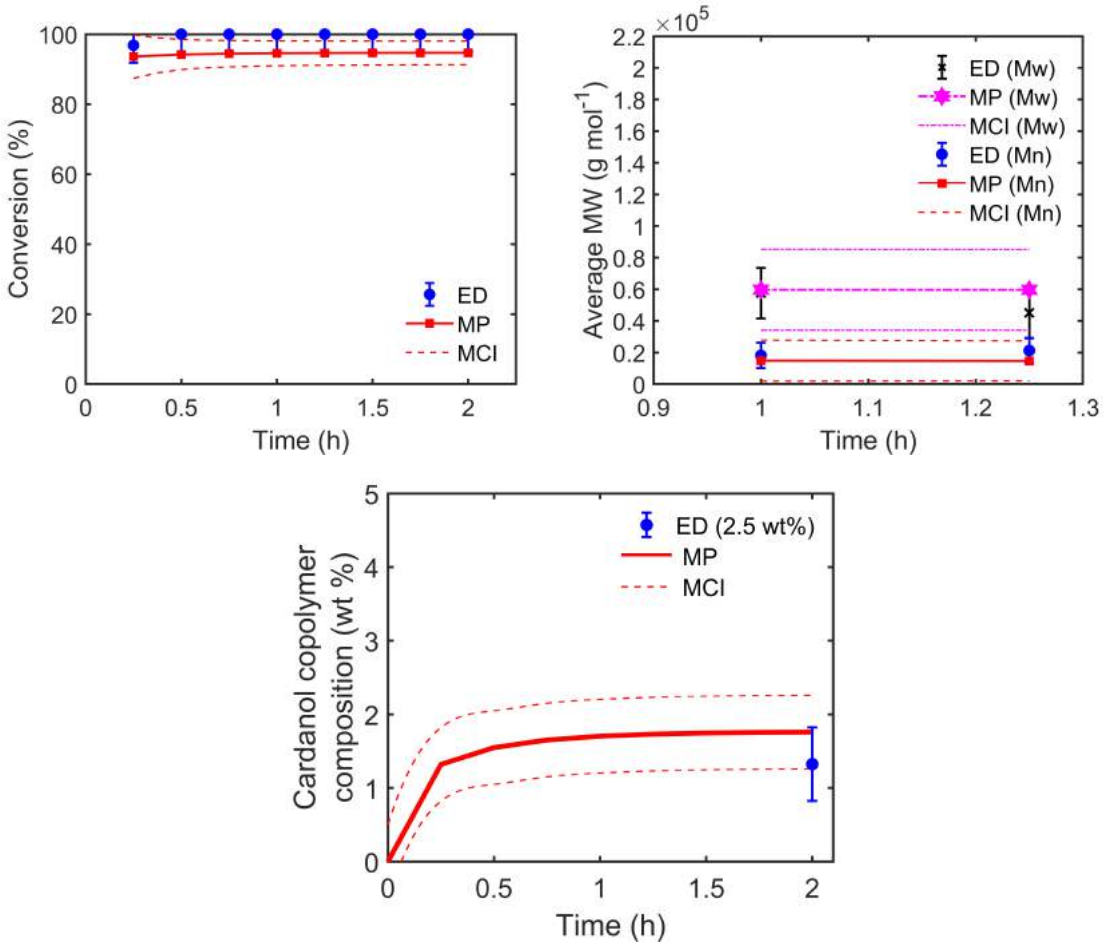


Figure 6.21: Predicted and experimental results for conversion, molecular weights and cardanol composition for a MMA/cardanol copolymer at conditions 110 °C and 2.5 wt % considering a $4^{th}$ parameter, $t_{1,2}$ (MCI = model confidence interval; MP = model predictions and ED = experimental data).

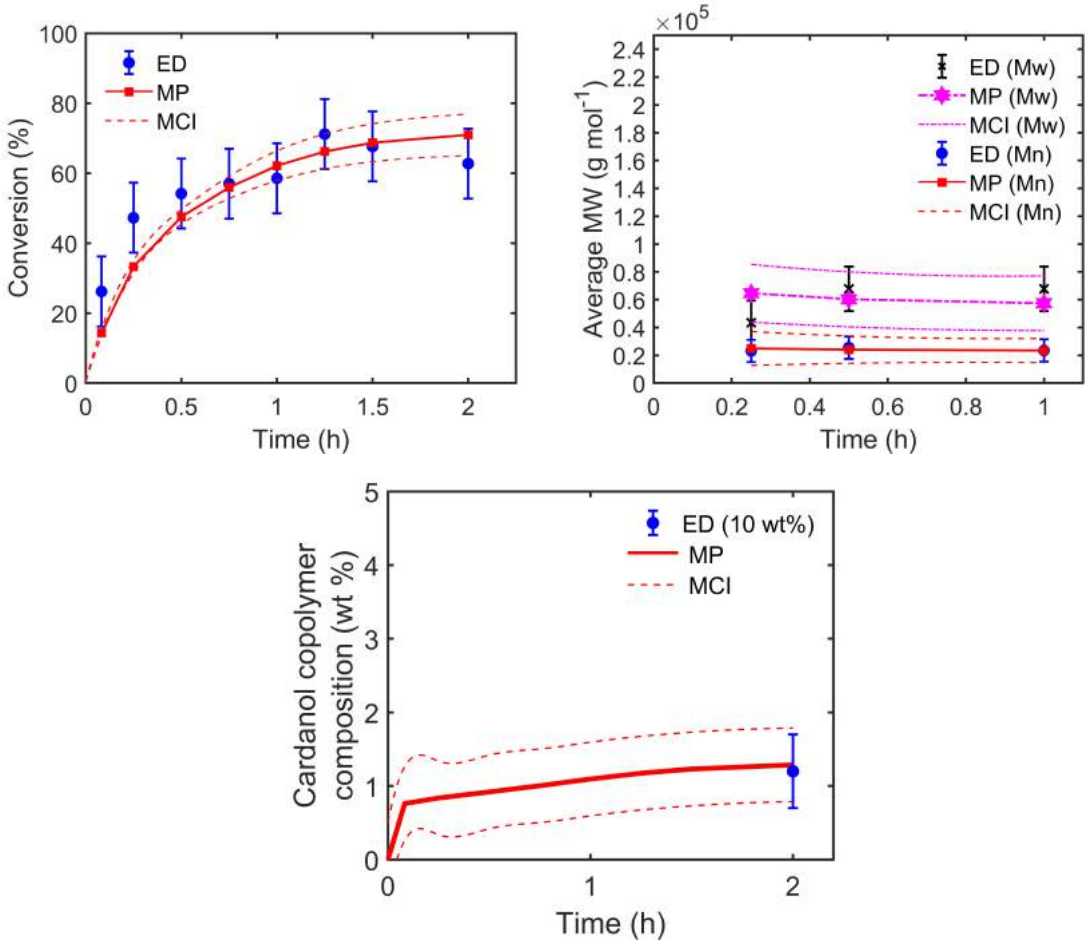


Figure 6.22: Predicted and experimental results for MMA/cardanol copolymer conversion, cardanol composition and molecular weights at 110 °C and 10.0 wt % considering a $4^{th}$ parameter, $t_{1,2}$ (MCI = model confidence interval; MP = model predictions and ED = experimental data).

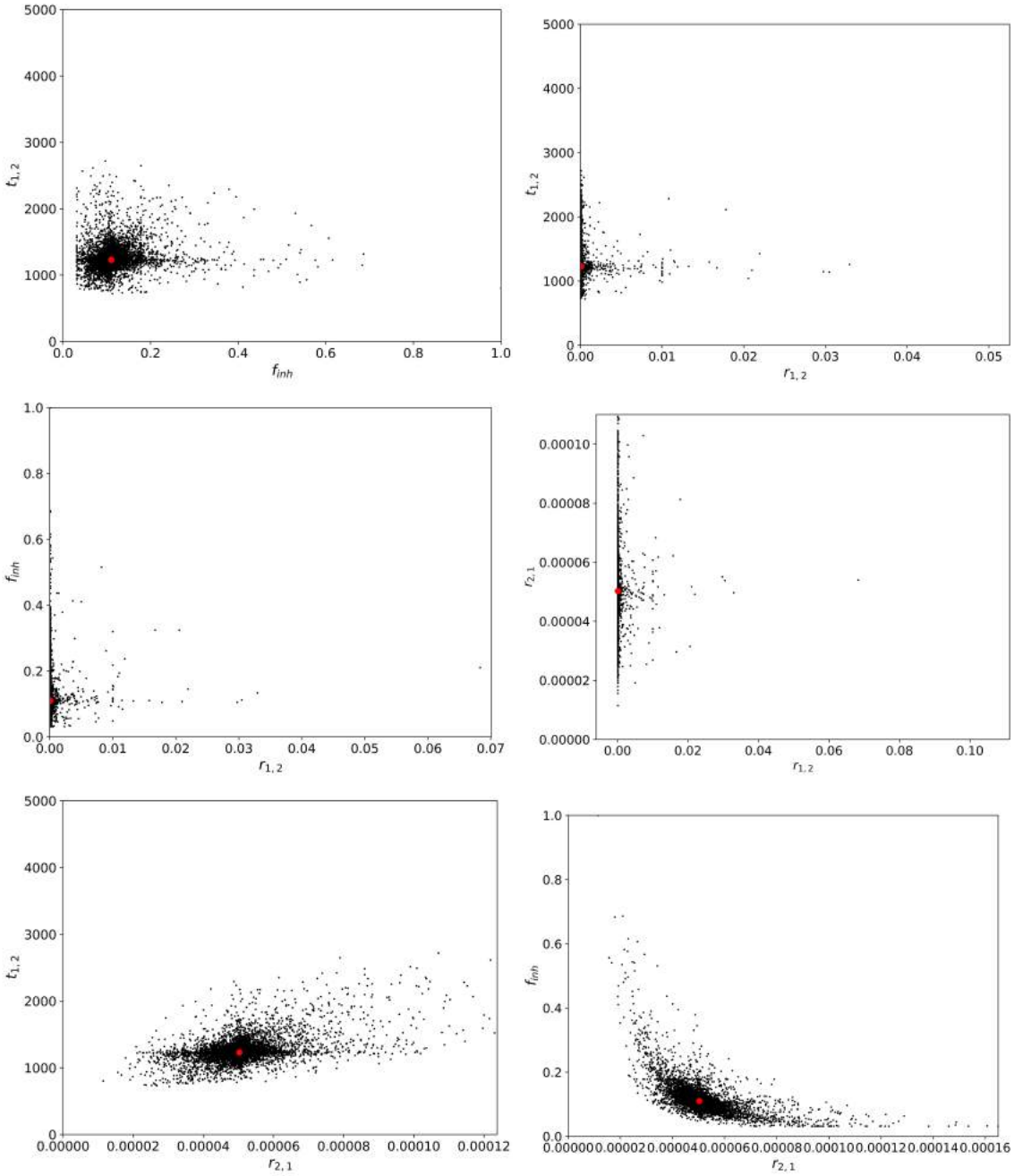


Figure 6.23: Confidence regions for 10 wt% MMA/cardanol copolymer, 110 °C.

## 6.8 Concluding Remarks

A kinetic mechanism was proposed and shown to represent adequately the polymerization systems under study. Firstly, a correction factor for styrene homopolymerization was estimated ($k_{tm11} = 1.211 \cdot k^0_{tm11}$), and experimental conversion and average molecular weights for styrene polymerization were well represented by the model. The kinetic model proposed for the copolymerization was able to follow available experimental data, although some assumptions were used: a) cardanol was represented as a lump of similar components with a variable number of unsaturations; b) cardanol was assumed to contain equally reactive sites, such as terminal unsaturation, internal unsaturations and hydroxyl groups; c) cardanol was assumed to inhibit the polymerization due to its internal unsaturations and hydroxyl group, which required the estimation of the $f_{inh}$ parameter to decrease the concentration of initiator; d) cardanol does not homopolymerize and it has a propagation constant ($k_{p22}$) equal to zero; e) it was considered the living polymer chains ending in cardanol also terminates with the same rate of polystyrene; and f) the quasi-state hypothesis and the terminal model were assumed to be valid for the polymerization.

Moreover, transfer reactions, although possible (mainly due to steric hindrance and availability of hydrogen atoms), were not considered initially for the cardanol mixture. Also, as the terminal unsaturation was the functional group most likely to continue propagation and incorporate cardanol. Although cardanol contained less than 50% of compounds with terminal unsaturation, it was considered that the whole lump was reactive in the proposed kinetic model proposed because, as explained, the compounds have many reactive sites. Nonetheless, the copolymerization parameters $r_{1,2}$ and $r_{2,1}$ were shown to depend little on the reaction temperature in the analyzed experimental range and to be equal to 1.627 - 3.210 and 0.015 - 0.026, respectively for styrene copolymerizations. As detected experimentally, the inhibition of cardanol at 90 °$C$ is more intense than at 110 °C for styrene copolymerizations. This reflected in a lower value for $f_{inh}$ obtained for 90 °$C$ (0.628) than for 110 °$C$ (0.731), meaning that it reduced the concentration of available radical molecules more the in last condition. From $^1$H-NMR analysis, it was possible to obtain copolymer composition and, therefore, predict cardanol compositions in the copolymer and in the reaction medium. For the conditions studied, cardanol is incorporated at the begging quite fast ($r_{1,2} > 1.0$) during early reaction times due to its multiple reactive sites.

For MMA/cardanol copolymerizations, without the transfer to monomer reaction (a MMA-ended living chain attacking a cardanol molecule), the model could not represent correctly the experimental data. As MMA is much more reactive than styrene, $r_{1,2}$ became lower than 1.0. The parameter for chain transfer reaction ($t_{1,2}$) turned out to be quite high to represent correctly average molecular weights while still represent-

ing the cardanol composition in the copolymer. With this model adaptation in relation to the one used for styrene copolymerizations, the model was able to follow available experimental data at in studied composition (2.5, 5 and 10 wt%) and temperatures for MMA copolymerizations.

# Kinetic Studies of Suspension Copolymerizations

## $2^{nd}$ Section

# Chapter 7

# Suspension Copolimerizations: Methodology

## 7.1 Materials

Cardanol (Taian Health Chemical, minimum purity of 99.5 wt% w/w, Taian, China), methyl methacrylate (MMA) (VETEC, Rio de Janeiro, Brazil, with minimum purity of 99.5 wt%) and styrene (STy) (Sigma-Aldrich, Rio de Janeiro, Brazil, with minimum purity of 99 wt%) were used as monomers. Benzoyl peroxide (BPO) (VETEC, Rio de Janeiro, Brazil, with minimum purity of 99 wt%, containing 25% of humidity) and azobisisobutyronitrile (AIBN) (Merck Millipore, São Paulo, Brazil, with minimum purity of 98.5 wt%) were used as initiator for the polymerizations. Poly(vinyl alcohol) (PVA) (Vetec Química Fina, Mw = 78 kDa, 86.5 – 89.5% of hydrolysis) was used as a suspension agent.

## 7.2 Experimental Set Up

For suspension polymerizations, a 1L glass reactor was used (Figure 7.1). The reactor was surrounded by a cooling jacket that was filled with a 50/50 mixture of hot water and ethylene glycol from a controlled hot bath, used to control the reaction temperature. A metal cap was used to allow for connection of a mechanical stirrer, a reflux condenser and a thermocouple, that was connected to the bath. Two holes were used for monomer feeding and aliquot withdrawal.

Figure 7.1: Set Up for Suspension Polymerizations

## 7.3 Kinetic Experiments

For the suspension polymerization, different phases were prepared separately. The aqueous phase was prepared on the day before the reaction to solubilize the PVA. The organic phase was prepared by mixing the monomer with the initiator instants before starting the polymerization. Every reaction is conducted at 85 $°C$ with agitation of $850 \pm 50$ rpm. For methyl methacrylate polymerizations, samples were taken during 2 hours; for styrene, samples were taken during 4 hours. Aliquots were taken every 15/30 minutes.

On the reaction day, the following procedure was used: (1) the heating bath was turned on with set point of 85 $°C$; (2) the PVA solution was added into the reactor; (3) stirring was turned on and kept around 500 rpm; (4) when the temperature of the PVA solution reached the desired value, the monomer was mixed with the initiator; (5) the monomer mixture was added to the reactor and the stirring rate was changed to 850 rpm; (6) samples were taken at specific time intervals and a solution of hydroquinone was added to halt the polymerization; (7) the heating bath was turned off after the planned reaction time; (8) after cooling, reaction samples were filtrated under vacuum; (9) samples were left at the recirculating oven under vacuum until complete drying.

Conditions for the suspension polymerizations are summarized in Table 7.1. Concentrations are presented in weight fraction. Variable X stands for cardanol and Y for styrene (Sty) or methyl methacrylate (MMA). Moreover, 1 wt% or 3 wt% of BPO were

Table 7.1: Experimental design of the suspension polymerizations reactions.

| Experiments | Organic Phase (30%) | | Aqueous Phase (70%) | | T (°C) | Stirring Rate (rpm) |
|---|---|---|---|---|---|---|
| | X (wt%) | Y (wt %) | Water (wt%) | PVA (wt%) | | |
| HomoY | 0 | 99 | 99.6 | 0.4 | 85 | 850 |
| 2.5% X | 2.5 | 96.5 | 99.6 | 0.4 | 85 | 850 |
| 5% X | 5 | 94 | 99.6 | 0.4 | 85 | 850 |
| 10% X | 10 | 89 | 99.6 | 0.4 | 85 | 850 |

added in respect to the total mass of monomer. Sometimes, BPO was replaced by AIBN. For reactions in the 1L reactor, the real masses were equal to: 180 g of monomer, 418.32 g of water and 1.68 g of PVA.

## 7.4 Gravimetric Analysis

Monomer conversion was obtained by gravimetry. The samples containing the polymer material were dried in the recirculating oven under vacuum until reaching the constant mass.

To obtain the conversion values, Equations 7.1 - 7.3 were used. However, $m_{polymer}$ had to be multiplied by 0.3 to consider the initial monomer/polymer fraction into heterogeneous medium. Therefore, the equations used to obtain the conversion of samples obtained with suspension polymerization were:

$$m_{monomer} = m_{initial} - m_{crucible} - m_{BPO} \tag{7.1}$$

$$m_{polymer} = m_{dry} - m_{crucible} - m_{BPO} - C_{sol,hydroquinone} m_{hydro} \tag{7.2}$$

$$Conversion\,(\%) = \frac{m_{polymer}}{0.3 m_{sample}} \cdot 100\% \tag{7.3}$$

where $m_{monomer}$ is the initial mass of monomer, $m_{BPO}$ is the mass added of droplets of ethanolic solution of hydroquinone, $m_{polymer}$ is the mass of the polymer formed and $C_{sol.hydro}$ is the alcoholic solution of hydroquinone concentration (0.01 g/L).

## 7.5 Characterizations

### 7.5.1 Contact Angle

In order to determine the degree of hydrophobicity of the produced polymeric materials, a tensiometer was used (Teclis, Marseille, France). Initially, the particles were compressed in a disk mold, using a press to form tablets. Each sample was then placed over an acrylic surface, and a drop of water as placed over the disk. The contact angle between the surfaces was then measured under atmospheric conditions at 25 $°C$ using the equipment software. The contact angle was used to infer the hydrophobicity of the polymer particles. Analyses were made in triplicate.

### 7.5.2 Interfacial Tension

The interfacial tension between the organic phase (containing only monomers, without BPO) and water (without PVA) was measured at 25 and 85 °C. Analyses were performed to see the possible role of cardanol as a suspension agent. Analyses were carried out with pure MMA, MMA with cardanol, styrene and styrene with cardanol. Measurements were performed with a tensiometer (Kruss Process, model K100, North Carolina, the United States). Analyses were repeated until attainment of constant interfacial tension. Data points were obtained every 30 seconds.

### 7.5.3 Particles Size

Particle size distributions were obtained through light scattering in aqueous medium. The equipment used was the particle size analyzer Master Sizer Hydro 2000S (Malvern, United Kingdom). The equipment counts on a detector system for front, side and back light scattering measurements. The light source was a helium neon laser with characteristic wavelength of 632.8 mm. The detection limits range from 0.01 to 3000 $\mu$m. Samples were prepared by dispersing 200 - 500 mg of sample in water. Analyzes were performed at room temperature.

### 7.5.4 Scanning Electron Microscopy (SEM)

The detailed visualization of the produced particles surface was carried out with the aid of a SEM microscope (Quanta 250, Fei Company, 30kV, Hillsboro, the United States) using vacuum and secondary electrons for image reconstruction. The photomicrographs were processed in an image analyzer provided by the SEM manufacturer.

### 7.5.5 Optical Microscopy (OM)

The morphology of produced particles was determined by optical microscopy. The micrographs were obtained with the optical microscope Axiovert 40 MAT equipped with a 1.4 megapixel camera, model Axiocam MRc, both provided by the manufacturer Carl Zeiss (Oberkochen, Germany), using the dark field technique. The microscope is associated with a computer running the Axiovision software version 4.8.1 from the same manufacturer. This software enables acquisition and analyses of images, provides scales and other measures.

# Chapter 8

# Suspension Copolymerization: Results

## 8.1 Introduction

As one of the main objectives of the present study is the future immobilization of enzymes and functionalization of polymers using natural CNSL or cardanol, the manufacture of copolymer particles in heterogeneous media is interesting (PAIVA *et al.* (2018), CAMPOS *et al.* (2016), MENDES *et al.* (2012)). Suspension polymerization present many advantages, including the easy separation of the polymer particles, easy removal of heat of reaction, easy temperature control and low levels of impurities and additives in the final polymer resin.Therefore, it is suitable for production of polymer resins intended for many distinct applications, including biotechnological, medical and dental applications (PINTO *et al.*, 2002).

Suspension copolymerizations were performed with cardanol and methyl methacrylate or styrene, as these systems resulted in the best bulk polymerization result. Benzoyl peroxide (BPO) was used as initiator at two different concentrations: 1 wt% and 3 wt%. However, some polymerizations were performed with azobisisobutyronitrile (AIBN). Although, average molecular weights and copolymer compositions have not been obtained so far, other aspects of this reaction and respective productions are studied. The interesting aspect is that, after the reaction, the mixtures were stable even when they were kept resting for several weeks. Thus the addition of cardanol enhanced the stability of the suspended particles due to reduction of the interfacial tension and combination of electrical and mechanical effects as described below.

## 8.2 Styrene-Cardanol Copolymer Particles

First of all, the interfacial tension between the organic phase (styrene and a styrene-cardanol mixture containing 10 wt % of cardanol in water) was characterized to evaluate whether cardanol might affect the particle size distributions and check if reaction

conditions should be adjusted in presence of cardanol, including the PVA concentration and the stirring rate. In Table 8.1, values of interfacial tension indicate addition of cardanol to the mixture causes the reduction of the interfacial tension. This occurs because cardanol is an amphiphilic molecule, which enhances the interaction between the organic phase and the aqueous phase (DE MARIA *et al.* (2005)). However, the reduction of the interfacial tension was not so high as observed with the addition of PVA in the aqueous phase which corresponds to 5 mN/m with 1 wt% of PVA in water (CARVALHO, 2011).

As an example of the good interaction between cardanol and water when the interfacial tension between cardanol and water was measured through pendant drop tensiometry, values could not be obtained due to the high interaction between the two phases, as cardanol was carried by the water phase and not remained in the drop (Figure 8.1-a). For measurements between styrene (or methyl methacrylate) and water using this method, the monomers remained in the droplets with perfect round shape. Cardanol probably moves to the interface, leaving styrene in the cores of the particles or the bottom of the crucible used to measure the interfacial tension (DE MARIA *et al.*, 2005). However, this is a good aspect of this systems as cardanol deposition on the particle surfaces allow for surface modification, rendering the particles compatible with different media, and finding potential use in various types of applications (BOHARA *et al.* (2016)).

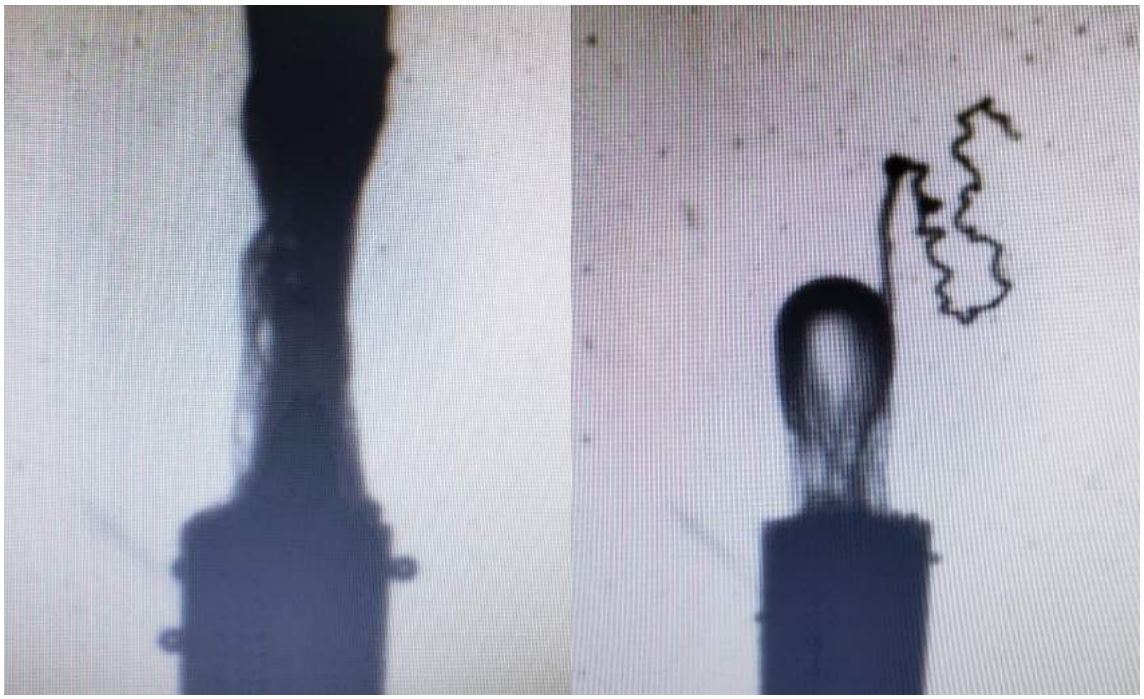

(a) (b)

Figure 8.1: Photographs of pendant upward drop tensiometry used for some non-reported interfacial tension calculations. (a) Test for cardanol-water (b) Test for styrene with cardanol in water.

Table 8.1: Interfacial tension between STy or STy-cardanol with distilled water.

| | **Average Value [mN/m]** | **Standard Deviation [mN/m]** |
|---|---|---|
| Sty | 18.0977 | 6.2072 |
| Sty + 10%C | 11.0678 | 0.4502 |

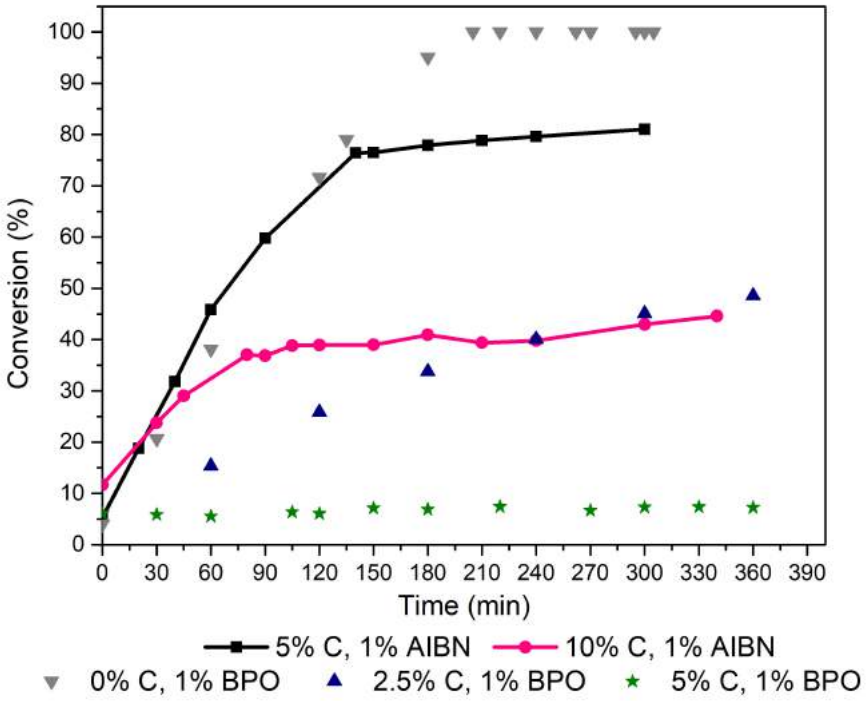


Figure 8.2: Conversion values for styrene-cardanol suspension polymerizations.

Styrene-cardanol copolymers were synthesized using 5 wt % of cardanol with 1 or 3 wt % of BPO and using 10.0 wt % of cardanol with 1.0 wt % of AIBN (Figure 8.2). The data for 2.5 wt% with 1 wt% BPO was obtained from GALVÃO (2016) for comparative purposes. Polystyrene trials reached 100% of conversion after 200 min of reaction when 1.0 wt% of BPO was used. However, cardanol inhibits the polymerization, reaching only 53% of conversion for 2.5 wt% of cardanol after 540 minutes and 7% for 5 wt% although the reasons were not clear, as suspension reactions are expected to follow the bulk kinetics (GALVÃO (2016) obtained 13.4% after 300 min) (PINTO *et al.*, 2002). Therefore, the kinetics was much slower when the reactions were performed in suspension. The possible presence of oxygen in the larger vessel may have exerted influence on the rates of hydrogen donation by the phenolic group (LARTIGUE-PEYROU, 1996). However, the possible concentration of cardanol molecules on the particle surfaces may also have affected the course of the polymerizations. When the initiator was changed for AIBN, monomer conversions increased very significantly: for 5 wt% of cardanol, conversion reached 80% and for 10 wt% of cardanol, conversion reached 45%, almost the value obtained with 2.5 wt% of cardanol and 1% of BPO. GALVÃO (2016)

observed total monomer conversion with 2.5 wt % of cardanol using AIBN. AIBN is known to be more reactive than BPO and this shows that cardanol inhibition can be less effective when more active initiators are used.

Analyses of contact angle were performed through deposition of water droplet on a copolymer surface. For styrene disks, the water droplet stayed on the surface throughout the analysis, and the contact angle (measured by image analysis using a software) remaining constant. However, the water droplet was quickly absorved by the copolymer disk so that contact angle could not be measured. This happened because the copolymer presented good affinity with water due to the presence of cardanol, indicating the cardanol incorporation by the particles.

## 8.3 Methyl Methacrylate-Cardanol Copolymer Particles

As performed for styrene, the interfacial tension was also evaluated for methyl methacrylate (with and without cardanol) in water. The obtained values are shown in Table 8.2. It can be seen that cardanol reduced the interfacial tension, but not go significantly as the 1 wt% aqueous solution of PVA. Therefore, PVA could not be replaced entirely by cardanol.

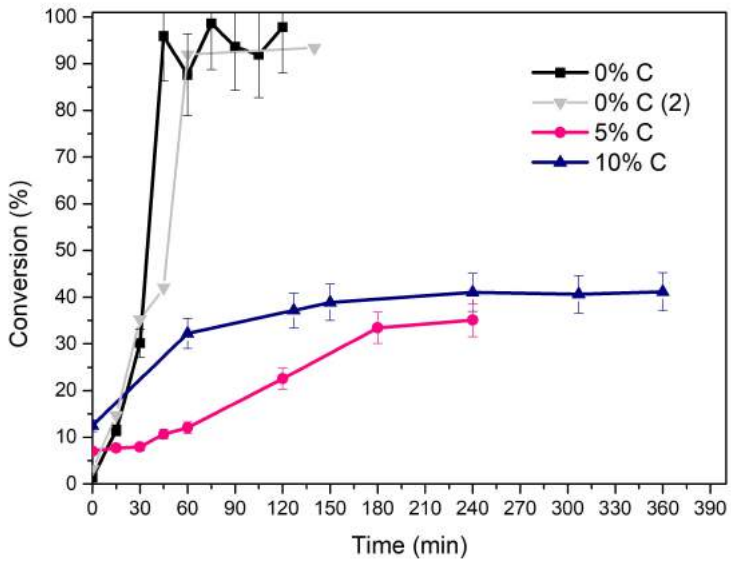


Figure 8.3: Conversion values for methyl methacrylate-cardanol suspension copolymerizations with 1.0 wt% of BPO.

Table 8.2: Interfacial tension between MMA or MMA-cardanol with distilled water

| | Average Value [mN/m] | Standard Deviation [mN/m] |
|---|---|---|
| MMA | 9.404 | 0.627 |
| MMA + 10%C | 6.555 | 1.015 |
| MMA + PVA | 1.335 | 1.262 |

Suspension polymerization performed with 1.0 wt % of BPO (Figure 8.3) were much slower than the ones perfomed in bulk with the same BPO concentration, as also reported for styrene. Because of the small monomer conversion, copolymer particles became small and very sticky as shows in Figure 8.4 and 8.5 (PINTO *et al.* (2002)). As a consequence, these polymer particles could not be filtrated efficiently because they clogged the pores of the paper filter (with pores of 14 $\mu$) and had to be freeze dried.

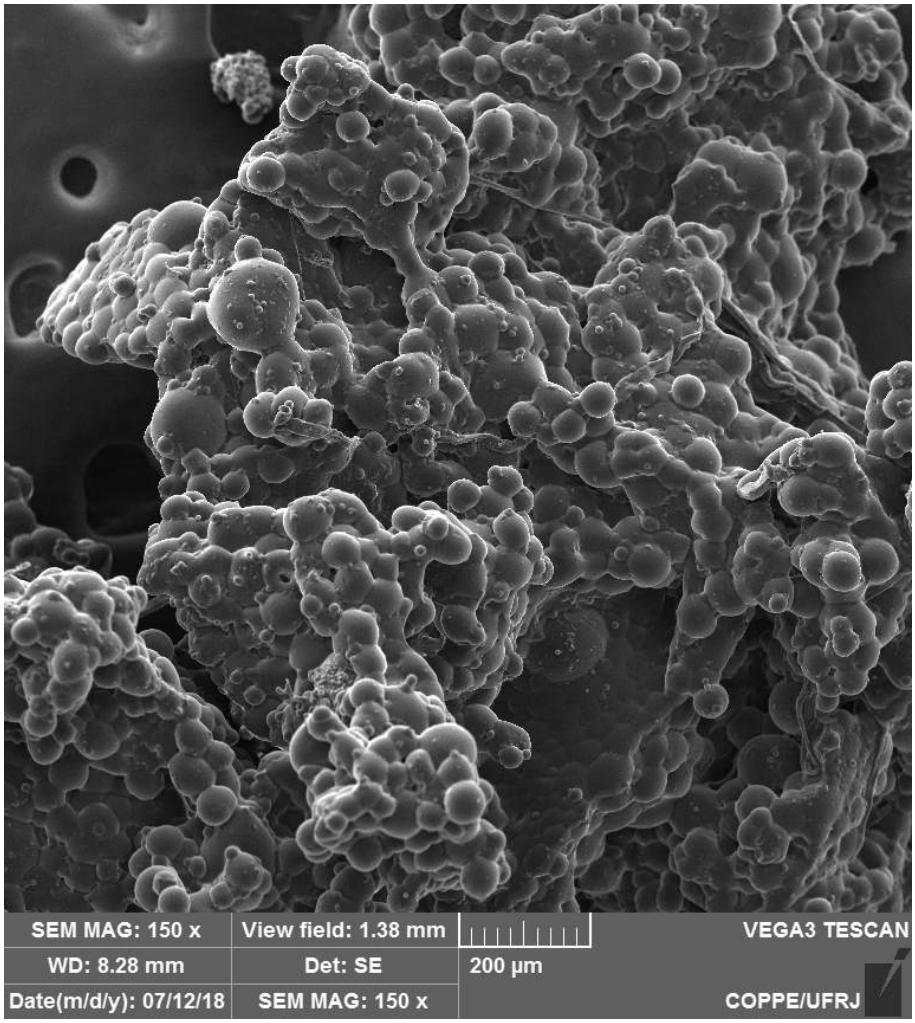


Figure 8.4: SEM micrograph of for methyl methacrylate-cardanol particles produced with 10 wt% of cardanol and 1 wt% of BPO after 6 hours of polymerization.

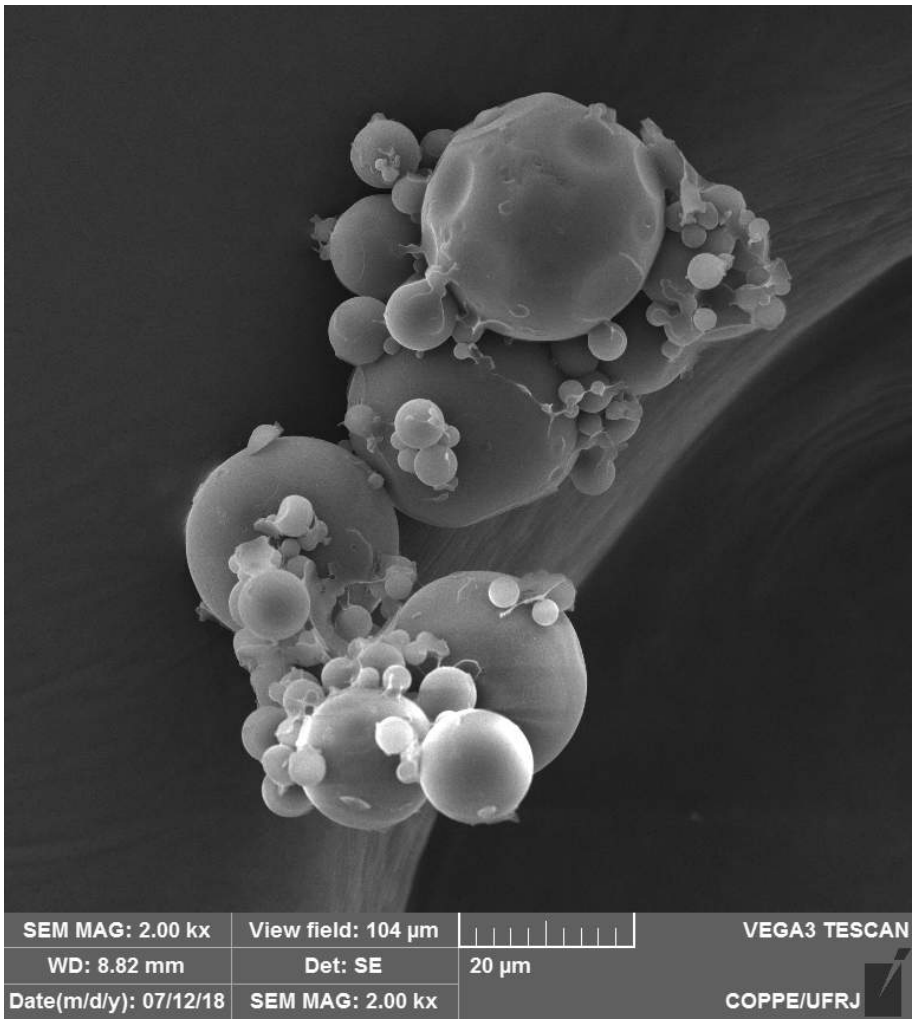


Figure 8.5: SEM micrograph for methyl methacrylate-cardanol particles produced with 5 wt% of cardanol and 1 wt% of BPO after 4 hours of polymerization.

The particles might also be small because of the amphiphilic characteristic of cardanol, as shown in Figure 8.6. Particularly, one day after the reaction, the particles were segregated by size, with the bigger and denser particles placed at the bottom of the becker, while the smaller and less dense particles were placed on top. After getting samples of each phase, optical microscopy images confirmed the size differences, as shown in Figure 8.8. The particle size segregation was also described by GALVÃO (2016) for styrene-cardanol copolymer particles, as shown in Figure 8.7.

Using 3.0 wt % of BPO (Figure 8.9), the conversion increased a little and this was sufficient to allow for filtration and introduction of larger particles, showing the importance of conversion for stabilization of particle sizes. Figure 8.10 shows the final particle size distribution obtained with 3 wt% of BPO and 2.5 wt% of cardanol. It is intersting to observe that, even reducing interfacial tension, the presence of cardanol in the copolymer particles could not avoid production of large particles, when compared to pure MMA.

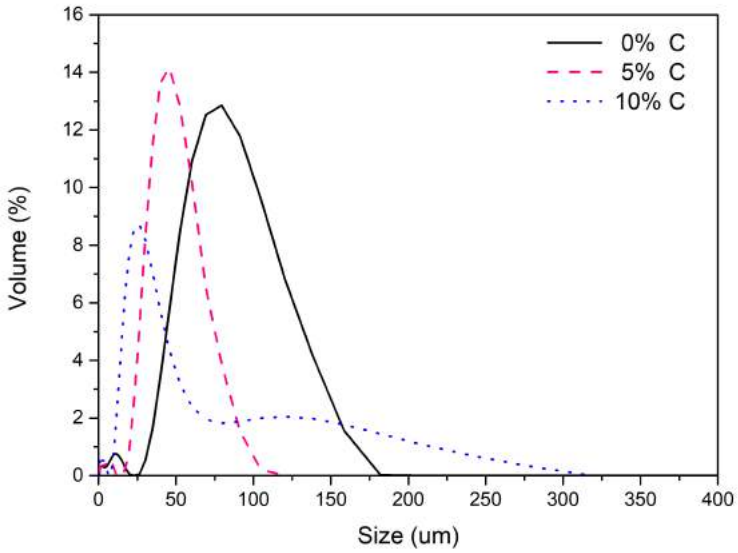


Figure 8.6: Particle size distribution for copolymer particles produced with 1 wt% of BPO.

Changing BPO by AIBN as initiator, conversions increased tremendously. This was tested with 5 and 10 wt% of cardanol, as one can be see in Figure 8.11. Even with 10 wt% of cardanol, conversion almost reached 100% (the average molecular weights of the final product were $M_n$ = 34478 Da and $M_w$ = 59340, values higher than obtained for bulk copolymerization with 1 wt% of BPO). AIBN is more reactive than BPO and its use may constitute a way to work around cardanol inhibition. However, the increase of conversion also led to increase of the average particle sizes. Figure 8.12 presents particle size distributions for the copolymers prepared with 5.0 wt% of cardanol and 1.0 wt% of BPO, and 5.0 wt% of cardanol and 1.0 wt% of AIBN. The average size for the copolymer with AIBN (143 $\mu m$) was even bigger than for pure PMMA (76 $\mu m$). It is important to emphasize that these differences in particle sizes are only due to changes in cardanol and/or BPO (or AIBN) concentration and initiator type (BPO or AIBN), as stirring rate and concentration of PVA were kept constant. Figure 8.12 shows once more the controlling effect of monomer conversion or particle size distributions and indicate that addition of cardanol may impose the modification of the remaining operation parameters in order to keep the particle size distribution constant.

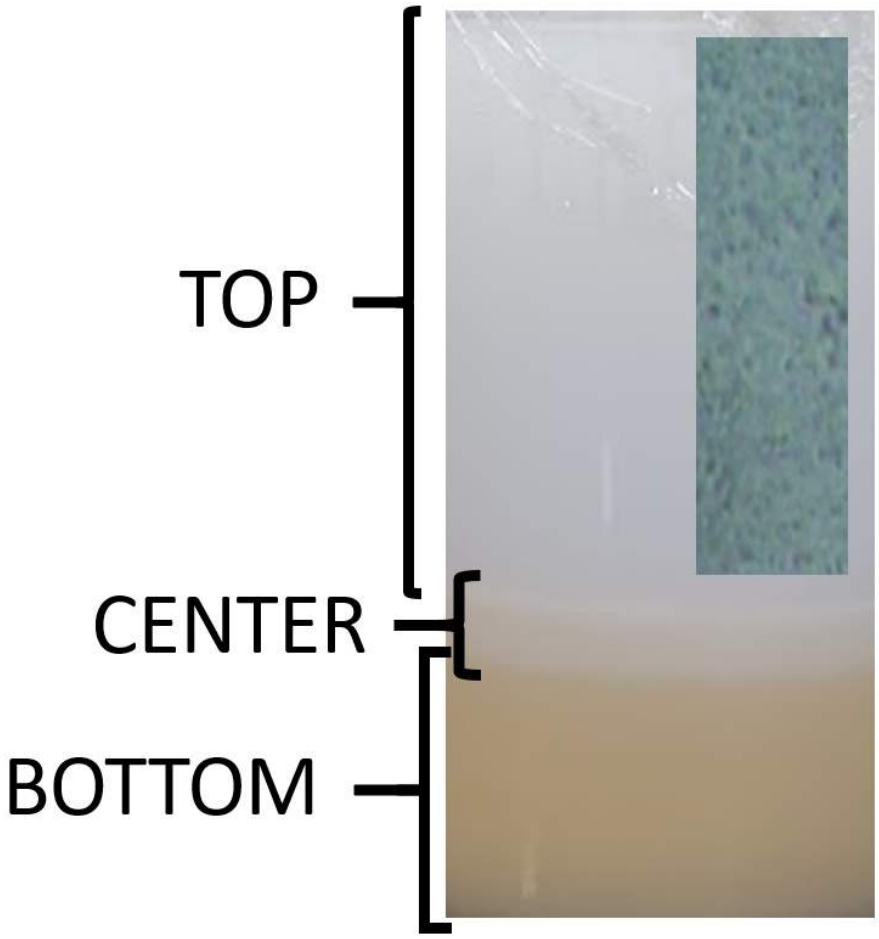


Figure 8.7: Photo of a becker containing the reaction mixture of methyl methacrylate and 5 wt% of cardanol one day after the reaction.

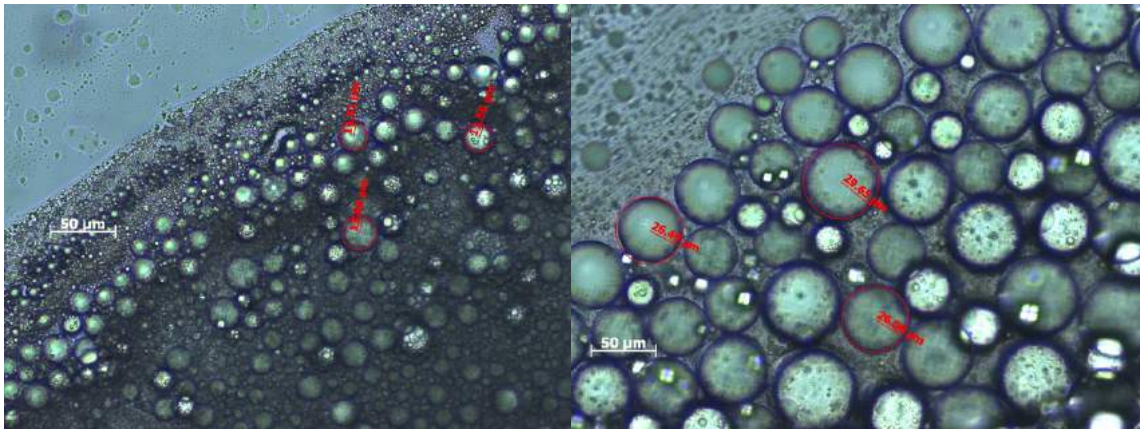


(a) (b)

Figure 8.8: Optical micrographs of particles present at the center (a) and bottom (b) of the becker for methyl methacrylate-cardanol copolymer particles.

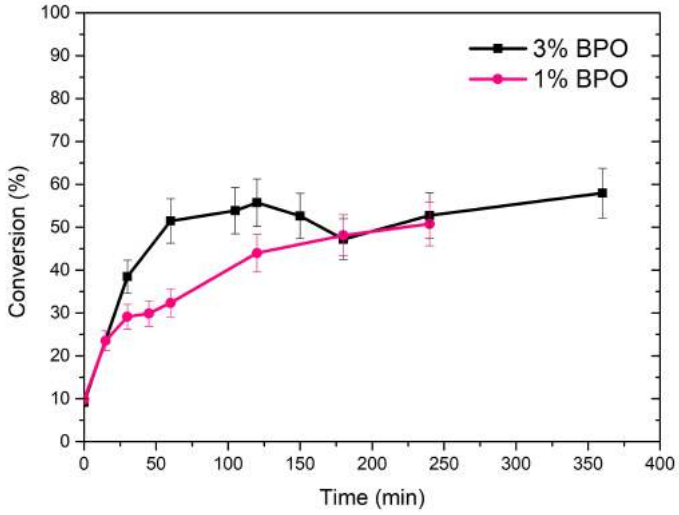


Figure 8.9: Conversion values for methyl methacrylate-cardanol suspension polymerizations with 5.0 wt% of cardanol and 1 or 3 wt% of BPO.

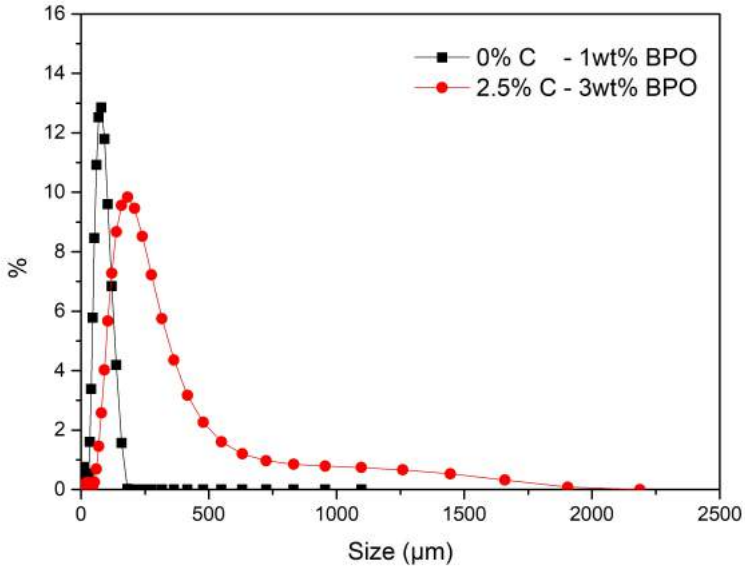


Figure 8.10: Particle size distribution for PMMA or copolymer particles made with 1 or 3.0 wt% of BPO respectively.

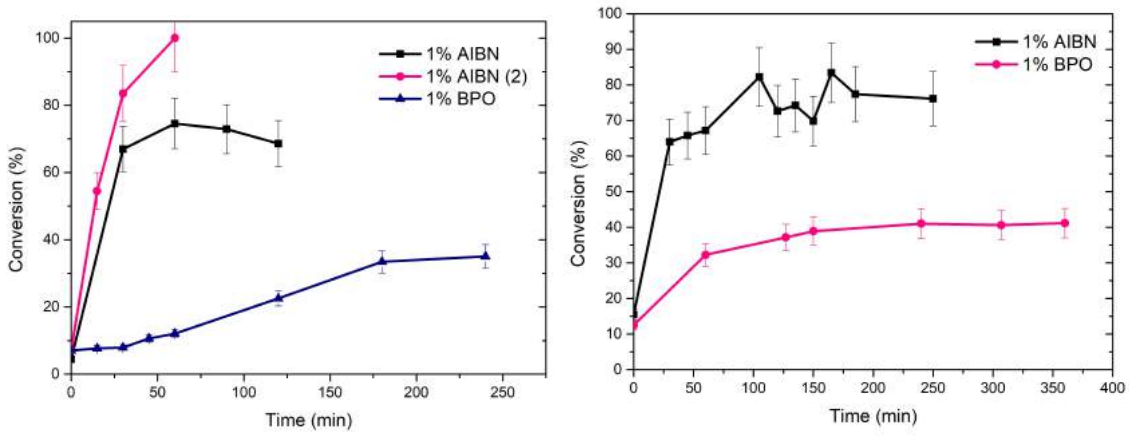


(a) (b)

Figure 8.11: Conversion data for methyl methacrylate-cardanol suspension polymerizations with 5.0 wt% (a) or 10.0 wt% (b) of cardanol and 1 wt% of AIBN. For (a), AIBN and AIBN(2) are duplicates.

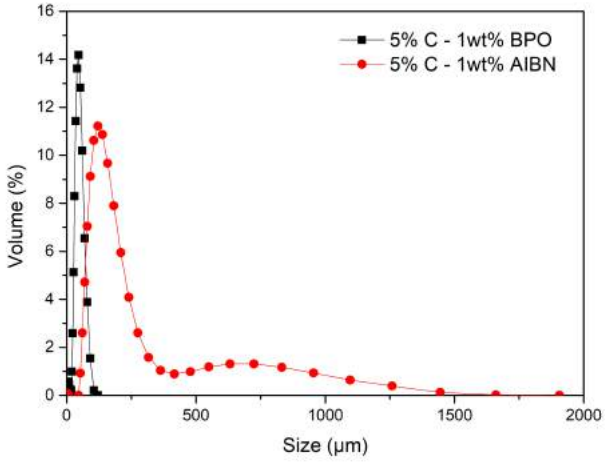


Figure 8.12: Particle size distributions for 5.0 wt% cardanol copolymer particles made with 1wt% of BPO or AIBN.

Contact angle analyses were performed to evaluate the hydrophobicity of produced copolymers in comparison to the PMMA homopolymer. In this case, a droplet of water was deposited over a disk of pressed particles and the contact angle could be measured through image analyses with the tensiometer software. For PMMA, a contact angle could be measured (results not reported). Figure 8.13 shows the water droplet on the polymer disk while contact angle was being measured. However, for the copolymers, the water droplet was quickly absorbed (less than 8 seconds). One can see how the contact angle changes while the drop is being absorbed in Figure 8.14. This happened even for the lowest concentration of cardanol (2.5 wt%). (The copolymer with 2.5 wt% was produced with 3 wt% of BPO, and reached over 80% of conversion). However, it is interesting that the $^{1}$H-NMR of the copolymer with 5 wt% of cardanol almost did not present any trace of cardanol, while the $^{1}$H-NMR of the copolymer produced with 10 wt% of cardanol shows a composition of 33.6% in mass (14.7% higher than what was obtained for the copolymer produced in bulk not precipitated, and 31.2% higher for the MMA/cardanol copolymer precipitated). Figure 8.15 present the $^{1}$H-NMR spectra for MMA/cardanol copolymers particle in comparison to the PMMA produced in bulk at 85 °C. $^{1}$H-NMR for 2.5 wt% of cardanol is not available. Although the composition data for 5 wt% do not show cardanol in the copolymer, the contact angle analysis confirms that cardanol could be incorporated due to difference in hydrophobicity.

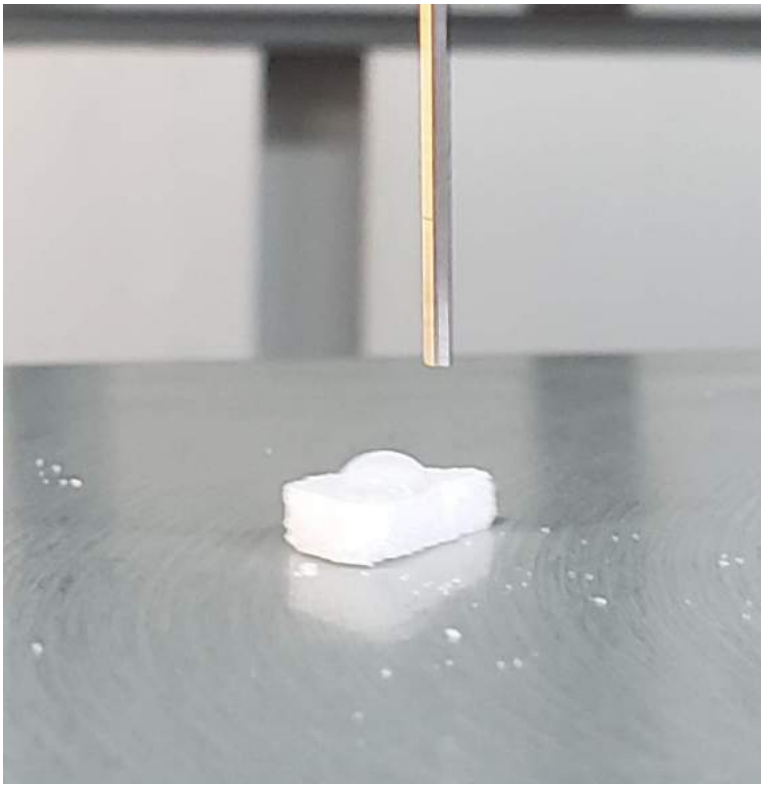

Figure 8.13: Experimental set up for PMMA-water contact angle measure.

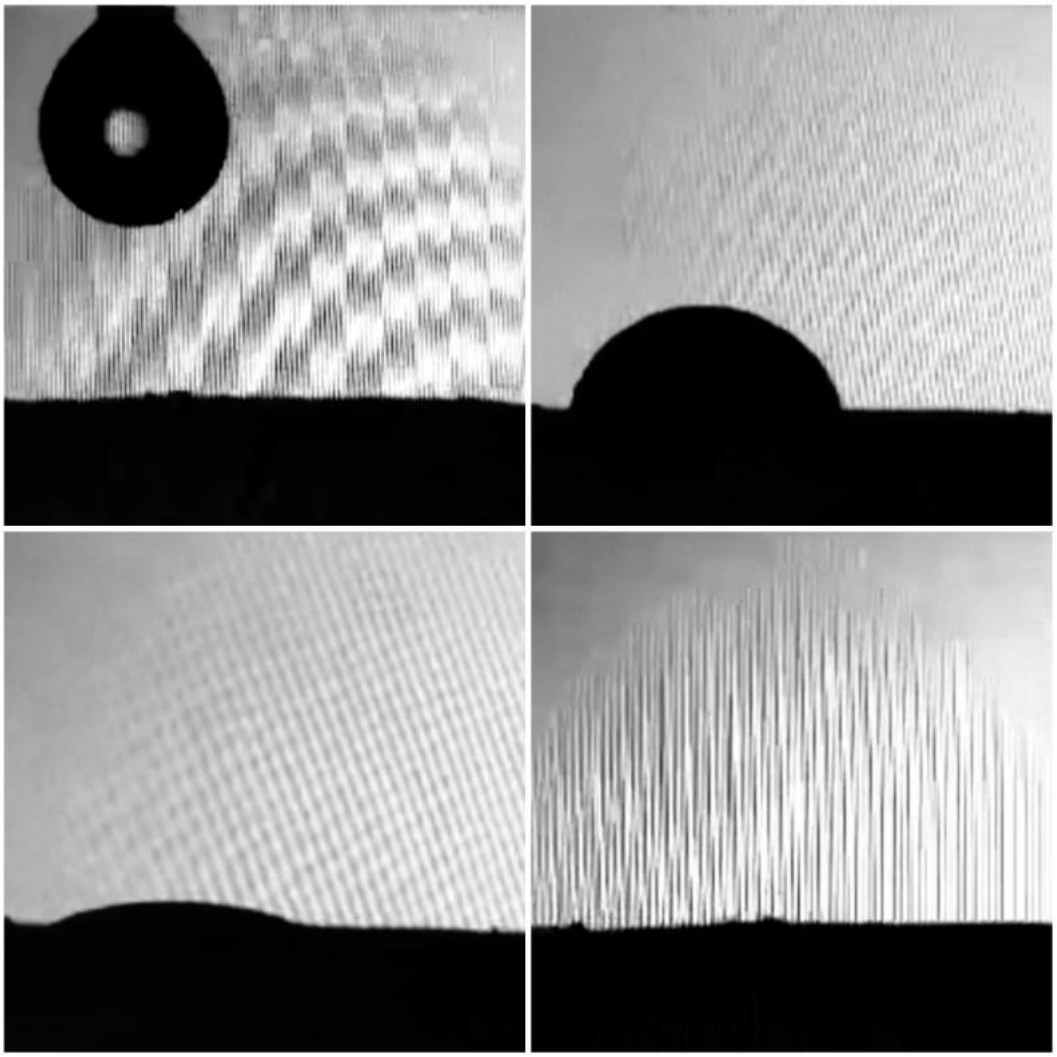

Figure 8.14: Photos taken while the contact angle analysis was being performed for a MMA/cardanol copolymer.

## 8.4 Concluding Remarks

Suspension polymerizations with cardanol were performed with methyl methacrylate and styrene as comonomers. Conversions were smaller than the ones obtained by bulk polymerization with BPO, which indicates the occurrence of unusual effects, as the kinetics of suspension and bulk polymerizations are expected to be similar. Although cardanol could reduce interfacial tension between the organic and the aqueous phase, it was not sufficient to stabilize completely the system. In order to increase the monomer conversion, BPO was changed for AIBN. For MMA, although the presence of cardanol molecules may cause the reduction of particle sizes, the size distributions were very broad and depend on the cardanol concentration, amount and type of initiator. Finally, it was interesting to see how the hydrophobicity of the particles changed with cardanol incorporation using contact angle technique. However, the particles became too hydrophilic and absorbed water, not allowing the measurements to be com-

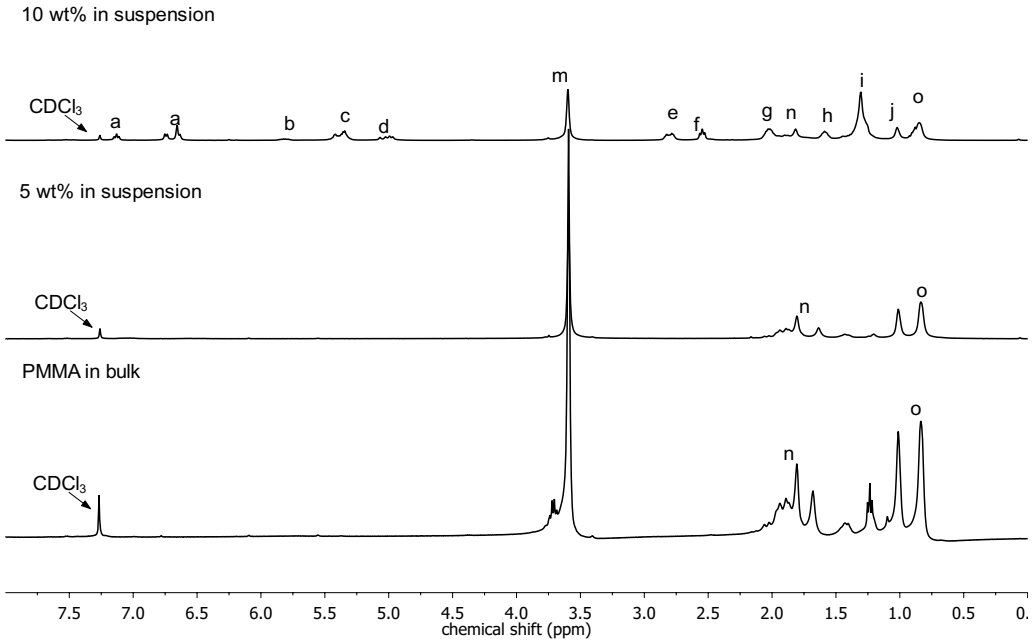


Figure 8.15: $^{1}$H-NMR of copolymer produced in suspension polymerization in relation to bulk polymerization. (Assignments were presented in Figure 5.34)

pleted. Despite that, it became obvious that copolymer particles of styrene or MMA with cardanol can be successfully prepared in suspension, using AIBN as initiator and after adjustments of agitation speeds and PVA concentrations to assure the control of the particle size distributions.

# Chapter 9

# Conclusions

Bulk polymerizations of cardanol and natural cashew nut shell liquid (CNSL) showed that oligomers can be formed through bulk free radical polymerizations, although with low conversions. The strong limitations to increase conversions arise from steric hindrance; addition of radicals to internal unsaturations of the side chain, forming stable radicals that do not propagate; and donation of protons by the phenolic group, stabilizing the aromatic ring due to resonance structures. Despite this, bulk copolymerizations of cardanol or natural CNSL with methyl methacrylate, styrene, vinyl acetate and acrid acid were performed successfully. The best results were obtained with styrene and MMA although inhibitory effects and lower reactions rates were present when the initial load of cardanol was increased. The obtained copolymers did not have high cardanol contents, but 1 wt% of cardanol in the copolymer was sufficient to improve thermal stability and reduce the glass transition temperature. Because the phenolic compounds contain many reactive sites and functional groups, analyses of FTIR and $^1H$-NMR revealed complex structures with peaks overleaping each other, but bonds for both compounds were detected and it is clear that phenolic group and unsaturations are reactive, i.e. their corresponding peaks decrease in intensity. Nonetheless, cardanol content in the copolymers was determined by $^1H$-NMR.

For vinyl acetate, cardanol acted as a strong inhibitor and, even worse, its presence in VAc polymeric chains decreased its strength and, thereby, decreased thermal stability. For acrylic acid, practically instant copolymerization happened. But, because of this, deep kinetic investigations could not be performed. Further reactions with acrylic acid should be done in heterogeneous medium to have a better control of polymerization, as bulk kinetic parameters for PAA polymerization is hard to find to study its kinetics.

Moreover, only mildly differences from cardanol kinetics to CNSL could be detected. For homopolymerizations, CNSL had higher conversions, but considering the high deviations of the obtained values, their oligomerization happened basically with

the same polymerization rate. For MMA-CNSL copolymerization, the biggest gap between its conversion and MMA-cardanol copolymerization conversion happened for the lowest temperature (85 °C). Therefore, CNSL had a lesser inhibition effect, but it still exert an inhibitory effect. This could have happened due to induction effect between the carboxyl and hydroxyl around the aromatic ring, decreasing the possibility of phenolic inhibition. However, even with this slightly difference, they are both lump mixtures and their kinetics can be considered the same. Furthermore, using CNSL, decreases one purification step to obtain cardanol, reducing process costs.

Therefore, based on the bulk results, one may expect to face strong limitations to maximize the cardanol/CNSL content of the copolymers. Despite that, for future studies, the production of copolymers with high CNSL compositions should be performed at much higher temperatures as it was shown that the increase in temperature led to a decrease in CNSL inhibition effect on kinetics. However, this might not translate in high CNSL copolymer compositions. Other possibility is using alternative processes, mainly polymerization under pressure to avoid traces of oxygen that can increase radical inhibition by the phenolics. This may lead to overall high conversions. Nonetheless, changing the initiator to a more reactive one, such as AIBN, can obtain high conversion. A good start for these future studies was the validation of a proposed kinetic model in which kinetic parameters for cardanol copolymerizations with styrene were estimated ($r_{1,2}$ and $r_{2,1}$). To characterize the inhibition, an inhibition factor responsible for reducing the concentration of free radicals was also estimated. These constants could be obtained for the studied range of cardanol concentrations and temperatures used with low objective functions. Thus, even with many hypothesis, the proposed model was able to follow monomer conversions, average molecular weights and copolymer compositions in a good range of conditions.

As polymerization in heterogeneous medium is more interesting for biomedical and other noble applications, MMA/cardanol or styrene/cardanol copolymerization were performed in suspension. Although worse rates for monomer conversion were obtained using the same mass fractions of reactants in the organic phase, the introduction of small amounts of cardanol into the copolymer backbone (below 2.5 wt%) is sufficient to modify the hydrophobicity of the final polymer product, which can be advantageous for biotechnological applications. From SEM photographies, the particles did not have a high porosity, and, in fact, their surface were smooth. Nonetheless, cardanol concentration reduces the interfacial tension, but not as much to substitute PVA in the aqueous phase. However, its amphiphilic characteristic affected the average particle size, reducing it from the average size of 76 $\mu m$ for pure PMMA to 30~45 $\mu m$ for 10 or 5.0 wt% of cardanol respectively. But particle sizes were influenced by differences in initiator concentration and type - as well as monomer conversion. Finally, the addition of chemical functionals groups on the polymeric chains (and mainly on

the surface of polymeric particles), renders them compatible and with the potential for various kind of applications.

## 9.1 Suggestion for Future Works

There are still many aspects and applications of cardanol or CNSL copolymers with vinyl monomers. To cite only a few suggestion for future works:

- Copolymerization kinetics should be studied with more reactive initiators such as AIBN;
- Apply chemical transformations to enhance the reactivity using activation functionalization or conjugation strategies in cardanol or natural CNSL and, then, perform new copolymerization reactions with these monomers.
- Although MMA is very applied in the biomedical field, copolymerizations with other vinyl monomers should be studied aiming enzyme immobilization and biomedical applications;
- Vinyl acetate copolymerizations with cardanol should be investigated in pressurized reactors at temperatures over 85 °C;
- Mechanical analysis of the copolymer produced may bring interesting results;
- Model parameters for homopolymerization of cardanol and natural CNSL should be estimated;
- More robust models for copolymerization should be proposed including cardanol homopolymerization rates, mainly for MMA;
- More tests to confirm the copolymer particles functionalization should be performed;
- Other characterization analysis should be investigated to improve copolymer characterizations such as gas chromatography, Raman spectroscopy or ultraviolet–visible spectroscopy.

# Bibliography


ANTONY, R., PILLAI, C., SCARIAH, K., 1990, "GPC studies on the cationic polymerization of cardanol initiated by borontrifluoridediethyletherate", *Journal of Applied Polymer Science*, v. 41, n. 7-8, pp. 1765–1775.

ASTM D2702, 2016, *Standard Practice for Rubber Chemicals — Determination of Infrared Absorption Characteristics*. Standard, ASTM International, West Conshohocken, PA.

BALGUDE, D., SABNIS, A. S., 2014, "CNSL: an environment friendly alternative for the modern coating industry", *Journal of Coatings Technology and Research*, v. 11, n. 2, pp. 169–183. doi: <10.1007/s11998-013-9521-3>. Availability: <http://link.springer.com/10.1007/s11998-013-9521-3>.

BESTETI, M. D., SOUZA JR, F. G., FREIRE, D. M., et al., 2014, "Production of core-shell polymer particles-containing cardanol by semibatch combined suspension/emulsion polymerization", *Polymer Engineering & Science*, v. 54, n. 5, pp. 1222–1229.

BESTETI, M. D., 2009, *Produção e Caracterização de Partículas Casca-Núcleo Obtidas pela Polimerização Simultânea em Suspensão e Emulsão*. Master dissertation, Programa de Engenharia Química (PEQ) - Federal University of Rio de Janeiro.

BEVINGTON, J., MELVILLE, H., TAYLOR, R., 1954, "The termination reaction in radical polymerizations. Polymerizations of methyl methacrylate and styrene at 25°", *Journal of Polymer Science*, v. 12, n. 1, pp. 449–459.

BHUNIA, H. P., NANDO, G. B., BASAK, A., et al., 1999, "Synthesis and characterization of polymers from cashewnut shell liquid (CNSL), a renewable resource III. Synthesis of a polyether", *European Polymer Journal*, v. 35, n. 9, pp. 1713–1722. doi: <http://dx.doi.org/10.1016/S0014-3057(98)00244-4>. Availability: <http://www.sciencedirect.com/science/article/pii/S0014305798002444>.

BILLMEYER, F. W., 1984, *Textbook of Polymer Science*. 3rd ed. United States of America, John Wiley & Sons.

BISANDA, E. T. N., ANSELL, M. P., 1992, "Properties of sisal-CNSL composites", *Journal of Materials Science*, v. 27, n. 6, pp. 1690–1700. doi: <10.1007/BF00542934>.

BOHARA, R. A., THORAT, N. D., PAWAR, S. H., 2016, "Role of functionalization: strategies to explore potential nano-bio applications of magnetic nanoparticles", *RSC Advances*, v. 6, n. 50, pp. 43989–44012.

BRANDÃO, A., 2017, *Mathematical modeling of chain branching reactions in olefin coordination polymerizations*. Phd thesis, Programa de Engenharia Química (PEQ) - Universidade Federal do Rio de Janeiro.

CAMPOS, I. M., FERRAZ, H. C., PINTO, J. C., 2016, "Production and Functionalization of P (MMA-co-AA) Nanoparticles by Miniemulsion Polymerization". In: *Macromolecular Symposia*, v. 368, pp. 70–77. Wiley Online Library.

CANEVAROLO JR., S., 2006, *Ciência dos Polímeros*. 2nd ed. São Paulo, Artliber Editora.

CARVALHO, E. P., 2011, *Uso do persulfato de amônio para estabilização da polimerização em suspensão do estireno*. Master dissertation, Programa de Engenharia Química (PEQ) - Universidade Federal do Rio de Janeiro.

CEPAGRO/IBGE, 2019, *Levantamento Sistemático da Produção Agrícola (LSPA)*. Relatório técnico, 1.

CERVANTES-UC, J., CAUICH-RODRÍGUEZ, J., VÁZQUEZ-TORRES, H., et al., 2006, "TGA/FTIR study on thermal degradation of polymethacrylates containing carboxylic groups", *Polymer degradation and stability*, v. 91, n. 12, pp. 3312–3321.

CHELIKANI, R., KIM, Y. H., YOON, D. Y., et al., 2009, "Enzymatic polymerization of natural anacardic acid and antibiofouling effects of polyanacardic acid coatings", *Applied Biochemistry and Biotechnology*, v. 157, n. 2, pp. 263–277. doi: <10.1007/s12010-008-8284-2>.

CHISHOLM, B. J., ALAM, S., KALITA, H., et al., 2014, *Monomers and polymers derived from natural phenols*. Nsdu Research Foundation. WO2014197041A2.

CORREIA, S. D. J., DAVID, J. P., DAVID, J. M., 2006, "Metabólitos secundários de espécies de Anacardiaceae", *Química Nova*, v. 29, n. 6, pp. 1287–1300.

COSTA, L. P., OECHSLER, B. F., BRANDÃO, A. L. T., et al., 2019, "Copolymerization of Styrene and Cardanol from Cashew Nut Shell Liquid. Part I – Kinetic Modeling of Bulk Copolymerizations", *Macromolecular Reaction Engineering*. doi: <10.1002/mren.201800065>. Availability: <https://onlinelibrary.wiley.com/doi/abs/10.1002/mren.201800065>.

DE MARIA, P., FILIPPONE, P., FONTANA, A., et al., 2005, "Cardanol as a replacement for cholesterol into the lipid bilayer of POPC liposomes", *Colloids and Surfaces B: Biointerfaces*, v. 40, n. 1, pp. 11–18.

FERREIRA, S. R., LOUZADA, H. F., DIP, R. M. M., et al., 2015, "Influence of the architecture of additives on the stabilization of asphaltene and water-in-oil emulsion separation", *Energy & Fuels*, v. 29, n. 11, pp. 7213–7220.

FERRIOL, M., GENTILHOMME, A., COCHEZ, M., et al., 2003, "Thermal degradation of poly (methyl methacrylate)(PMMA): modelling of DTG and TG curves", *Polymer degradation and stability*, v. 79, n. 2, pp. 271–281.

FINEMAN, M., ROSS, S. D., 1950, "Linear method for determining monomer reactivity ratios in copolymerization", *Journal of Polymer Science*, v. 5, n. 2, pp. 259–262.

GALVÃO, L. D. A., 2016, *Estudo da Copolimerização de Estireno e Cardanol em Meios Homogêneo e Heterogêneo*. Master dissertation, Programa de Engenharia Química (PEQ) - Federal University of Rio de Janeiro.

GEDAM, P., SAMPATHKUMARAN, P., 1986, "Cashew nut shell liquid: extraction, chemistry and applications", *Progress in Organic Coatings*, v. 14, n. 2, pp. 115–157.

GONDINS, A., 1973, "A agro-industria do caju no Nordeste-Situacao atual e perspectivas", *Banco do Nordeste do Brasil SA, Departamento de Estudos Economics do Nordeste (ETENE), Fortaleza (Brazil)*.

HARVEY, M. T. "Process of destructively distilling cashew nut shell liquid (*US*2098824)". .

HERMANSON, G. T., 2013, *Bioconjugate techniques*. Academic press.

IKEDA, R., TANAKA, H., UYAMA, H., et al., 2000a, "Enzymatic Synthesis and Curing of Poly(cardanol)", *Polymer Journal*, v. 32, n. 7, pp. 589–593.

IKEDA, R., TANAKA, H., UYAMA, H., et al., 2000b, "New crosslinkable polyphenol from renewable resource", *American Chemical Society, Polymer Preprints,*

*Division of Polymer Chemistry*, v. 41, n. 1, pp. 83–84. doi: <10.1002/(SICI)1521-3927(20000501)21:8<496::AID-MARC496>3.0.CO;2-G>.

KAEWCHADA, A., BORVORNPONGSAKUL, C., JAREE, A., 2012, "Synthesis of molecularly imprinted polymers from AnAc for the separation of $\gamma$-oryzanol", *Korean Journal of Chemical Engineering*, v. 29, n. 9 (sep), pp. 1279–1284. doi: <10.1007/s11814-012-0021-4>. Availability: <http://link.springer.com/10.1007/s11814-012-0021-4>.

KALFAS, G., RAY, W. H., 1993, "Modeling and experimental studies of aqueous suspension polymerization processes. 1. Modeling and simulations", *Industrial & engineering chemistry research*, v. 32, n. 9, pp. 1822–1830.

KASHIWAGI, T., INABA, A., BROWN, J. E., et al., 1986, "Effects of weak linkages on the thermal and oxidative degradation of poly (methyl methacrylates)", *Macromolecules*, v. 19, n. 8, pp. 2160–2168.

KELEN, T., TÜDŐS, F., 1974, "A new improved linear graphical method for determing copolymerization reactivity ratios", *Reaction Kinetics and Catalysis Letters*, v. 1, n. 4, pp. 487–492.

KIM, K. J., CHOI, K. Y., ALEXANDER, J. C., 1992, "Dynamics of a continuous stirred tank reactor for styrene polymerization initiated by a binary initiator mixture. II: Effect of viscosity dependent heat transfer coefficient", *Polymer Engineering & Science*, v. 32, n. 7, pp. 494–505.

KIM, K., CHOI, K., 1989, "Modeling of free radical polymerization of styrene catalyzed by unsymmetrical bifunctional initiators", *Chemical engineering science*, v. 44, n. 2, pp. 297–312.

KIM, Y. H., AN, E. S., SONG, B. K., et al., 2003, "Polymerization of cardanol using soybean peroxidase and its potential application as anti-biofilm coating material", *Biotechnology Letters*, v. 25, n. 18, pp. 1521–1524. doi: <10.1023/A:1025486617312>.

KUMAR, S., DINESHA, P., ROSEN, M. A., 2018, "Cashew Nut Shell Liquid as a Fuel for Compression Ignition Engines: A Comprehensive Review", *Energy and Fuels*, v. 32, n. 7, pp. 7237–7244. doi: <10.1021/acs.energyfuels.8b00579>.

LARTIGUE-PEYROU, F., 1996, "The use of phenolic compounds as free-radical polymerization inhibitors". In: *Industrial Chemistry Library*, v. 8, Elsevier, pp. 489–505.

LEMOS, T. S. M., 2014, *Modelagem Estocástica da Formação de Produtos Copoliméricos com Microestrutura Controlada em Reatores Contínuos*. Master dissertation, Programa de Engenharia Química (PEQ) - Federal University of Rio de Janeiro.

LI, W. S. J., NEGRELL, C., LADMIRAL, V., et al., 2018, "Cardanol-based polymer latex by radical aqueous miniemulsion polymerization", *Polymer Chemistry*, v. 9, n. 18, pp. 2468–2477. doi: <10.1039/C8PY00167G>. Availability: <http://xlink.rsc.org/?DOI=C8PY00167G>.

LOCHAB, B., SHUKLA, S., VARMA, I. K., 2014, "Naturally occurring phenolic sources: monomers and polymers", *RSC Adv.*, v. 4, n. 42, pp. 21712–21752. doi: <10.1039/C4RA00181H>. Availability: <http://xlink.rsc.org/?DOI=C4RA00181H>.

LOUIE, B. M., CARRATT, G. M., SOONG, D. S., 1985, "Modeling the free radical solution and bulk polymerization of methyl methacrylate", *Journal of applied polymer science*, v. 30, n. 10, pp. 3985–4012.

LOUREIRO, T., DIP, R. M. M., LUCAS, E., et al., 2017, "Cardanol Polymerization Under Acid Conditions By Addition And Condensation Reactions", *Journal of Polymers and the Environment*, v. 0, n. 0, pp. 1–12. doi: <10.1007/s10924-017-0969-6>.

LUBI, M. C., THACHIL, E. T., 2000, "Cashew nut shell liquid (CNSL) - a versatile monomer for polymer synthesis", *Designed Monomers & Polymers*, v. 3, n. 2, pp. 123–153. doi: <10.1163/156855500300142834>. Availability: <http://www.tandfonline.com/doi/full/10.1163/156855500300142834>.

MAHABADI, H. K., O'DRISCOLL, K., 1977, "Absolute rate constants in free-radical polymerization. III. Determination of propagation and termination rate constants for styrene and methyl methacrylate", *Journal of Macromolecular Science—Chemistry*, v. 11, n. 5, pp. 967–976.

MAHANWAR, P. A., KALE, D. D., 1996, "Effect of processing parameters on refining of CNSL", *Indian Journal of Chemical Technology*, v. 3, n. July, pp. 191–193.

MAHON, E., SALVATI, A., BOMBELLI, F. B., et al., 2012, "Designing the nanoparticle–biomolecule interface for "targeting and therapeutic delivery"", *Journal of Controlled Release*, v. 161, n. 2, pp. 164–174.

MANJULA, S., KUMAR, V. G., PILLAI, C. K., 1992, "Kinetics and mechanism of oligomerization of cardanol using acid catalysts", *Journal of Applied Polymer Science*, v. 45, n. 2, pp. 309–315. doi: <10.1002/app.1992.070450213>.

MANRING, L. E., SOGAH, D. Y., COHEN, G. M., 1989, "Thermal degradation of poly (methyl methacrylate). 3. Polymer with head-to-head linkages", *Macromolecules*, v. 22, n. 12, pp. 4652–4654.

MAYO, F. R., LEWIS, F. M., 1944, "Copolymerization. I. A basis for comparing the behavior of monomers in copolymerization; the copolymerization of styrene and methyl methacrylate", *Journal of the American Chemical Society*, v. 66, n. 9, pp. 1594–1601.

MAZZETTO, S. E., LOMONACO, D., MELE, G., 2009, "Óleo da Castanha de Caju: Oportunidades e Desafios no Contexto do Desenvolvimento e Sustentabilidade Industrial", *Quim. Nova*, v. 32, n. 3, pp. 732–741.

MCNAUGHT, A. D., WILKINSON, A., 1997, *IUPAC. Compendium of Chemical Terminology (the "Gold Book")*. 2 ed. Oxford, Blackwell Scientific Publications. ISBN: 0-9678550-9-8.

MELO, C. K., SOARES, M., CASTOR, C. A., et al., 2014, "In Situ Incorporation of Recycled Polystyrene in Styrene Suspension Polymerizations", *Macromolecular Reaction Engineering*, v. 8, n. 1, pp. 46–60.

MENDES, A. N., HUBBER, I., SIQUEIRA, M., et al., 2012, "Preparation and cytotoxicity of poly (methyl methacrylate) nanoparticles for drug encapsulation". In: *Macromolecular Symposia*, v. 319, pp. 34–40. Wiley Online Library.

MINARI, R. J., CACERES, G., MANDELLI, P., et al., 2011, "Semibatch Aqueous-Solution Polymerization of Acrylic Acid: Simultaneous Control of Molar Masses and Reaction Temperature", *Macromolecular Reaction Engineering*, v. 5, n. 5-6, pp. 223–231.

MISRA, A. K., PANDEY, G. N., 1984, "Kinetics of alkaline-catalyzed cardanol–formaldehyde reaction. I", *Journal of Applied Polymer Science*, v. 29, n. 1 (jan), pp. 361–372. doi: <10.1002/app.1984.070290134>. Availability: <http://doi.wiley.com/10.1002/app.1984.070290134>.

MISRA, A. K., PANDEY, G. N., 1985, "Kinetics of alkaline-catalyzed cardanol–formaldehyde reaction. II. Mechanism of the reaction", *Journal of Applied Polymer Science*, v. 30, n. 3, pp. 969–977. doi: <10.1002/app.1985.070300307>.

MUBOFU, E. B., MGAYA, J. E., 2018, "Chemical Valorization of Cashew Nut Shell Waste", *Topics in Current Chemistry*, v. 376, n. 2, pp. 1–15. doi: <10.1007/s41061-017-0177-9>. Availability: <https://doi.org/10.1007/s41061-017-0177-9>.

MUBOFU, E. B., 2016, "From cashew nut shell wastes to high value chemicals", *Pure and Applied Chemistry*, v. 88, n. 1-2, pp. 17–27. doi: <10.1515/pac-2015-0603>.

ODIAN, G., 2004, *Principles of Polymerization*. 4th ed. New York, John Wiley & Sons, Inc.

OECHSLER, B. F., 2016, *Análise Dinâmica de Modelos de Mistura Imperfeita em Reatores de Polimerização via Radicais-livres em Solução*. Phd thesis, Universidade Federal do Rio de Janeiro (UFRJ).

OLIVEIRA, L. D. M. DE, 2007, *Síntese, Caracterização e Funcionalidade de Aditivos de Lubricidade, Derivados do LCC*. Master dissertation, Universidade Federal do Ceará.

OTSUKA, T., FUJIKAWA, S. I., YAMANE, H., et al., 2017, "Green polymer chemistry: The biomimetic oxidative polymerization of cardanol for a synthetic approach to 'artificial urushi'", *Polymer Journal*, v. 49, n. 3, pp. 335–343. doi: <10.1038/pj.2016.118>. Availability: <http://dx.doi.org/10.1038/pj.2016.118>.

PAIVA, F. F. D. A., GARRUTTI, D. D. S., SILVA NETO, R. M. D., 2000, *Aproveitamento industrial do caju*. Relatório técnico, Embrapa Agroindústria Tropical, Fortaleza. Availability: <http://ainfo.cnptia.embrapa.br/digital/bitstream/CNPAT-2010/4835/1/Dc-038.pdf>.

PAIVA, T., VIEIRA, L., MELO, P., et al., 2018, "In Situ Incorporation of Praziquantel in Polymer Microparticles through Suspension Polymerization for Treatment of Schistosomiasis", *Macromolecular Reaction Engineering*, p. 1800064.

PARAMASHIVAPPA, R., KUMAR, P. P., VITHAYATHIL, P., et al., 2001, "Novel method for isolation of major phenolic constituents from cashew (Anacardium occidentale L.) nut shell liquid", *Journal of Agricultural and Food Chemistry*, v. 49, n. 5, pp. 2548–2551.

PATEL, R. N., BANDYOPADHYAY, S., GANESH, A., 2006, "Extraction of cashew (Anacardium occidentale) nut shell liquid using supercritical carbon dioxide", *Bioresource Technology*, v. 97, n. 6, pp. 847–853.

PEIXOTO, A. C. B., 2013, *Funcionalização de Nanopartículas Poliméricas para Liberação de Medicamentos Sítio-Dirigida*. Phd thesis, Programa de Engenharia Química (PEQ) - Federal University of Rio de Janeiro.

PEKLAK, A. D., BUTTÉ, A., STORTI, G., et al., 2006, "Gel effect in the bulk reversible addition–fragmentation chain transfer polymerization of methyl methacrylate: Modeling and experiments", *Journal of Polymer Science Part A: Polymer Chemistry*, v. 44, n. 3, pp. 1071–1085.

PERDRIAU, S., HARDER, S., HEERES, H. J., et al., 2012, "Selective conversion of polyenes to monoenes by RuCl3-catalyzed transfer hydrogenation: The case of cashew nutshell liquid", *ChemSusChem*, v. 5, n. 12, pp. 2427–2434. doi: <10.1002/cssc.201200503>.

PHILIP, J. Y., BUCHWEISHAIJA, J., MKAYULA, L. L., et al., 2007, "Preparation of molecularly imprinted polymers using anacardic acid monomers derived from cashew nut shell liquid", *Journal of Agricultural and Food Chemistry*, v. 55, n. 22, pp. 8870–8876. doi: <10.1021/jf0718289>.

PICHOT, C., 2004, "Surface-functionalized latexes for biotechnological applications", *Current Opinion in Colloid & Interface Science*, v. 9, n. 3-4 (nov), pp. 213–221. doi: <10.1016/j.cocis.2004.07.001>. Availability: <http://linkinghub.elsevier.com/retrieve/pii/S1359029404000688>.

PINTO, J., RAY, W., 1995, "The dynamic behavior of continuous solution polymerization reactors—VII. Experimental study of a copolymerization reactor", *Chemical engineering science*, v. 50, n. 4, pp. 715–736.

PINTO, M. C. C., SANTOS JR., J. G. F., MACHADO, F., et al., 2013, "Suspension Polymerization Processes". In: *Encyclopedia of Polymer Science and Technology*, American Cancer Society. ISBN: 9780471440260. Availability: <https://onlinelibrary.wiley.com/doi/abs/10.1002/0471440264.pst597>.

PINTO, M. C., SANTOS JR, J. G., MACHADO, F., et al., 2002, "Suspension polymerization processes", *Encyclopedia of Polymer Science and Technology*.

PRETSCH, E., BUEHLMANN, P., AFFOLTER, C., et al., 2000, *Structure determination of organic compounds*. Springer.

RAMOS, I. M. F. C., 2018, *Nanopartículas Poliméricas Funcionalizadas para Liberação de Fármaco no Sistema Nervoso Central*. Phd thesis, Universidade Federal do Rio de Janeiro (UFRJ).

RODRIGUES, F. H., FRANÇA, F. C., SOUZA, J. R., et al., 2011, "Comparison between physico-chemical properties of the technical Cashew Nut Shell Liquid (CNSL) and those natural extracted from solvent and pressing", *Polímeros*, v. 21, n. 2, pp. 156–160.

RODRIGUES, F. H. A., FEITOSA, J., RICARDO, N. M., et al., 2006, "Antioxidant activity of cashew nut shell liquid (CNSL) derivatives on the thermal oxidation of synthetic cis-1, 4-polyisoprene", *Journal of the Brazilian Chemical Society*, v. 17, n. 2, pp. 265–271.

RODRIGUEZ, F., COHEN, C., OBER, C. K., et al., 2015, *Principles of Polymer Systems*. 6th ed. New York, Taylor & Francis Group.

SATHIYALEKSHMI, K., 1993, "Studies on structure and properties of CNSL novolac resins prepared with succinic acid catalyst", *Bulletin of Materials Science*, v. 16, n. 2, pp. 137–150. doi: <10.1007/BF02745329>.

SCHWAAB, M., PINTO, J., 2007, *Análise de Dados Experimentais: I. Fundamentos de Estatística e Estimação de Parâmetros*.

SCHWAAB, M., BISCAIA JR, E. C., MONTEIRO, J. L., et al., 2008, "Nonlinear parameter estimation through particle swarm optimization", *Chemical Engineering Science*, v. 63, n. 6, pp. 1542–1552.

SCORAH, M., DHIB, R., PENLIDIS, A., 2006, "Modelling of free radical polymerization of styrene and methyl methacrylate by a tetrafunctional initiator", *Chemical engineering science*, v. 61, n. 15, pp. 4827–4859.

SECEX/MDIC, 2019, *Castanha de Caju - Comex Vis: Principais Produtos Exportados*. Relatório técnico, Secretaria de Comércio Exterior, Ministério da Economia, Indústria, Comérico Exterior e Serviços. Availability: <http://www.mdic.gov.br/comercio-exterior/estatisticas-de-comercio-exterior/comex-vis/frame-ppe?ppe=1130>.

SERRANO, L. A. L., 2016, "Sistema de produção do caju". In: *Sistema de produção, 1*, Embrapa Agroindústria Tropical, Fortaleza. Availability: <http://ainfo.cnptia.embrapa.br/digital/bitstream/item/147861/1/SPR16001.pdf>.

SILVA, F. M., LIMA, E. L., PINTO, J. C., 2004, "Control of the copolymer composition in suspension copolymerization reactions", *Industrial & engineering chemistry research*, v. 43, n. 23, pp. 7312–7323.

SMITH, B. C., 1998, *Infrared spectral interpretation: a systematic approach*. CRC press.

SOUZA JR., F. G., PINTO, J. C., RODRIGUES, M. V., et al., 2008a, "New polyaniline/polycardanol conductive blends characterized by FTIR, NIR, and XPS", *Polymer Engineering & Science*, v. 48, n. 10 (oct), pp. 1947–1952. doi:

<10.1002/pen.21047>. Availability: <http://doi.wiley.com/10.1002/pen.20921http://doi.wiley.com/10.1002/pen.21047>.

SOUZA JR., F. G., RICHA, P., DE SIERVO, A., et al., 2008b, "New in situ blends of polyaniline and cardanol bio-resins", *Macromolecular Materials and Engineering*, v. 293, n. 8, pp. 675–683. doi: <10.1002/mame.200800077>.

SURESH, K. I., KISHANPRASAD, V. S., 2005, "Synthesis, structure, and properties of novel polyols from cardanol and developed polyurethanes", *Industrial and Engineering Chemistry Research*, v. 44, n. 13, pp. 4504–4512. doi: <10.1021/ie0488750>.

TIAN, H., TANG, Z., ZHUANG, X., et al., 2012, "Biodegradable synthetic polymers: Preparation, functionalization and biomedical application", *Progress in Polymer Science (Oxford)*, v. 37, n. 2, pp. 237–280. doi: <10.1016/j.progpolymsci.2011.06.004>. Availability: <http://dx.doi.org/10.1016/j.progpolymsci.2011.06.004>.

TIDWELL, P. W., MORTIMER, G. A., 1965, "An improved method of calculating copolymerization reactivity ratios", *Journal of Polymer Science Part A: General Papers*, v. 3, n. 1, pp. 369–387.

TIDWELL, P. W., MORTIMER, G. A., 1970, "Science of determining copolymerization reactivity ratios", *Journal of Macromolecular Science—Reviews in Macromolecular Chemistry*, v. 4, n. 2, pp. 281–312.

TSOUKAS, A., TIRRELL, M., STEPHANOPOULOS, G., 1982, "Multiobjective dynamic optimization of semibatch copolymerization reactors", *Chemical Engineering Science*, v. 37, n. 12, pp. 1785–1795.

TYCHOPOULOS, V., TYMAN, J. H., 1990, "Long chain phenols—the thermal and oxidative deterioration of phenolic lipids from the cashew (Anacardium occidentale) nut shell", *Journal of the Science of Food and Agriculture*, v. 52, n. 1, pp. 71–83.

VILLALOBOS, M. A., HAMIELEC, A. E., WOOD, P. E., 1993, "Bulk and suspension polymerization of styrene in the presence of n-pentane. An evaluation of monofunctional and bifunctional initiation", *Journal of applied polymer science*, v. 50, n. 2, pp. 327–343.

VIVALDO-LIMA, E., WOOD, P. E., HAMIELEC, A. E., et al., 1998, "Kinetic model-based experimental design of the polymerization conditions in suspension copolymerization of styrene/divinylbenzene", *Journal of Polymer Science Part A: Polymer Chemistry*, v. 36, n. 12, pp. 2081–2094.

WAY, D. V., 2017, *Uso de Click Chemistry para a Bioconjugação de Polímeros Visando ao Tratamento do Câncer*. Phd thesis, Programa de Engenharia Química (PEQ) - Universidade Federal do Rio de Janeiro.

WELSCH, N., LU, Y., DZUBIELLA, J., et al., 2013, "Adsorption of proteins to functional polymeric nanoparticles", *Polymer*, v. 54, n. 12, pp. 2835–2849.

YADAV, R., SRIVASTAVA, D., 2007a, "Kinetics of the acid-catalyzed cardanol-formaldehyde reactions", *Materials Chemistry and Physics*, v. 106, n. 1, pp. 74–81. doi: <10.1016/j.matchemphys.2007.05.020>.

YADAV, R., SRIVASTAVA, D., 2007b, "Kinetics of the acid-catalyzed cardanol–formaldehyde reactions", *Materials Chemistry and Physics*, v. 106, n. 1, pp. 74–81.

YOON, D. Y., KIM, D. S., 2009, "Molecular design of anti-biofouling materials from natural phenolic compounds", *Korean Journal of Chemical Engineering*, v. 26, n. 2, pp. 433–437. doi: <10.1007/s11814-009-0073-2>.

ZALDÍVAR, C., DEL SOL, O., IGLESIAS, G. D., 1998, "On the preparation of acrylic acid/vinyl acetate copolymers with constant composition—1. copolymerization reactivity ratios", *Polymer*, v. 39, n. 1, pp. 245–246.

# Appendix

## Using GPC for polymer conversion

Gel permeation chromatography (GPC) is a liquid chromatography technique that separates molecules according to their size and it is used to determine the molar mass distribution of a polymer. It is similar to high performance liquid chromatography (HPLC), but a GPC uses thermodynamic conditions that avoids enthalpic interactions with the stationary phase. Low polydispersity polymer standards with known molar masses are used to form a calibration curve. From this calibration curve, the distribution of an unknown polymer can be transformed in a molar mass distribution with its statistical averages.

In addition, the weight fraction is an output of the analyze. So, you know the weight fraction of each small section of the chromatogram and, simultaneously, the cumulative weight fraction and the average molecular weight distribution. Therefore, using only the essential mechanism of GPC, you can obtain the conversion by comparing weight fractions between the polymer and monomer of a same chromatogram (if the polymer was not previously treated).

Therefore, the conversion was calculated by the Equation bellow:

$$conversion(\%) = \frac{weight\ fraction_{polymer}}{weight\ fraction_{polymer} + weight\ fraction_{monomer}} * 100\%$$

The figure bellow presents an example of the area taken for calculation of conversion for cardanol and natural CNSL oligomers.

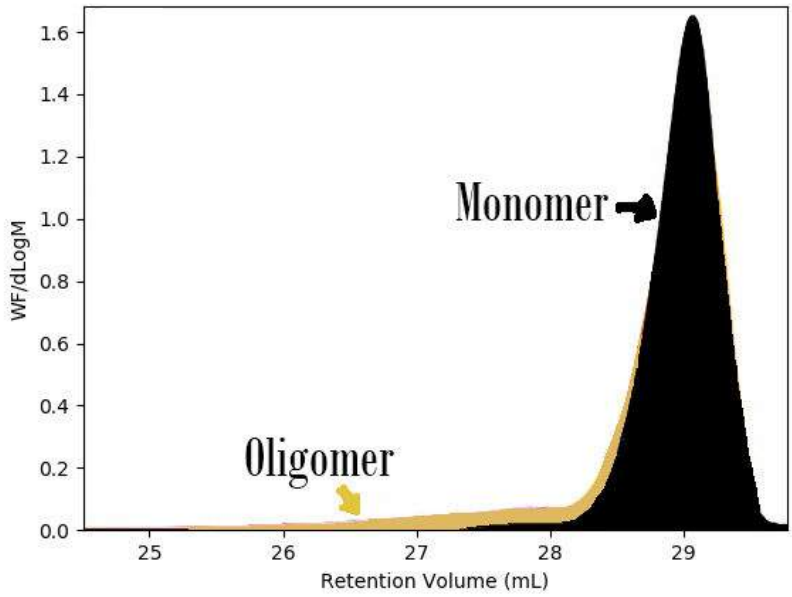


Chromatogram for a cardanol oligomer sample showing the area taken for calculation of oligomer conversion.

## Average molecular weights for oligomers of cardanol and natural CNSL

Average molecular weights for cardanol at 85 and 110°C using 1 wt% of BPO

| | 110 °C | | |
|---|---|---|---|
| | Mn | Mw | PDI |
| 1 h | 1081 | 1552 | 1.436 |
| 3 h | 1192 | 1641 | 1.376 |
| 5 h | 1241 | 1711 | 1.467 |
| 6 h | 1138 | 1544 | 1.356 |
| 8 h | 1239 | 1870 | 1.510 |
| | 85 °C | | |
| | Mn | Mw | PDI |
| 2 h | 992 | 1287 | 1.299 |
| 4 h | 972 | 1210 | 1.245 |
| 7 h | 962 | 1171 | 1.219 |
| 8h30 | 993 | 1279 | 1.289 |
| 10h30 | 936 | 1136 | 1.214 |

Average molecular weights for natural CNSL at 85 and 110°C using 1 wt% of BPO

| | 110 °C | | |
|---|---|---|---|
| | Mn | Mw | PDI |
| 1 h | 1197 | 1679 | 1.402 |
| 3 h | 1213 | 1830 | 1.509 |
| 5 h | 1205 | 1727 | 1.433 |
| 6 h | 1144 | 1557 | 1.360 |
| 8 h | 1135 | 1627 | 1.434 |
| | 85 °C | | |
| | Mn | Mw | PDI |
| 2 h | 1091 | 1451 | 1.329 |
| 4 h | 1199 | 1593 | 1.328 |
| 7 h | 1140 | 1474 | 1.292 |
| 8h30 | 1106 | 1498 | 1.355 |
| 9h | 1159 | 1517 | 1.308 |

# $^{1}$H-NMR of styrene-cardanol copolymer

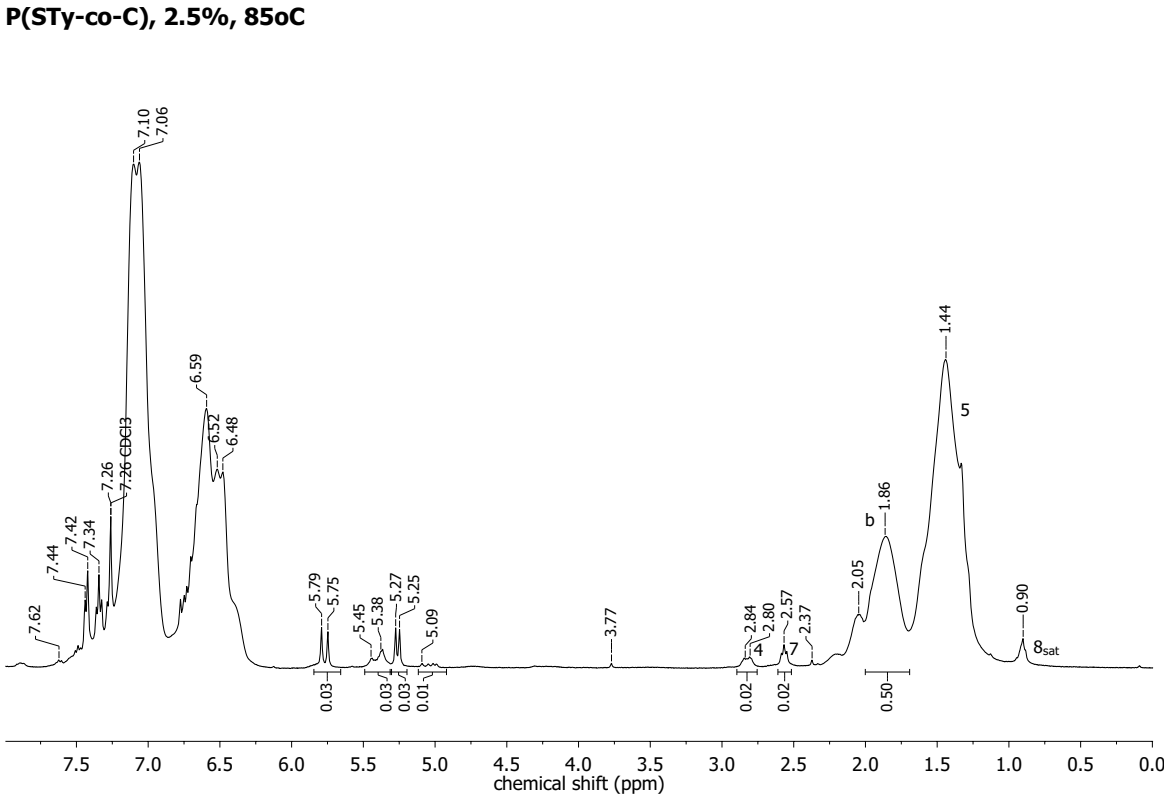


$^{1}$H-NMR of 2.5 wt% of cardanol, 85 °C, 5 hours

**P(STy-co-C), 5%, 85oC**

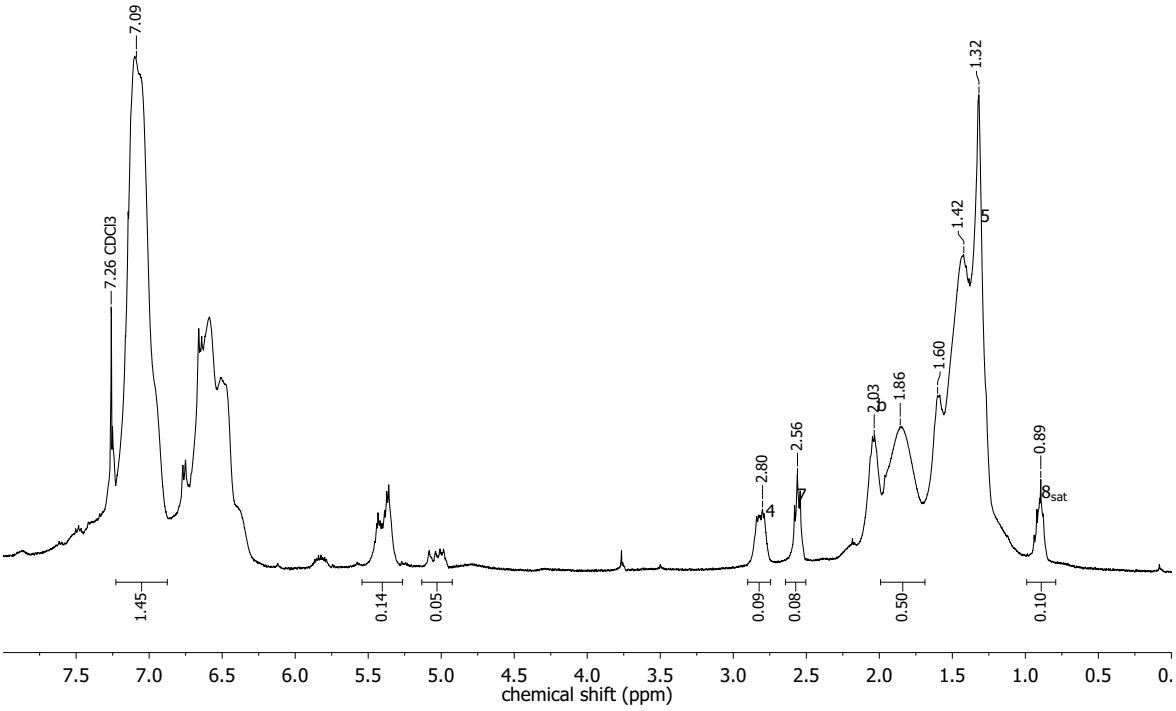


$^{1}$H-NMR of 2.5 wt% of cardanol, 85 °C, 5 hours

**P(STy-co-C), 10%, 85oC**

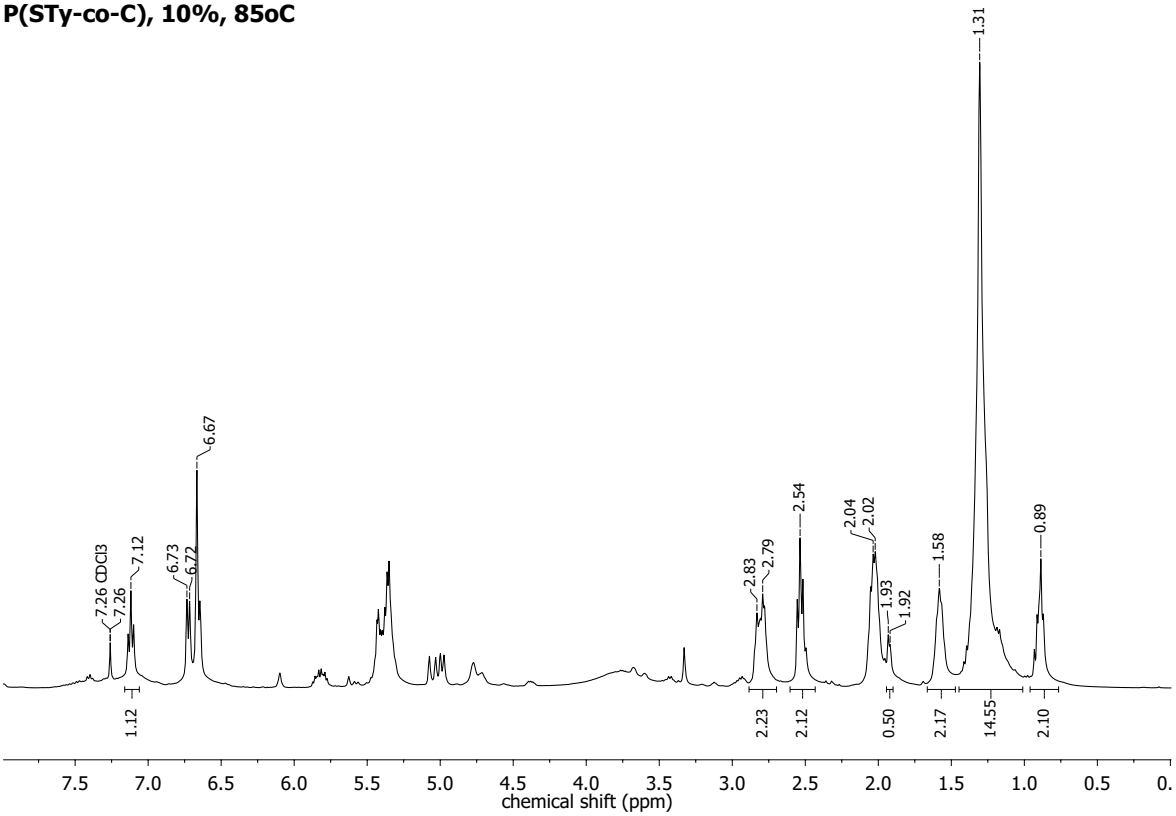


$^{1}$H-NMR of 10 wt% of cardanol, 85 °C, 5 hours

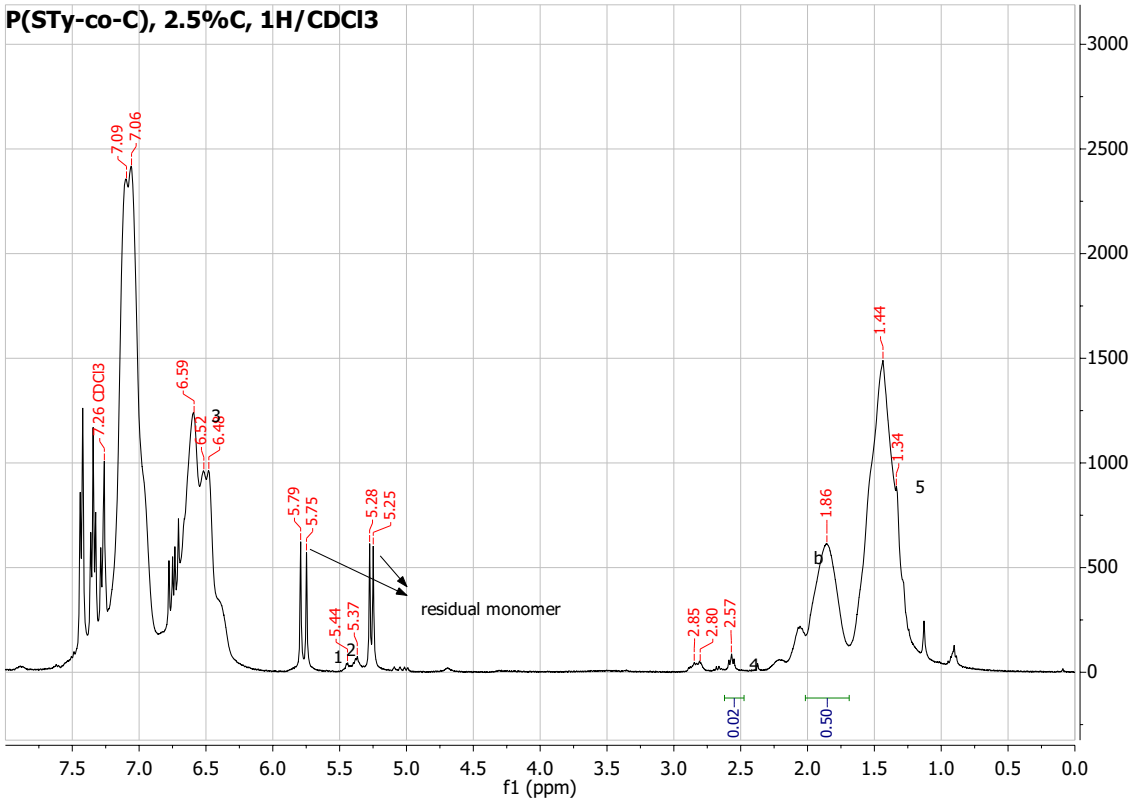


$^{1}$H-NMR of 2.5 wt% of cardanol, 110 °C, 5 hours

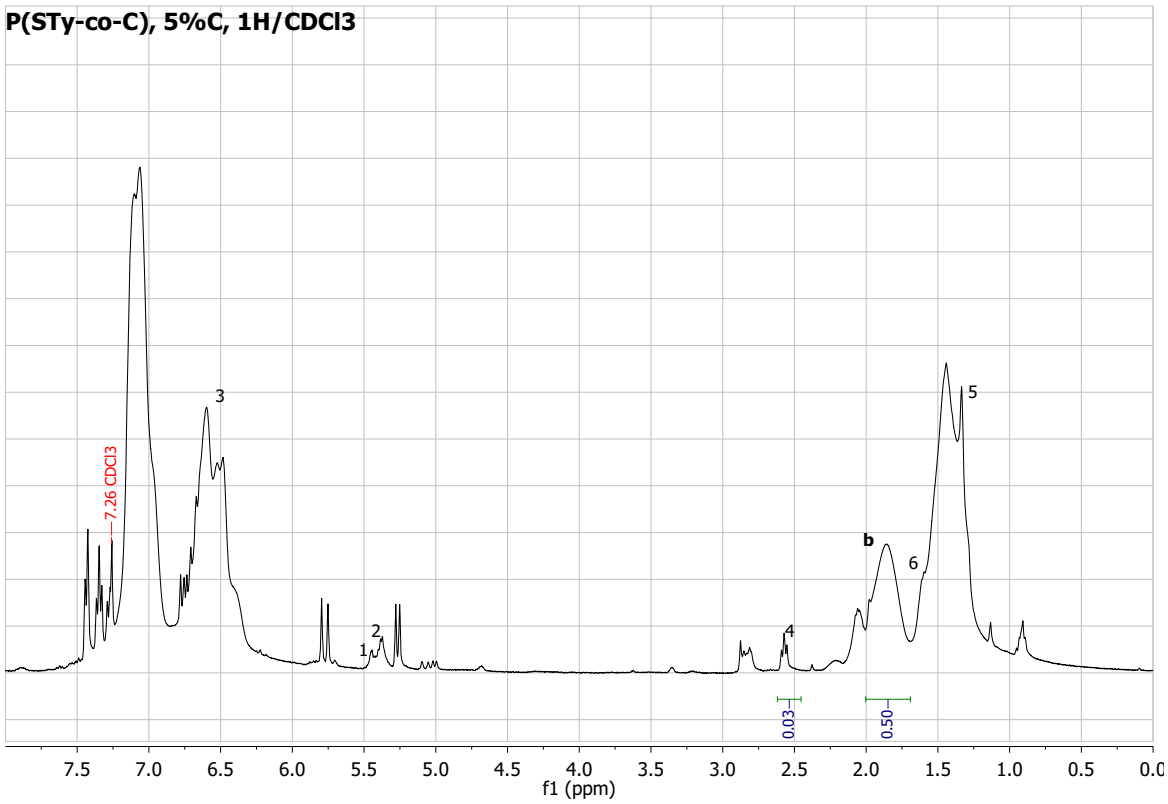


$^{1}$H-NMR of 2.5 wt% of cardanol, 110 °C, 5 hours

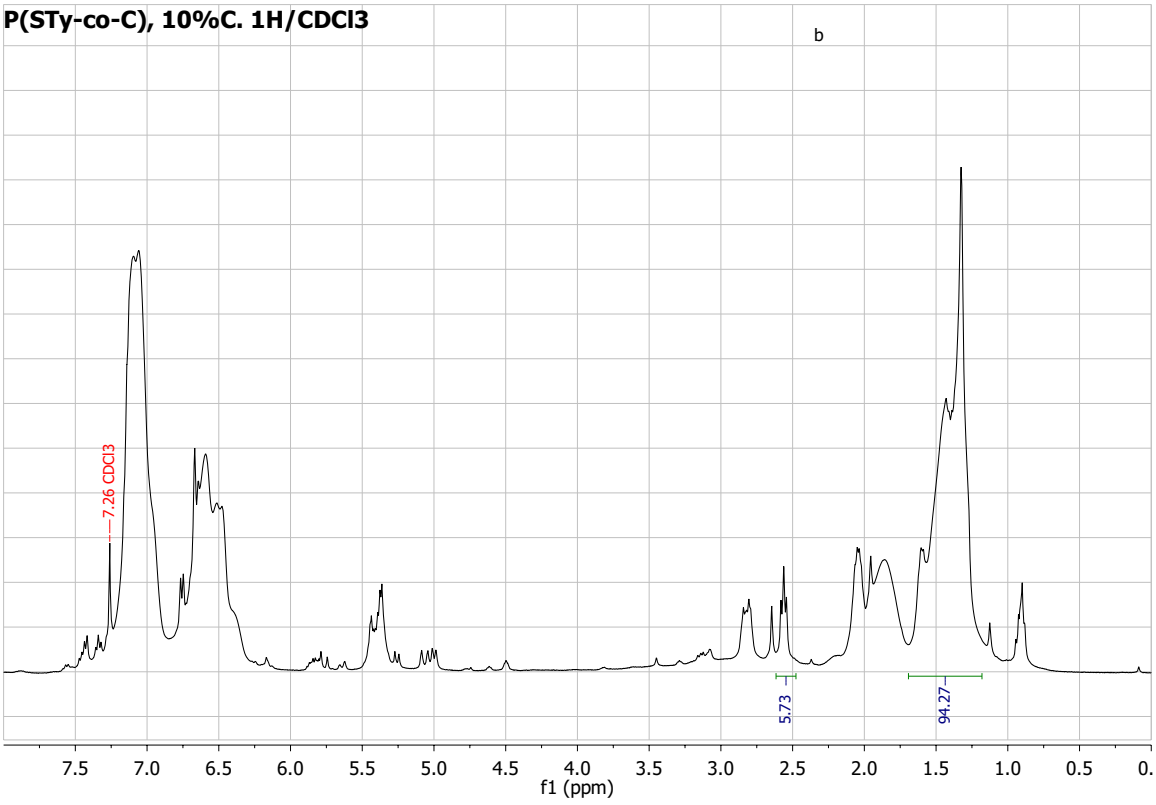


$^{1}$H-NMR of 10 wt% of cardanol, 110 °C, 5 hours

# $^{1}$H-NMR of reprecipitated styrene-cardanol copolymer

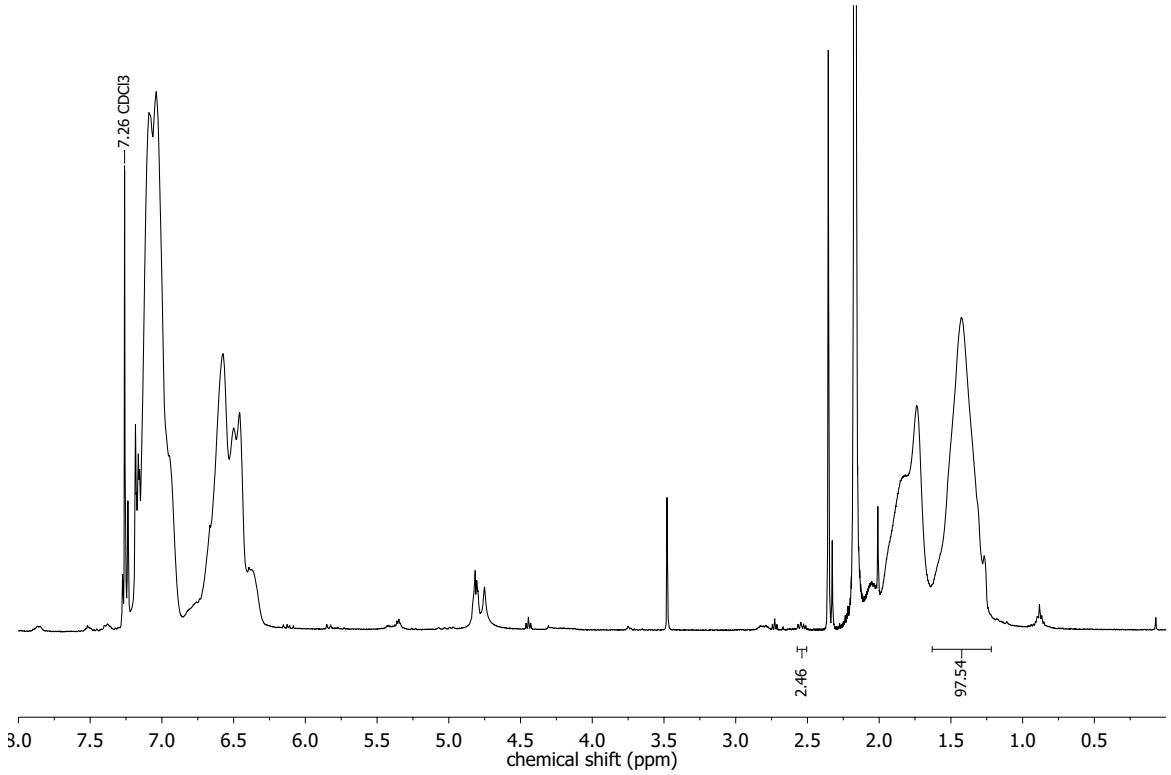


$^{1}$H-NMR of 2.5 wt% of cardanol, 85 °C, 3 hours

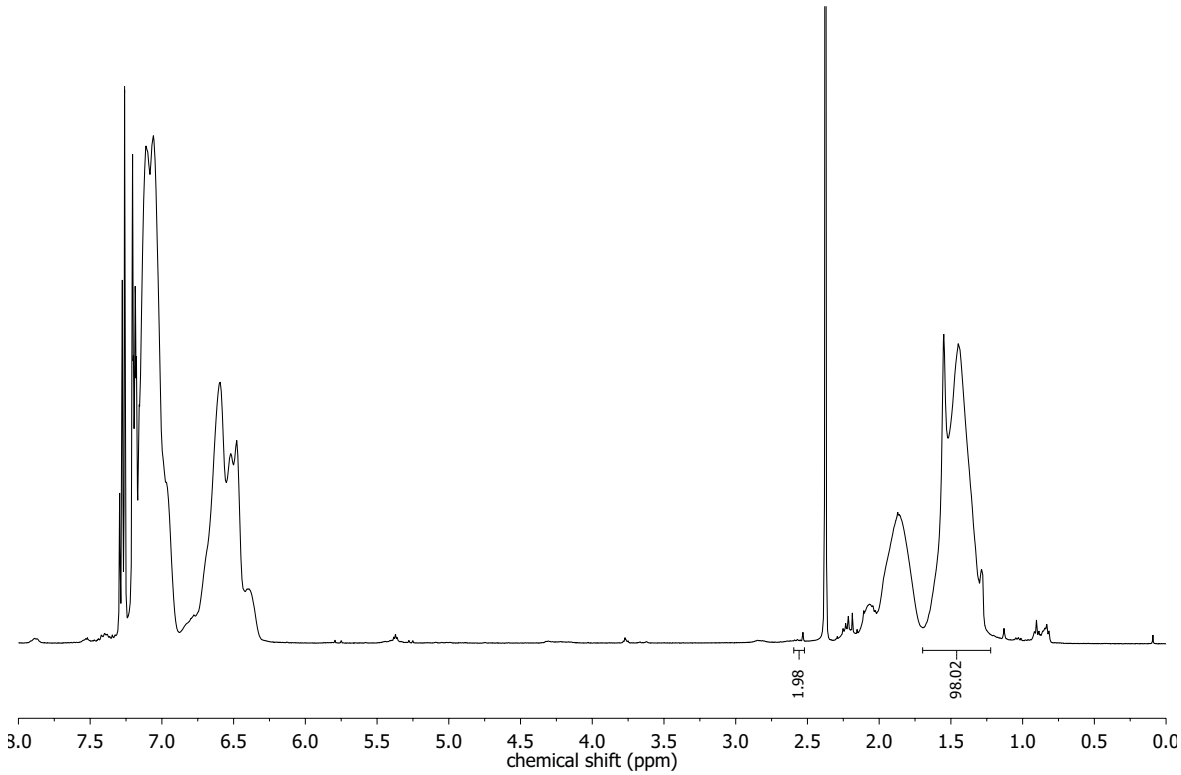


$^{1}$H-NMR of 2.5 wt% of cardanol, 85 °C, 5 hours

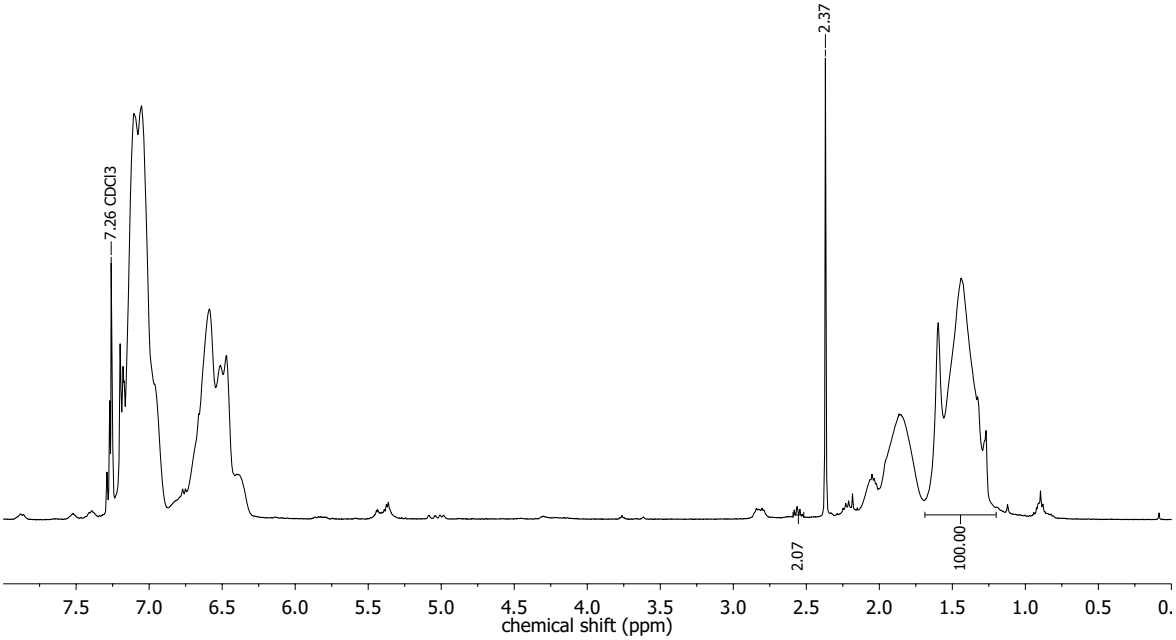


$^{1}$H-NMR of 5 wt% of cardanol, 85 °C, 3 hours

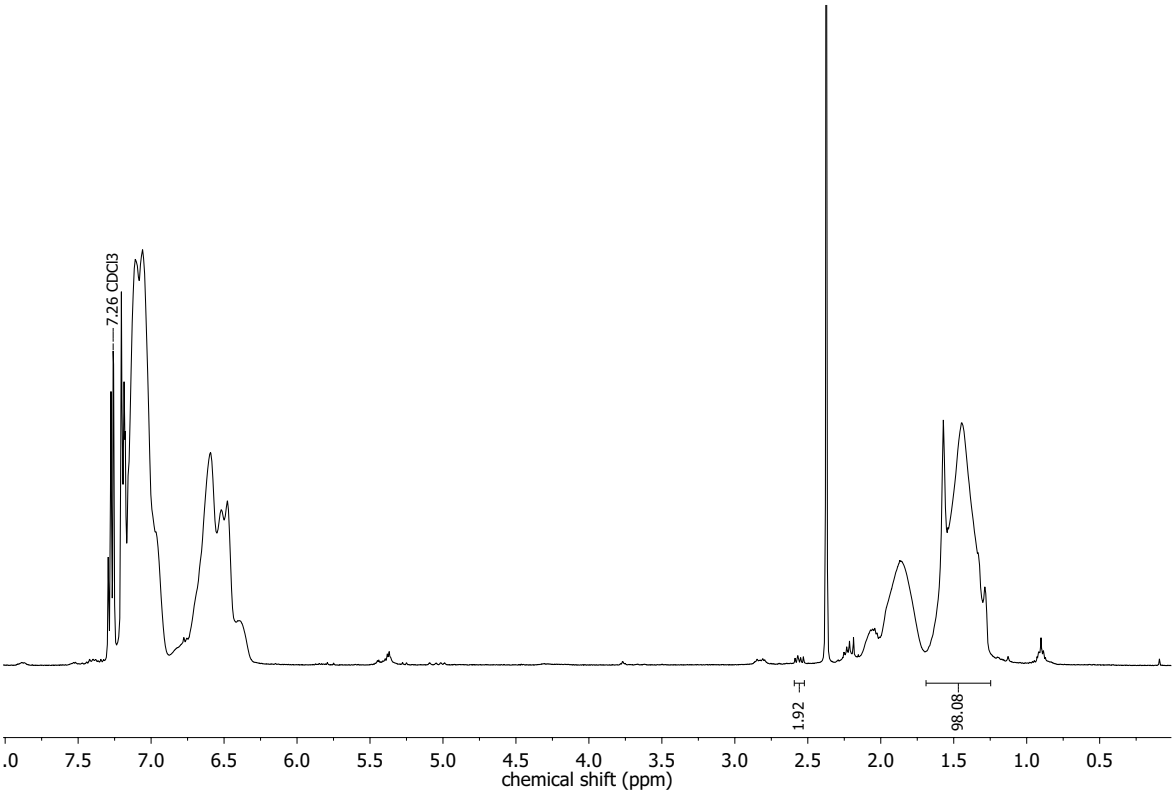


$^{1}$H-NMR of 5 wt% of cardanol, 85 °C, 5 hours

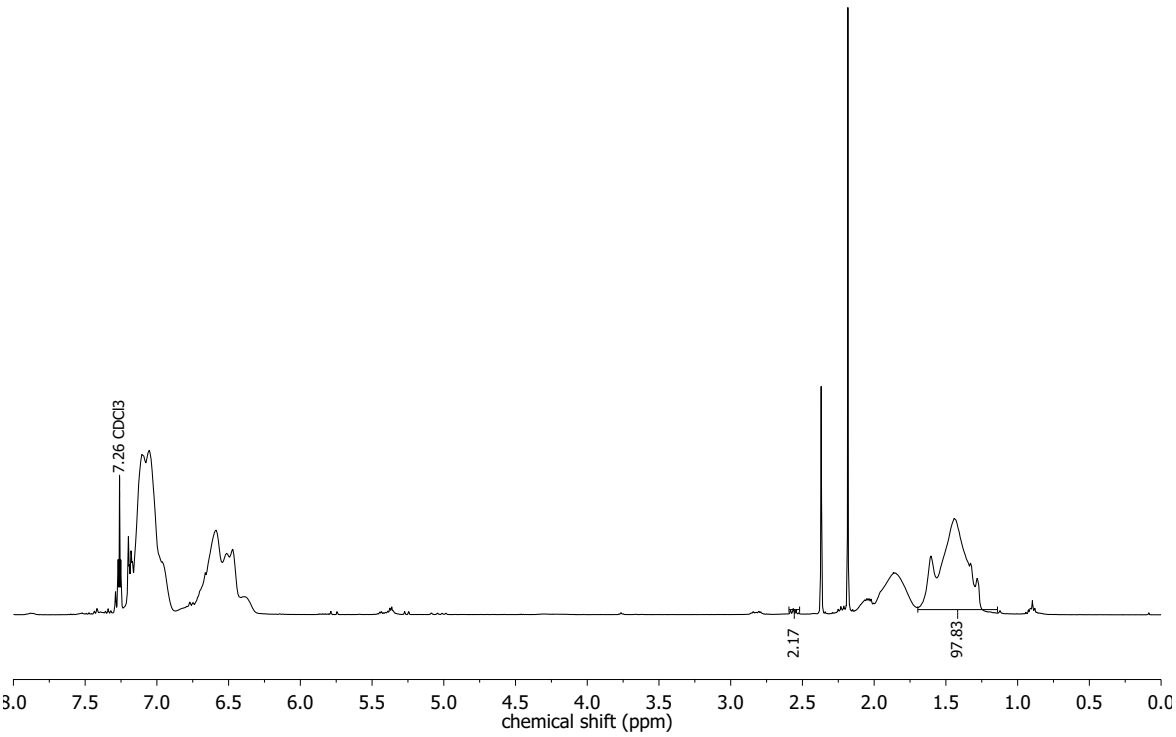


$^{1}$H-NMR of 2.5 wt% of cardanol, 110 °C, 3 hours

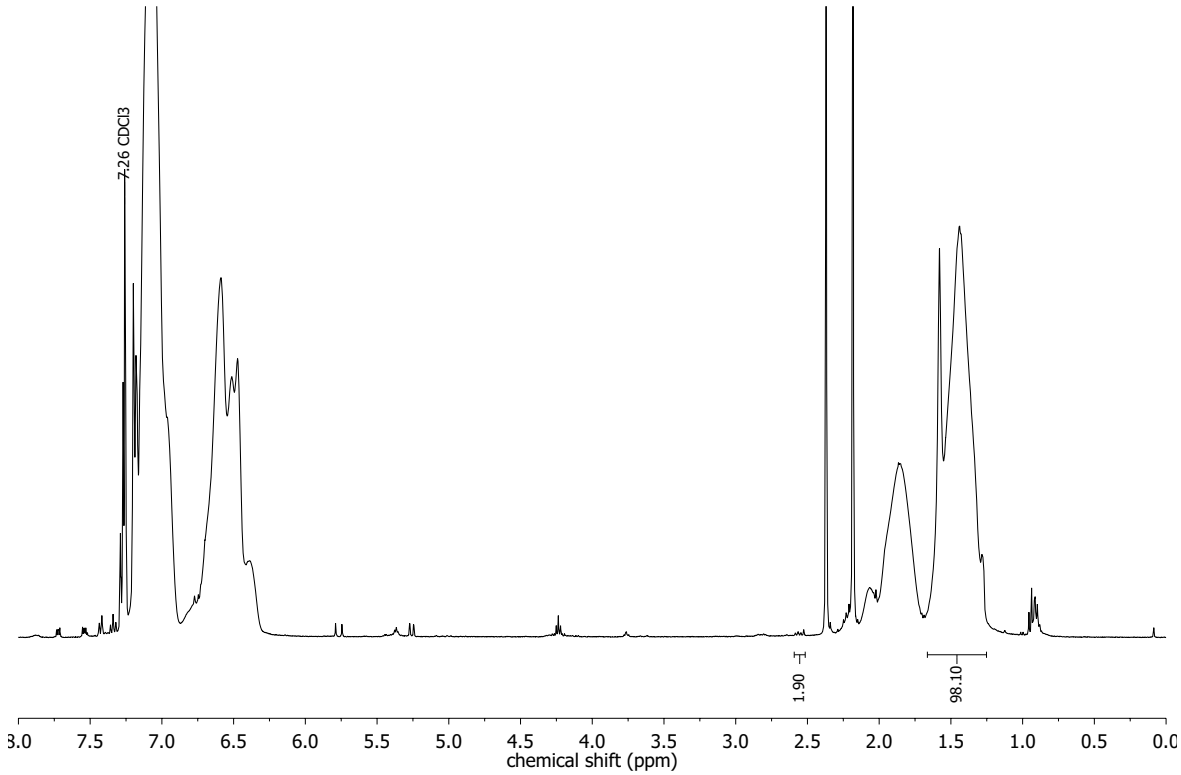


$^{1}$H-NMR of 2.5 wt% of cardanol, 110 °C, 5 hours

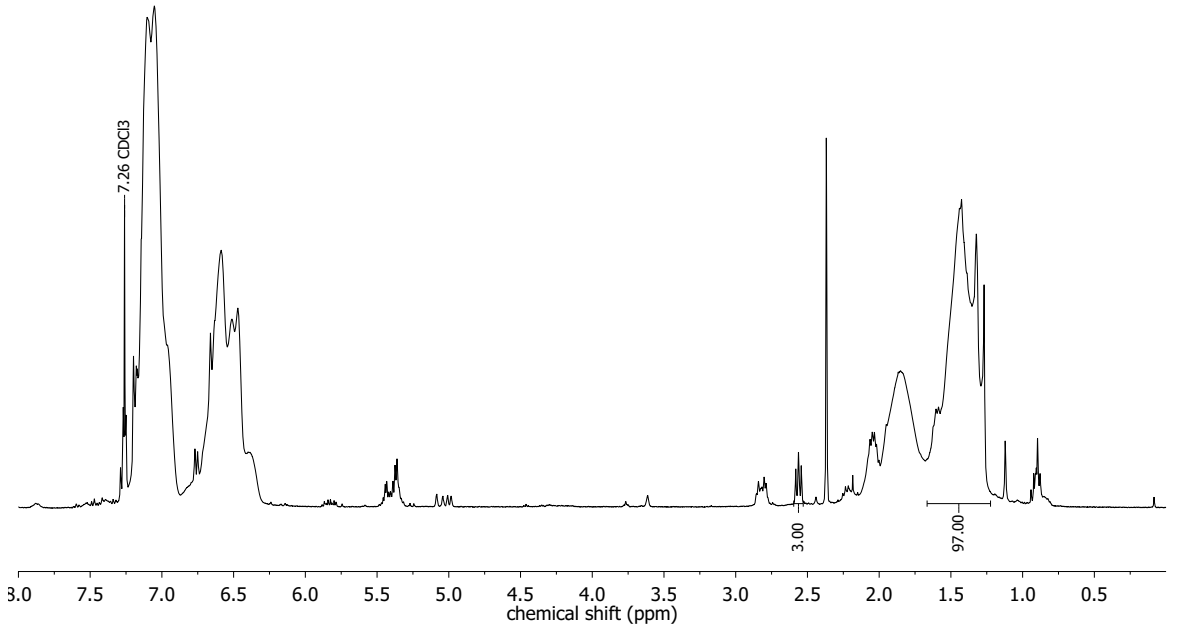


$^{1}$H-NMR of 5 wt% of cardanol, 110 °C, 3 hours

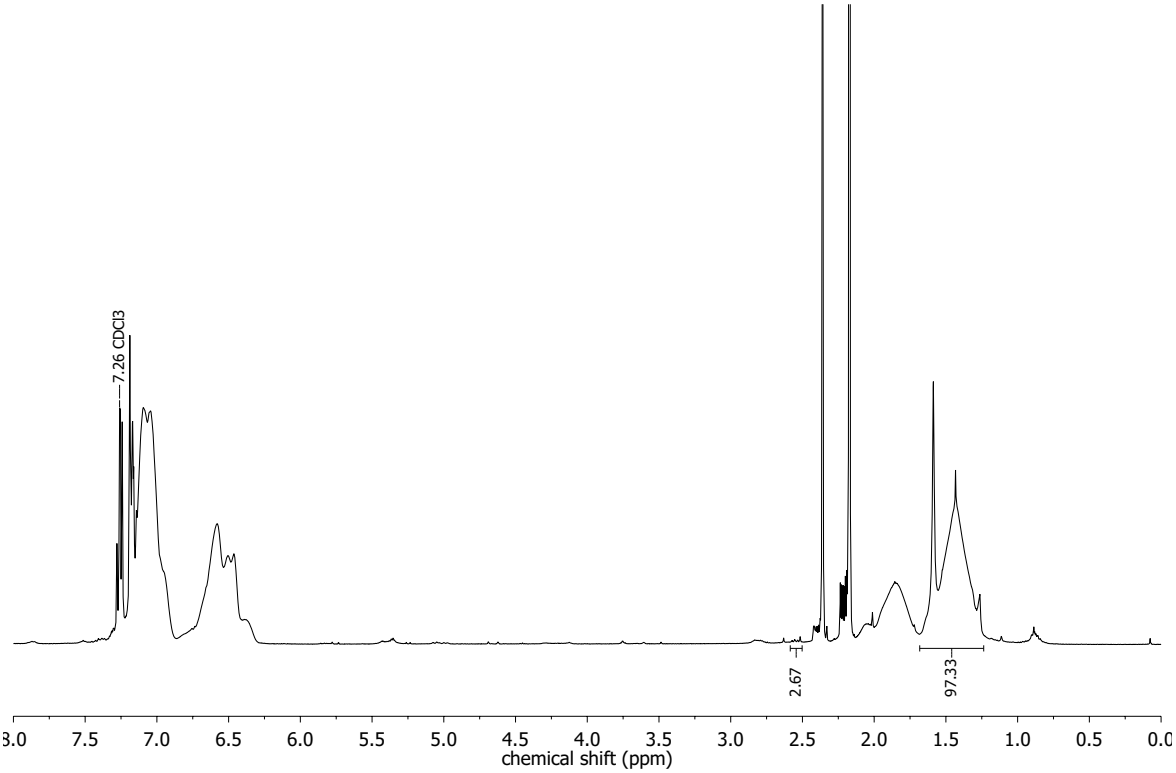


$^{1}$H-NMR of 5 wt% of cardanol, 110 °C, 5 hours

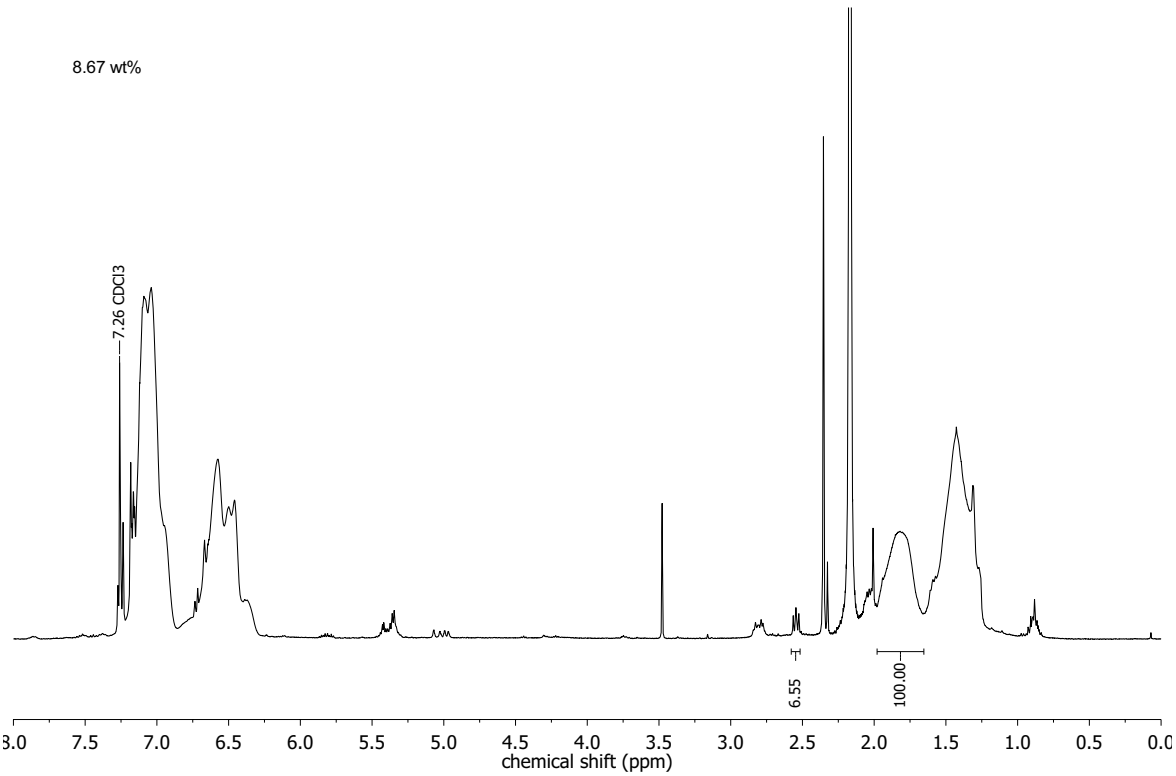


$^{1}$H-NMR of 10 wt% of cardanol, 110 °C, 3 hours

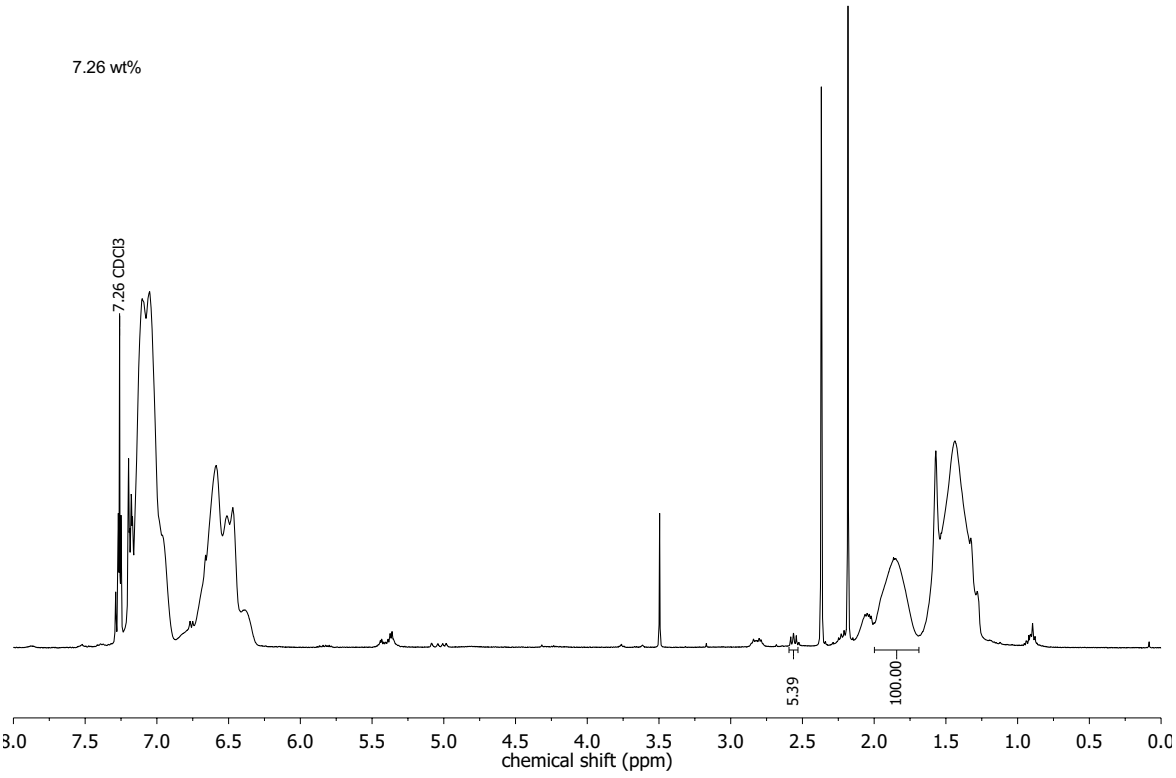


$^{1}$H-NMR of 10 wt% of cardanol, 110 °C, 5 hours

# $^{1}$H-NMR of MMA-cardanol copolymer

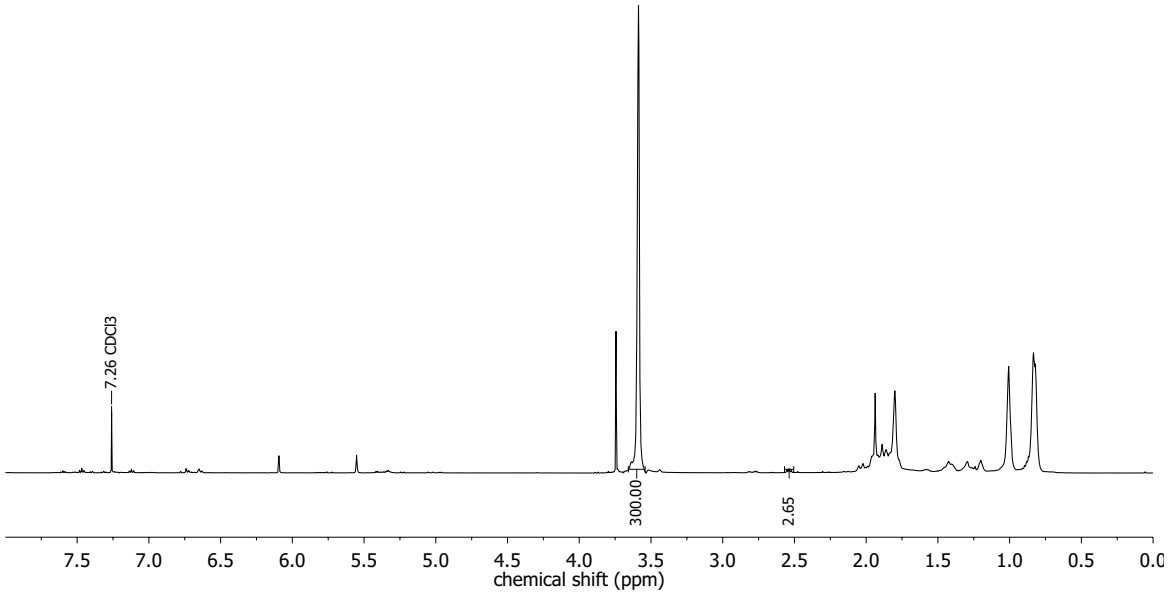


$^{1}$H-NMR of 2.5 wt% of cardanol, 85 °C, 2 hours

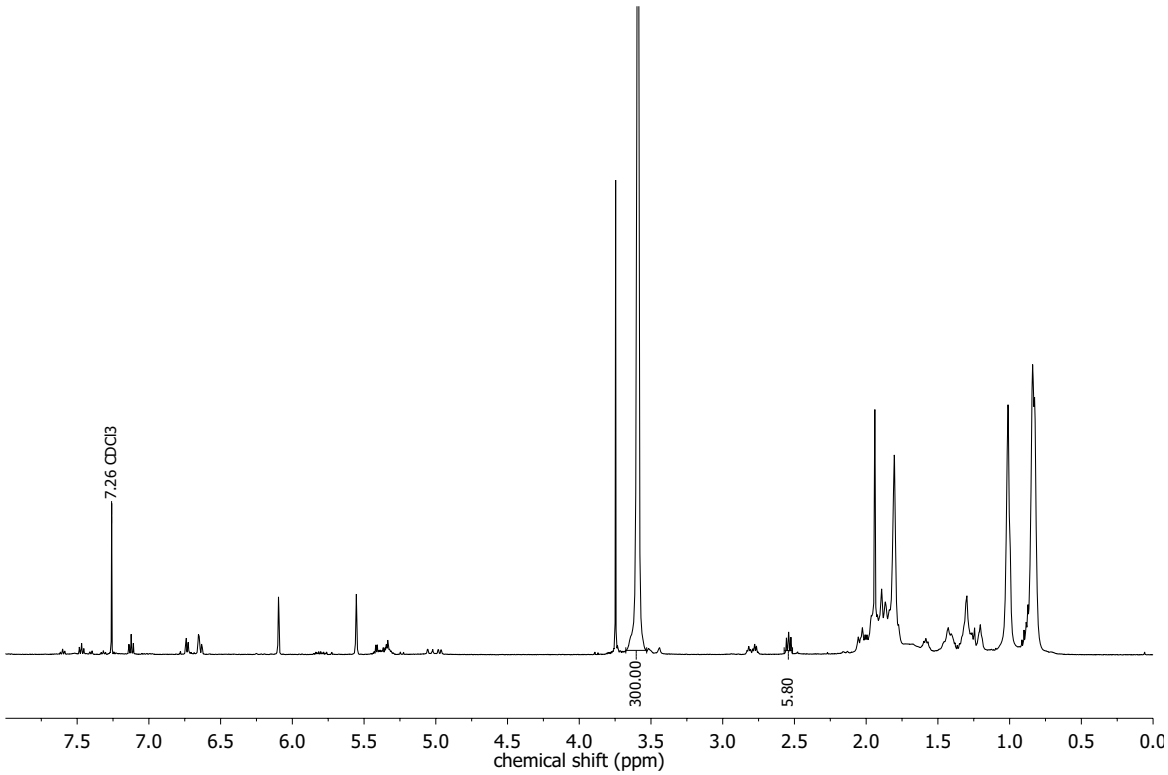


$^{1}$H-NMR of 5 wt% of cardanol, 85 °C, 3.5 hours

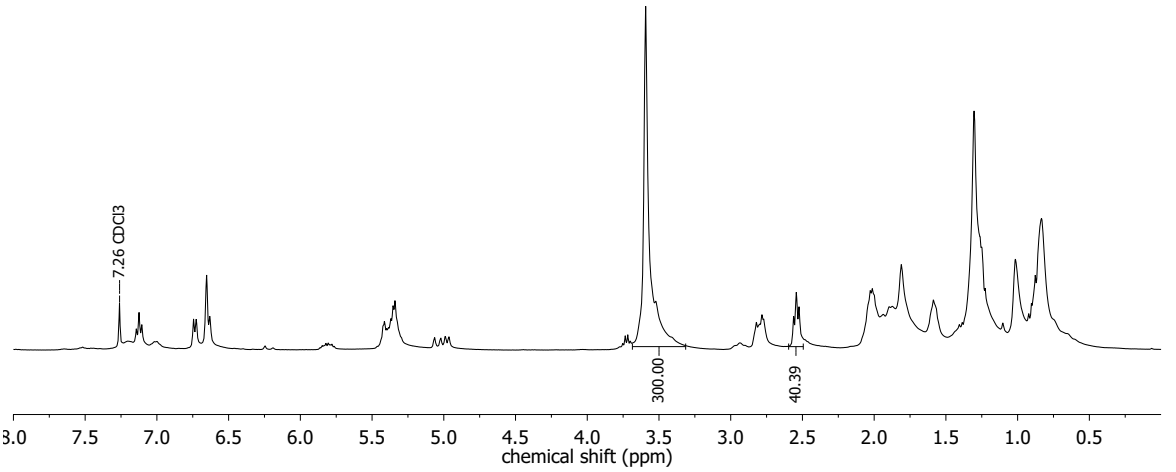


$^{1}$H-NMR of 10 wt% of cardanol, 85 °C, 6 hours

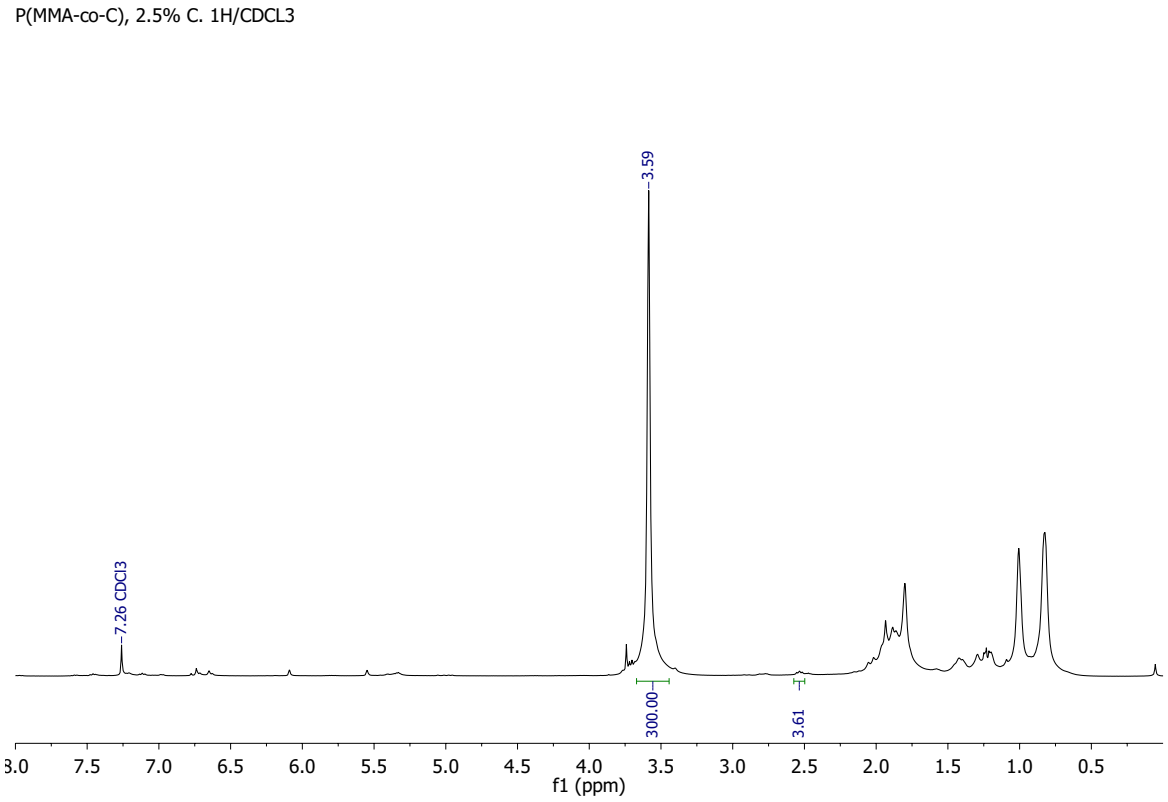


$^{1}$H-NMR of 2.5 wt% of cardanol, 110 °C, 2 hours

**P(MMA-co-C), 5%, 1H/CHCl3**

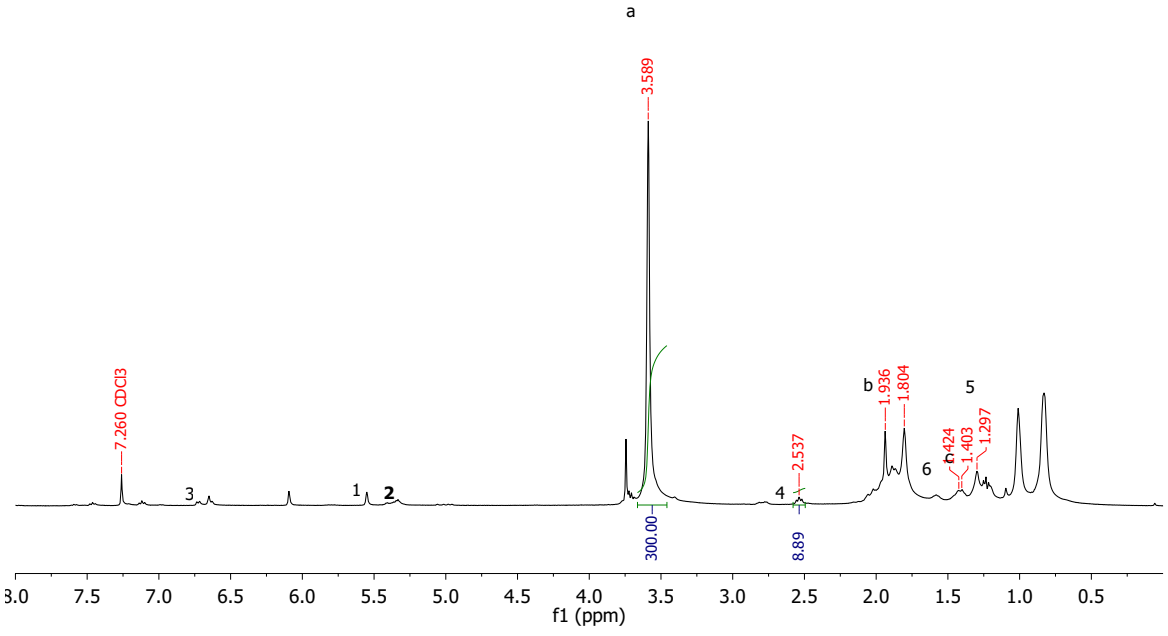


$^{1}$H-NMR of 5 wt% of cardanol, 110 °C, 2 hours

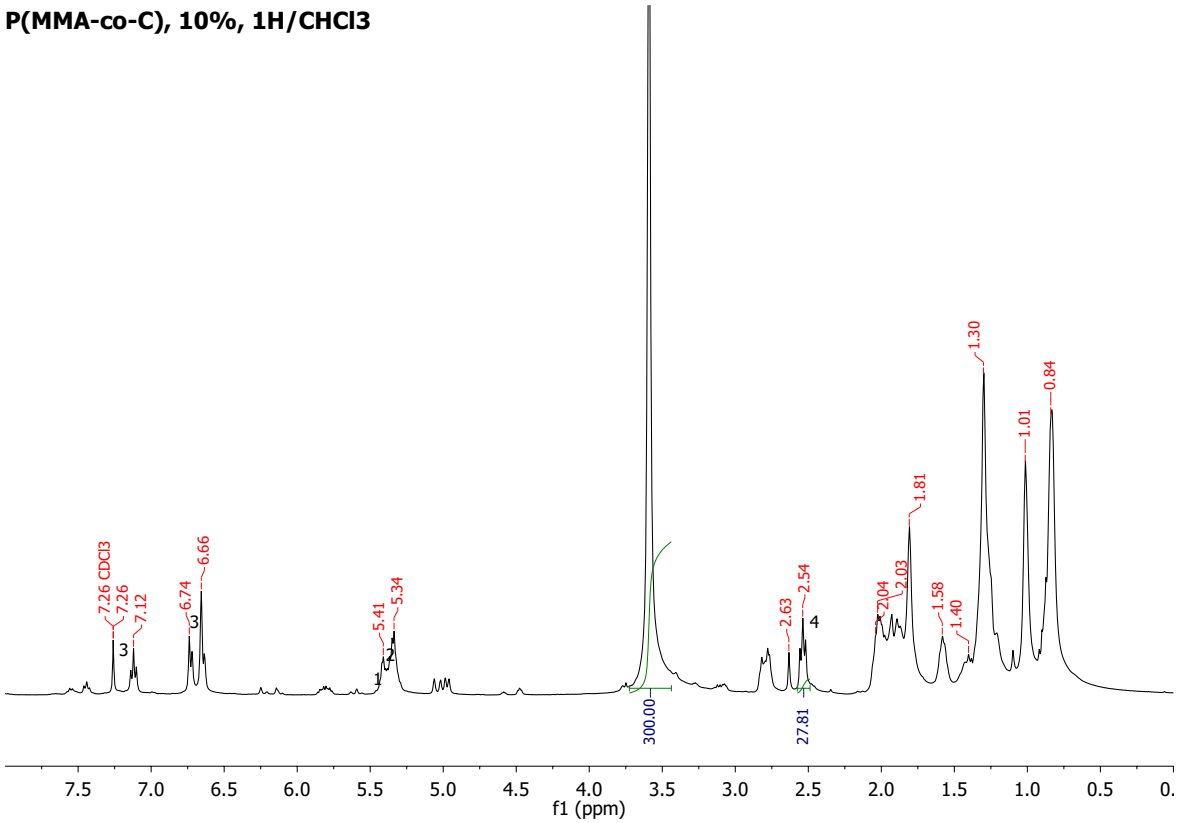


$^{1}$H-NMR of 10 wt% of cardanol, 110 °C, 2 hours

# $^{1}$H-NMR of reprecipitated MMA-cardanol copolymer

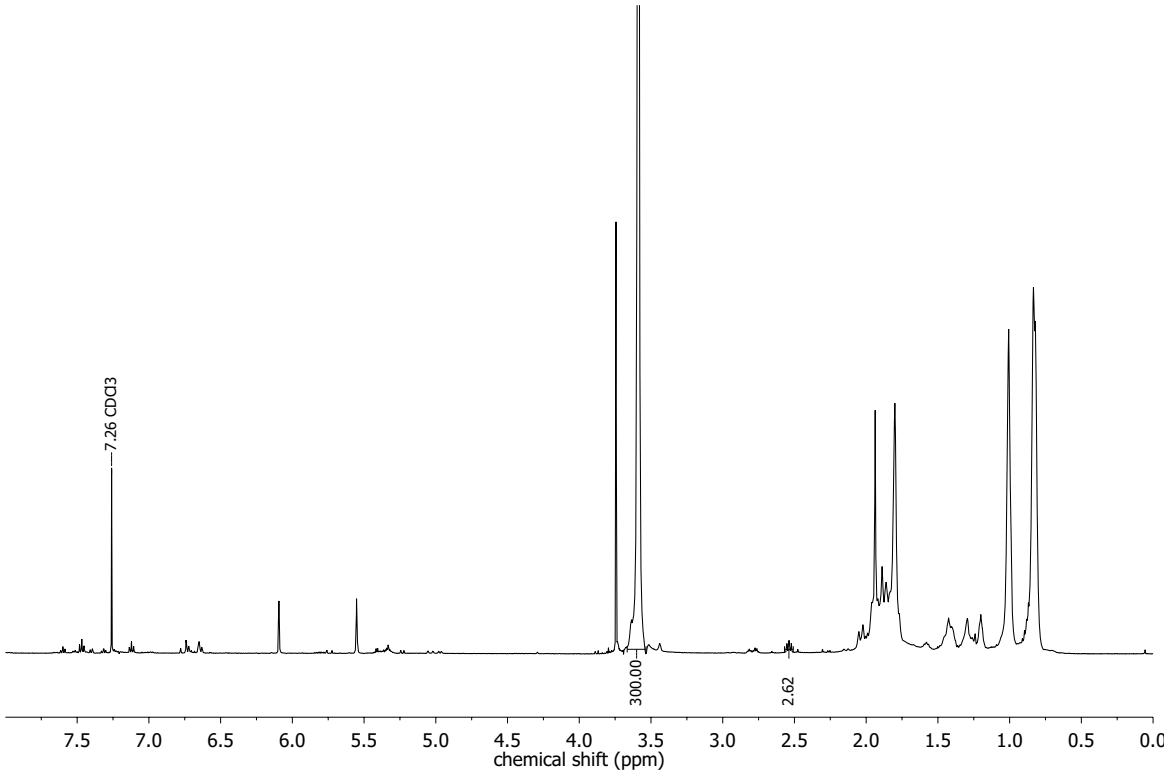


$^{1}$H-NMR of 2.5 wt% of cardanol, 85 °C, 2 hours

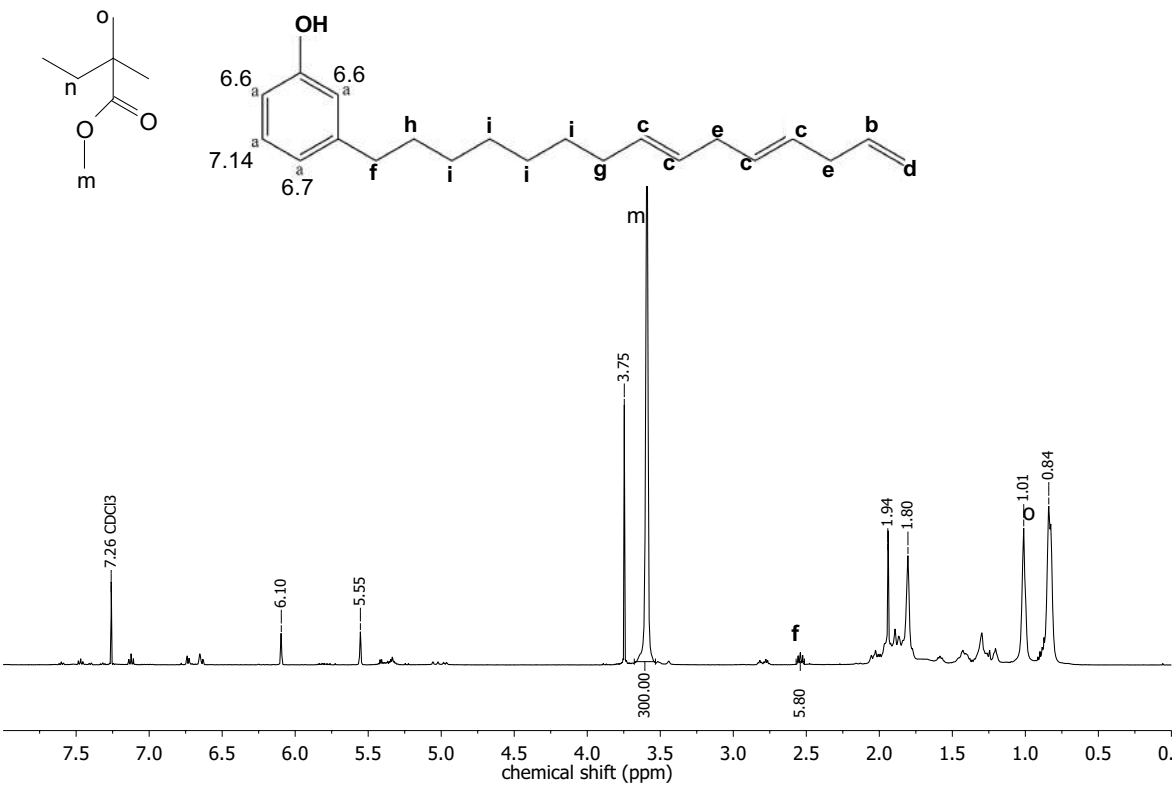


$^{1}$H-NMR of 5 wt% of cardanol, 85 °C, 3.5 hours

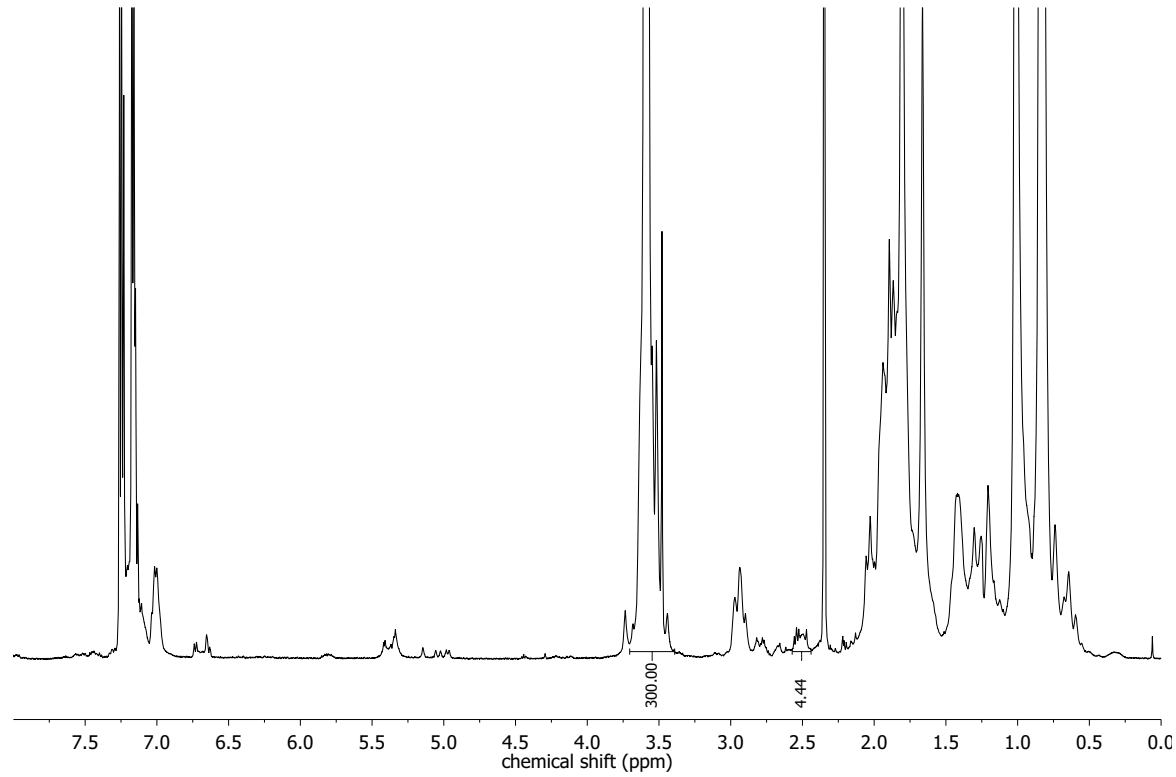


$^{1}$H-NMR of 10 wt% of cardanol, 85 °C, 6 hours

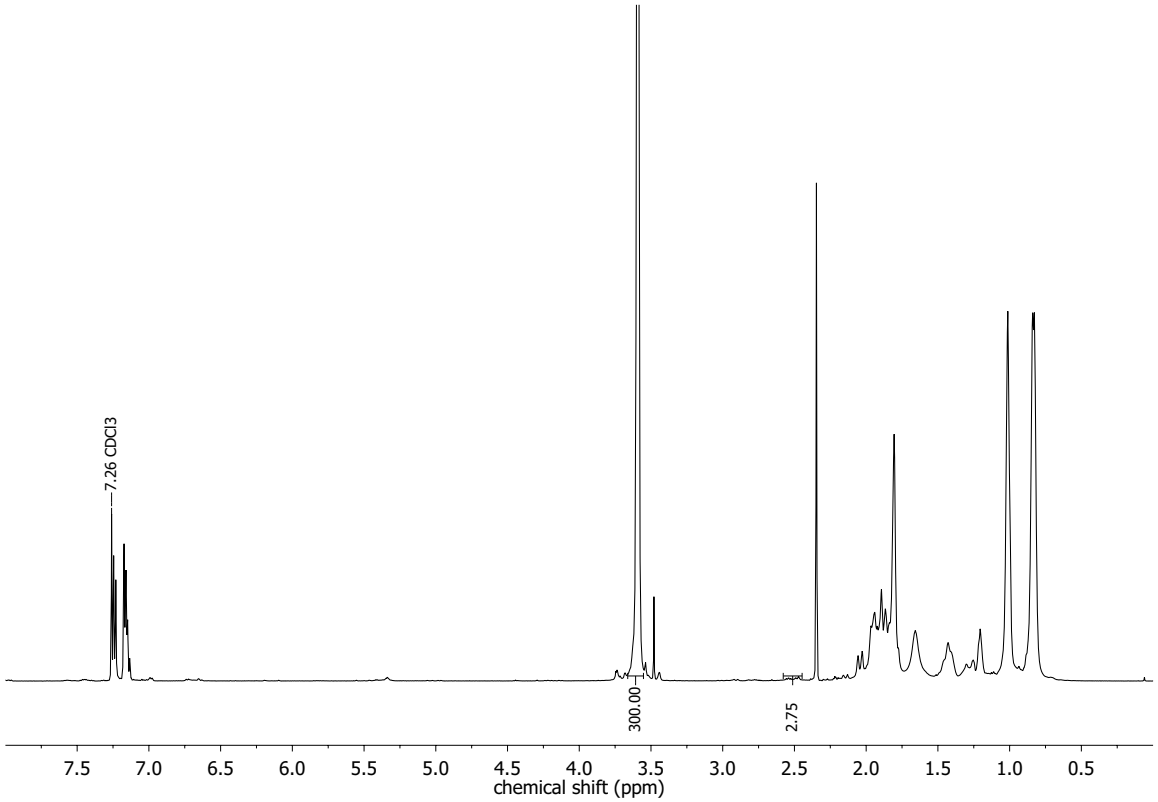


$^{1}$H-NMR of 2.5 wt% of cardanol, 110 °C, 2 hours

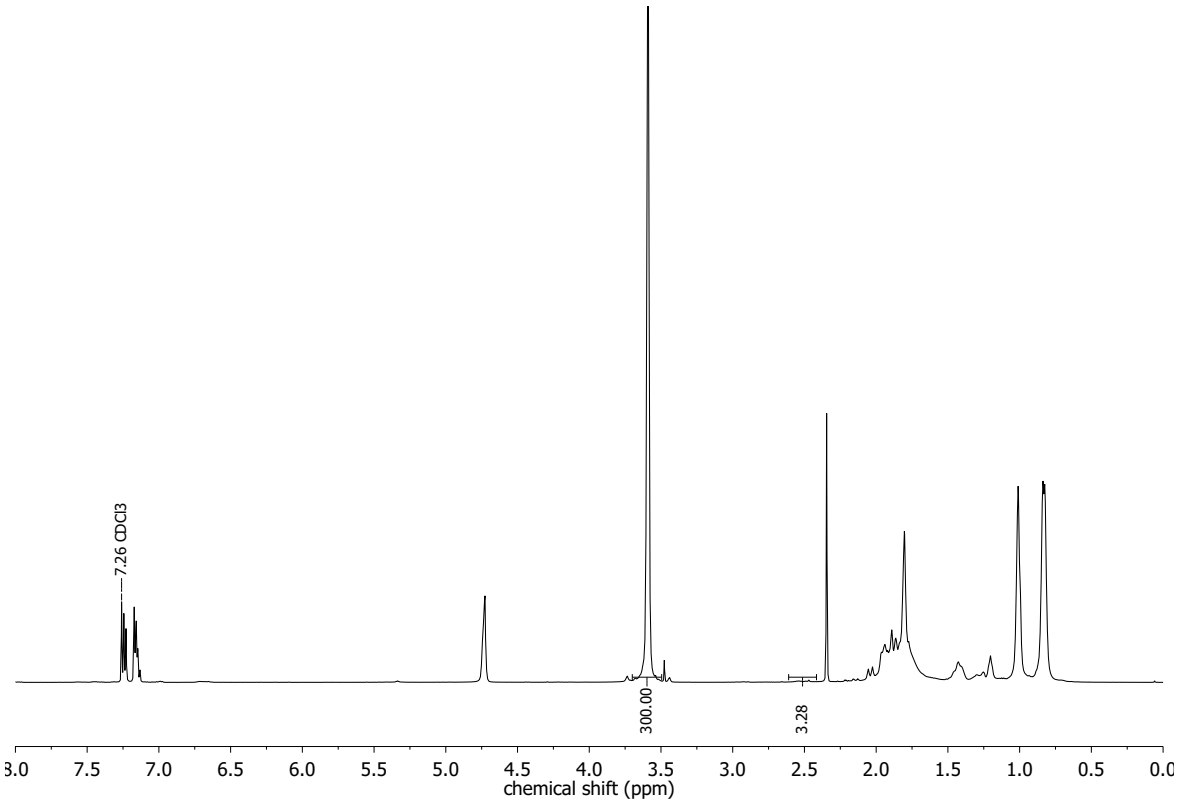


$^{1}$H-NMR of 5 wt% of cardanol, 110 °C, 2 hours

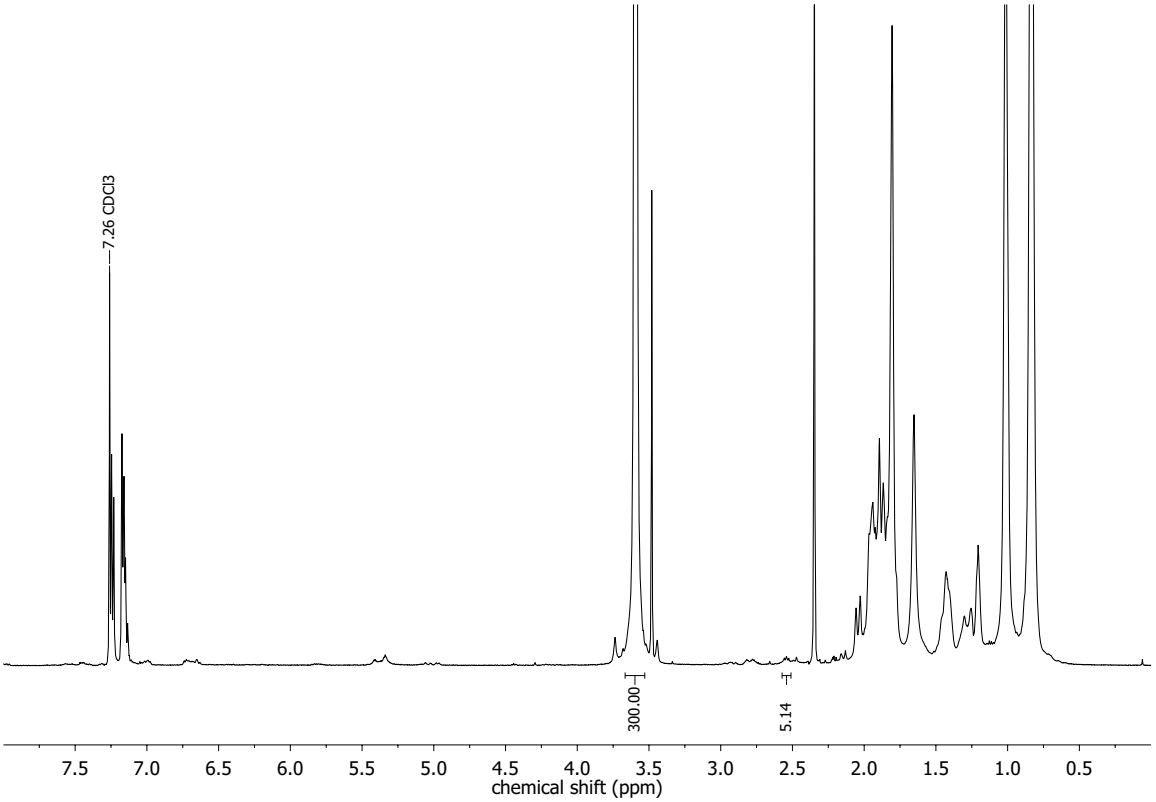


$^{1}$H-NMR of 10 wt% of cardanol, 110 °C, 2 hours

## Graphic comparison between FTIR transmittances

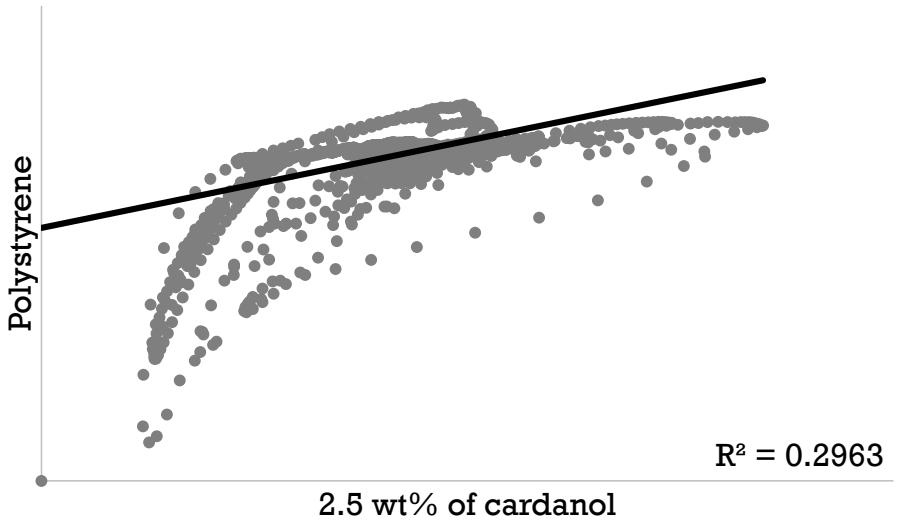


Graphic comparison between FTIR transmittance of the final product of poly(styrene-co-cardanol) with 2.5 wt% and of polystyrene produced at 110 °C.

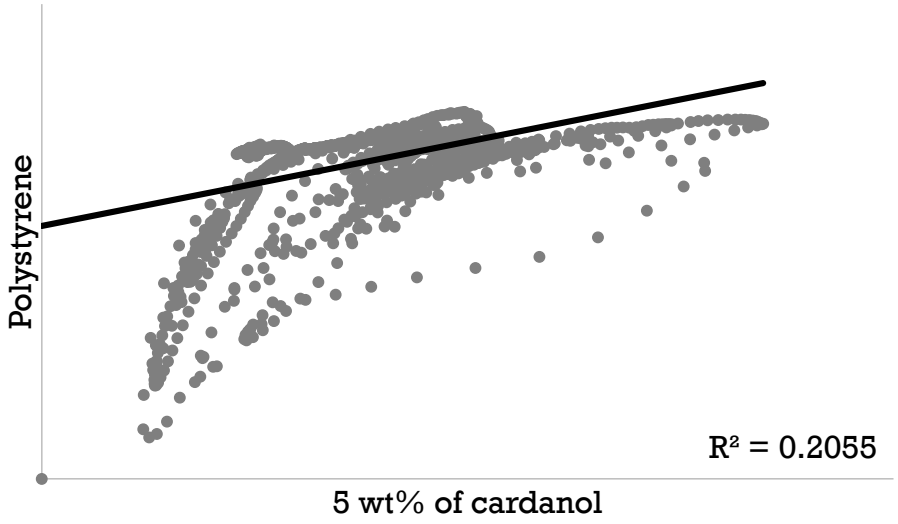


Graphic comparison between FTIR transmittance of the final product of poly(styrene-co-cardanol) with 5 wt% and of polystyrene produced at 110 °C.

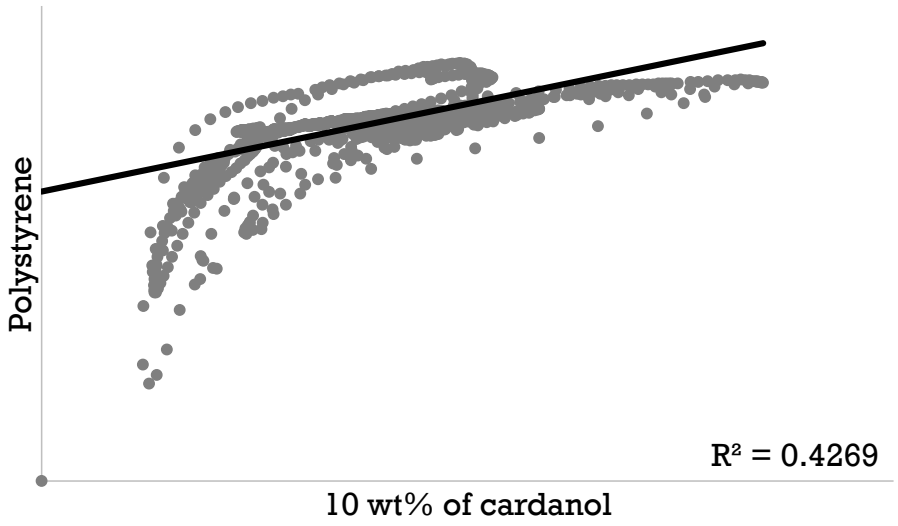


Graphic comparison between FTIR transmittance of the final product of poly(styrene-co-cardanol) with 10 wt% and of polystyrene produced at 110 °C.

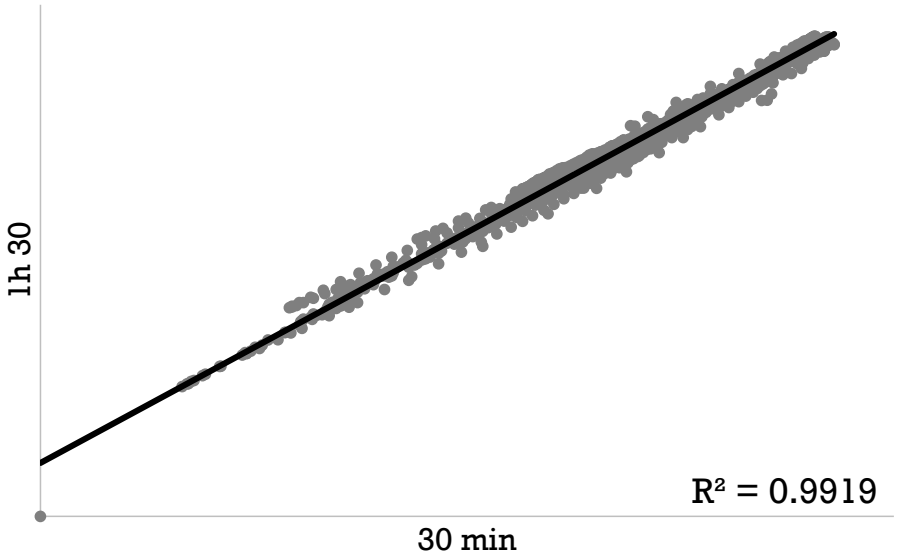


Graphic comparison between FTIR transmittance of collected poly(MMA-co-cardanol) sample with 5 wt% of cardanol after 30 minutes and 1h30 of reaction produced at 85 °C.

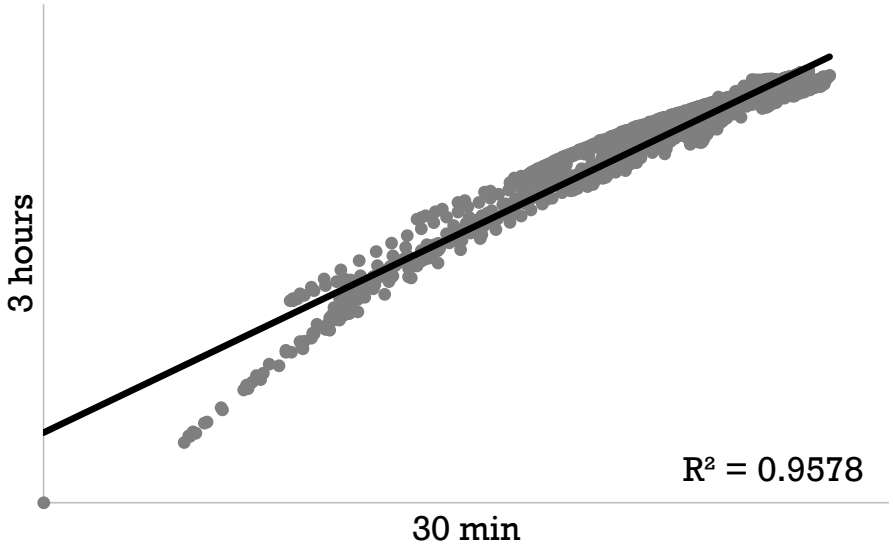


Graphic comparison between FTIR transmittance of collected poly(MMA-co-cardanol) with 5 wt% of cardanol after 30 minutes and 3 hours of reaction produced at 85 °C.

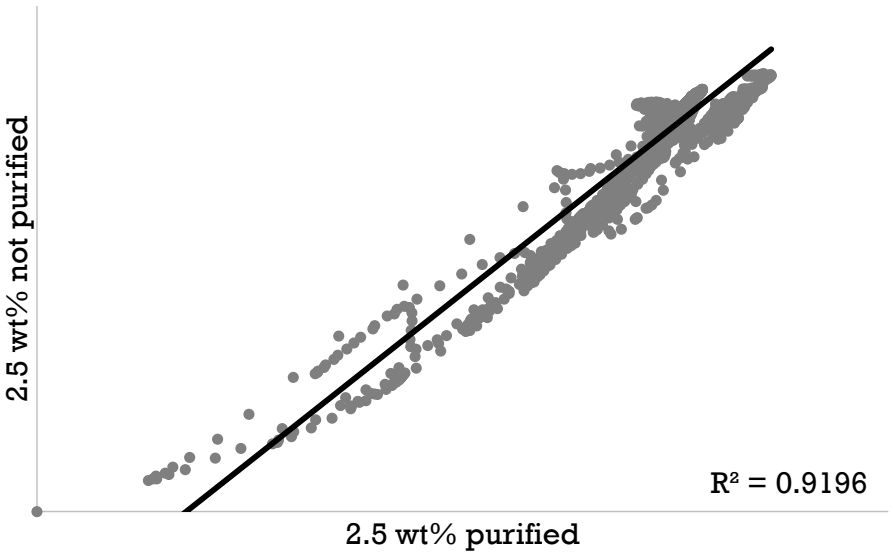


Graphic comparison between FTIR transmittance the final poly(MMA-co-cardanol) product with 2.5 wt% of cardanol at 110 °C before and after reprecipitation.

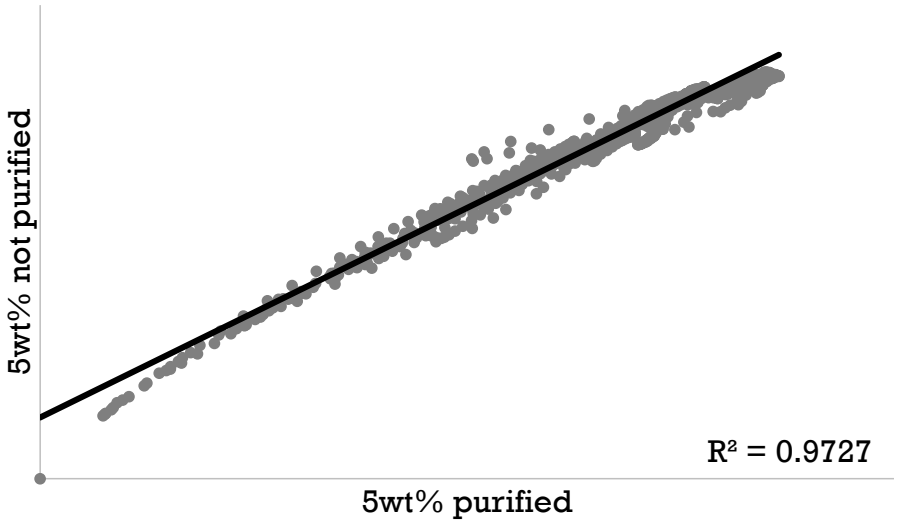


Graphic comparison between FTIR transmittance the final poly(MMA-co-cardanol) product with 5 wt% of cardanol at 110 °C before and after reprecipitation.

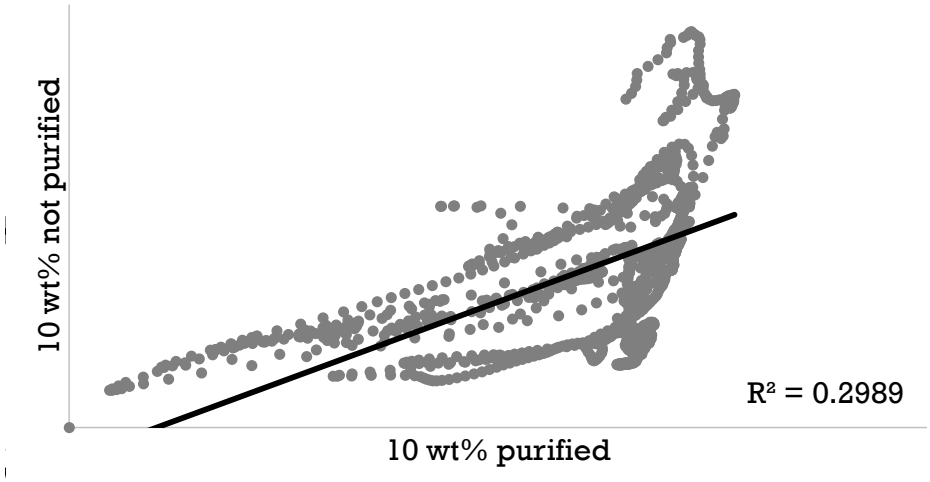


Graphic comparison between FTIR transmittance the final poly(MMA-co-cardanol) product with 10 wt% of cardanol at 110 °C before and after reprecipitation.

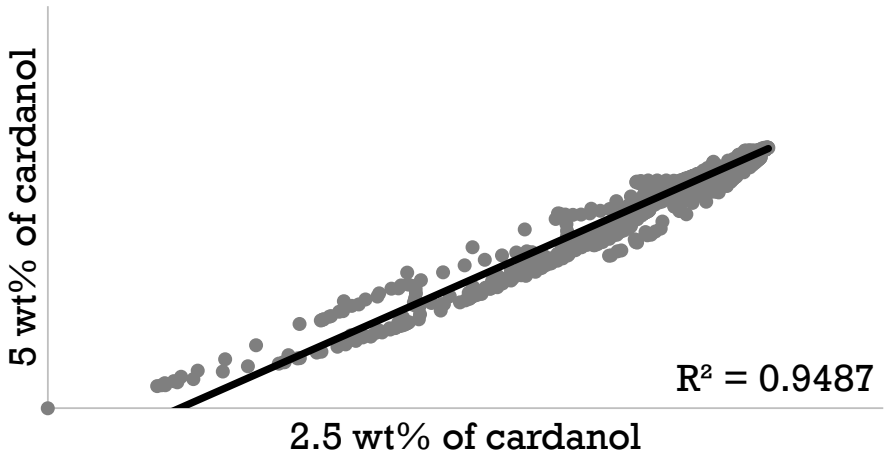


Graphic comparison between FTIR transmittance for purified copolymers samples produced with MMA and cardanol at 110°C before and after reprecipitation. 2.5 wt% versus 5 wt% of cardanol

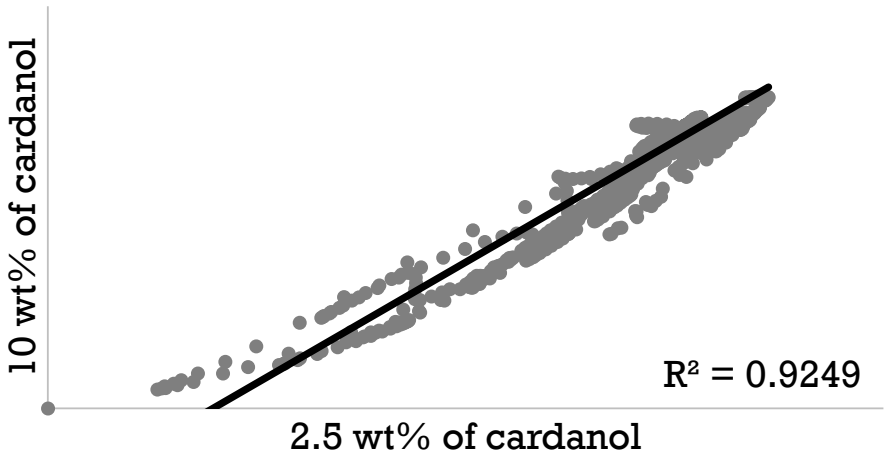


Graphic comparison between FTIR transmittance for purified copolymers samples produced with MMA and cardanol at 110°C before and after reprecipitation. 2.5 wt% versus 10 wt% of cardanol

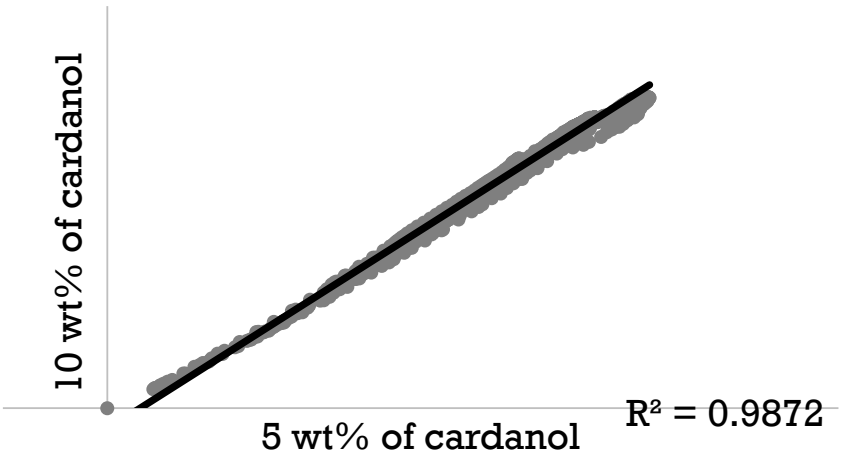


Graphic comparison between FTIR transmittance for purified copolymers samples produced with MMA and cardanol at 110°C before and after reprecipitation. 5 wt% versus 10 wt% of cardanol